Low Damage Steel Base Connections

Jamaledin Borzouie

A thesis
presented for the Degree

of

Doctor of Philosophy

in

Civil and Natural Resources Engineering
at the
University of Canterbury
Christchurch, New Zealand

University of Canterbury
2016

This thesis is dedicated in memory of my father,

Dariush Borzouie 1951-1994

Abstract

Base connections link column to ground and essentially provide a building fixation to the foundation. Seismic damage to these connections can significantly raise repair cost and the risk of demolition if costs are too high. This thesis explores the experimental and analytical studies on performance of steel column base connections under seismic demands to develop low damage base connections.

Tested base connections include exposed base plate connections with and without anchor rod preloading, bases with different patterns of asymmetric friction connections, and bases with yielding angles. Analytical studies are used to quantify the effect of base flexibility on structural demands. The overall goal is to develop low damage base connections.

The experimental results indicate that the proposed details for base connections with friction connections provide repeatable cycles without strength degradation or any requirements for repair or replacement following an earthquake. However, some stiffness degradation was observed, particularly after cycles on axially loaded specimens in the weak axis direction. In addition, the construction details of these connections are practical for construction and can be easily detailed by engineers.

Comparing the performance of tested base connections shows that if low strength loss is important, then bases with friction connections are rational selections. If simple detailing and construction is a top priority, then bases with yielding angles are potentially better choice. Finally, exposed base plate connections provide more stiffness for connections expected to

have lower rotational demands. Initial rotational stiffness can be set for all connection types by changing the design and detailing parameters for the specific connection, making them customizable for design.

Macro models of these base connections were developed or modified to enable design of these base connections by practitioners. These models are critical as they enable the translation of this research into industries and direct practices. Thus, they are a final link between the experimental results, new designs and potential new construction.

Acknowledgements

I would like to express my appreciation and thanks to all people who generously contributed to the research presented in this thesis. Special mention goes to my principal supervisor, Associate Professor Greg MacRae, for his patience, thoughtful guidance and warm encouragements. He has insprired me the latitude to become an independent researcher during this thesis. Without his guidance and useful feedback this PhD would not have been achievable. My thanks go to co-supervisors, Distinguished Professor Geoffrey Chase, and Dr Geoffrey Rodgers who generously spent their time to offer me valuable comments, support, advice and encouragement throughout my PhD. I also would like to thank Associate Professor Charles Clifton whose involvement was extremely helpful.

The financial support provided by the Natural Hazard Research Platform is gratefully acknowledged. Without the financial aid from this organization, my PhD research and experimental tests would not have been possible.

My acknowledgment is also extended to the technicians and staff of the Department of Civil and Natural Resources Engineering who helped me on this project. In particular, I would like to acknowledge Russell McConchie, Mosese Fifita, Gavin Keats, Peter Course, Grant Dunlop, John Maley, Alan Poynter for their support during experimental tests of this thesis. I want to thank Alan Jolliffe and Elizabeth Ackermann for their support and managing administrative tasks during my PhD study.

I would like to extend my deepest gratitude to my mother, Zahra, brother and sister, Sadra

and Shima, for providing me with lots of encouragement and love. Thank you for all of your support over the past 30 years. Without your support and dedication, I would not be where I am today. Finally, I am immensely appreciative of my wife, Atefeh, for being the source of my joy, inspiration and unwavering support during my PhD project.

Table of Contents

List of Figures

List of Tables

Chapter 1: Introduction

1.1. Background

For structures to be reusable after major earthquake, components of the structure including column base connection should have undergone little damage and be easily reinstated. Evidence of the need for low damage structures comes from behaviour observed in past earthquakes, such as the Canterbury, 2010, Darfield, 2010, where many significantly damaged buildings were required to be demolished. For those buildings that were repaired, the repair process was difficult, time consuming and expensive.

Recently, a new generation of seismic design was introduced with the objective to minimize structural damage. This new approach to seismic design has been termed "Low Damage Design". One significant performance objective of a low damage building is "immediate occupancy" to allow business continuity (MacRae, 2013). A low damage construction approach eliminates expensive repairs and limits the financial loss to the owner and the tenant.

Efforts around the world to develop low damage steel structures, where the frame systems are not expected to perform linearly, have emphasized low damage column moment resisting joints (e.g. Clifton, 2005; Koetaka et al., 2005; Inoue et al., 2006; Rodgers et al., 2007; Oh et al., 2009; MacRae et al., 2010; Latour et al., 2011; Rodgers et al., 2012; Latour et al., 2013; Latour et al., 2015), or the use of braces (e.g. Pall and Marsh, 1982; Fitzgerald et al., 1989; Chanchí et al., 2014), or post tensioned rods (e.g. Christopoulos et al., 2002), and the

consideration of slab effect (e.g. Hobbs et al., 2013; Chaudhari et al., 2014). Some of these techniques have been used in new construction (e.g. Gledhill et al., 2008; Latham et al., 2013).

One promising method to dissipate energy is friction. Friction was successfully used in sliding hinge joints for beam to column connection by Clifton (2005) and in braces by Pall and Marsh (1982). However, more tests and design methods are required for its usage at the base connection, where damage is extremely difficult and costly.

Issues with the commonly used exposed base plate connections were reported by Tremblay (1995) and Midorikawa et al. (2012) in the Northridge (1994), Kobe (1995), and Tohuku (2011) earthquakes. In particular, inelastic rotations are expected at this location with the associated cost to repair. More specifically, if all low-damage structural elements around the structure remain undamaged after an event, but the column base connections experience damage, it is likely that the whole structure will need to be replaced since these columns support the rest of the structure. Hence there is a significant need to extend low damage design to these connections.

Recently, some uni-directional studies have focused specifically on low-damage base connections (Tamai et al., 2004; Chi and Liu, 2012; Piluso et al., 2014). Friction device, and post tensioned bars with yielding plates were used in these connections. However, there is still a lack of practical details for low damage base connections, as well as experimental tests of base connections under the likely bi-directional loading including the axial force of building weight, which would be expected in an earthquake.

The demand on the base connection is also affected by the flexibility of the foundation, soil underneath of the foundation, and the stiffness of the specific base connection. A number of studies have been conducted to evaluate the effect of base flexibility (Maan and Osman, 2002; Aviram et al., 2010; Ruiz-Garcia and Kanvinde, 2013; Zareian and Kanvinde, 2013). However, analytical study is not available to determine the effect of base flexibility on the nonlinear base rotation for wide range of structural periods, thus limiting the impact of these studies on design practice.

1.2. Specific Need

It may thus be seen that for confidence to be developed in low damage base connections, there is a significant need for base connection systems that have no-damage through use of devices under bi-directional loading as well as the likely demands, or are easily repaired. In addition, there is a need to determine the likely demands on base connections due to the base flexibility. Finally, there is a need to translate and predict these results to industry practitioners to enable of uptake new solutions.

1.3. Objective and Scope

To address these needs this research investigates the feasibility of low damage performance of yielding and frictional base connections. In particular, analytical and experimental studies are conducted to study the cyclic performance of the exposed base plate, base connections with yielding and frictional techniques. In addition, analytical study is performed to quantify base connection demands due to base flexibility. Specific answers are sought to the following

questions:

1. What base connections have the potential to perform as low damage base connections under large column deformation according to qualitative assessment?

2. Under what circumstances may exposed base plate connections be categorized as low damage base connections?

3. What is the effect of base flexibility on the damage at the column base?

4. What is the cyclic performance of low damage base connection candidates under axial load and bi-directional bending?

5. Can macro-models suitable for use in design by practitioners for low damage base connections be developed?

1.4. Preface

Chapter 2 presents the detailing of innovative base connections that have the potential to perform as low damage base connections. A subjective quantitative assessment (SQA) method is used to compare these base connections and evaluate their potential. Finally, the general test setup and loading regime proposed for the experimental program are described. In particular, this chapter seeks to answer Question 1.

Chapter 3 presents experimental cyclic lateral testing of exposed base plate connections with different failure types tested under in-plane, and 2-D clover leaf cyclic tests, with and without

applied axial force in order to answer Question 2.

Chapter 4 presents in-plane cyclic testing of columns with exposed base plate connections, with and without anchor rod pre-loading and column axial force. Based on these experimental tests, simple procedures are proposed to estimate the effect of anchor rod tensile force on base rotational stiffness and calculate of the anchor rod tensile force. This chapter answers Question 2.

Chapter 5 presents the effects of column base rotational stiffness on the seismic demand of single storey frames with a range of periods using linear and nonlinear time history analysis. This chapter answers Question 3.

Chapter 6 and 7 present an experimental investigation of an asymmetric friction connection (AFC) at the base of steel columns such as may be used in a moment-frame. The column base strong axis aligned asymmetric friction connection (SAFC) and the column base weak axis aligned asymmetric friction connection (WAFC) are investigated in these chapters. In-plane, out-of-plane and 2-D clover leaf cyclic tests were conducted of columns both with and without applied axial force. Simple models are developed to estimate the force-displacement hysteresis loop envelope behaviour. This chapter answers Question 4.

Chapter 8 presents the development and verification of a macro-model to represent the hysteretic moment-rotation backbone curve of column base friction connections under strong and weak axis displacements. The friction connections considered were (i) aligned with the column weak axis, sticking out from the column flange, or (ii) with the column strong axis, being flat against the column flange. This chapter answers Question 5.

Chapter 9 presents the experimental testing of asymmetric friction connections (AFCs) using 2 M16 Grade 10.9 bolts with higher strength, but less ductility, compared to Grade 8.8 bolts. This chapter provide more details for the answer to Question 4.

Chapter 10 presents the design and experimental testing of column base with replaceable angles bending about their strong and weak axis with and without applied axial force. This chapter seeks for the answer Question 4.

Chapter 11 presents the comparison of the exposed base plate connection, column base strong axis aligned asymmetric friction connections (SAFC), and column base weak axis aligned asymmetric friction connections (WAFC) and base connection with yielding angles in terms of damageability, stiffness and construction. This comparison enables the selection of base connections in real design.

Chapters 12 presents the overall conclusions to the research and discusses possible extensions and future work.

1.5. Summary

This chapter has presented the motivation and main scope of this research. Overall, seismic building performance can be increased using low damage systems. However, these improvements are rendered useless if the column base connection is damaged. Hence, there is a significant need to extend low damage approaches to these connections.

To date, there is still lack of practical low damage base details, and experimental testing of

base connections under realistic conditions including bi-directional loading and axial force. The scope of this research is to develop low damage steel base connections. The experimental studies in this research have been conducted to study the cyclic performance of column bases with the exposed base plate connections, asymmetric friction connection (AFC), and yielding angles. In addition, analytical studies are used to quantify the effect of base flexibility on structural demands. The overall goal is to develop and characterize low-damage base connections, and quantify their performance experimentally and in models suitable for use in design by practitioners.

Chapter 2: Candidates for Low Damage Base Connections

2.1. Introduction:

Base connection failures were reported in the Northridge (1994), Kobe (1995), and Tohuku (2011) earthquakes by Tremblay (1995), Midorikawa et al. (2012) as shown in Figure 2-1. Generally, the seismic performance of base plate connections in past earthquakes has not been widely reported, since the base is placed at the lowest part of the building and is typically hidden by flooring. In addition, the observed performance of exposed base plate connections in past experimental tests indicates that they cannot perform as a low damage connection at high drift levels. Because lateral column displacement and increased damage and fracture were observed in the columns, base plates, anchor rods and welding between the base plate and the column. Figure 2-1 shows examples of this damage.

However, all base connections could be low damage, if demands are small enough. (Dewolf and Sarisley, 1980; Picard and Beaulieu, 1985; Thambiratnam and Paramasivam, 1986; Astaneh et al., 1992; Jaspart and Vandegans, 1998; Burda and Itani, 1999; Fahmy et al., 1999; Adany et al., 2000; Myers et al., 2009; Gomez et al., 2010). In particular, replacing the yielded or fractured element is often difficult at the level of the base connection. Moreover, yielding of the base connection may cause the residual displacement on the column top, and building straightening is difficult. Thus, there is significant cost associate with their repair, creating a significant economic motivation to develop low or no damage base connections.

Fracture of the base plate (Website of California State University)

Elongation of anchor bolts in an exposed base plate (Midorikawa et al., 2012)

Cracking of asphalt showed base plate yielding (Midorikawa et al., 2012)

Fracture of anchor bolts, out-of-plane deformation of base plate (Midorikawa et al., 2012)

Fracture of anchor bolts (Midorikawa et al., 2012)

Spalling of concrete covering a column base (Midorikawa et al., 2012)

Figure 2-1: Photos of Tohuku (2011) and Northridge (1994) from Midorikawa et al. (2012) and Website of California State University

In this chapter, innovative base connections are detailed that have the potential to perform as low damage base connections. A subjective quantitative assessment (SQA) method is used to compare these base connections and evaluate their potential. Finally, the general test setup and loading regime proposed for the experimental program are described. In particular, answers are sought to the following main question:

- What base connections have the potential to perform as low damage base connections under large column deformation?

2.2. Low Damage Base Connections Candidates

2.2.1. Rocking Steel Column by Post Tensioned Steel Bars

For rocking steel columns (Chi and Liu, 2012), the column is connected to the base plate by post tensioned rods that are anchored by couplers under the base plate, as shown in Figure 2-2. The post tensioned rods are anchored from the top to the structure and from the bottom to the couplers that are placed in the concrete. Several holes are drilled in the base plate by which rods can pass through the base plate. This base connection can be designed for two different limit states: 1) yielding of rods before column yielding and; 2) rods remain elastic under applied demands.

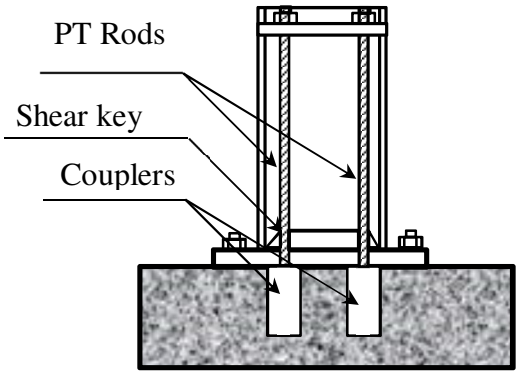

Figure 2-2: Base connection with PT rods

However, this design does not offer enough potential for further experimental tests. The pros and cons of this design include:

- Additional energy dissipators can be added to this base connection, such as the buckling restrained steel (BRS) plates by Chi and Liu (2012). Therefore, structural damage at column bases is limited to the replaceable dissipators.

- Rocking behaviour of this connection causes a small amount of damage in this base connection.

- The cables in the structural steel are exposed, which is dangerous if a cable or anchorage fails. Note that in similar rocking concrete structures, the prestressed cable is enclosed in the column.

- It is difficult to prestress steel cables or rods. There are two ways for prestressing cables or rods. In the first way, cables are prestressed by the stressing jack, which also requires a large space around the anchor. The prestress tendons also have to be located at the top of the columns to use the stressing jacks in the steel structure, which can create with multi-storey constructions. In addition, the anchorages are a major addition to the cost. In the second method, bars are post tensioned by torque wrench, where friction makes prestressing difficulty for high tensile bars.

- Tightening on one side causes column bending deformation so a sequence of steps must be implemented, adding time and cost to construction.

- Long bars are required when the base connections are designed for high drifts. In this case, rods must pass through the first level beam-column joint, and special added detailing is thus required, adding further cost.

- If the rod fractures below the base plate, then replacing of the fractured bar is difficult.

Thus, this design approach is not considered suitable for further experiments.

2.2.2. Column Base with Yielding Elements

The use of anchor bolts (or rods), a base plate, and an angle that connects the column to the base plate are candidates to be designed as the weakest link in the base connection chain, as shown in Figure 2-3. Japanese design procedures proposed criteria for the base connection designed with yielding anchor bolts, as described by Grauvilardell et al. (2005). The yield strength over the tensile strength of the anchor bolt (yield ratio) is less than 0.75 to ensure yielding of the bolt shank, as well as the threads. In addition, in fully threaded rods, it increases the fracture deformation. Finally, the yield ratio of Grade 8.8 anchor bolts is about 0.8, which implies anchor bolts fracture in this type of connection so there is low deformation capacity. However, if during a large earthquake, these bolts fracture in the threaded region, then there is no moment and shear strength at the base, and replacing of the fractured anchor bolts is not possible. Hence, it is not always practical to develop the base connection with yielding anchor bolts using steel materials for partially threaded anchor bolts in New Zealand. To address this issue, Tamai et al. (2003) proposed connecting a shape memory alloy (SMA) rod to an ordinary steel bolt via coupler. Overall, both experimental and analytical results demonstrate this type of rod can increase the performance of building column bases.

The yielding base plate could be an option for rocking frames, but not moment resisting

frames, as tested by Midorikawa et al. (2010) and shown in Figure 2-3. Two drawbacks can be found in this type of base connection. First, the yielded base plate causes residual displacement of the column. Second, damage occurs in the base plate that is not easily repaired or replaceable.

The base connection with yielding angles that connects the column to the base plate, as also shown in Figure 2-3, is a candidate for low damage base connections. In particular, the yielding mitigates to the replaceable angle and the structure can be easily straightened. Thus, it offers a much lower repair cost and time.

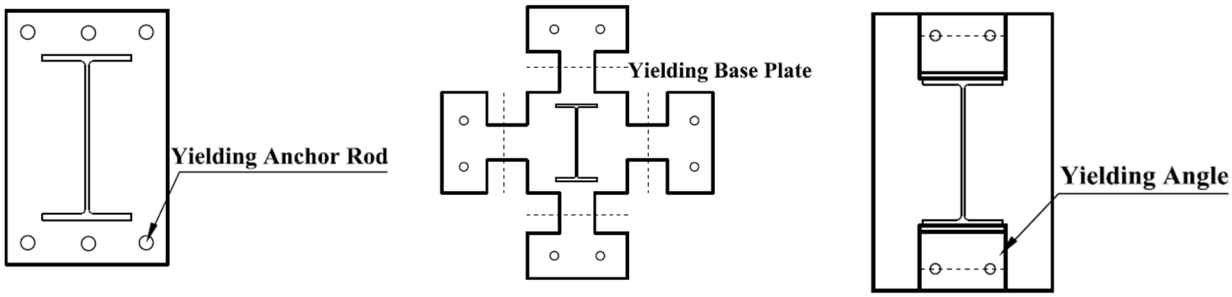

a. Yielding anchor rod

b. Yielding base plate (Midorikawa et al., 2010)

c. Yielding angle

Figure 2-3: Base connections with yielding elements

2.2.3. Column Base with Asymmetric Friction Connection (AFC)

The sliding hinge joint (SHJ) beam-to-column friction connection as shown in Figure 2-4 is a type of asymmetric friction connection (AFC). It was invented by Clifton (2005) and has been further developed by MacRae et al. (2010). In this design approach, the top flange of the beam is fixed to a plate extending from the column, referred to as the *top flange plate*. There is also a bottom flange plate and a web plate with elongated holes to permit bolt sliding. A

shim is placed between the bottom flange plate and beam. Another shim is placed between the column flange plate and a floating, or cap, plate. The floating plate is shown in the figure as the *bottom flange cap plate* and it is only connected to the subassembly through the bolts. There is a similar configuration beside the web, but the holes at the top of the web are not elongated and the bolts in these holes are designed to carry the beam shear forces.

During large lateral movements, beam end rotation occurs about the top flange. Sliding first occurs at the interface between the bottom flange plate and the beam/shim. Later, it occurs at the interface between the bottom flange plate and the floating plate/shim. Because sliding does not initiate at the same displacement on each side of the bottom flange plate, it is referred to as an *asymmetric friction connection* (AFC). Similar behaviour occurs beside the web. Since energy is dissipated by friction sliding, rather than by yielding or buckling, reinstatement of the joint may only require replacement of the bolts and possibly shims. For this reason it may be considered to be a low-damage or no-damage connection.

It should be noted that during large lateral deformations the bottom plate must deform causing significant demands on the plate and plate-column weld. Even if no bolts exist in the connection, lateral deformation of the beam about its strong axis causes the upper and lower beam plates to pry apart, thus resisting some moment, but also reducing clamping force and friction. In practical situations, the prying forces in this prying connection are small. However, if the top and bottom flange plates consist of large thick steel plates, it is possible that the beam flexural strength would be fully developed by prying alone, without any bolts.

The AFC base connection of Figure 2-4, has been proposed for the base of one-way moment frames (Gledhill et al., 2008, MacRae et al., 2009). It has some similarities to the SHJ base

connection except that sliding may occur beside either flange and gravity forces discourage vertical movement of the column. Hence, it is very similar in design and use of the beam column AFC connection.

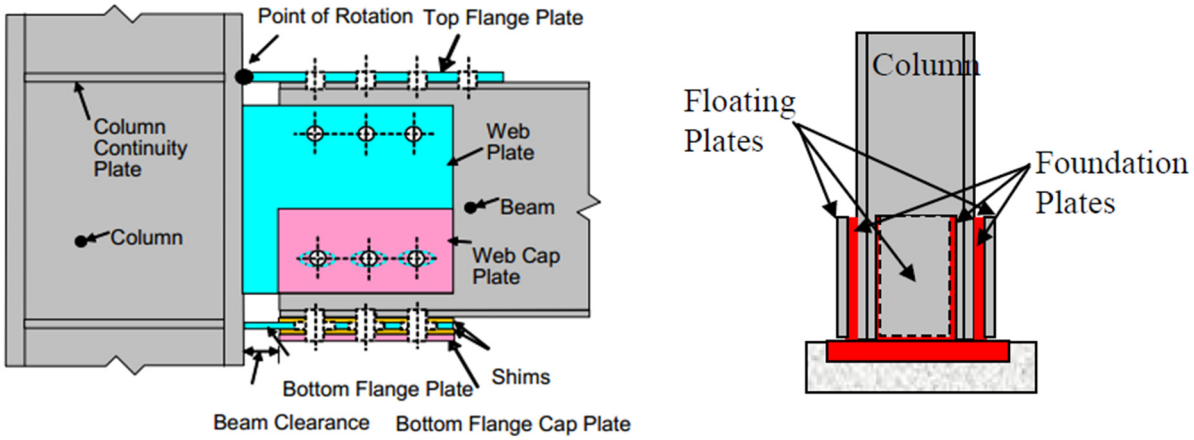

Figure 2-4: Flexural AFC Connections. Left is sliding hinge joint (MacRae et al., 2010). Right is the base with SHJ (MacRae et al., 2009)

Two categories of column base AFC are: (1) the weak axis aligned asymmetric friction connection (WAFC), where friction surfaces are parallel to the web on plates outstanding from the column flange, as shown in Figure 2-5, and (2) the strong axis aligned asymmetric friction connection (SAFC), where the friction surfaces are parallel to the flanges as shown in Figure 2-5. Boundary plates pry apart as the column base rotates providing moment resistance in addition to that obtained from the sliding friction and axial force effects, when the column bends about its strong axis for the SAFC, and the weak axis of the WAFC. In contrast, the prying of the boundary plates does not affect the base moment resistance when the column bends about the weak axis of SAFC and the strong axis of WAFC. The base plate of the WAFC is larger than SAFC base due to the orientation of AFCs in the WAFC.

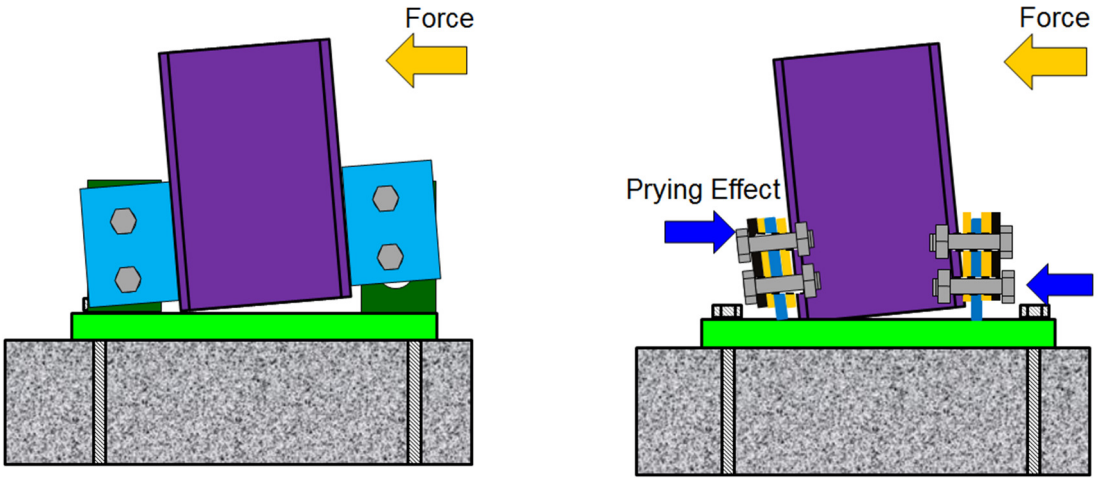

Figure 2-5: Column Base Connections using AFC, the weak axis aligned asymmetric friction connection (WAFC) on left, and the strong axis aligned asymmetric friction connection (SAFC) on right

Both AFC base connections in Figure 2-5 have the following characteristics that make them candidates for low damage base connections:

i) The column and the base plate are in full contact, but without direct welding.

ii) Nonlinear deformation is mainly in the AFC rather than in the base plate or column.

iii) Untightening AFC bolts allows post-earthquake residual displacement to be removed.

iv) Damage is limited to the bolts and shims that can be replaced after an earthquake.

v) Prying can occur on both types depending on the direction of loading.

vi) One of the main advantages of this type of connection is decoupling of the strength and deformation capacity. The strength comes from number and size of the bolts, friction coefficient between sliding surfaces, but the deformation capacity is related to size of clearances and holes.

2.2.4. Comparison

Table 2-1 summarizes the mentioned pros and cons for the possible low damage base connections.

Table 2-1: Pros and Cons of Possible Low Damage Base Connections

Base Connection	**Pros**	**Cons**
PT bars	Additional energy dissipators can be added to this base connection	Failure of cable and anchorage are serious hazards
		It is difficult to prestress steel cables or rods
		Sequence of steps for rod tightening must be implemented that add time and cost to construction.
	Small amount of damage due to the rocking behavior	Special detailing is required at the beam to column joint to pass rods.
		Replacing of the fractured bar is difficult if it happens under the base plate
Yielding Elements	Yielding angle is replaceable	Yielded base plate causes residual displacement of the column
	No residual deformation remains in the base with yielding angle after replacement	Replacing of fractured anchor rod and base plate is difficult in the case with yielding rod and base plate respectively.
Friction Connection	Nonlinear deformation is mainly in the AFC rather than in the base plate or column.	Construction is more difficult compare to the other base connections
	Untightening AFC bolts allows post-earthquake residual displacement to be removed.	
	Damage is limited to the bolts and shims that can be replaced after an earthquake.	
	Decoupling of the strength and deformation capacity.	

2.3. Subjective Quantitative Assessment (SQA) of Base Connections

SQA is a decision making tool used in many fields of engineering to assess design alternatives (Dieter and Schmidt, 2012). This method is simple, and does not require advanced mathematics or optimisation. SQA involves rating different characteristics in terms of what may be better according to a subjective scale. In this method, the effective parameters of the topic are identified, and then points are assigned for each parameter. These numbers can be combined to obtain an overall assessment, as is commonly conducted in many areas.

In this section, SQA is applied to the mentioned candidates of low damage base connections in Section 2.2, as well as the traditional exposed base plate connection, to asses them in terms of low damage concept, cost, and constructability. The main parameters for the evaluation are replaceability, permanent deformation, damage to the column, cost, and difficulty of construction. Note that replaceability includes the cost and ease of repair. Table 2-2 shows parameters selected and their weight on total estimation of the bases.

Table 2-2: Qualitative parameters for evaluation of base connections

Parameters	Range	Min	Max
Replaceability	[0-3]	0:hard to be replaced	3: easy to be replaced
Permanent deformation	[0-3]	0: high permanent deformation	3: low permanent deformation
Damage to column	[0-2]	0: high damage	2: low damage
Cost	[0-1]	0: expensive	1: cheap
Difficulty of construction	[0-1]	0: hard installation	1: easy installation
Total*	[0-10]	0:unsuitable	10: very suitable

Since these factors are mainly evaluated from low damage perspective, the majority of the total values (80%) belongs to the replaceability of the deformed elements, permanent deformation after loading, and the possibility of damage to the column. In addition, construction and installation cost of the base plates are a small part of total construction cost for the whole of the building. Therefore, the effect of cost on evaluation of different details of base plate was selected to be 2 out of 10. For example, for an interior column of a 10 storey building, only one base connection is required compared to about 40 beam to column joints. In addition, the cost of this long column and the attached beams is much larger than a much smaller base connection.

The exposed base plate connection and the base with yielding base plate have lower SQA scores, as shown in the reality SQA score summary in Table 2-3. The main factors behind this result are the permanent deformation in the base plate and the column. In addition, these deformed elements cannot be replaced since it adds considerable cost. However, their construction is easy and low cost. Because of difficulties in prestressing the rods, as well as the problems associated with long rods, the cost and construction SQA scores of the base with post tensioned rods are also low valued. In addition, if the rod fractures below the base plate, which is the most probable location, then replacing the fractured bar is not simple. Hence, low a SQA value results for the replaceability of the base with post tensioned rods, and the base with yielding anchor rods. The base with AFC and angle are the best candidates from a low damage, cost, and constructability standpoint according to SQA, as seen in Table 2-3.

Table 2-3: SQA results summary

Parameters \ Detail		Exposed base plate	Base with post-tensioned rods	Base with yielding			Base with AFC
				Base plate	Anchor rod	Angle	
Replaceability	[0-3]	0	1	0	1	3	3
Permanent deformation	[0-3]	1	3	0	3	3	3
Damage to column	[0-2]	0	1	1	2	2	2
Cost	[0-1]	1	0	1	1	1	1
Difficulty of construction	[0-1]	1	0	1	1	1	1
Total score*	[0-10]	3	5	3	8	10	10

*0 means unsuitable and 10 means very suitable

2.4. Experimental Program

2.4.1. Test Setup

Figure 2-6 shows the overall experimental setup for the selected concepts. Actuator A pushes in the west-east direction causing bending about the column strong axis. Actuators B and C push in the north-south direction causing weak axis bending. They also prevent twist during strong axis deformation alone, where they are programmed to prevent any out-of-plane movement. Three potentiometers positioned parallel to each actuator are used to monitor and control displacement. A hydraulic jack with a ball bearing joint, was placed on top of the column to allow for the application of an axial force of 320 *kN,* equal to 20% of the gross column section axial capacity ($0.2\phi AF_y$). Axial force was kept constant through the lateral deformations imposed. It was measured by two load cells on top of a SHS section cross-beam above the jack at the top of the column.

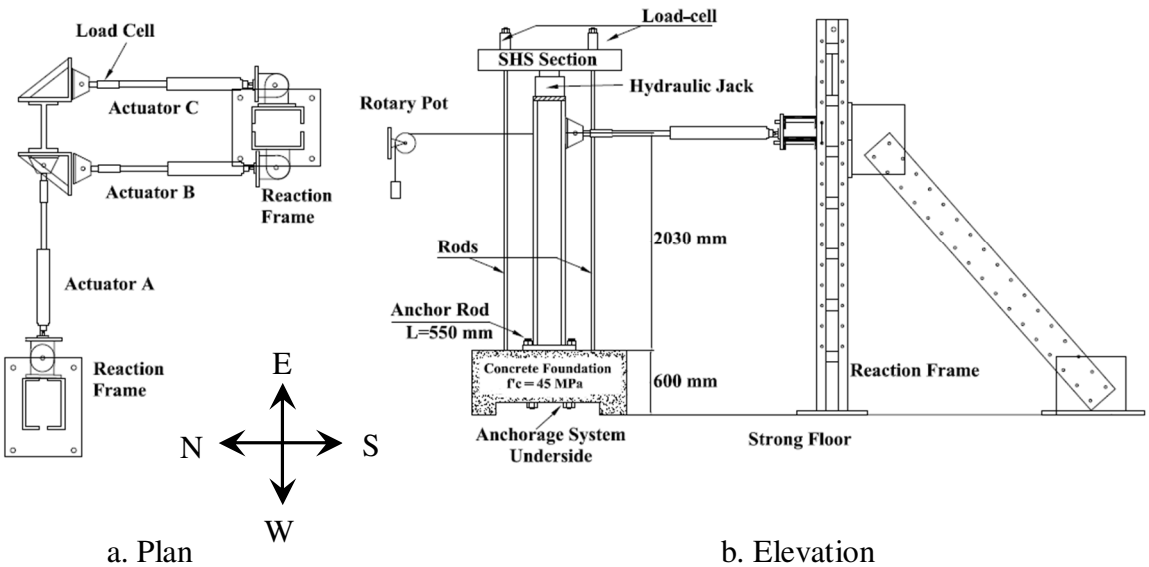

a. Plan

b. Elevation

c. Experimental test set-up

Figure 2-6: Test set-up , where (a) shows plan of the experimental test set-up; (b) shows the elevation of the test set-up ; and (c) shows a picture from top side of the test set-up

2.4.2. Loading Regime

Cyclic loading according to ACI Report T1.1-01 (2001) was applied to each specimen. Initial loading started from 0.2% drift, which is a 4 mm top displacement, and finished at 4% drift, corresponding to a displacement of 80 mm. The increase in each new drift is 1.25 to 1.5

times that of the previous step. For uni-directional loading for each level of drift, three full cycles were applied, as shown in Figure 2-7. At the end of each drift increment, a full cycle with half of the drift amplitude is included. Since buildings typically move in two-directions under earthquake excitation, bi-directional displacements were also applied. A clover pattern is defined: x = a sin(2θ)cos(θ) and y = a sin(2θ)sin(θ), where x and y are the displacement of the actuator in x and y directions respectively, a is displacement amplitude that is constant for each level of drift, and θ is the angle between the load path and X axis that is changed from zero to 2π for each level of drift as shown in Figure 2-7. At each drift increment, one cycle is applied in the X direction, then one full cycle in the Y direction, and then the clover bi-directional pattern.

The clover leaf pattern could be a representative of the demand on a column base under an earthquake. The pattern applies the loading in the following directions: (+X,+Y), (+X,-Y), (-X,+Y), (-X,-Y). The Cloverleaf pattern is pretty common and widely accepted loading protocol as it was used before in several experimental by Solberg et al. (2009), Muir (2014), Mashal (2015).

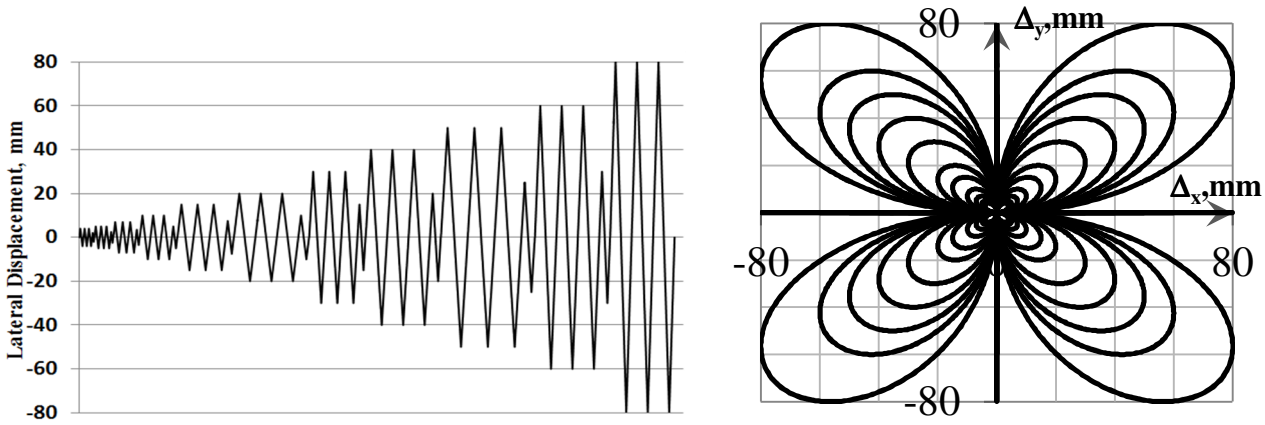

Uni-directional loading Bi-directional loading

Figure 2-7: Test loading regime for (left) uni-directional loading, and (right) bi-directional loading

2.5. Summary

In this chapter the candidates for low damage base connections are introduced and the advantages and disadvantages were described. A subjective quantitative assessment (SQA) rubric was used to compare these base connections based on low damage, cost, and construction. The main results show:

i) The base with post-tensioned rods, yielding base plate, yielding anchor rods, yielding angle, and AFC have potential to perform as a low damage base connections.

ii) It was conclude from the SQA and the mentioned drawbacks for these connections that the base connections with yielding angles and AFC have higher potential for further experimental tests that are described in future chapters.

The plan and details of test set-up were proposed that can apply axial force and bi-directional loading. In addition, the proposed cyclic loading regimes for uni-directional and bi-directional loading for use in later chapters were presented.

Chapter 3: Experimental Studies on Cyclic Performance of Exposed Base Plate Connection

3.1. Introduction

Exposed base plate connections are widely used in mid- and low rise steel buildings. The column is directly welded to the base plate and the base plate is connected to the concrete foundation by anchor rods. Grout is placed between the steel base plate and the concrete foundation. The base components are shown in Figure 3-1.

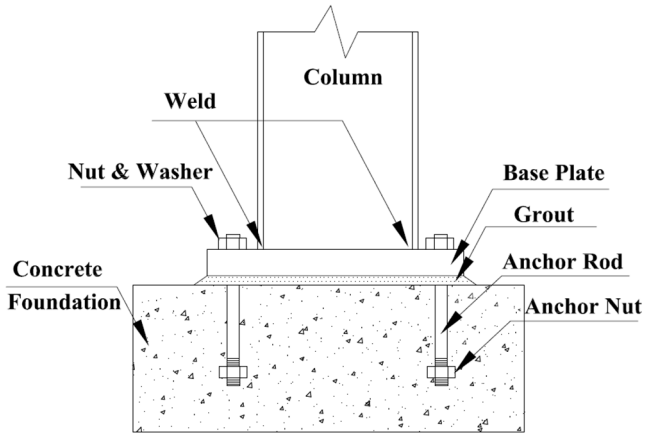

Figure 3-1: Typical exposed base plate connection components

In most analytical studies, the base of the structure with this type of connection is modelled as fully fixed or fully pinned. The choice of base flexibility assumption can significantly change the demands on the structure, as described by Aviram et al. (2010), Borzouie et al. (2013), Zareian and Kanvinde (2013), and Ruiz-Garcia and Kanvinde (2013). All actual structures have a base rotational stiffness, k_θ, defined as the base moment, M, divided by the base rotation, θ, between these two extremes. However, Eurocode 3 (2005) defines base connections into categories depending on k_θ, as shown in Figure 3-2. Here, k_θ is normalized

by *EI/H*, where *EI* is the flexural stiffness of the column section and *H* is the storey height of the column independent of rotational fixity of the top of the column. Column bases with a rotational stiffness, k_θ, of 30*EI/H* or more are expected to not change the column ultimate strength by more than 5% or column lateral displacement under service load by more than 10% from the fixed base case according to Jaspart et al. (2008). In this case, the connection is defined as fully rigid. Base connection stiffnesses lower than *0.5(EI/H)* are considered to capture the fully pinned condition. For rotational stiffness between these two boundaries, connections are categorized as semi-rigid, and the rotational stiffness should be explicitly considered in design. While cast in concrete columns are likely to have "rigid" connections and those with a perfect pin are likely to be in the "pinned" category, for realistic base plate connections that can experience bidirectional loading, it is not always clear what k_θ should be used.

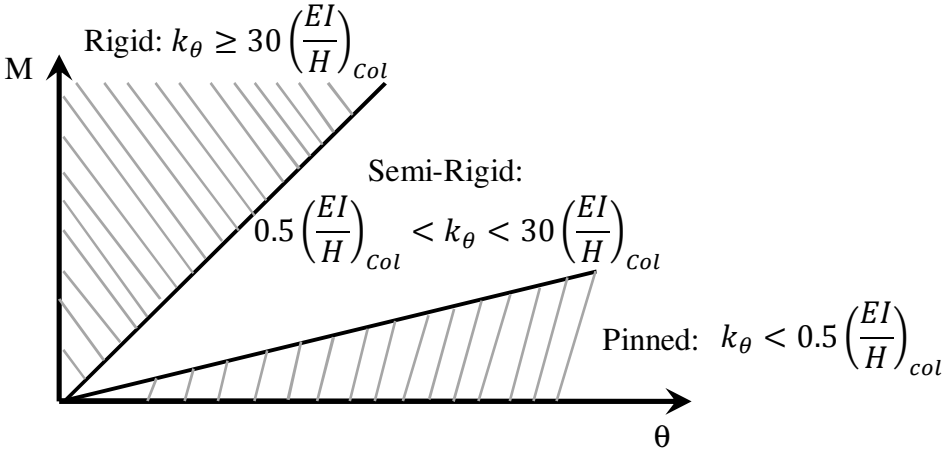

Figure 3-2: Eurocode 3 (2005) Column Base Rotational Stiffness Boundaries

Exposed base plate connection failures in the Northridge (1994), Kobe (1995), and Tohuku (2011) earthquakes were reported by Tremblay (1995), and Midorikawa et al. (2012). The dominant reported failures were brittle base plate fracture, excessive anchor bolt elongation, and anchor rod failure. Moreover, previous conducted experimental studies on the exposed

base plate connections (e.g. Dewolf, 1978; Dewolf and Sarisley, 1980; Akiyama, 1984; Hon and Melchers, 1988, Astaneh et al., 1992; Akiyama et al., 1998; Jaspart and Vandegans, 1998; Burda and Itani; Fahmy et al., 1999; Adany et al., 2000; Miyasaka et al., 2001; Somiya et al., 2002) showed that although for low levels of drift these connections remain elastic, for greater levels of deformation some inelastic behaviour and failures are expected at the column base. Gomez (2010) summarized reported failures of base connections in the previous tests that are rod steel failure in tension, compression and shear, rod fatigue, rod nut stripping, washer bearing failure, washer failure in shear, base plate bending from bearing stress, and anchor rod forces, base plate fracture, column to base plate weld failure, column failure, shear key steel failure, base plate bending due to shear key, shear key weld failure.

Numerous analytical studies (e.g. Salmon et al., 1957, Voce, 1958) and experimental studies (e.g. Dewolf, 1978, Murray, 1983) form the basis for design recommendation to prevent connection failure. However, most of these studies considered only uni-directional behaviour.

It may be seen from the discussion above that methods are needed to quantify the stiffness of base plate connections for design, also to ensure that premature failure does not occur under the possible earthquake demands to which the connection may be subjected. Studying the cyclic performance of the exposed base plate connection under bi-directional bending is also provide useful information for understanding the behaviour of this connection. To address some of these needs answers are sought to the following questions:

(i) Can we confirm the behaviour of exposed base plate connections as reported in past research and how does bi-directional loading affect the exposed base plate performance?

(ii) What is the stiffness, strength, and failure modes of some typical exposed base plate connections:

a. Exposed base plate with yielding anchor rods without axial load under strong axis bending.
b. Exposed base plate with elastic anchor rods without axial load under strong axis bending.
c. Exposed base plate with elastic anchor rods with axial load under strong axis bending.
d. Exposed base plate with elastic anchor rods under bidirectional bending and axial load.

(iii) Should typical base plate connections be characterized as pinned, semi-rigid or rigid?

(iv) How much does bidirectional loading increase anchor rod forces?

3.2. Methodology

3.2.1. Design and Detailing of Exposed Base Plate Specimens

The fundamental tests used in this chapter are described in in Table 3-1. The test column section was a Grade 300, 310UB46.2 section (σ_y=320 MPa from tensile test), and the distance from top of the base plate to the column point of contraflexure was 2 m. All of the column drift values are based on this height. A UB section was used because they are the most common in drift-governed applications, and ductile moment resisting frame are typically drift governed.

The base plate was placed on a 5mm layer of dental plaster to provide full contact. The base plate was attached to the concrete by 4 M24 Grade 8.8 or 10.9 snug-tightened un-bonded rods

anchored at the bottom of the concrete foundation block. The exposed base plate connections were designed according to AISC's Design Guide 1 Fisher and Kloiber (2006), as shown in Figure 3-3, where 50% of the flexural yielding moment of the column (197 kN.m) section was considered as the design moment of the base plate to observe the effect of base plate yielding in total performance of the base connection. Two different types of anchor rods, Grade 8.8 and Grade 10.9, were used for connecting the base plate to the foundation. The computed base moment for column yielding when the column extreme fibres first begin to yield (197 kN.m) and for anchor rod tension yielding (193 kN.m) was approximately equal for the base plate with 4M24 Grade 8.8 rods. However, for the base plate with Grade 10.9 bolts, the computed base moment causing yielding of anchor rods (269 kN.m) was 1.36 of the column yielding moment (197 kN.m) and 1.11 of the nominal section moment capacity (219 kN.m). All anchor rods were unbounded with an effective length of 550 mm, they passed through steel tubes placed in the concrete foundation and were anchored at the bottom of the foundation.

Table 3-1: Conducted tests properties

Test No	Specimen	Axis of Bending	Axial force	Anchor Rod Grade
1	A	Strong	Zero	8.8
2	A	Strong	Zero	10.9
3	B	Strong	320kN ($0.20N_s$)	10.9
4	C	Bi-directional	320kN ($0.20N_s$)	10.9

The column to base plate connection consisted of partial joint penetration (PJP) welding together with fillet welding. For the partial joint penetration welding, the bevel groove weld was carried out from the outside flange face up to 85% of the flange thickness (10mm), as shown in Figure 3-3. In addition, 12 mm fillet welding was used on the inside face of the flanges and the web. This combination of PJP and fillet welding provides a total throat

thickness 80% larger than the flange's thickness.

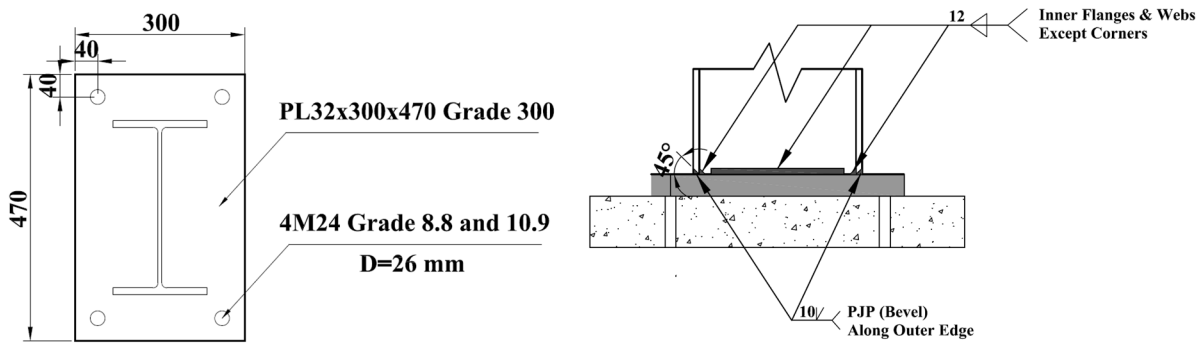

a. Detail of the base plate connection b. Column to base plate weld detail

Figure 3-3: Base plate detailing, detail of base plate connection on left, and column to base plate weld detail on right

This detail was selected based on the design practice survey for steel moment resisting frame in the US (Myers et al., 2009, Gomez et al., 2010). This survey states that this detail is effective for high seismic performance based on experimental tests with different types of welding between the column and baseplate. This detail is different with full penetration welds, allowing easier alignment of the column to the base plate.

3.2.2. Test Setup and Loading Regime

The loading regime and test setup are as described in Chapter 2.

3.2.3. Instrumentation of the base Connection

Foundation rods passing through 125mm long 30mm diameter 600 kN load cells recorded anchor rod tension, while holding down the baseplate. Nine linear potentiometers with 25 mm stroke were placed on top of the base plate to monitor the base plate deformation.

Three potentiometers monitored the sliding of the base plate in both directions. Seven potentiometers were attached around the concrete foundation to monitor if there was any sliding or uplift between the foundation and the laboratory strong floor. Some of these sensors are visible in Figure 3-4. Strain gauges, with 6mm gauge length, were placed on the column flange, and column base plate to measure localised strains.

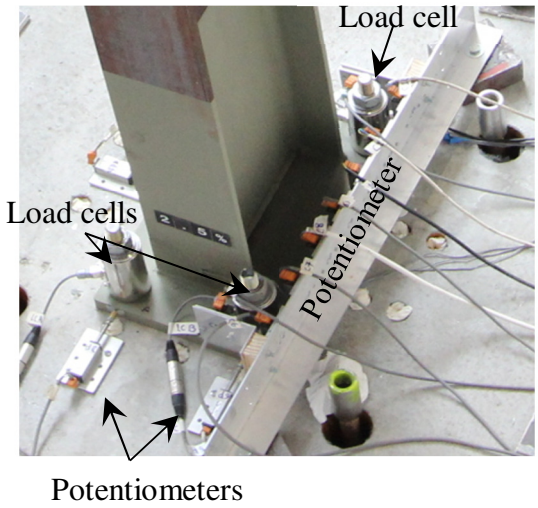

Figure 3-4: Instrumentation of the exposed base plate connection with sensors

3.2.4. Test Specimen and Run

The four cyclic tests conducted are shown in Table 3-1. Since the main deformation in the first test occurred in the anchor rod, specimen A was reused for Test No. 2 and the anchor rods were changed to Grade 10.9 rods. In addition, since the base plate and welding between the base plate and the column of specimen A experienced cyclic loading up to 4% drift during Test No.1, only 4% cycles were applied in Test No. 2. For Test No. 1 and No. 2, the sliding of the base plate was restricted by placing shear keys around the base plate that were connected to the foundation since no axial force was applied to provide shear resistance. These shear keys did not contribute to moment resistance.

3.2.5. Interpretation of Test Data

The column base moment, M_{Base}, and column base rotation, θ_{Base}, were computed from the column lateral force, V, and lateral displacement, Δ_{top}, according to:

$$M_{Base} = V \times H_{col} \tag{3-1}$$

$$\theta_{Base} = (\Delta_{top} - \frac{V \times {H_{col}}^3}{3 \times E_{col} \times I_{col}}) \times \frac{1}{H_{col}} \tag{3-2}$$

Here, V is the lateral force at column top, H_{col} is height of the column from the base plate to the point of contraflexure, Δ_{top} is top displacement of the column, E_{col} is the elastic modulus of the column, I_{col} is the second moment inertia of the column in the direction of testing. The shear deformation was ignored as it is small in long member. Also, p-delta effects were ignored as the axial force applied by the rods was inclined at the peak displacement making this effect small. The lateral drift is calculated by dividing top displacement of the column by the height of the column from base plate up to the point of contraflexure.

For each test, a base moment-rotation hysteresis curve, and a multi-linear idealized moment-rotation curve showing moment-rotation at different limit states were plotted. The failure modes are also presented in a drawing for each base connection. Yielding of the base plate and the column was recognized from paint flaking and from strain gauge measurements. Yielding of the anchor rod was obtained from the load cells and from column rotation at zero moment.

The secant stiffness is calculated at the first yielding of the column. It is presented in two

ways: (i) the actual value (kN.m /rad); and (ii) normalized to *EI/H*, where *H=2.0 m* is the height of the column from base plate up to the point of contraflexure. This definition is different from that in Eurocode (2005) that *H* is the storey height. Plastic rotation of the base plate in the strong axis deformation at the end of the test was calculated by dividing the deformation of the base plate recorded by potentiometers at flange tips, over their horizontal offset distance of 300mm. The plastic deformation of the column top at the end of the test was obtained from the residual displacement after unloading from 4% drift. Plastic residual rotation of the column was computed as the column top plastic deformation minus the plastic rotation of the base plate. Plastic anchor rod elongation can be obtained by recording the nut rotation of the anchor rod, which was tightened by the snug tightening method at the end of the test.

3.3. Results and Discussion

3.3.1. Test Results Summary

The summary of the experimental test measurements are presented in Table 3-2. The measurements are the average of the maximum moments of the base connection at ±4% drift, M_{Max}; the secant rotational stiffness of the base connection, K_θ; the residual force at top of the column at zero displacement, after the cycles to 4% drift at the end of the test, $P_{\Delta=0}$; plastic rotation of the column at zero displacement the end of the test, $\theta_{P\text{-}Col}$; the plastic rotation of the base plate at zero displacement at the end of the test, $\theta_{P\text{-}BP}$; the permanent anchor rod elongation at zero displacement at the end of the test, $\Delta_{P\text{-}rod}$; the permanent plastic deformation of the column top at zero force after the cycles to 4%, $\Delta_{P\text{-}col}$; and the tension

force of the anchor rod at 4% drift T_{Rod}.

Table 3-2: Experimental tests outputs for Tests No. 1 to 4

Test No		M_{Max} kN	K_θ kN.m/rad	EI/H	$P_{\Delta=0}$ kN	$\theta_{P\text{-}Col}$ $\times 10^{-3}$ rad	$\theta_{P\text{-}BP}$ $\times 10^{-3}$ rad	$\Delta_{P\text{-}rod}$ mm	$\Delta_{P\text{-}col}$ mm	T_{Rod} kN
1		224	14736	1.47	0	3.7	1.1	3.8	9.6	292
2		251	14736	1.47	35	9.37	5.63	0.3	30	318
3		255	23254	2.33	67	11.4	3.57	0	30	279
4	X Dir	240	38181	3.82	70	18	3.63	0	44	253
	Y Dir	45	14569	16.2	15	28.8	0	0	57.5	

3.3.2. Test No. 1 –Strong Axis Bending without Axial Force of Base Plate with Grade 8.8 Anchor Rods

Figure 3-5 shows maximum strong axis moment for the column base with 4M24 Grade 8.8 rods reaches 224 kN.m, which is 96% of the nominal column section moment capacity, M_{sx} (233 kN.m). At overall drift of 0.1% drift, the base plate on the tension side separated from the concrete foundation. The base plate on the tension side started to yield at 0.85% drift corresponding to 6×10^{-3} rad of base connection. The column and the anchor rods both yielded at 2.5% drift (0.018 rad) that can be identified as points 3 and 4 in Figure 3-5. The base rotational stiffness was also reduced to 15% of the original secant rotational stiffness.

The performance of the base connection was affected by elongation of the anchor rod after this level. The recorded tension force (292.5 kN) in the anchor rods at 4% drift (0.032 rad) was close to the specified maximum tensile strength of the rods (292 kN). Therefore, further deformation would likely have resulted in fracture. However, no fracture of anchor rods occurred. The hysteretic curve of this base connection after anchor rod yielding is similar to that of a pair of tension braces, because, after anchor-rod elongation due to yielding on a

previous cycle, the connection has no moment resistance up to the point that the base plate contacts the nut on the tension side.

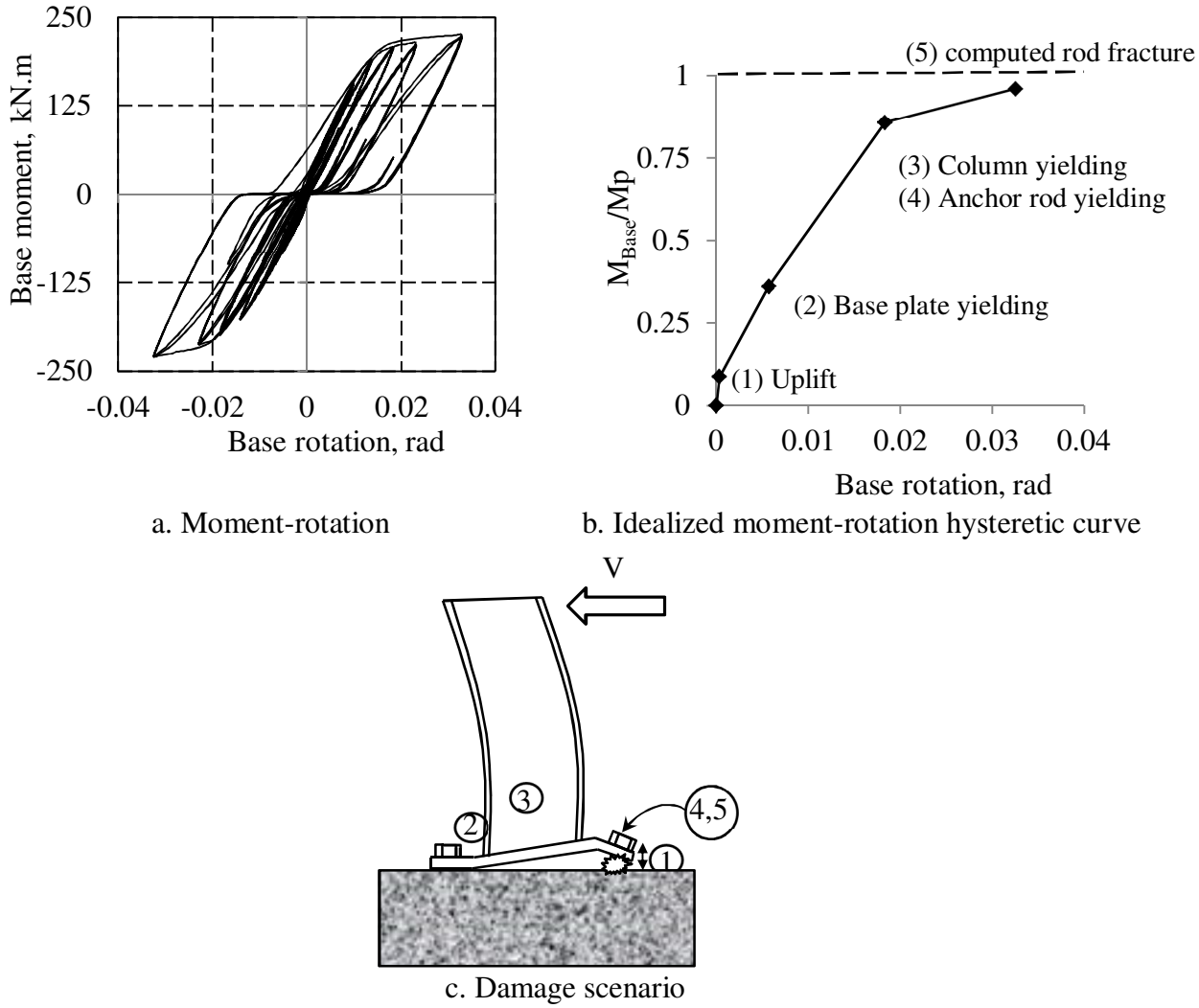

a. Moment-rotation

b. Idealized moment-rotation hysteretic curve

c. Damage scenario

Figure 3-5: Moment-rotation and damage scenario for Test No. 1 , Figure a is the base moment against base rotation, Figure b is the idealized base moment- base rotation hysteretic curve, and Figure C is the order of damage scenario as labelled in Figure b.

The possibility of anchor rod fracture causing projectile motion of the rod end and a sudden strength decrease is the main disadvantage of this base connection design. Japanese design procedures (Grauvilardell et al., 2005) proposed criteria to mitigate this failure by forcing the use of ductile anchor bolts, unless the base plate connection is designed for two times the

anticipated demands on the base. A yield ratio is defined as the yield strength of the rod shank divided by the tensile strength due to fracture in the threaded region. In the ductile anchor rod, this ratio is required to be less than 0.75 to encourage yield to be spread out over the rod length. Therefore, the yield strength of the unthreaded part should be less than the strength at fracture of the threaded section.

The yield ratio is equal to 0.8 for standard Grade 8.8 bolts, so they cannot be considered as a ductile anchor bolts. However, for Grade 4.6 bolts, this ratio 0.6, which satisfies this criteria, but has lower strength. According to Table 3-2, the level of base plate plastic rotation was small and caused only 2.2 mm (0.0011 rad) of column top displacement. The main source of deformation was the anchor rods that were permanently elongated by 3.8 mm.

The maximum difference between calculated tension force in the anchor rods according to AISC's Design Guide 1 (Fisher and Kloiber, 2006) computed before the test and the recorded values is 6%. This result is shown in Figure 3-6, and indicates that the uniform bearing stress assumption is reasonably accurate. Hence, the proposed AISC design method can predict the tension force of anchor rods with the reasonable accuracy.

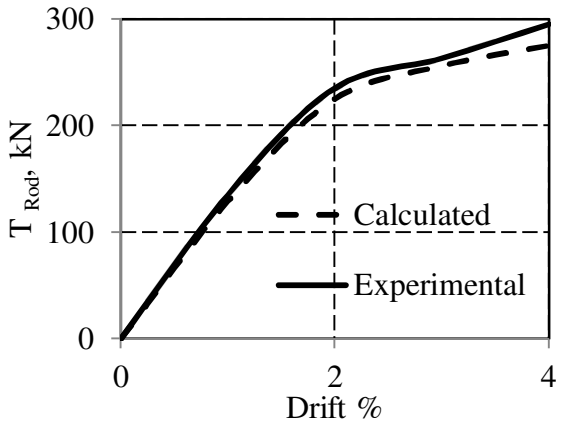

Figure 3-6: Calculated and recorded tension force in the anchor rod

3.3.3. Test No. 2 –Strong Axis Bending without Axial Force of Base Plate with Grade 10.9 Anchor Rods

In this test, the anchor rods were replaced by M24 Grade 10.9 rods, and only 4% cycles were applied on the same specimen used for Test No. 1. Changing the anchor rods from Grade 8.8 (Test No. 1) to Grade 10.9 (Test No.2) shifted the anchor bolt yielding from 2.5% drift (0.018 rad base rotation) to 3.9% (0.03 rad base rotation), and the maximum moment was increased by 12%, as shown in Figure 3-7. Therefore, the main plastic deformation occurred in the base plate that yielded at 0.85% drift (0.0057 rad base rotation), and column that yielded from 2.5% drift (0.018 rad base rotation), as can be identified by points 2 and 3 in Figure 3-7. Table 3-2 states that the contributions of $\theta_{P\text{-}col}$, and $\theta_{P\text{-}BP}$ to $\Delta_{P\text{-}col}$ are approximately similar. In addition, $\theta_{P\text{-}col}$ and $\theta_{P\text{-}BP}$ were up to 2 and 5 time that of the first test, respectively. This high bending of the column and the base plate caused the fracture of column base welds at 4% drift (Point 5 in Figure 3-7). Initial weld cracking occurred on the corner of the flange on the tension side, which appeared at the first cycle of 4% drift as shown in Figure 3-8. In the second cycle this crack extended, reducing the base moment by 5%, and finally, full weld fracture occurred in the third cycle reducing the base moment by 22% compared to the second cycle, as shown in Figure 3-7. As the welding was undertaken by a certified welder, and procedural defects present in this testing could equally also be present in field applications of this design approach.

According to Table 3-2, increasing the strength of the anchor rods did not have an effect on rotational stiffness, since the base plate yielded before any other elements. However, residual displacement of the column at zero applied force, $\Delta_{P\text{-}col}$, rotation of column, $\theta_{P\text{-}Col}$, and the base plate, $\theta_{P\text{-}BP}$, were increased by factors of 3, 2.5, and 5, respectively. The main mode of failure was changed from yielding and fracture of anchor rod to fracture of the weld between

the column and base plate.

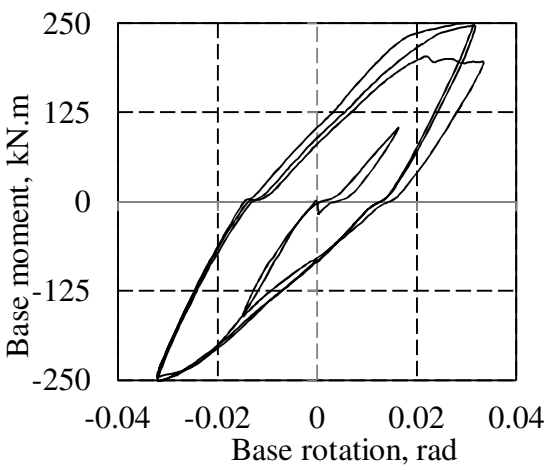

a. Moment-rotation

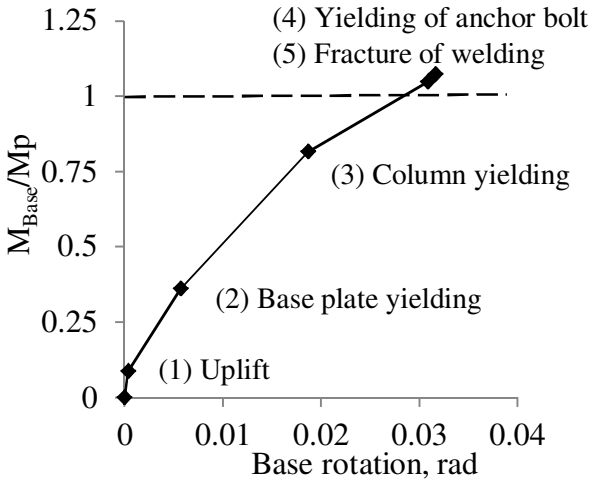

b. Idealized moment-rotation hysteretic curve

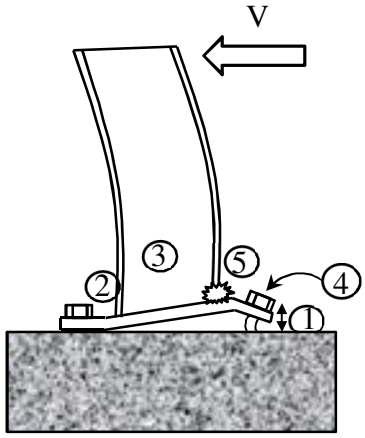

c. Damage scenario

Figure 3-7: Moment-Rotation and Damage Scenario for Test No. 2 , Figure a is the base moment against base rotation, Figure b is the idealized base moment- base rotation hysteretic curve, and Figure C is the order of damage scenario as labelled in Figure b.

a. First cycle

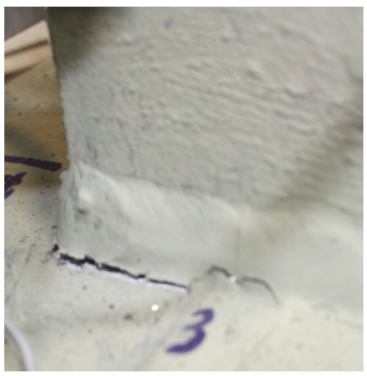

b. Second cycle

c. Third cycle

Figure 3-8: Fracture of welding in Test No.2 for cycles of 4% drift

3.3.4. Test No. 3 –Strong Axis Bending with Axial Force of Base Plate with Grade 10.9 Anchor Rods

The base moment at 4% drift was similar to that of Test No. 2, and 8% more than M_{sx}, as shown in Figure 3-9. The base plate started to uplift on the tension side at 0.25% drift (0.0008 rad base rotation). The axial force that caused the start of column yielding was reduced from 2.5% drift (0.018 rad base rotation) in Test No. 2 to 1% drift (0.0056 rad base rotation), as observed by column paint flaking. The base moment was 0.56 M_{sx} when the column started to yield. The base plate yielded at 1.25% drift (0.007 rad base rotation), as shown as point 3 in Figure 3-9. The flanges started to buckle at 3.5% drift (0.0266 rad base rotation), with the base moment of 1.08 M_{sx} (point 5 in Figure 3-9). As the lateral drift was increased the column web also buckled. After one full cycle of 4% drift (0.0315 rad base rotation) the test was stopped due to the possibility of instability due to column buckling. No crack was observed in the welding of the column to the base plate. The maximum anchor rod tension force was 275 kN, which is 83% of the ultimate tension capacity of the rods, and they remained elastic. The plastic rotation of the column, $\theta_{P\text{-}Col}$, was 3.2 times the plastic deformation of the base plate, which shows that the column hinging was the main contributor to the column performance. Residual displacement of the column, $\Delta_{P\text{-}col}$, was 30 mm, which is equal to 37% of the peak deformation. According to Table 3-2, the axial force increased the rotational stiffness of the base plate connection by 1.6 times, as well as the residual displacement, $\Delta_{P\text{-}col}$, of the column top, plastic rotation of the column, $\theta_{P\text{-}Col}$, and residual force at zero displacement, $P_{\Delta=0}$. In contrast, plastic rotation of the base plate, $\theta_{P\text{-}BP}$, and tension force in the anchor rods, T_{Rod}, were reduced. In addition, the main source of damage changed from fracture of the welding to the flange and web buckling of the column section. Therefore, the

type of damage was shifted from tensile to compressive type by the presence of comprehensive axial force, as anticipated by the AISC design method.

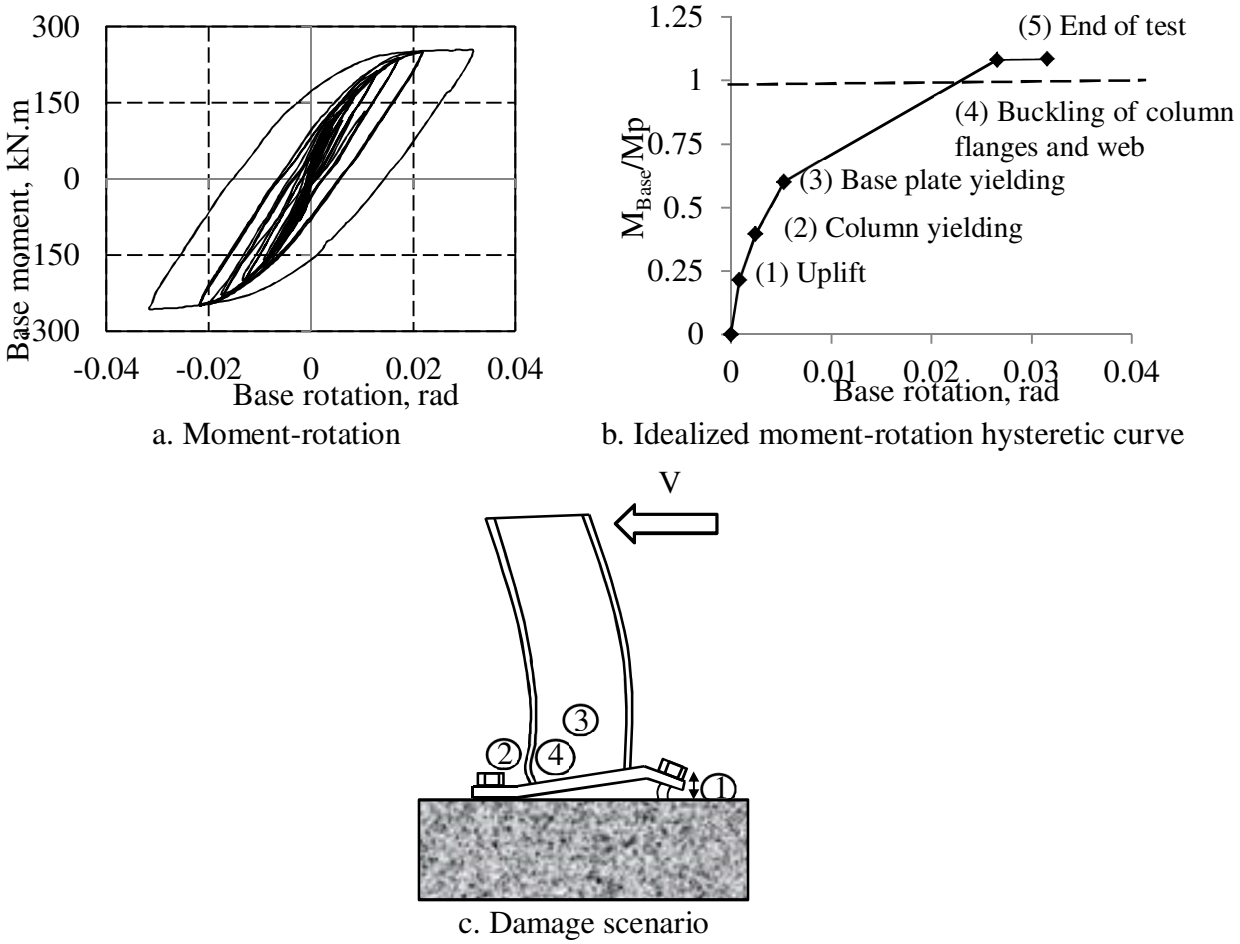

a. Moment-rotation

b. Idealized moment-rotation hysteretic curve

c. Damage scenario

Figure 3-9: Moment-Rotation and Damage Scenario for Test No. 3 , Figure a is the base moment against base rotation, Figure b is the idealized base moment- base rotation hysteretic curve, and Figure C is the order of damage scenario as labelled in Figure b.

3.3.5. Test No. 4 –Bi-directional Bending with Axial Force of Base Plate with Grade 10.9 Anchor Rods

The maximum moment about strong axis was 240 kN.m which is 1.03M_{sx}, and maximum moment about the weak axis was 45 kN.m, which is 0.86 times of the nominal section moment capacity about the weak axis, M_{sy} (52 kN.m), as shown in Figure 3-10. The column,

and the base plate yielded at 0.5% drift (0.0022 rad base rotation about the X direction and 0.0007 rad base rotation about the Y direction), as observed from paint flaking shown as points 2 and 3 in Figure 3-10. The corresponding moment for yielding about the strong axis was 83.5 kN.m ($0.36M_{sx}$), and about the weak axis was 11.4 kN.m ($0.22M_{sy}$). The column flanges then buckled at 2% drift (0.017 rad base rotation about the X direction and 0.01 rad base rotation about the Y direction), and the corresponding moments about the strong and weak axes were $1.03M_{sx}$, and $0.77M_{sx}$, respectively. Increasing the lateral deformation reduced the base resisting moment and buckling occurred in the column web, as shown in Figure 3-11. The base moments about the strong and weak axes were reduced by 17.5%, and 35%, respectively, in the third cycle of 4% drift compared to the point where flange buckling started. Plastic rotation of the base plate, $\theta_{P\text{-}BP}$, at the end of the test was 16% of the total plastic base rotation.

Applying bi-directional loading with axial force caused permanent deformation of the column at the end of the test, which was 2.4 times that of the tests with the column bending about the strong axis with applied axial force, as shown in Table 3-2. Plastic rotation of the column, $\theta_{P\text{-}Col}$, was 9.3 times the plastic rotation of the base plate, $\theta_{P\text{-}BP}$, which shows the main hinge was formed in the column, and the plastic rotation of the base plate, $\theta_{P\text{-}BP}$, was less than 2% different for the test with unidirectional bending with axial force. The secant rotation stiffness of the base plate about the strong axis, $K_{\theta x}$, in Test No.4 was increased 1.63 times compared to Test No. 3 since the column yielded at the same force, but lower rotation. Although rotational stiffness about the strong axis, $K_{\theta x}$, was 2.6 times of the rotational stiffness about the weak axis, $K_{\theta y}$, when K_{θ} is normalized to EI/H, $K_{\theta y}$ was 4.2 times $K_{\theta x}$. This outcome indicates that the column base plate that underwent bi-directional bending acted more rigidly

about the weak axis and as a semi-rigid base about the strong axis.

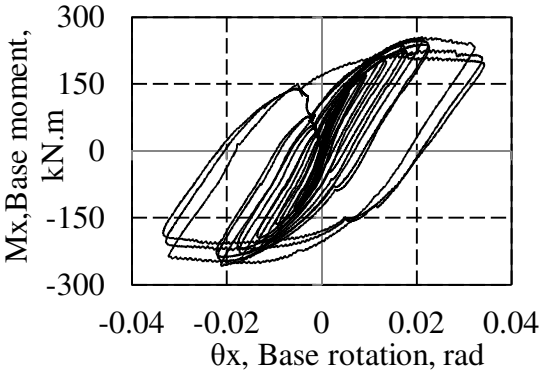

a. Moment-rotation about strong axis

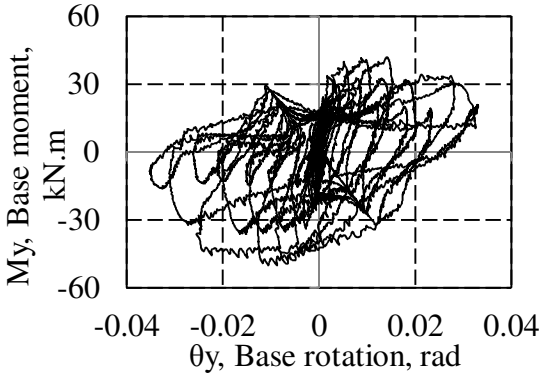

b. Idealized moment-rotation hysteretic curve

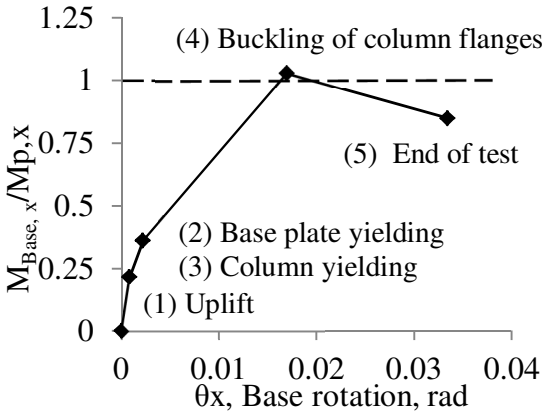

c. Idealized moment-rotation hysteretic curve for strong axis bending

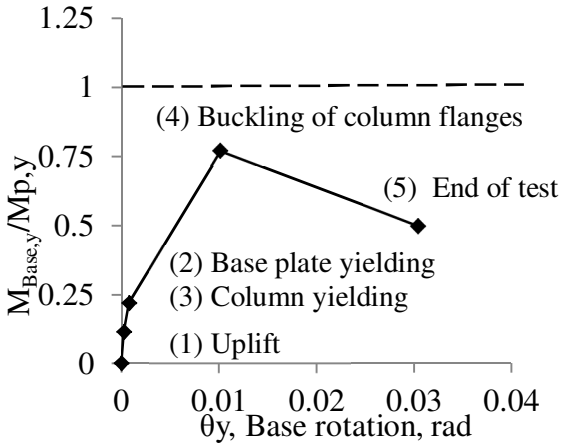

d. Idealized moment-rotation hysteretic curve for weak axis bending

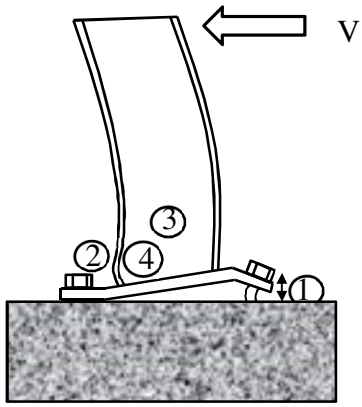

e. Damage scenario

Figure 3-10: Moment-Rotation and Damage Scenario for Test No. 4 , Figures a, and b are the base moment against base rotation, Figures c, and d are the idealized base moment- base rotation hysteretic curve, and Figure e is the order of damage scenario as labelled in Figures s, and d.

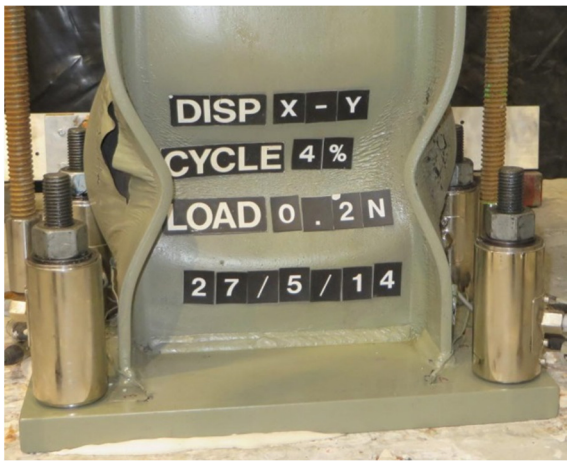

Figure 3-11: Buckled column at the end of Test No.4

The tension force of the anchor rod during bi-directional loading (Test No. 4) was higher than Test No. 3 for the same level of drift because it is subject to force from both loading directions. However, the tension force of the anchor rod at 4% drift in the X direction and 2.5% drift in Y direction is 10% lower than the tension force of the anchor rod at 4% uni-directional (x) drift in Test No. 3 according to Table 3-2. The reason for this observation is higher deformation of the base plate in Test No. 4, due to the concentration of the tension force in only one corner of the base plate that caused a reduction of base plate uplift. Figure 3-12 shows the displacement from potentiometers beside the column that is consistent with these outcomes. In this case, there is a reduction in uplift at the critical tension anchor rod by about 12%, which is similar to the 10% seen in Table 3-2.

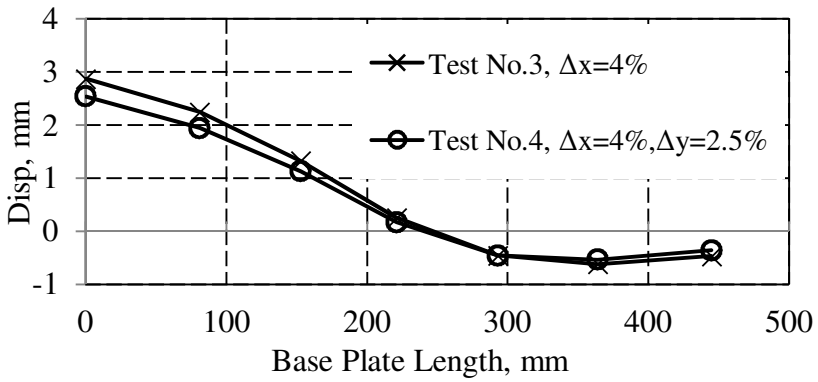

Figure 3-12: Base Plate Uplift

3.4. Summary

This chapter describes the experimental testing of steel I-shaped columns with exposed base plate connections and different levels of axial force bending about their strong axis and about both axes. In particular, the main results show:

1. The results of these experimental tests confirm that damage to the base connection started at low levels of drift (less than 1% drift), and in larger levels of drift more yielding and in some cases fracture occurred. This behaviour is consistent with previous studies. Furthermore, bi-directional bending with axial force caused column yielding starting from one-third of the level of drift at which the column yielded under uni-directional bending with axial force. Nonlinear deformation mainly occurred in the column rather than the base plate and anchor rods. Although the base plate was designed as the weakest component, no fracture or considerable permanent rotation was observed in the base plate during bi-direcitonal loading up to 4% drift.

2. The stiffness of the tested base plate connections ranged from 1.47 *EI/H* to 3.82 *EI/H* under strong axis bending, but was as high as 16 *EI/H* for weak axis bending. The strength did not increase by more than 12% for the specimen considered with 320 kN ($0.2\phi N_s$) axial force. The mechanism and failure mode did not change significantly depending on the test. In general, more column yielding resulted in greater possible residual displacements.

3. Typical exposed base plate connections not specifically designed to be rigid, such as those used here, may have rotational stiffnesses, K_θ, less than 3.8 *EI/H* under strong

axis bending implying that they may be modelled as being semi-rigid. In addition, the column base plate weak axis rotational stiffness may be much greater than that for the strong axis. In this test, rotational stiffness of the weak axis bending was also semi-rigid.

4. Bi-directional loading did not increase anchor rod forces for yielding columns due to biaxial bending.

In the next chapter the cyclic performance of the exposed base plate connections is described to evaluate the exposed base plate connection damageability for different levels of anchor rod preloading.

Chapter 4: Cyclic Performance of Column Base Plates Considering Anchor Rod Pre-Loading

4.1. Introduction

Anchor rod elongation is one of the main sources of base connection flexibility, as described by Kanvinde et al. (2012). He developed a macro model of the exposed base plate connection to estimate its rotational stiffness for snug tightened anchor rods without additional pre-loading. According to this model, if anchor rod elongation is prevented, then the base connection rotational stiffness is increased and some of the structural displacement demands are reduced.

Pre-loading of anchor rods, and increasing number and size of anchor rods are methods to limit anchor rod elongation. This approach has been recommended at the base of the structures subject to vibration or cyclical loads to limit the possibility of bolt fatigue or progressive loosening of anchor rod nuts (ASCE, 1997; AISC Design Guide 1 by Fisher and Kloiber, 2006; AISC Steel Construction Manual 13th Edition, 2005). However, none of these references proposed design criteria for pre-loaded rods. HERA Design and Construction Bulletin No 56 (Clifton, 2000) recommended tightening of the anchor rods to approximately half of the yield strength to eliminate potential sources of undesirable connection flexibility. However, this recommendation was not experimentally tested or validated.

AISC Design Guide 1 (Fisher and Kloiber, 2006) proposed two details for base connections with pre-loaded rods. In the first, anchor rods pass unbonded through steel sleeves and are

anchored in the concrete, as shown in Figure 4-1. The steel sleeves transfer the anchor rod force to the base plate and prevent reduction of pre-loaded force by concrete creep and shrinkage. The second detail is recommended for large building columns. The stool-type detail shown in Figure 4-1 is proposed where the rods are placed in a sleeve for easy insertion and replacement. There is no recommendation about the required length of unbonded rod in either case.

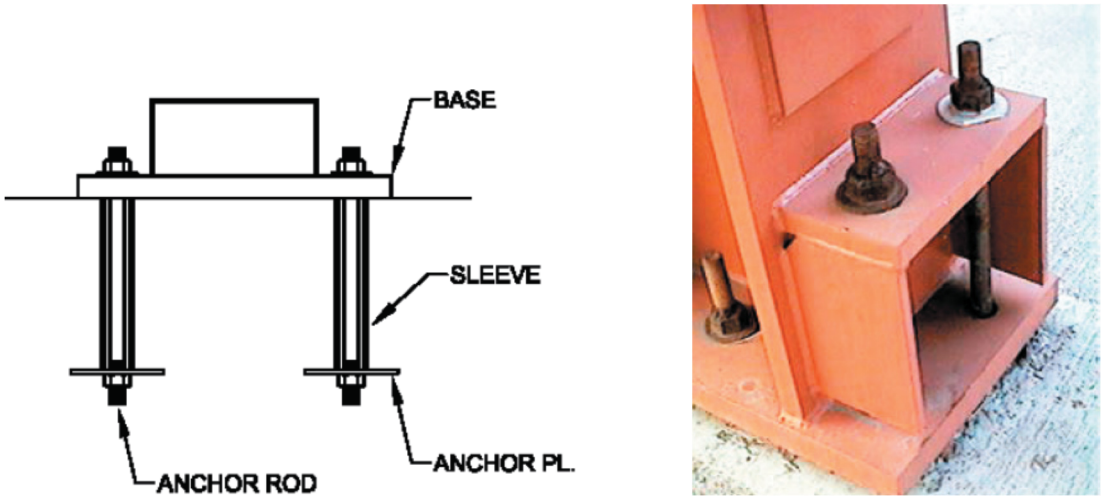

Figure 4-1: Details for pre-loaded joint Fisher and Kloiber (2006). Left is the anchor rod with sleeves, and the column base detail with stools is on right.

Anchor rods can be pre-loaded using a hydraulic jack, or long wrench following the nut-rotation or turn-of-the-nut method. According to PIP (2006), use of the hydraulic jack can most accurately provide the required force if there is installation space. In contrast, the turn-of-the-nut method is not as precise, but simpler and less costly to implement.

There are many experimental studies on the performance of base plate connections without preloaded anchor rods (e.g. Fahmy et al., 1999), and some macro models were developed based on them. Kanvinde et al. (2012) developed a macro model of the exposed base plate

connection to estimate its rotational stiffness for snug tightened anchor rods without additional pre-loading. According to his model, if anchor rod elongation is prevented, then the base connection rotational stiffness is increased and some of the structural displacement demands are reduced.

Very few studies considered the effect of anchor bolt tightening on performance of the base connection. Cannon (1992) carried out a series of baseplate connection tests considering finger and snug tightened rods. Anchor bolt preloading to the snug tight condition had no effect on the anchorage capacity, but significantly increased the anchorage elastic stiffness. Effect of higher anchor rod pre-loading, rotational stiffness, and non-linear mechanisms were not reported.

Hence, it may be seen that anchor rod preloading can significantly affect column performance. However, little work has been done to characterize effect of tightening on stiffness, strength, yielding modes and failure point. This lack of information creates a void in design methods and codes.

A set of experimental tests was conducted on exposed base plate connections without the anchor rod pre-loading using different numbers and strengths of anchor rod, different column axial forces, and column loading directions. These tests were described in Chapter 3, as shown again for clarity in Table 4-1. The columns and base plates were designed according to the AISC Design Guide 1 (Fisher and Kloiber, 2006).

Table 4-1: Tests on Exposed Base Plate Connections

Test No	Column and base plate	Axis of bending	Axial force	Anchor rods	Anchor rod pre-loading
I	A	Strong	Zero	4M24Grade 8.8	30 kN
II	A	Strong	Zero	4M24Grade 10.9	30 kN
III	B	Strong	320kN ($0.20N_s$)	4M24Grade 10.9	30 kN
IV	C	Bi-directions	320kN ($0.20N_s$)	4M24Grade 10.9	30 kN

This chapter uses experimental tests to address the issues delineated. In particular, answers are sought to the following questions:

(i) What is the effect of anchor rod pre-loading on seismic performance of column base plate connections with and without column axial force?

(ii) Can a simple method be developed to determine the strength of some types of column base connections considering anchor rod total pre-loading?

(iii) Can column base connection rotational stiffness considering anchor rod pre-loading be simply estimated?

4.2. Methodology

4.2.1. Test Specimen Design and Detailing

The test column section was a Grade 300, 310UB46.2 section with measured tensile yield stress of 320 MPa, and the distance from top of the base plate to the column point of contraflexure was 2 *m*. All of the drift values are based on this height. A universal beam (UB) section was used because they are most common in drift-governed frames, and ductile

moment resisting frames are typically drift governed. Two tests discussed in this chapter are a subset of tests in Table 4-1, as shown in Table 4-2. These tests were selected because they have the same bolt type and were tested about the strong axis. For Test No. 1 in Table 4-2, which is the same as Test No. II in Table 4-1, only 4% drift cycles were applied. In addition, Test No.3 in Table 4-2 is the same as Test No. III in Table 4-1. Two additional tests, Test No. 2 and Test No. 4 were conducted with high rod pre-loading to observe the performance of the base connections with high anchor rod preloading.

Table 4-2: Tests conducted in Chapter 4 to study the performance of the base plate connections with different levels of anchor rod preloading

Test No	Axial force	Anchor Rods	Anchor rod Pre-loading	Drift
1	Zero	4M24Grade 10.9	30 kN	4%
2	Zero	6M24Grade 10.9	185 kN	0.2%-4%
3	320kN (0.20N_s)	4M24Grade 10.9	30 kN	0.2%-4%
4	320kN (0.20N_s)	6M24Grade 10.9	185 kN	0.2%-4%

The computed moment causing first yield at an extreme fibre of the section due to bending about the strong axis using the measured material strength and nominal section dimensions ignoring axial force effects is 197 kN.m. The base plate was designed for one half of this moment (98.5 kN.m) to allow some base plate yielding. In addition, if the base plate is too strong it will act as a rigid body and be uneconomical, and if it is too weak, the flexural resistance at the column base will be compromised.

The AISC Design Guide 1 (Fisher and Kloiber, 2006) was used for design of base plate as shown in Figure 4-2. The column to base plate connection consisted of partial joint penetration (PJP) welding together with fillet welding. For the partial joint penetration welding, the bevel groove weld was carried out from the outside flange face up to 85% of the

flange thickness (10mm), as shown in Figure 4-2. In addition, 12 mm fillet welding was carried out on the inside face of the flanges and the web. This combination of PJP and fillet welding provides a total throat length 80% larger than the flange's thickness. This detail was selected based on the design practice survey for steel moment resisting frames in the US (Myers et al., 2009. Gomez et al., 2010). These surveys are based on experimental tests with different types of welding between column and baseplate, and state that this detail is effective for high seismic performance.

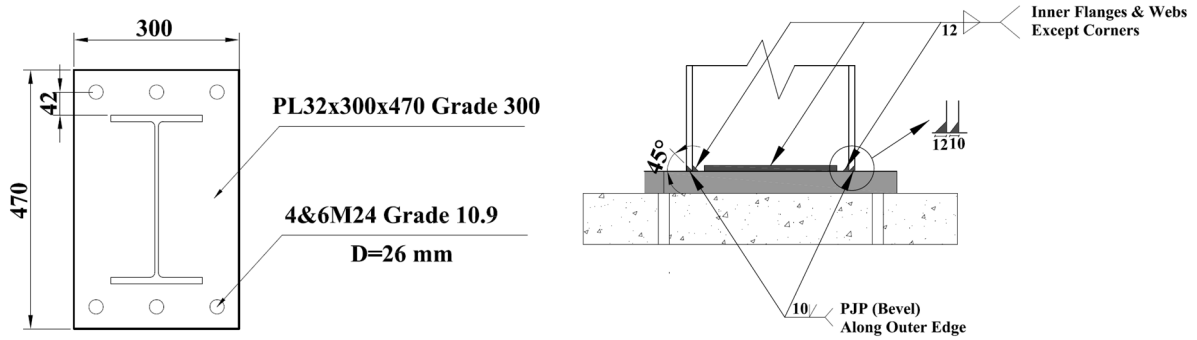

a. Detail of the base plate connection b. Column to base plate weld detail

Figure 4-2: Base plate detailing. Left is the detail of the base plate connection, and right is the column to the base pate detail, and left is.

The 550 mm long unbonded M24 Grade 10.9 anchor rods passed through steel tubes placed in the concrete foundation. They were anchored at the bottom of the foundation. Configurations with either 4 or 6 anchor rods were used, as described in Table 4-2. The computed base moment at anchor rod tensile failure was 1.25 times of the column yielding moment, and 2.5 times the nominal yielding of the plate when 4M24 Grade 10.9 were used. Pre-loading to 77% of the nominal bolt tension strength (185 kN) or 0.63 of the proof load of 292 kN according to Bickford (1995) was carried out on six anchor rods configuration. The pre-loading force was calculated to prevent rod elongation up to the nominal section moment capacity, M_{sx} (233 kN.m) following the method described in Section 2.5.

The base plate was placed on a 5mm layer of dental plaster to provide full contact. Initially, all of the nuts were snug tightened to ensure the nuts and the foundation plate were in full contact. All of the nuts were then tightened to 50% of the full pre-loading force. The preloading force was checked using load cell measurements. Finally, they were tightened to the final pre-loading force, as recorded by connected load cells according to the ASCE (1997) method. The nuts were tightened in an order in a shape of a star pattern, which described by FHWA (2005), as numbered in Figure 4-3.

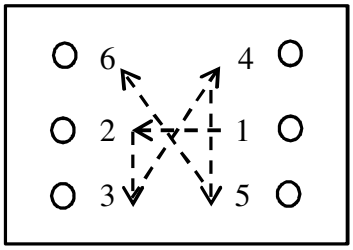

Figure 4-3: Tightening sequence star pattern

Four cyclic tests shown in Table 4-2, comparing Tests No. I, II, III, and IV from Table 4-1, were conducted about the column strong axis. Axial loads of 0 and 320 *kN,* which is 20% of the gross column section axial capacity ($0.2\phi AF_y$) were applied to evaluate this effect. For Test No. 1, horizontal sliding of the base plate was restricted by shear keys connected to the foundation. In the other tests, no shear key was provided as either the axial force or bolt preloading provided some shear resistance. For Tests No. 1 and 3, the anchor rods were snug tightened to 30 *kN*. Furthermore, a long torque wrench was used for pre-loading the rods in Tests No. 3 and 4. Contact surfaces between nuts and washers were greased and no rotation of the load cells was observed during tightening.

The applied torque, T_{apply}, and anchor rod tension force, T_{PT}, measured when rods with

diameter, D, were used to enable computation of the torque coefficient, K (Till and Lefke, 1994):

$$T_{apply} = K \times D \times T_{PT} \quad (4\text{-}1)$$

In Tests No. 2, and 4, the applied torque for tightening of the anchor rods was 620 N.m for well-lubricant rods and nut, and 960 N.m when no lubricant was used. Thus, the torque coefficient is equal to 0.14, and 0.216, respectively, as given by Equation 4-1. These factors are close to the factors from the AISC Design Guide 1 (Fisher and Kloiber, 2006), which are 0.12 for common size and coating, and 0.2 for less well lubricated anchor rods.

4.2.2. Test Setup and Loading Regime

The loading regime and test setup are as described in Chapter 2.

4.2.3. Instrumentation of the Base Connection

Foundation rods passed through 125 mm long 30 mm diameter load cells with 600 kN capacity. They recorded anchor rod tension while holding down the baseplate. Nine linear potentiometers with 25 mm stroke were placed on top of the base plate to monitor the base plate deformation. Three potentiometers monitored the sliding of the base plate in both directions. In addition, seven potentiometers were attached around the concrete foundation to monitor if there was any sliding or uplift between the foundation and the laboratory strong floor. Some of these sensors are shown in Figure 3-4. Strain gauges, with 6mm gauge length, were placed on the column flange and column base plate to measure local strains.

4.2.4. Analytical Modelling Prediction of Performance

- **Anchor Rod Tensile Force**

The AISC (2006) method for calculation of anchor rod tensile load assumes an initial anchor rod pre-load, T_{PT}=0. Therefore, it is modified to consider anchor rod preload. For a baseplate that uplifts on the tension side, as illustrated in Figure 4-4, the net moments about the tension rod (point A) should be equal to zero:

$$\sum M_A = 0 \rightarrow q_{max} Y \left(\frac{N}{2} - \frac{Y}{2} + f\right) - P_r(e+f) - T_{PT}(2x + d_c) = 0 \qquad (4\text{-}2)$$

The bearing length, Y, can be calculated by:

$$Y = \left(f + \frac{N}{2}\right) \pm \sqrt{\left(f + \frac{N}{2}\right)^2 - 2 \times \frac{P_r(e+f) + T_{PT}(2x + d_c)}{q_{max}}} \qquad (4\text{-}3)$$

Where:

$$f_p = 0.65 \times 0.85 \times f_c' \times \min\left\{2, \sqrt{\frac{A_{foundation}}{B \times N}}\right\} \qquad (4\text{-}4)$$

Where f_p is the bearing stress between the baseplate and concrete, as given in Equation 4-4, $A_{foundation}$ is the foundation area, e is the axial load eccentricity, which provides the moment at the centre of the column ($M=P_r e$) that cannot exceed the column plastic capacity (M_p). M and P are obtained from the applied forces of the column. B is the base plate width, N is the length of the base plate, f_c' is specific compressive strength of concrete, P_r is applied axial force, q_{max} is uniform bearing stress per width $=f_p \times B$, T_{PT} is pre-load tensile force of the rods,

x is the length of the base plate from the rods up to the column flange, d_c is depth of the column section.

Vertical force equilibrium, and the final tensile force of the rods, T_{rod}, are then defined:

$$\sum F_{vertical} = 0 \rightarrow T + 2T_{PT} + P_r = q_{max}Y \quad (4\text{-}5)$$

$$T = q_{max}Y - 2T_{PT} - P_r \quad (4\text{-}6)$$

If T>0 then $T_{rod} = T + T_{PT}$ otherwise $T_{rod} = T_{PT}$ (4-7)

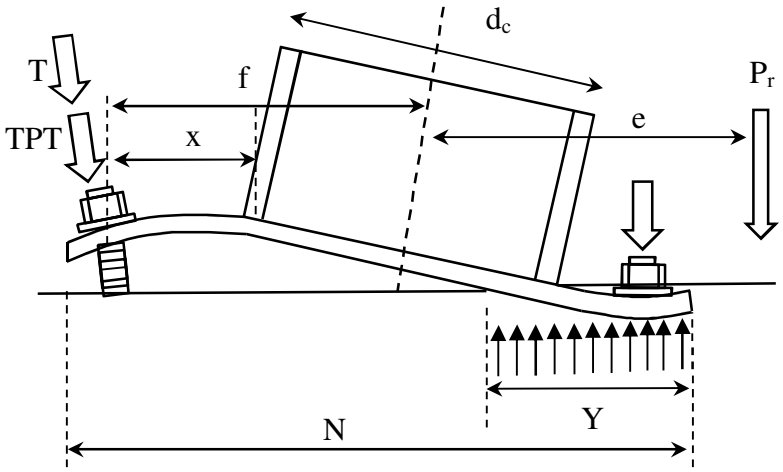

Figure 4-4: Base plate with pre-loaded rods and large moment including all terms in Equations 4-5 to 4-7

- **<u>Rotational Stiffness of Exposed Column Base with Pre-loaded Anchor Rod</u>**

Kanvinde et al. (2012) proposed a mathematical model for calculation of the rotational stiffness of exposed base plate connections that was modified by 14 experimental test results. This method is modified to calculate the rotational stiffness of the exposed base plate connection with pre-loaded anchor rods. The main base connection deformation under high eccentricity according to this method comes from elongation of the anchor rod, flexural

deformation of the base plate on the tension side, $\Delta_{plate}^{tension}$, and compression side, $\Delta_{plate}^{compression}$, and compressive deformation under the toe of the base plate, $\Delta_{concrete}$, as shown in Figure 4-5 before lift-off.

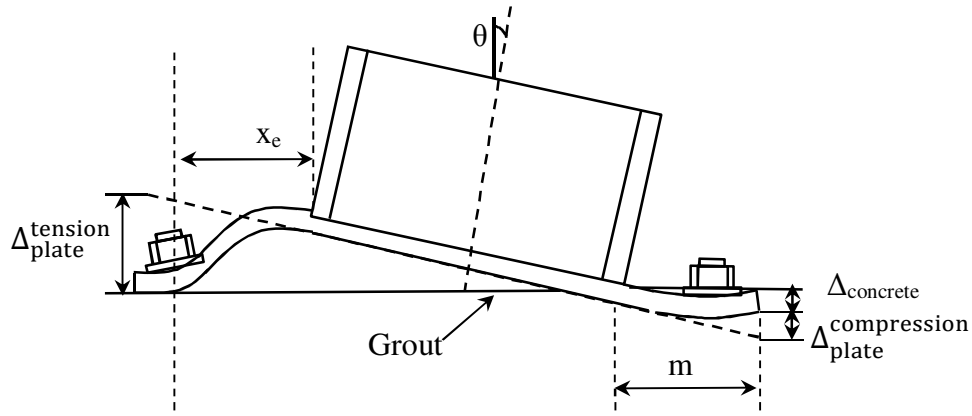

Figure 4-5: Deformation of components to calculate stiffness of exposed base plate before lift-off

It is assumed that the plate in the tension side performs as a cantilever and the flexural deformation of the base plate, $\Delta_{plate}^{tension}$, can then be calculated:

$$\Delta_{plate}^{tension} = \left(\frac{T_{BP} \times x_e^3}{3 \times E_{BP} \times I_{BP}}\right) + \left(\frac{T_{BP} \times x_e}{G \times A_{BP}}\right) \quad (4\text{-}8)$$

Where x_e is the distance between the edge of the column flange up to the centre of the anchor rod in the tensions side, I_{BP} is the base plate moment of inertia that is $B_{BP} \times t_{BP}^3/12$, A_{BP} is the effective shear area that is $(5/6) \times B_{BP} \times t_{BP}$, B_{BP} is width of the base plate, t_{BP} is thickness of the base plate, E_{BP} is the elastic modulus of base plate, and T_{BP} is the tension force on the tension side of the base plate.

The anchor rods do not elongate when $T_{rod} < T_{PT}$ .Therefore, another bearing area is formed on the tension side with length of Y_2, as shown in Figure 4-6. For computational simplicity,

Y_2 is assumed symmetric around the tensile rod. Hence, the length of bearing in the compression side is similar to Equation 4-3, and Y_2 can be calculated by vertical equilibrium, yielding:

$$Y_2 = \frac{2T_{PT} + P_r - q_{max}Y_1}{q_{max}} \tag{4-9}$$

Where T_{PT} is the pre-load force of the anchor rods, P_r is the applied axial force at the column top, q_{max} is the concrete bearing stress per width over Y_1 and Y_2, and Y_1 is the bearing length on the compression side. Therefore, when the anchor rod does not elongate, the net downward force on the base plate at the location of tension bolts force use in Equation 4-8 T_{BP} is defined:

$$T_{BP} = T_{PT} - q_{max}Y_1 \tag{4-10}$$

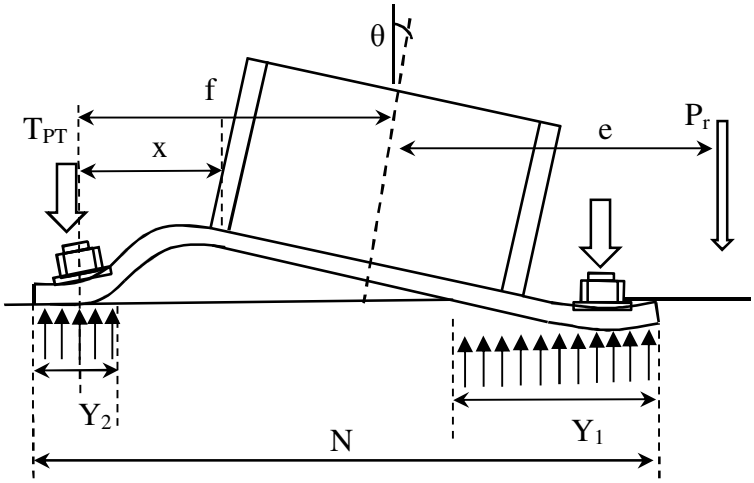

Figure 4-6: Base plate with large moment before uplift

When the base plate uplifts, this force is equal to T_{rod} in Equation 4-7. The elongation of the anchor rod for the case with uplift ($T_{rod} > T_{PT}$) is defined:

$$\Delta_{rod} = \frac{T \times L_{rod}}{n_{AB} \times A_{rod} \times E_{rod}} \tag{4-11}$$

Where T is the tensile force of the anchor rods on the tension side above that from the total tension side anchor rod pre-load given by Equation 4-6, n_{AB} is number of anchor rods in the tension side, and L_{rod} and A_{rod} are the length, and area of the anchor rod. When there is no uplift ($T_{rod} < T_{PT}$), T=0, and according to Equation 4-7, the anchor rod elongation is Δ_{rod}=0. For the case that anchor bolts are cast directly into the foundation, L_{rod} is de-bonded length before yielding of anchor rod.

No further modifications are required for calculation of $\Delta_{plate}^{compression}$ and $\Delta_{concrete}$ shown in Figure 4-5 to compare to the proposed method by Kanvinde et al. (2012). These calculations are defined:

If Y≥m:

$$\Delta_{plate}^{Compression} = f_{max} \times B_{BP} \times \left(\frac{m^4}{8 \times E_{BP} \times I_{BP}} + \frac{m^2}{2 \times A_{BP} \times G_{BP}}\right) \tag{4-12}$$

If Y<m:

$$\Delta_{plate}^{Compression} = \frac{f_{max} \times B_{BP}}{8 \times E_{BP} \times I_{BP}}\left(m^4 - \frac{1}{3}(m-Y)^3(3m+Y)\right) + \frac{f_{max} \times B_{BP} \times Y}{8 \times E_{BP} \times I_{BP}}\left(m + {}^{Y}/_{2}\right) \tag{4-13}$$

$$\Delta_{concrete} = \frac{f_{max}}{E_{concrete}} \times d_{footing} \tag{4-14}$$

Where m is distance from edge of the base plate up to edge of the column flange, as shown in Figure 4-5, f_{max} is the maximum bearing stress, B is the width of the base plate, E_{BP} and G_{BP} are the elastic modulus and the shear modulus of the base plate, respectively, Y is length of

the stress block that can be calculated according to AISC method (Fisher and Kloiber, 2006), and d_{footing} is the footing height.

The base connection rotation, θ, may be calculated, as shown in Figure 4-6, and defined:

$$\theta = \frac{\Delta_{plate}^{tension} + \Delta_{plate}^{Compression} + \Delta_{concrete}}{L_{total}} \tag{4-15}$$

Where $\Delta_{plate}^{tension}$ and $\Delta_{plate}^{compression}$ are the flexural deformation of the base plate on the tension and compression sides, respectively, and $\Delta_{concrete}$ is compressive deformation under the toe of the base plate. The secant base rotational stiffness up to the first yielding of the exposed base plate connection is thus defined:

$$K_\theta = \frac{M_y}{\theta} \tag{4-16}$$

Where M_y is moment of the base at the first yielding of the section or connected elements, and θ is base rotation at this level.

Under low-eccentricity (i.e. low moment) conditions, where the whole base plate is in compression bearing on the concrete due to column axial force, the strain in the supportive grout or concrete due to base moment determines the rotation of the base connection. In this case, no tension force is applied to the anchor rod, and the anchor rod does not affect base plate rotational stiffness.

4.2.5. Interpretation of Test Data

For each test, a base moment-rotation hysteresis curve is plotted and compared with the computed column plastic moment ignoring axial force affects. Multi-linear moment-rotation curves from the tests are also used to show when different limit states are reached. Yielding of the base plate and the column were recognized by paint flaking, and from strain gauges readings. Yielding of the anchor rod was monitored by the load cells beneath the anchor rod nuts. The column base moment, M_{Base}, and column base rotation, θ_{Base}, were computed from the column lateral force and lateral displacement according to:

$$M_{Base} = V \times H_{col} \tag{4-17}$$

$$\theta_{Base} = (\Delta_{top} - \frac{V \times {H_{col}}^3}{3 \times E_{col} \times I_{col}}) \times \frac{1}{H_{col}} \tag{4-18}$$

In these experiments, V is the lateral force at column top, H_{col} is height of the column from the base plate to the point of contraflexure, Δ_{top} is top displacement of the column, E_{col} is the elastic modulus of the column, I_{col} is the second moment inertia of the column in the direction of testing. The shear deformation was ignored as it is small in long member. P-delta effects were also ignored, as the axial force applied by the rods was inclined at the peak displacement making this effect small. The lateral drift is calculated by dividing the top displacement of the column by the height of the column from base plate up to the point of contraflexure.

The secant stiffness is calculated at the first observed yielding point of the column, plate or other component from the test, as described. The secant stiffness is presented in two ways:

(1) the actual value (kN.m /rad); (2) normalized to the stiffness of the column (*EI/H)*, where *H* is the height of the column from base plate up to the point of contraflexure, which is 2.0 *m* in these tests.

Displacement ductility capacity was calculated by dividing the displacement at the initiation of any fracture or column local web and flange buckling to the column first yield displacement. Plastic rotation of the base plate at the end of the test was calculated by dividing the recorded deformations of the base plate measured by the potentiometers at the flange tips at the end of the test by the distance between them. The plastic deformation of the column top at the end of the test was obtained from the moment-rotation plot at zero force after unloading from 4% drift. Column plastic residual rotation was then calculated by deducting the plastic rotation of the base plate from the total plastic rotation of the base. Residual force was defined as the force at zero displacement in the first cycle to 4% drift.

4.3. Results and Discussion

4.3.1. Hysteretic Curve and Damage Scenario

Test No. 1: The maximum moment for the first test with snug tightened anchor rod (30 kN) preloading, labelled as w/o PT in Figure 4-7, and without column axial force was 1.08 times of the nominal section moment capacity M_{sx} (233 kN.m) and the base experienced 32×10^{-3} rad rotation, as shown in Figure 4-7. This figure shows the base plate during the 3 cycles to 4% drift and the following cycle to 2% drift, as described in Section 2.4.2. The dashed line in Figure 4-7 indicates the level of nominal section moment capacity.

Base plate uplift occurred at a lateral drift of 0.1%, as shown in Figure 4-9, corresponding to a base rotation of 0.3×10^{-3} rad since the applied tension force in the anchor rods by snug tightening method was 30 kN and column self-weight was insufficient. The base plate yielded at a lateral drift of 0.85% corresponding to a base rotation of 5.7×10^{-3} rad, as recorded by strain gauges. The main plastic deformation occurred in the column that yielded at a lateral drift of 2.5% corresponding to a base rotation of 18×10^{-3} rad, as observed by paint flaking. High bending of the column and the base plate with inherent weakness of the welding against tension actions caused the fracture of the welds at 4% column drift (0.031 rad base rotation), as shown in Figure 4-8. Initial welding crack appeared on a corner of the flange on the tension side on the first cycle of 4% drift. Full fracture of the welding occurred in the third cycle of 4% drift, which reduced the base moment to 88% of the second cycle.

Test No. 2: Pre-loading of the anchor rod to 185 kN for the column base without axial force caused a 20% reduction of base rotation in the level of the column yielding compared to Test No. 1 at 4% drift because the column took a higher proportion of the total deformation. The base moment at 4% drift was increased 11% to 286 kN.m by pre-loading of the anchor rods, as shown in Figure 4-7 for Test No.2. Initial yielding of the base plate was recorded by strain gauges at a lateral drift of 0.6% corresponding to a base rotation of 1.6×10^{-3} rad, as shown in Figure 4-9. Finally, on the first cycle of 4% lateral drift (3.7×10^{-3} rad base rotation) the column flange buckled and the weld fractured at the same displacement. In the second cycle, fracture of the weld developed in the flange and part of the web, and the test was stopped in the third cycle.

Figure 4-8 shows Test No. 2 with welding fracture, as well. The column fractured from the corner of the column flange and about 10 mm above the base plate at the top of the weld in

the first cycle to 4%. It then travelled along the flange and through the weld to below the weld in the 2nd cycle.

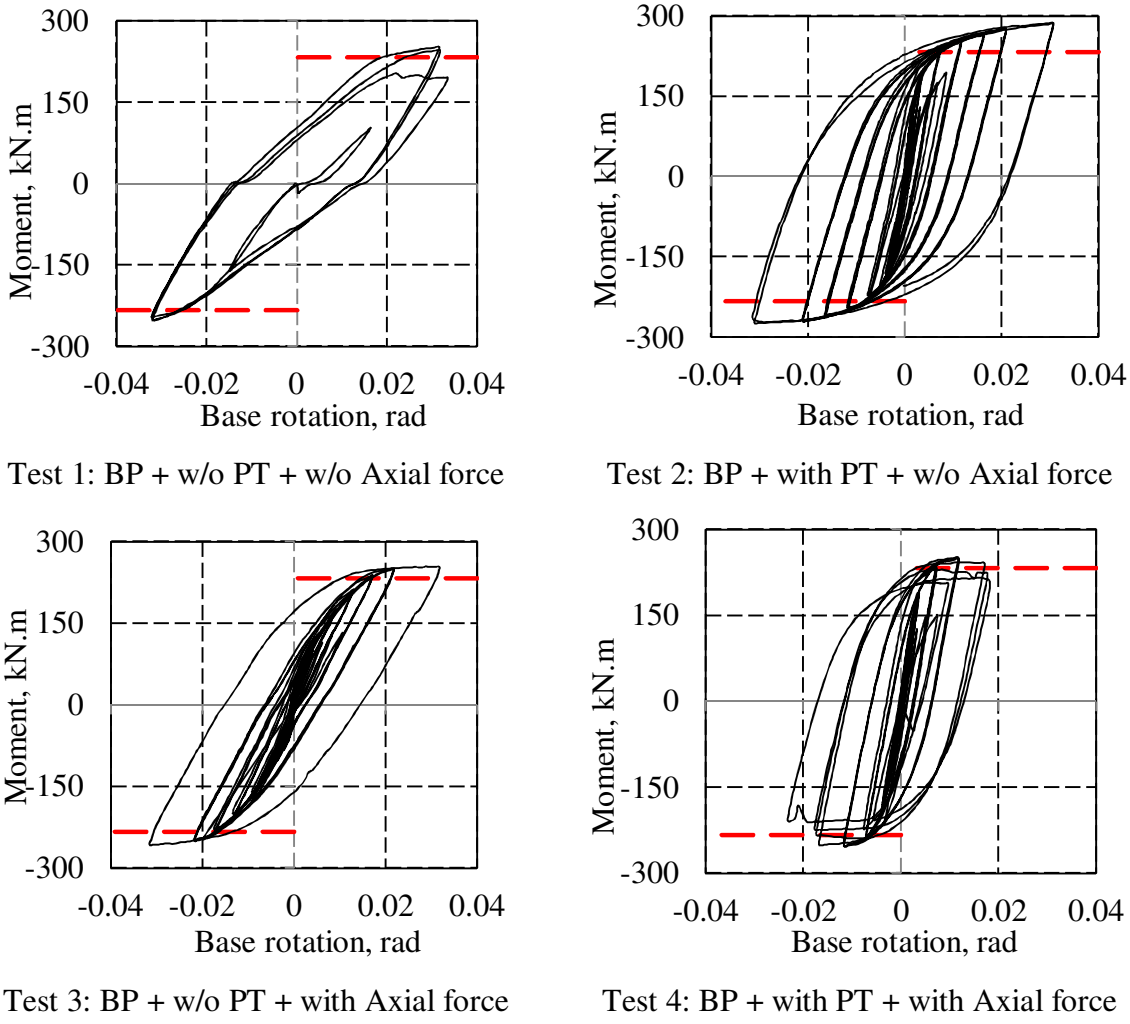

Test 1: BP + w/o PT + w/o Axial force

Test 2: BP + with PT + w/o Axial force

Test 3: BP + w/o PT + with Axial force

Test 4: BP + with PT + with Axial force

Figure 4-7: Base moment- base rotation curves for Tests 1-4

According to Table 4-3, the rotational stiffness increased 3.4 times by pre-loading the anchor rods for the column base without axial force. In addition, ductility, residual displacement and residual force at the end of the test were increased by 2.5, 1.4, and 2.7 times, respectively. The contribution of base plate residual deformation at the end of the test to total residual deformation was reduced from 38% to 10% by the presence of pre-loaded anchor rods. Pre-

loading of the anchor rod also led to hinge formation in the column and significantly reduced the yielding in the base plate for the columns without applied axial force.

Test No. 1

Test No. 2

Figure 4-8: Type of welding fracture in Test No. 1 on left and test No. 2 on right

Table 4-3: Results of Tests No. 1-4

Test No	PT rods	Axial force	M_{max} kN.m	K_θ		μ	$P_{\Delta=0}$ kN	$\theta_{P\text{-}Col}$ $\times 10^{-3}$rad	$\theta_{P\text{-}BP}$ $\times 10^{-3}$ rad	$\Delta_{P\text{-}Col}$ mm
				kN.m/rad	EI/H					
1	No	Zero	251	14736	1.47	1.6	35	9.37	5.63	30
2	Yes	Zero	280	50357	5.04	4	95	19.25	2.25	43
3	No	320kN ($0.20N_s$)	255	23254	2.33	3.5	67	11.4	3.57	30
4	Yes	320kN ($0.20N_s$)	251	55443	5.54	2.7	85	16.7	0.79	35

Test No. 3: The anchor rods were snug tightened, column axial force was applied and the column was bent about its strong axis. The base plate started to uplift on the tension side at a lateral drift of 0.25%, corresponding to a base rotation of 0.8×10^{-3} rad. The axial force that caused the start of column yielding shifted from 2.5% lateral drift (18×10^{-3} *rad* base rotation) in Test No. 1 to 1.5% lateral drift (9×10^{-3} rad base rotation), as observed by column paint flaking. The base moment was $0.75M_{sx}$ when the column started to yield. The base plate then yielded at 1.25% lateral drift (7.2×10^{-3} rad base rotation), as recorded by strain gauges.

The flanges started to buckle at 3.5% column lateral drift (26.6×10^{-3} rad base rotation) when the base moment was 1.08 M_{sx} on the first cycle to 4% drift, as shown in Figure 4-9 for Test No. 3. Column web buckling continued for higher levels of drift. After one full cycle of 4% lateral drift (31.5×10^{-3} rad base rotation) the test was stopped due to the possibility of instability caused by column buckling. Rotational stiffness, K_θ, of this specimen is half of the column base with pre-loaded anchor rods and without axial force (Test No. 2), as described in Table 4-3.

Test No. 4: The anchor rods were pre-loaded, axial force applied to the column, and it was bent about its strong axis. When the axial force was applied, the tensile force of the pre-loaded rods was reduced by 0.86%. This reduction in tensile force is small, and it shows that in real construction, the rods can be pre-loaded before applying the full axial force associated with the weight of the building.

The column yielded at 0.75% lateral drift (2.6×10^{-3} rad base rotation) as observed by paint flaking, and then the flange started to buckle at 2% lateral drift (11.7×10^{-3} rad base rotation), as shown in Figures 4-10 and 4-11. Buckling of the web and more deformation of the flange was observed as the lateral drift of the column was increased, as shown in Figure 4-10. The test was stopped after half a cycle at 3% lateral drift (23×10^{-3} rad base rotation) due to high deformation of the flange for buckling and the possibility of anchor rod load-cell damage.

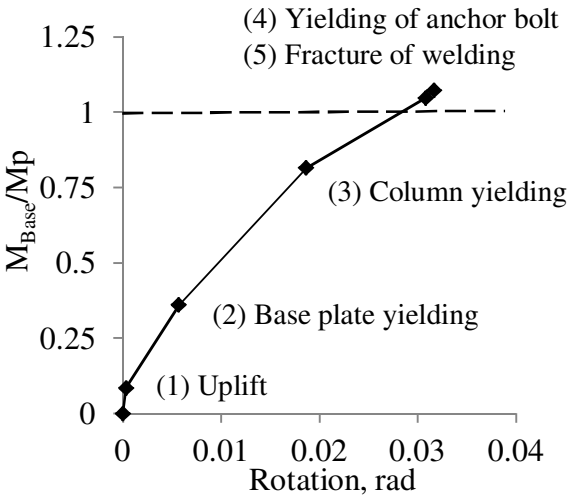

Test 1: BP + w/o PT + w/o Axial force

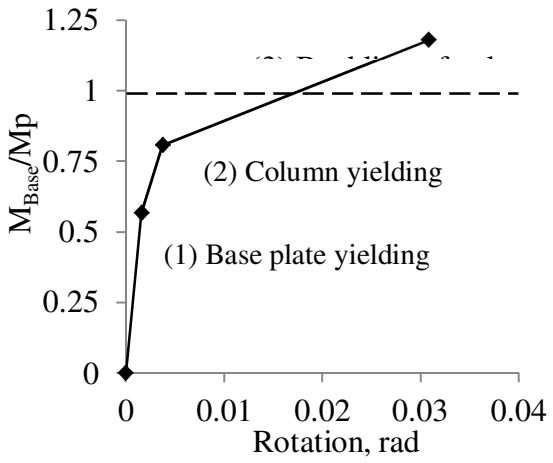

Test 2: BP + with PT + w/o Axial force

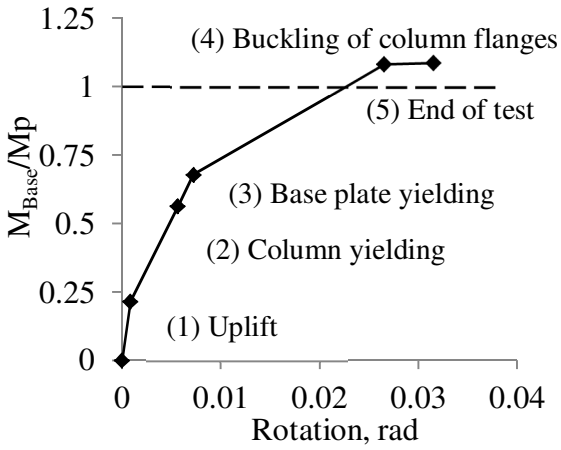

Test 3: BP + w/o PT + with Axial force

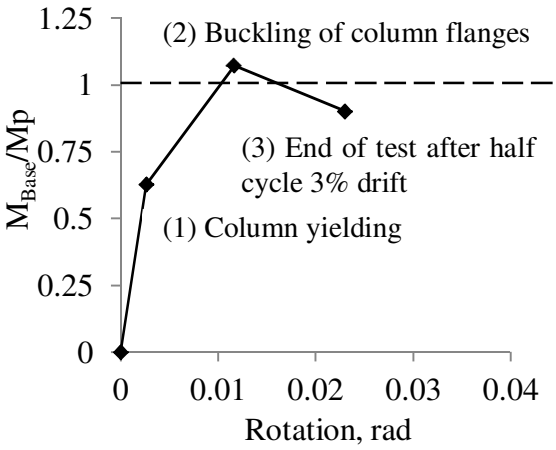

Test 4: BP + with PT + with Axial force

Figure 4-9: Damage scenario and multi-linear moment rotation curve for Tests No. 1-4

Figure 4-10: Specimen at the end of Test No. 4 showing buckling of the column web and the flanges

The following points can be stated based on these results:

1. The rotational stiffness of the specimen in Test No. 4 with pre-loaded anchor rods and axial force was 2.4 times that of the column base in Test No. 3, where the anchor rods were snug-tightened and axial force was applied, as described in Table 4-3.

2. The rotational stiffness was increased 10% by applying axial force to the specimen in Test No. 2 in the base with pre-loaded anchor rods. However, the rotational stiffness of the base plate with snug-tightened rods (Test No. 1) is more sensitive to axial force as it increased 158%.

3. Residual displacement at the end of the Test No. 4 and the residual force at zero displacement of the last cycle was increased by the pre-loading of anchor rods as shown in Table 4-3.

4. Although applying axial force to the base plate without pre-loaded rods (Test No. 1) reduced the contribution of base plate plastic deformation on residual rotation from 38% in Test No. 1 to 24% in Test No. 3, this contribution dropped to 4.5% by pre-loading of the anchor rods in Test No. 4 according to Table 4-3. As a result, the position of the plastic hinge was shifted to the column by applying axial force and anchor rods pre-loading.

5. Figure 4-11 shows vertical deformation of the base plate profile. It shows, the main deformation in Tests No. 1 and No. 3 came from base plate and anchor rod elongation. However, for Tests No. 2 and No. 4, elongation of the rods was zero and deformation of the base plate was highly reduced. As a result, the main deformation occurred in the column instead.

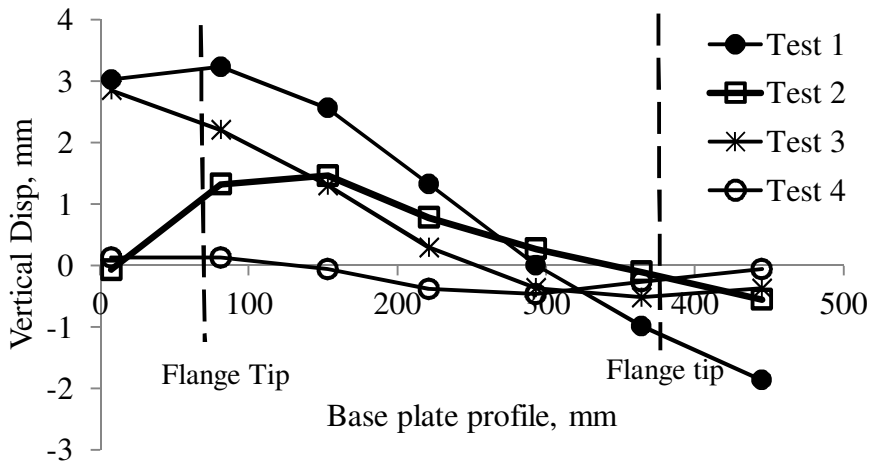

Figure 4-11: Profile of base plate vertical deformation at 3% drift for Tests No. 1-4

4.3.2. Tension Force of Rods

Tensile force in the anchor rods, *T* in Equation 4-7, in Tests No.1 and 3 at different column drifts are compared with the method proposed in Section 1.7 and with the AISC method, which does not consider anchor rod tightening, in Figure 4-12. Since the applied pre-loading to the anchor rods was small (30 kN), there is no obvious difference with AISC method, and the AISC method can be used for estimation of rod tensile force. The average difference of the proposed method and the experimental tensile force is 10% for Test No. 1 and 22% for Test No. 3.

For Tests No. 2 and No. 4 with high levels of pre-loading (185 kN), the AISC method cannot provide an accurate estimation of anchor rod tensile force giving significant errors, as shown in Figure 4-13. However, the proposed method estimated the anchor rod tensile force with average difference of 3.5% and 4.5% for Tests No. 2 and 4, respectively. Thus, the proposed method offers significant improvement for use in predictive design.

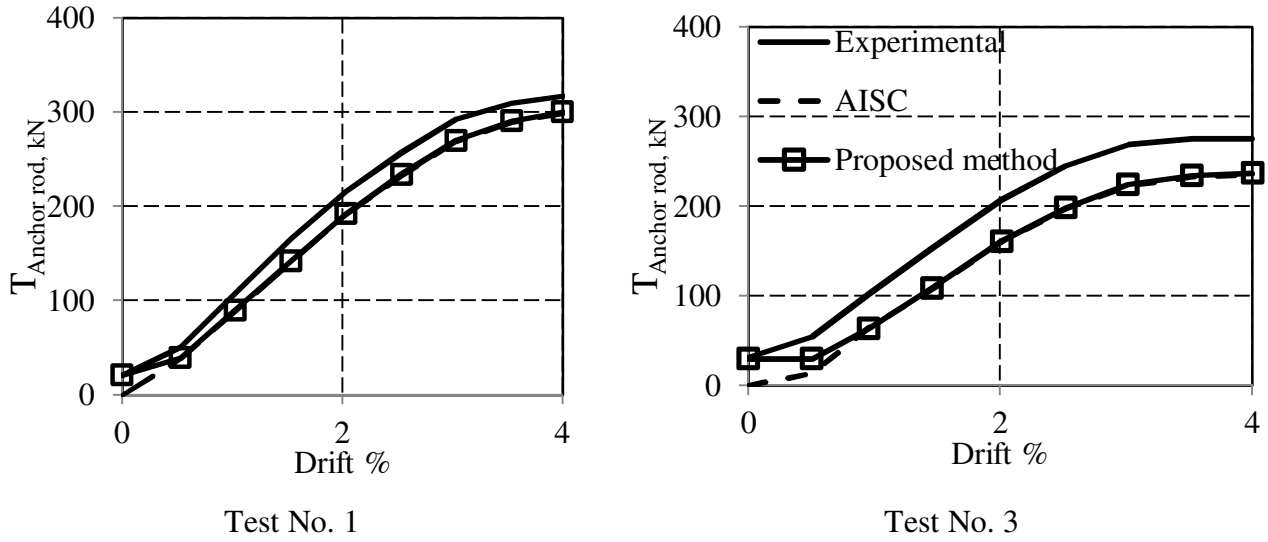

Test No. 1 Test No. 3

Figure 4-12: Anchor rod tension force for Test No.1 (on left) and Test No. 3 (on right) from experimental tests compare to the AISC and proposed methods

An example calculation for tension force of anchor rod in Test No. 3 is presented in the following. At 3% drift, the lateral force at top of the column was 137.6 kN. The uniform bearing stress per width, q_{max}, is 49.7 MPa, as given in Equation 4-4 for concrete with concrete compressive stress of 45 MPa. The bearing length, Y, as given in Equation 4-3 is 85 mm. Therefore, T equals 158.6 kN for three anchor rods following Equation 4-6, and the final tensile force of the rod, T_{rod}, is 248 kN, as given in Equation 4-7. The recorded tensile force from the experimental test was 250 kN, which is less than 5% difference from the analytical results of the proposed method.

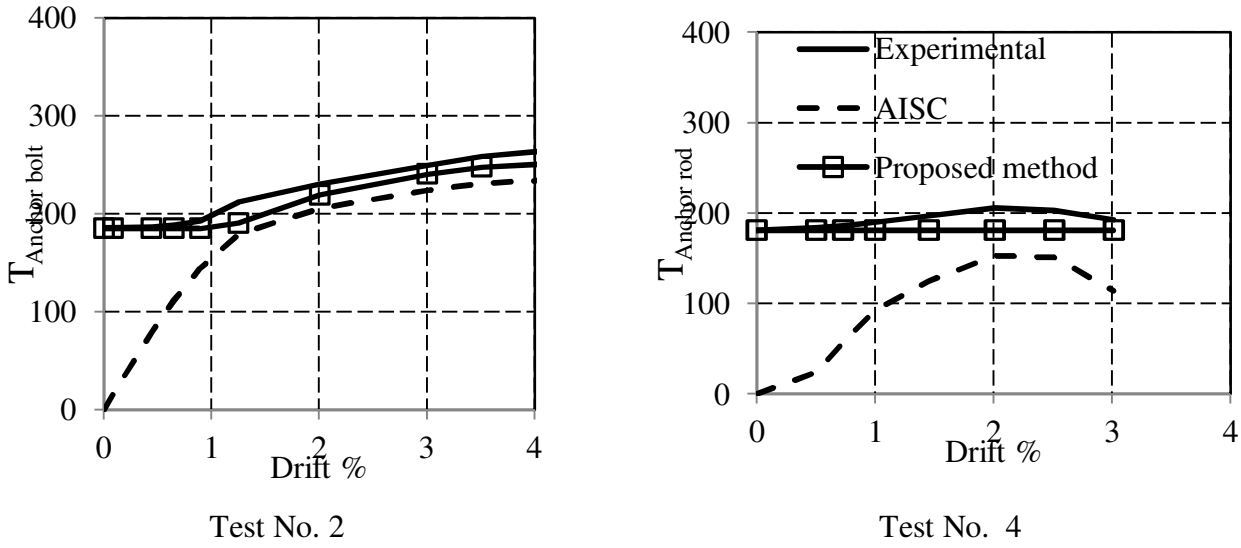

Figure 4-13: Anchor rod tension force for Test No. 2 (on left) and Test No. 4 (on right) from experimental tests compare to the AISC and proposed methods

4.3.3. Rotational Stiffness

Table 4-4 shows that the median ratio of calculated experimental rotational stiffness to the analytical estimation of Equation 4-16 is 0.97 for all four tests. The agreement between the experimental and analytical rotational stiffness is not as good for Test No. 4 with axial force and anchor rod pre-loading of 185 kN. In this test, the applied axial force and high anchor rod preloading that acted as a compression force on the concrete surface caused the rotational stiffness to become more sensitive to the base plate-footing interaction. This result is consistent with the same results by Kanvinde et al. (2012) for the base plate with high axial load. This effect, which tends to exactly predict the rotational stiffness, is not considered in the proposed method due to several simplifying assumption. Hence, its exclusion does affect the resulting analytical estimation.

Table 4-4: Experimental and Analytical Rotational Stiffness Calculations for Tests No. 1-4

Test No	Experimental kN.m/rad	Analytical kN.m/rad	$K_{\theta,exp}$/ $K_{\theta,Analytical}$
1	1.47	1.82	0.81
2	5.04	4.38	1.15
3	2.33	2.97	0.78
4	5.54	3.5	1.58

4.4. Summary

This chapter describes the experimental testing of four columns with exposed column base plates connected to the foundation with both high pre-loading and snug-tightened anchor rods. The columns were loaded to induce bending about their strong axis and subject to an axial force ratio of zero or $0.2\phi A f_y$. The main outcomes are summarized:

1. Axial load from preloading of anchor rods or column axial force tends to decrease the base plate and anchor rod contribution to the displacement at the top of the column. This behaviour increases the overall observed column stiffness and strength.

2. The AISC method was modified to consider the anchor rod pre-loading, and gave similar results to the AISC method when the pre-loading was small, but matched experimental results much better than the AISC method for high pre-loads.

3. Methods by Kanvinde et al. (2012) for calculation of rotational stiffness of base plate connections were modified to consider anchor rod preloading. This change enabled the stiffness to be estimated with a maximum 22% accuracy except for columns with high axial force, where column stiffness is underestimated.

Overall, the experimental tests in Chapters 3, and 4 show that the base connections remained

elastic at low levels of drift. They can be categorized as “low damage” at these low levels. Beyond this point, plastic base rotation occurred, leading to brittle fracture or residual column deformation, and thus significant damage for even moderate drift demands. In the next chapter, the effect of base flexibility, which comes from the soil, foundation and the base connection, on demands of the structure, will be studied to determine whether or not base flexibility can reduce base connection damage.

Chapter 5: Spectral Assessment of the Effects of Base Flexibility on Seismic Demands of a Structure

5.1. Introduction

The rotational stiffness at the base of a column affects the force and displacement demands on frame elements during an earthquake. In most analyses conducted for design, the column base is considered to be fully fixed. However, in real structures, foundation flexibility exists due to the soil, foundation, and base connection, all of which can change the base rotational stiffness, potentially leading to increased structural demands.

Observations of the performance of base plate connections during the experimental studies described in Chapters 3 and 4 showed they did not perform as low damage connections at high drift levels. However, it may be possible that changing the base flexibility could reduce base demands, such that the base connection acts as a low damage connection.

A number of studies have been conducted to evaluate the effect of base flexibility. Maan and Osman (2002) modelled five and ten storeys buildings with different column base flexibilities. They showed that pinned to fully fixed column base cases bounded the responses for all frames. While frame displacements increased with increasing base flexibility, the frame displacement capacity also increased. The location of inelasticity can also change with base flexibility and could also the inelasticity increase at some levels. Aviram et al. (2010) showed that increasing base flexibility increased displacement demands and concentrated deformations in the first storey of a three storey building. Ruiz-Garcia and Kanvinde (2013) showed that ideal pinned based connections lead to larger inter-storey drift demands, but

smaller residual drift demands compared to the fixed base condition. Zareian and Kanvinde (2013) found that increasing base flexibility results in the development of a collapse mechanism with large deformations concentrated in fewer storeys in 2, 4, 8 and 12 storey steel moment resisting frames.

From this discussion there appears a need to evaluate the effect of the base flexibility on structural demands for a wide range of structural periods.

This chapter addresses this need for a single storey moment frame structure by seeking answers to the following questions:

- What rotational stiffness is likely at the base of columns in realistic steel frames?

- What is the effect of column base flexibility on the frame top displacement, column top moment, and nonlinear base rotation?

5.1.1. Code Background Related to Connection flexibility

Few standards state much about the column base rotational stiffness, k_θ, which may be defined as the base moment, M, divided by the base rotation, θ. However, Eurocode 3 (2005) divides base connections into categories depending on k_θ, as shown in Figure 5-1. Here k_θ is normalized by EI/H where EI is the flexural stiffness of the column section, and H is the storey height of the column independent of rotational fixity of the top of the column. Column bases with a rotational stiffness, k_θ, of $30EI/H$ or more do not change the column ultimate

strength by more than 5% or column lateral displacement under service load by more than 10% from the fixed base case according to Jaspart et al. (2008). In this case, the connection may be considered fully rigid. Base connection stiffnesses lower than *0.5(EI/H)* capture the fully pinned condition and connections may be modelled as being fully pinned. It is suggested that if the real rotational stiffness is between these two boundaries, then the rotational stiffness should be explicitly considered in the analyses.

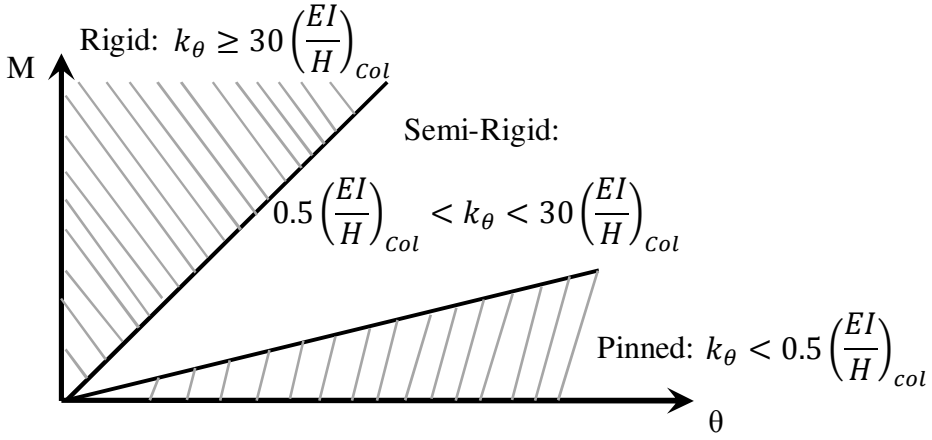

Figure 5-1: Eurocode 3 (2005) column base rotational stiffness boundaries

5.1.2. Base Connections and Flexibility

The most common column base connections used in practice are either: (1) exposed base plate connections (EPBC); or (2) embedded column bases (ECB), as illustrated in Figure 5-2 respectively. The EPBC, with the column directly welded to the base plate and the base plate bolted to the foundation, has been most widely used on low to medium rise structures (Cui et al., 2009). In these cases, the rotation of the column, θ_{column}, under the column moment is equal to the footing rotation, $\theta_{footing}$, plus the baseplate rotation, θ_{plate}, and the base and footing stiffnesses can be considered as two rotational springs in series. For the ECB, with the base embedded in the reinforced concrete foundation, the beam and the footing rotations,

θ_{beam} and $\theta_{footing}$ are the same as the column rotation, $\theta_{footing}$, and the rotational stiffness of the base may be considered to result from the two rotational springs of the footing and the beam in parallel.

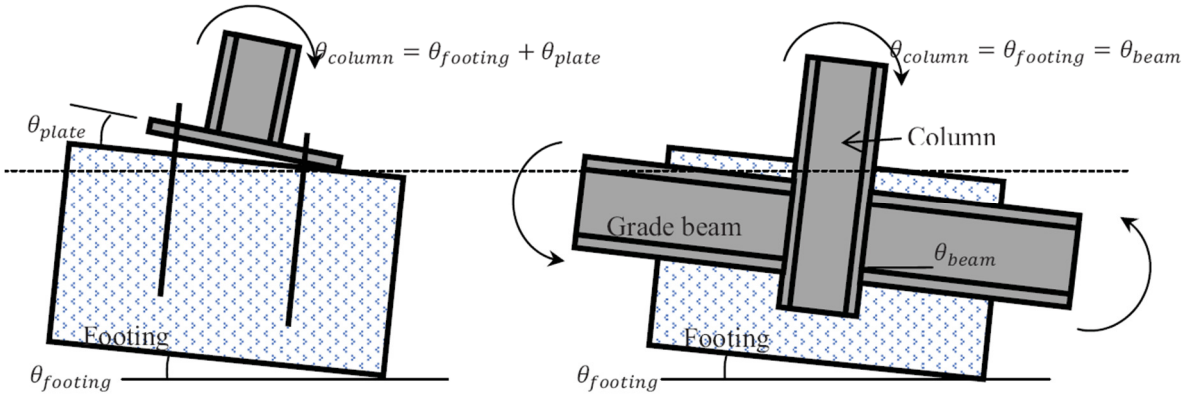

a. Exposed base plate connection (EBPC) b. Embedded column base (ECB)

Figure 5-2: Common base connections (Zareian and Kanvinde, 2013). Exposed base plate connection (EBPC) on left and embedded column base (ECB) on right.

- **<u>Exposed Base Plate Connection (EBPC)</u>**

Picard and Beaulieu (1985) showed that axial loading increased the base plate connection rotational stiffness of an EBPC with snug tightened nuts through the baseplate. Rotational stiffness, k_θ, defined as the 70% of the maximum applied, divided by the base rotation at that moment, θ, ranged between 662kN.m/rad and 14492 kN.m/rad for the range of sizes and axial forces considered. Rotational stiffness may be expressed as a degree of fixity, as per Eurocode 3 (2005), by writing it in terms of *EI/H*, where, *EI* is the material elastic modulus multiplied by the second moment of area for the tested column section, but the actual column base rotational stiffness, k_θ, is dependent only on moment and rotation, and is independent of the position of loading *H*.

The appropriate value of *EI/H* depends not only on the column section, but also on the likely height to the point of contraflexure from the base for that particular column. In this research, the column stiffness ranges above may be written as lying between 1.65EI/H_{st} and 7.6EI/H_{st}, where H_{st} is simply taken as 2.2m and *EI* is different since three different column sections were tested. This length is approximately 63% of the base storey column height of a 3.5m to the point of contraflexure for a typical full size column.

Robertson (1991) tested a frame where the column base rotational stiffness could be set. He used rotational stiffnesses of 150 kN.m/rad (0.1 EI/H_{st}), 1500 kN.m/rad (1.3 EI/H_{st}), 3300 kN.m/rad (2.8 EI/H_{st}) representing a pinned, and 2 different degrees of semi-rigid base, respectively. Robertson also stated that for typical 20mm thick base plate connections in real construction, the rotational stiffness was likely to range from 500kN.m/rad (0.4 EI/H_{st}) to 3500 kN.m/rad (3 EI/H_{st}).

Gomez et al. (2010) assessed the effect of axial load, base plate thickness and anchor-rod strength on total performance where the nuts were snug tightened. The rotational stiffness of these base connections were in the range of 7,760 kN.m/rad (1.2 EI/H_{st}) to 41,310 kN.m/rad (5.8 EI/H_{st}). Deformation of the plate, of the concrete under the compression side, and elongation of the anchor bolts were the main sources of observed flexibilities.

- **Embedded Steel Column Base (ECB)**

Nakashima and Igarashi (1986), Morino et al. (2003), and Grauvilardell et al. (2005) categorised the performance of ECB connections based on embedded length. For deeply embedded types, when the embedded length was no less than two times the lateral dimension

of the column cross section in the plane of bending, the column may be assumed to be fixed. For shallower embedding, rotational stiffness decreased and the failure mechanism changed from column yielding to cracking of the concrete and yielding of the anchor bolts.

5.1.3. Foundation and Soil Flexibilities

The soil below the foundation also contributes to overall column base stiffness. This aspect was investigated for different soils by Winterkorn and Fang (1975) and modified by Melchers (1992) to consider uplift effects. The main result of these studies was developing the macro model of the foundation and soil flexibilities.

5.1.4. Preface

It may be seen from this review that column bases may not be rigid as a result of connection, foundation and soil flexibility. Previous studies quantified these effects individually. In addition, the base flexibility effect on a number of individual frames has been quantified. However, none of these studies was general enough to provide design guidance for buildings with different periods. In addition, all these studies have evidenced failure or nonlinear deformation in base connections, although they are designed to remain elastic. Finally, studying the impact of nonlinear base behaviour with different levels of strength is also required, but not yet done. In this study, the likely range of rotational stiffness considering the combination of connection, foundation and soil flexibility is first obtained. Linear and nonlinear spectral analysis is then conducted to determine the likely change in response for a wide range of structural periods and strengths to understand the likely range of response of

single storey structures due to this base flexibility. These analyses are designed to provide the foundation for design guidelines.

5.2. Methodology

A single storey steel moment frame is modelled by MATLAB. Also, this model was verified with OpenSees. The MATLAB code is presented in appendix A. Figure 5-3 represents half of a single storey frame with the beam roller pin support providing a zero moment connection at the beam mid-length. The base of the column is fixed laterally, but can rotate. The rotational stiffness of the beam can be represented by a rotational spring with stiffness, K_{top}, as shown in Figure 5-3. K_{bot} represents the total base rotational flexibility from the connection, foundation and soil below.

The resulting column degrees of freedom consist of one mass degree of freedom, Δ_{top}, and two massless degrees of freedom, θ_{top} and θ_{bot}. The associated forces are shown in Figure 5-3, where M_{top}, M_{bot}, V_L are the top and base moment and lateral shear force applied to the frame. The period of the structure is changed from 0.3s to 5s in steps of 0.1s by changing the mass, m. Tangent stiffness proportional damping with a ratio of 5% is assumed for the first mode.

To estimate realistic column base rotational stiffnesses for analysis, the base connection stiffness of Gomez et al. (2010), together with the soil effect from Melchers (1992), is used, as shown in Table 5-1. It may be seen that baseplate rotational stiffness, $K_{\theta BP}$, is less than $6EI/H_{st}$. When soil flexibility is also considered, assuming a 1.2m x 1.2m foundation block on different soil types, such as soft clay, loose sand, dense sand and gravel, and basalt, the total

foundation flexibility, $K_{\theta,total}$, is obtained considering the springs in series. According to Table 5-1, the column base plate connection stiffness is significantly less than the rigid level of $30EI/H_{st}$ of Eurocode 3 (2005), implying no base plate connections should be considered to be fully rigid, and that these connection stiffnesses must be included in design analyses.

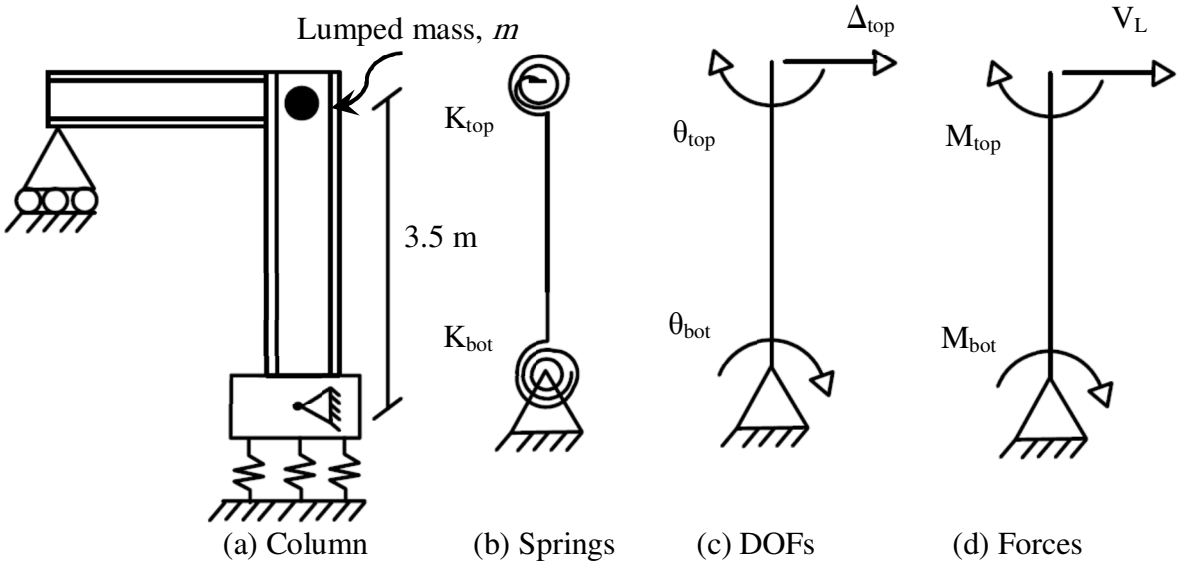

Figure 5-3: Analysis model of the single storey structure

In this study, rotational stiffnesses of *0EI/H* , which is fully pinned, *5EI/H* , which has intermediate stiffness, and *2000EI/H* , which can be considered as fully fixed, are considered. Here, *H=3.5m* is the height of the frame, as the point of contraflexure depends on the end conditions. Baseplate connections will generally result in sfiffnesses between about *0EI/H* and *5 EI/H* while those with greater stiffness represent embedded connections with stiff beams on hard soil.

The double curvature period, T_{dc}, is used in this analysis because the period of the structure is only affected by the stiffness and mass of the frame, and it is independent from rotational stiffness at the top and the base. T_{dc} is the period of the column when it is rotationally fixed at the base and the top with a lateral stiffness of $12EI/H^3$. For example, the true period of a fully

fixed base column that is pinned at the top with lateral stiffness of $K_L=3EI/H^3$ is twice that of the double curvature period, T_{dc}. Therefore, for a fixed base structure with top stiffnesses of 0*EI/H*, 5*EI/H*, 2000*EI/H*, the actual period, T, is $2T_{dc}$, $1.22T_{dc}$ and $1.0\ T_{dc}$, respectively. This approach allows consistent comparison across all cases analysed, and is easily converted to a normal period.

Table 5-1: Test data of base plate from Gomez (2010) tests and evaluation of K_θ for different types of soil based on Melchers (1992)

BP thickness *mm*	N^*/N_s [d]	$K_{\theta,BP}$ [a,b] (EI/H_{st})	Type of Soil	$K_{\theta footing}$ [a,c] (EI/H_{st})	$K_{\theta,total}$ [a] (EI/H_{st})
25.4	0	1.24	Soft clay	0	0
			Loose sand	0	0
			Dense sand and gravel	0	0
			Basalt	0	0
	0.16	3.49	Soft clay	0.14	0.14
			Loose sand	1.82	1.20
			Dense sand and gravel	8.55	2.48
			Basalt	3590	3.49
	0.27	5.81	Soft clay	0.15	0.15
			Loose sand	1.95	1.46
			Dense sand and gravel	9.19	3.56
			Basalt	3863	5.80
38.1	0.16	3.07	Soft clay	0.12	0.12
			Loose sand	1.57	1.04
			Dense sand and gravel	7.33	2.17
			Basalt	3097	3.07
50.8	0.16	3.02	Soft clay	0.12	0.12
			Loose sand	1.54	1.02
			Dense sand and gravel	7.25	2.13
			Basalt	3046	3.01

[a] The test's column section was W200 x 7, Grade 300
[b] For tests that were conducted several times the median results are presented in the table.
[c] The footing is assumed rigid relative to the soil that it rests, with dimension of 1.2m x 1.2m.
[d] N_s is nominal column section capacity, and N^* is the applied axial force to the column

Twenty medium suite earthquake records from the SAC steel project (Somerville et al., 1997)

for Los Angeles with a probability of 10% in 50 years (La 10 in 50) were used for time history analysis. The elastic spectral displacement for these records and the median value are shown in Figure 5-4. All 20 records were used for each configuration of structure, and the median result presented.

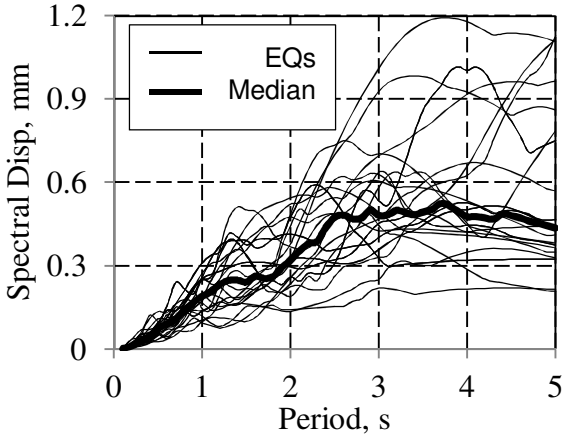

Figure 5-4: Median and record displacement response spectrum for SAC La 10 in 50 suites

The elastic analysis study involves the following parameters:

- K_{top} of *0EI/H, 5EI/H*, and *2000EI/H*
- K_{bot} of *0EI/H, 5EI/H*, and *2000EI/H*
- Double curvature period, T_{dc}, between 0.3s to 5.0s, ΔT_{dc} = 0.1s

The results are shown as a spectral plot ratio of $x^{Ktop=\beta EI/H}_{Kbot=\alpha EI/H}$ to $x^{Ktop=\beta EI/H}_{Kbot=fixed}$ over T_{dc}, where x is the demand parameter, such as top displacement, and top moment, k_{top} and k_{bot} are top and base rotational stiffness, respectively. When the response causes greater demands than for the rigid base case, the ratio is greater than one.

The entire study is repeated for nonlinear analysis where the column is rotationally fixed at

the top and the same column base flexural strength. Top rotational stiffness was kept fixed and period of structure, base rotational stiffness, and base yielding moment were varied. The nonlinear base rotation of a frame with column base rotational flexibility is compared with that for a rigid base over a range of T_{dc}. Note that P-Δ effects were not considered in either the linear or non-linear analysis as the effect is small for the range of stiffnesses considered. The base yielding moment is defined according to the maximum elastic moment of the fixed top and base column, $M_{Elastic,FB}$.

The Menegotto and Pinto (1973) M-θ hysteretic curve was used for modelling the nonlinear column moment-rotation behaviour as shown in Figure 5-5. Curve properties and model parameters are given in Table 5-2. The curve is not fully piecewise linear due to rounding of the corners represented by γ. This nonlinearity is used to consider yielding of the base connection.

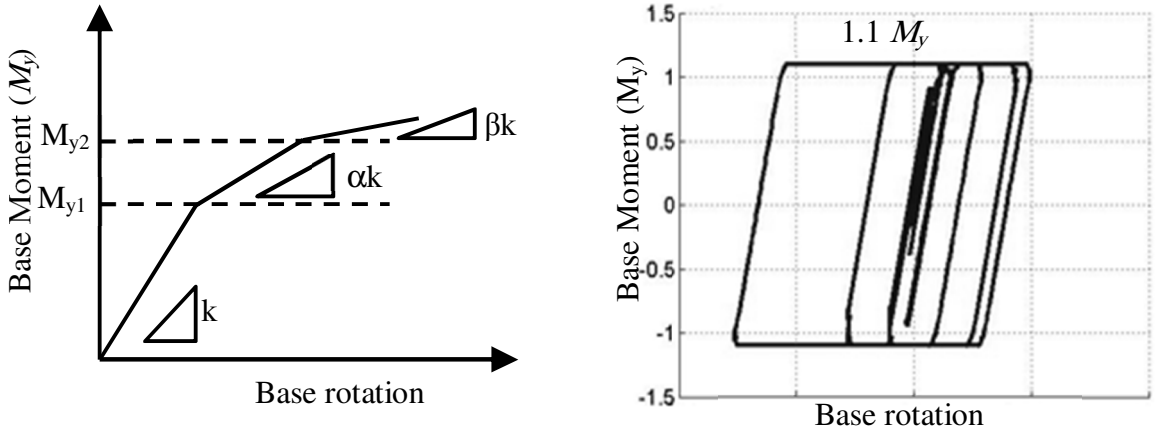

(a) Idealized loading response for first half cycle

(b) Cyclic response

Figure 5-5: Menegotto-Pinto hysteretic loop. Idealized loading response for first half cycle on left and the cyclic response is on right side

For nonlinear analysis, the results are presented as a plot that is the ratio of the nonlinear base

rotation for a frame that is fixed at the top with base rotational stiffness, $\theta_{NL,Kbot}$, to nonlinear base rotation of the fixed top and base frame, $\theta_{NL,Fixed}$, over base yielding moment, M_y, and base rotational stiffness, K_{bot}. This ratio is presented for three ranges of T_{dc} to simulate short, $0.3s \leq T_{dc} < 1s$, medium, $1s \leq T_{dc} < 3s$, and long periods, $3s \leq T_{dc} < 5s$. For each level of M_y in the range $0.3\ M_{Elastic,FB} \leq M_y \leq 0.9\ M_{Elastic,FB}$, and K_{bot} in the range $1\ EI/H \leq K_{bot} \leq 9\ EI/H$, the maximum value of this ratio over the range of T_{dc} is plotted. Ratios larger than one represents a non-conservative design, and ratios less than 1.0 show the design is conservative.

Table 5-2: Properties of the Menegotto-Pinto hysteretic loop and its governing equation

Properties	Value
α	0.1
β	0
M_{y2}	1.1My1
ϒ (curvature of loop's corners)	10
Equation: $F = \frac{k}{\left(1+\left(\frac{k}{M_y}\right)^{\gamma}\right)^{1/\gamma}}$	

Based on simple theoretical considerations it would be expected that for a frame with a rigid beam, by changing from a fixed base to a pinned base, the frame stiffness decreases by a factor or 4 ($=3EI/H^3/(12EI/H^3)$) and that the resulting period thus doubles. For structures in the range where the response spectra increases linearly with period and when the equal displacement method holds, the doubling of period is associated with a doubling of total displacement. In the elastic range, this doubling results in the same moment at the top of the column as for the rigid base case because the displacement is double and the moment diagram is in single, rather than double, curvature. It also reduces the moment at the top of the column and the base plastic hinge rotational demand in the inelastic case. For this reason, it is possible that, apart from displacement demands, other moment and plastic hinge demands may be reduced. However, there may be significant variation from this expected

behaviour due to the actual beam stiffness, the shape of the response spectra, variation from the equal displacement assumption and other factors.

5.3. Results and Discussion

5.3.1. Elastic Response Variation

Figure 5-6 shows the roof displacement, Δ_{top}, increased with reduction of base rotational stiffness relative to a fixed base structure with T_{dc} less than 1.5s, 2.4s, and 3s for K_{top}=*0, 5EI/H,* 2000*EI/H*, respectively. For T_{dc} greater than these values (1.5s, 2.4s, 3s) the displacements do not change very much from the fixed base assumption. The demands are consistent with the response spectrum of Figure 5-4, where longer periods see an increase in spectral displacement up to a true period of about 3.0s, which is consistent for the T_{dc} given. The response is greater than 2 times that of the fixed base elastic response for the column with top stiffness and short period, T_{dc} <0.8s. This difference is because of the shape of the elastic spectra is not linear with period. The case of pinned top and pinned base case is not shown in Figure 5-6, because it is statically unstable.

Figure 5-7 shows the moment demand at the top of the column, M_{top}, increases with the base flexibility when $T_{dc} < 0.8s$. Such an increase in moment increases the possibility of yielding at the top of the column, as well as the likelihood of a soft storey mechanism. This increase in moment response is consistent with the range of period causing amplification of displacement by more than 2 according to the theoretical considerations noted previously.

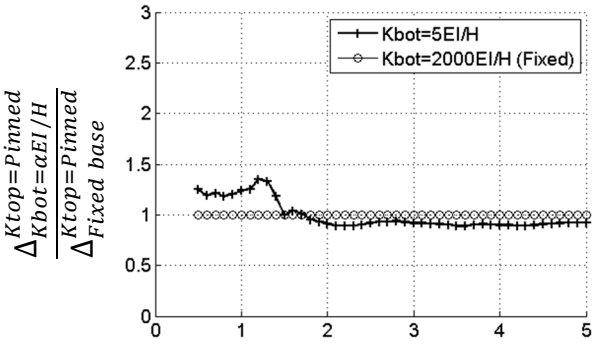

(a) Pinned top, K_{top}=0 EI/H

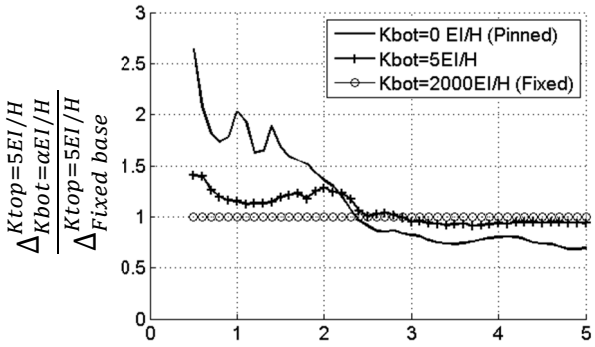

(b) K_{top}= 5EI/H

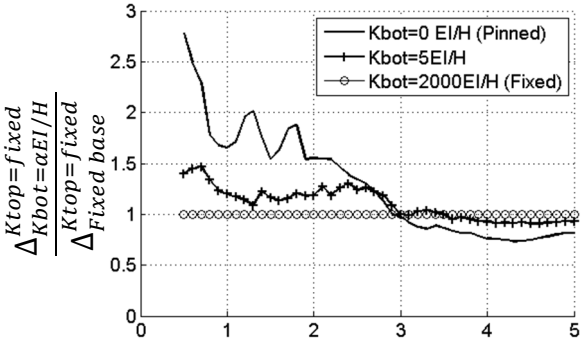

(c) Fixed top, K_{top}=2000 EI/H

Figure 5-6: The column median lateral displacement with a top flexibility of $\beta EI/H$ and the base flexibility of $\alpha EI/H$ ($\Delta^{Ktop=\beta EI/H}_{Kbot=\alpha EI/H}$) to the lateral displacement of the column that is fixed at the base with the same top flexibility ($\Delta^{Ktop=\beta EI/H}_{Kbot=Fixed}$) for various periods. β is 0, 5, and 2000 for Figures a, b, and c, respectively.

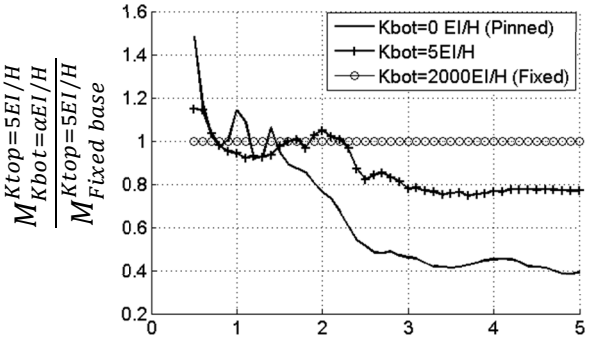

(a) K_{top}= 5EI/H

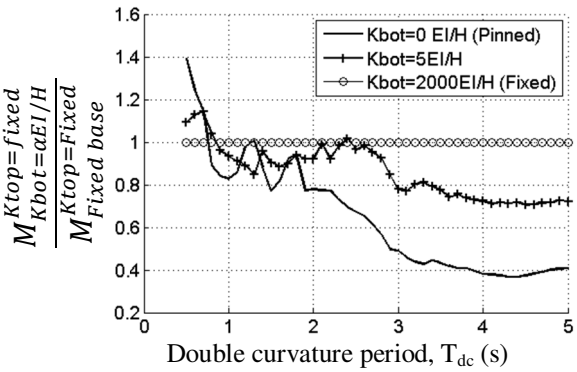

(b) Fixed top, K_{top}=2000EI/H

Figure 5-7: The column median top moment with a top flexibility of $\beta EI/H$ and the base flexibility of $\alpha EI/H$ ($\Delta^{Ktop=\beta EI/H}_{Kbot=\alpha EI/H}$) to the top moment of the column that is fixed at the base with the same top flexibility ($\Delta^{Ktop=\beta EI/H}_{Kbot=Fixed}$) for various periods. β is 5 and 2000 for Figures a, b, respectively.

5.3.2. Nonlinear Base Rotation Variation

Figure 5-8 shows the ratio of the median maximum nonlinear base rotation considering base flexibility, $\theta_{NL,Kbot}$, to that with a fixed base, $\theta_{NL,Fixed}$. The column is rotationally fixed at the top, the rotational stiffness at the base, $K_{bot}/(EI/H)$, ranges from *0EI/H to 9EI/H*, and the yield strength, M_y ranges from 0.3 to 0.9 $M_{elastic}$. In this case, M_y is computed for each record based on $M_{elastic}$ for each record. For $M_y > 1.0\ M_{elastic}$ the base performs elastically. For $M_y = 0$ $M_{elastic}$ the base is considered pinned. In both cases, there is no inelastic base rotation, so these cases were not considered.

The ratio of $\theta_{NL,Kbot}/\theta_{NL,Fixed}$ is plotted for period ranges of $0.3s \leq T_{dc} \leq 1.0s$, $1s < T_{dc} \leq 3.0s$, and $3s < T_{dc} \leq 5.0s$ in Figure 5-8. It may be seen that $\theta_{NL,Kbot}/\theta_{NL,Fixed}$ tends to increase as T_{dc} decreases, K_{bot} increases and M_y decreases. The shaded area in Figure 5-8 is the range associated with greater nonlinear rotation of the base compared to a fixed base case, where $\theta_{NL,Kbot}/\theta_{NL,Fixed} > 1.0$. This ratio increases with lower T_{dc}, and lower M_y. In the figures shown, it also generally increases with greater K_{bot} , except in Figure 5-8 where it peaks and is starting to reduce, but $\theta_{NL,Kbot}/\theta_{NL,Fixed}$ will return to unity as K_{bot} tends to infinity. This ratio is up to about 20% more than the fixed base rotation.

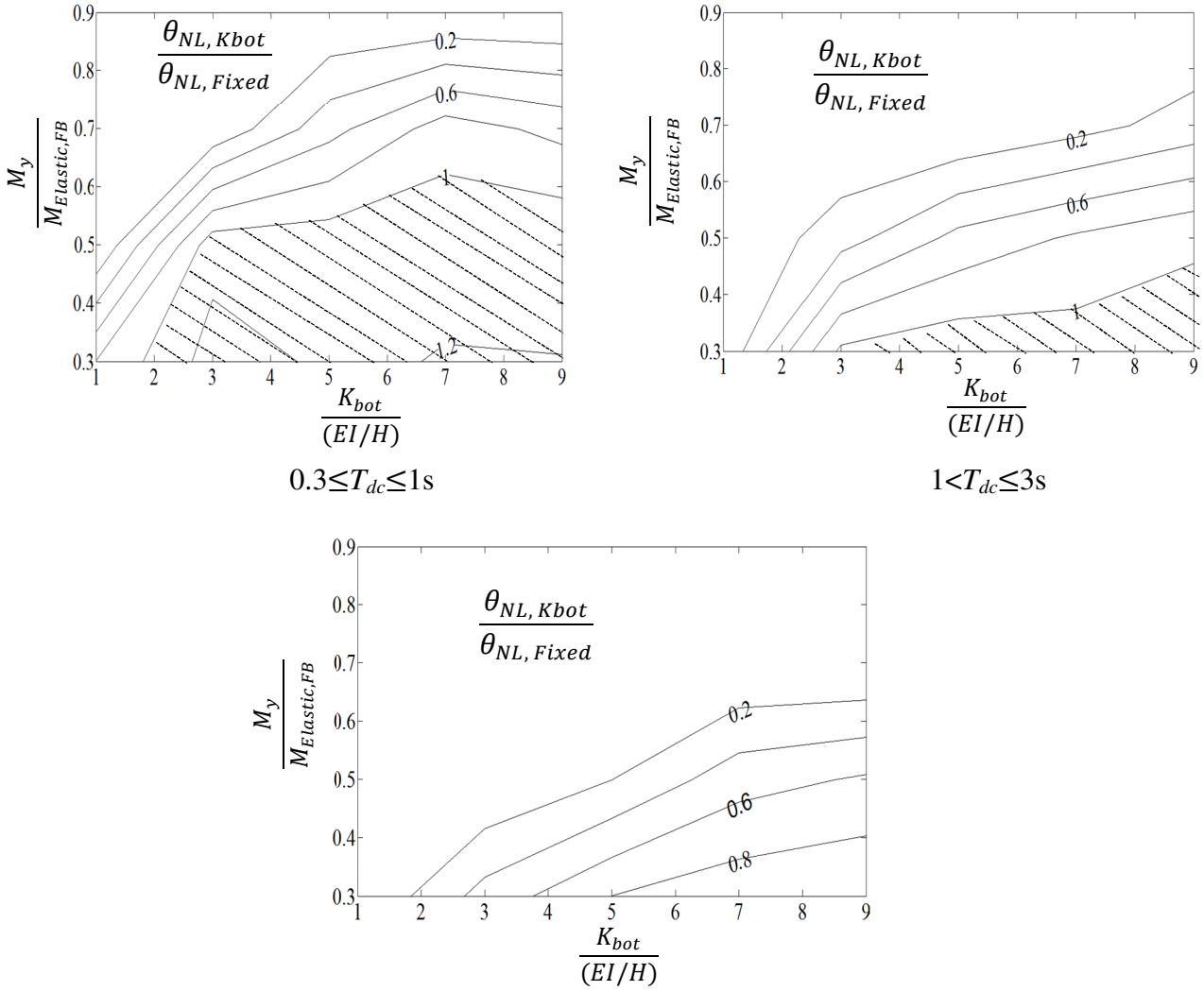

Figure 5-8: Median nonlinear base rotation ratio, $\theta_{NL,Kbot}/\theta_{NL,Fixed}$, for different base rotational stiffness ($K_{bot}/(EI/H)$) and yielding moment ratio ($M_y/M_{Elastic}$) for the suite of twenty records for three range of period: (a) is for short period structures $0.3 \leq T_{dc} \leq 1$s, (b) is for medium period range of structures $1 < T_{dc} \leq 3$s, and (c) is for long period structures $3 < T_{dc} \leq 5$s

5.4. Summary

This chapter presents linear and nonlinear spectral analyses of the impact of base flexibility on seismic demands over a suite of design level ground motions. It was found that:

1. Column base flexibility is affected by the flexibility of the column base connection, the foundation beneath the connection, and the soil supporting the foundation and can vary from being pinned to rigid. Rigid ones are likely to be embedded columns. For typical base plate connections, it is difficult to get a rotational stiffness greater than 6EI/L. Since base flexibility affects the response, it should be considered in design.

2. The amount base flexibility affects the seismic demands depends on the period of the frame, and fixities at the column ends, and strength. In particular:

   i. For top displacement of elastically responding frames, the rigid base assumption was conservative for structures with periods above 3s period for all cases. Results are non-conservative below periods of 3s for fixed top connections, reducing to 1.5s for pinned top connections. Displacements were more than twice the fixed base displacement for periods less than 0.8s.

   ii. The moment demand in an elastically responding frame at the top of the column is increased for periods below 0.8s. This behaviour is consistent with the displacement change.

   iii. The nonlinear base rotation increased by up to about 20% on average for structures with low period, moderate K_{bot} and low M_y.

For these reasons, neglecting the base flexibility effects arising from soil, foundation and base connection flexibility, can lead to non-conservative designs. In addition, nonlinear base rotation has a direct relation to the base connection damage and is not generally reduced by

the base flexibility. Therefore, base flexibility effects may not reduce damage as is often assumed.

These outcomes apply to the exposed base plate connection described in Chapters 3 and 4. They also apply to the nonlinear friction connections described in the following chapter. In particular, in the next chapter, the cyclic performance of the base connection with friction connections is described.

Chapter 6: Experimental Studies on Cyclic Performance of Column Base Strong Axis Aligned Asymmetric Friction Connections

6.1. Introduction

If all low-damage structural elements around the structure remain undamaged after an event, but column bases experience damage, it is likely that the whole structure will need to be replaced since these columns support the rest of the structure. Recently, studies have focused specifically on low-damage base connections (Tamai et al., 2003; Chi and Liu, 2012; Piluso et al., 2014). Friction devices, shape memory alloy anchor rods, and post tensioned bars with yielding plates were used in these connections. However, there is still lack of innovative base connection details, and realistic experimental tests of base connections under bi-directional loading including axial force.

One way to develop low damage base connections is to use friction, following its successful performance in beam column joints (Clifton, 2005; Latour and Rizzano, 2011; Latour et al., 2011; Latour et al., 2015) and braces (Pall and Marsh, 1982; Fitzgerald et al., 1989). In these devices, energy is dissipated by sliding friction between two surfaces in direct contact, and the sliding friction force is increased by clamping force from pre-tensioned high strength bolts. The length of sliding and the force at which the device starts to slide are the only parameters required to be calculated by the designer. These parameters are affected by the choice of friction surface due and to the clamping force impacted by the bolts. Several studies (Ratner and Sokol'skaya, 1956; Khoo et al., 2012a; Chanchí et al., 2013; Latour et al., 2014;

Khoo et al., 2012b) were conducted to evaluate the effect of sliding plate material on the performance of frictional devices. The main objective of these studies was to find shim materials that provide a friction connection with stable performance. Chanchí et al. (2012b), Loo et al. (2014), Chanchí et al. (2012b), and Khoo et al. (2014) tested friction components under large displacements with many cycles of loading compared to what they are likely to experience in severe earthquakes, and no low cycle fatigue was reported, although bolt stretch and loss of force occurred under realistic prying load inputs.

The sliding hinge joint (SHJ) beam to column friction connection is a type of low damage asymmetric friction connection (AFC) invented by Clifton (2005) and further developed by MacRae et al. (2010), as described in Chapter 2. This connection has been used in real construction for beam-column joints, rocking and column bases (e.g. Gledhill et al., 2008). However, SHJ cannot be directly used for base connections since the column bends under bi-directional response loading and also because of the applied axial force on the column. Thus, new details are required.

Therefore, there is a need to develop low-damage detailing for columns at the base of a structure by modifying the SHJ connection considering that can tolerate axial force and bi-directional bending. This chapter describes experimental tests of a column base strong-axis-aligned asymmetric friction connection, SAFC base, to:

(i) Evaluate if it can be considered low damage considering the modes of deformation involved under in-plane loading, out-of-plane loading, and 2-D horizontal deformation,

(ii) Determine if a simple model can represent the behaviour, and

(iii) Learn any new lessons about the behaviour of such columns.

6.2. Methodology

6.2.1. Design and Detailing of SAFC Base

The SAFC base connection considered in this study is illustrated in Figure 6-1. Both flanges may uplift from the base/end plate, axial force increases the flexural resistance and the column member may be subject to lateral movement in the two horizontal directions resulting in biaxial bending. These aspects make the connection different from beam-to-column SHJ connections.

In the SAFC base connection the AFCs are placed parallel to the flange. The primary moment resisting mechanisms result from friction and from the axial force. There is also moment resistance due to prying as the column bends about its strong axis. When it bends about its weak axis no prying occurs.

A shear key is provided of sufficient height to resist likely shear forces at the maximum expected uplift. The corners of the shear keys were cut on an angle to enable them to resist shear without binding and limiting column rotation. Therefore, the shear key does not affect the moment resistance.

Since yielding is not a primary energy dissipation mechanism, it offers a low amount of material damage. Such damage is likely to primarily occur in the bolts and shims that may readily be replaced after a major earthquake. The bolted connection also makes for easy straightening if there is a net base post-earthquake rotation. Hence, it is a potential low- or

no- damage connection, design.

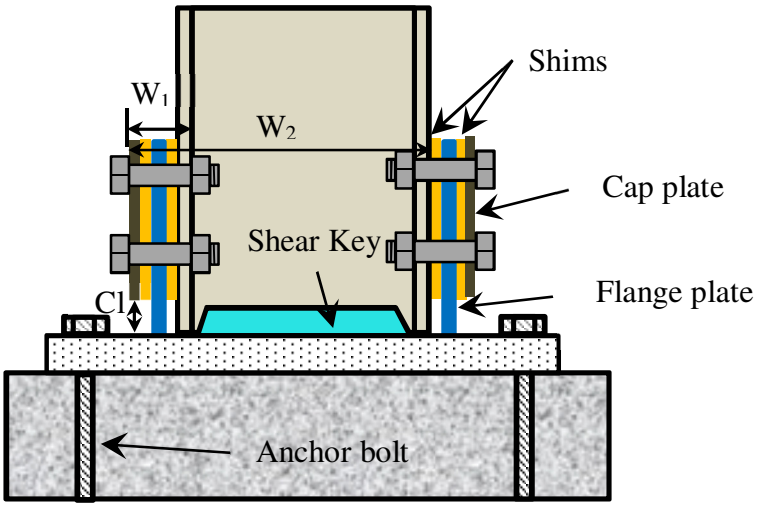

Figure 6-1: SAFC base design showing boundary plates, shear key, column, base plate, anchor rods, and clearances

The SAFC base connection shown in Figure 6-1 has the following characteristics:

i) The column and the base plate are in full contact, but without direct welding.

ii) Flange plates welded to the base plate extend on the outside of each flange to make AFC connections.

iii) Holes in the flange plates are provided with sufficient diameter to prevent the bolts from touching the flange plates during the expected lateral deformations in both directions of loading.

iv) Bisalloy500 (2012) shims are placed on the sliding surfaces either side of the flange plates, based on results from Chanchí et al. (2012b).

v) Floating cap plates are placed on the outside of the shim beside the flange plates.

vi) Grade 8.8 high strength proof loaded bolts are used for all friction connections.

vii) Shear keys are welded to the base plate, between the column flanges and on each side of the web, to provide shear resistance at the base.

The flange plate, shims, and cap plate are placed a distance *Cl* from the base plate as shown in Figure 6-1 to prevent contact with the base plate under large rotations.

The base plate and anchor rod for SAFC connection can be designed similar to the common exposed base plate and anchor rods. The only modification is the position of the tensile force is shifted from the tensile column flange to the flange plate in the tension side that is closer to the tensile anchor rods.

The mechanism of sliding for this base connection, when the column bends about the strong axis, is shown in Figure 6-2. When the base moment demand is greater than the resistance from axial force and friction on one shear plane, column base uplift occurs and sliding initiates between the column and the flange plate. At this stage, sliding does not occur between the cap plate and the flange plate. As sliding continues with increased top displacements the bolts move on an angle and provide a shear force on the cap plate, as shown in Figure 6-2. At this point, the cap plates start sliding up together with the column and prying provides the only base rotational stiffness. The prying in this base connection means prying apart of the flange plates. This mechanism can resist force even if there are no bolts. When the load is reversed, slip initially occurs on the shear plane between the flange plate and the column, as shown in Figure 6-2. For larger reverse deformation, sliding occurs on both sides of the flange plate.

Base moment resistance can be increased by changing the size and number of the bolts. To

prevent column yielding above the connection, the maximum strength at the connection should be less than the column flexural strength considering the bolt holes. For bending about the weak axis, the bolts move sideways in the holes and flange plates are not pried apart, maintaining a more constant friction force.

The column design base rotation, θ_{rock}, is estimated from:

$$\theta_{rock} = \frac{\Delta_{total} - \Delta_{FB}}{H} \quad (6\text{-}1)$$

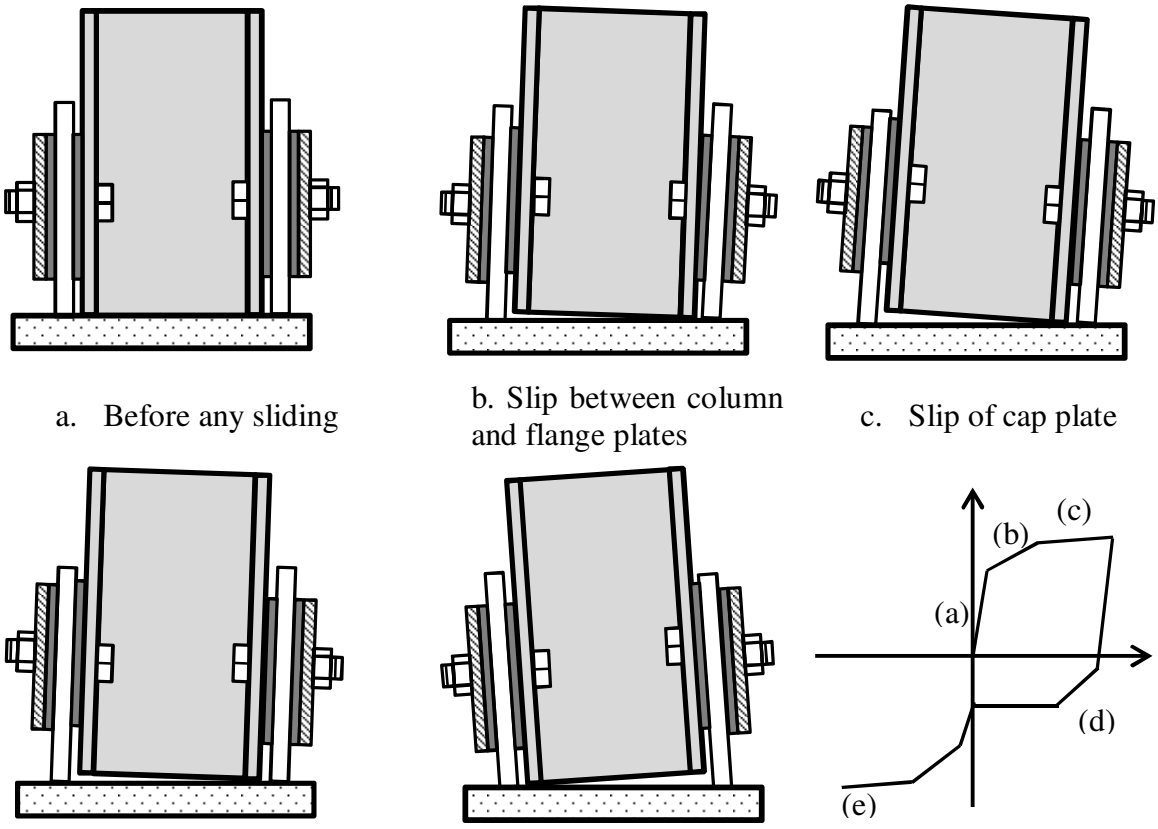

a. Before any sliding

b. Slip between column and flange plates

c. Slip of cap plate

d. Reverse loading, slip between column and flange plates

e. Maximum rotation in reverse cycle

f. Moment- Rotation

Figure 6-2: SAFC base performance with axial force

Where Δ_{total} is the displacement at the column point of inflection that is a distance H up the column from the base and Δ_{FB} is the elastic displacement of the column alone under the lateral force used to obtain Δ_{total}. For real design, the column base rotation can be determined

by structural linear or nonlinear analysis for specific performance and hazard.

Conservatively assuming that rotation occurs about the inside face of the flange, the distance/clearance *Cl* from the cap plate and shims to the base plate is given by:

$$Cl = \theta_{rock} \times W_1 \tag{6-2}$$

Where W_1 is total thickness of the shims, column flange, flange plate, and cap plate on one side of the column as shown in Figure 6-1. The diameter of the flange plate holes, *D*, is given in

$$D = 2(\theta_{rock} \times W_2) + d_{Sh} + 2mm \tag{6-3}$$

Where d_{sh} is the bolt shank diameter and W_2 is the minimum of: (i) the depth of the column plus W_1 for strong axis bending; and (ii) the distance from the flange tip to the furthest bolt for weak axis bending. When the column bends bi-directionally, the required clearance and size of the hole in the flange plate may be obtained by vector superposition of required motion in each direction.

Safety factors should be considered for size of clearances and holes to avoid contacting of the hole edges and bolts. If this displacement is exceeded during an earthquake, yielding of anchor rods can provide ductile response without residual deformation. Therefore, anchor rods can be designed to yield after AFC sliding stops to have a desirable chain of limit states and ensure a ductile response of the connection.

It is desirable to have a strong base connection to resist moment and decrease the possibility

of a soft-storey mechanism forming at the ground floor. However, the over strength of the connection should not cause significant column yielding. Based on recommendations used in construction (Leslie et al., 2013) an overstrength factor of 1.4 is reasonable. This overstrength factor is influenced by construction factors including variability of bolt tightening and different sliding surfaces. Based on this approach, the target base connection strength should be 1/1.4 that is 70% of the column flexural capacity considering axial force.

MacRae et al. (2010) and Khoo et al. (2014) proposed models for interaction of AFC bolt demands. According to these studies there is a correlation between the thickness of the plates and the resisted force.

6.2.2. Experimental Program

- **Test Specimen and Tests Run**

The test column section was a 310 UB 46.2 Grade 300 since universal beam (UB) and welded beam (WB) sections are more efficient and thus more common in drift-governed ductile moment resisting frames than universal column (UC) and welded column (WC) sections. The distance from top of the base plate to the point of lateral force application was 1980 mm. All drift values are based on this height.

The calibrated torque control method was used for tightening bolts over the sliding surfaces of the AFCs to the proof load. Simple experimental tests were carried out to determine the required torque as follows. Five specimens with total thickness equal to thickness of the plates, which was 60mm, in the friction connection were tightened with M20 Grade 8.8 bolts

torqued from 40 N.m up to 800 N.m. In each step the specific level of torque was first applied, and then the bolt elongation and turn-of-nut were recorded. The bolt axial deformation equivalent to the proof load was calculated considering threaded and shank areas and lengths and the torque corresponding to this deformation was applied to the bolts (Chanchí et al., 2012b). The applied torque at the proof load was equal to 480 N.m for the M20 Grade 8.8 bolts based on the above procedure.

The grip length is 64 mm (thickness of the plates plus washers), and M16 bolts were cut at length of 80 mm. The torque control method also provides an opportunity to estimate the nonlinear deformation of the bolts and degradation of the friction plates. This assessment was made by retightening the bolts to the target torque at the end of each test and recording the associated nut rotation. A nut rotation of 0.1 rad caused 0.03mm elongation of the bolt that approximately corresponds to 15% of the proof load for these bolts with 2mm thread pitch.

The base plate was placed on a 5mm layer of soft dental plaster to provide full contact on top of the concrete block. It was held down by 6 M24 Grade 10.9 bolts anchored at the bottom of the concrete foundation as shown in Figure 6-3. The anchor rods were post tensioned until the axial force measured by the load cells beneath the nuts was 85% of the bolt minimum proof load, while twisting of the load cells was prevented. The value of 85% is required to prevent base plate uplift. A 50mm thick base plate with post tensioned anchor bolts was used to minimise base flexibility.

Full penetration welding was used to connect the flange plate to the base plate. Using fillet welding can cause interruption of the base connection performance as the welding may prevent sliding of the shims and the cap plate for high level of rotation. In addition, the full

penetration welding can provide high resistance against applied bending and tensile demands to the flange plate compared to the fillet welding.

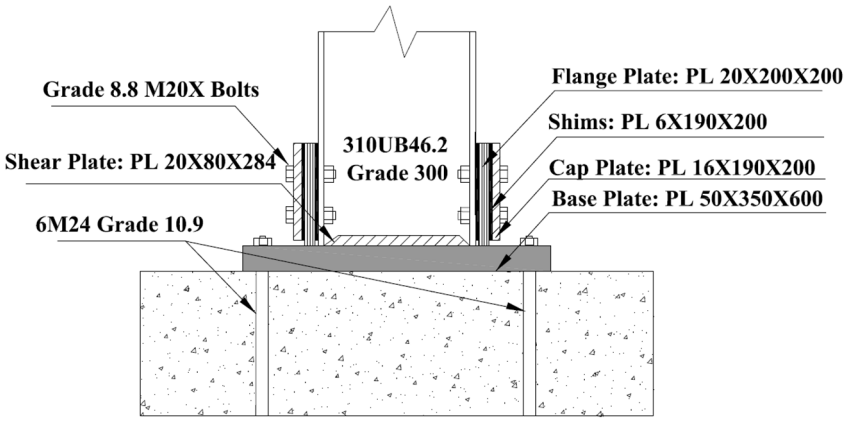

Figure 6-3: Detail of the SAFC base connection

The cyclic tests considered different numbers of bolts, axial force levels, axes of bending as shown in Table 6-1 also shows the order of the tests as conducted.

Table 6-1: Tests conducted

No	Axis of Bending	Axial force	No. AFC bolts
1	Strong	Zero	Zero
2	Strong	Zero	Four
3	Weak	Zero	Four
4	Strong	320kN (0.20Ns)	Four
5	Weak	320kN (0.20Ns)	Four
6	Bi-directional	320kN (0.20Ns)	Four
7	Strong	320kN (0.20Ns)	Zero

- **Test Setup and Loading Regime**

The loading regime and test setup are as described in Chapter 2.

- **Test Instrumentation**

Foundation rods passed through 125mm long 30mm internal diameter load cells, with a capacity of 600kN, to record the anchor rod tension force. These load cells were placed on

top of a washer that in turn was sitting on the base plate. Another washer was placed on top of the load cell below a nut at the very top, as shown in Figure 6-4.

Four linear potentiometers with 25mm stroke were attached between the column flange tips and the baseplate to monitor column vertical uplift. Two potentiometers measured movements between the cap plate and baseplate. Two other potentiometers recorded horizontal deformation of the top of the flange plate. One was connected between a vertical support at the middle of the baseplate and the flange plate, and the other connected tops of the flange plates. One more potentiometer on top of the base plate captured base plate uplift relative to the concrete block.

Some of these sensors are shown in Figure 6-4. Strain gauges with 6mm gauge length were also used in the column flange, and the flange plates. These last sensors were used to record any localised strain in these components.

Since small (washer sized) load cells to record bolt tensile force during and after cyclic loading was not available, it is not possible to verify the bolt interaction models that were suggested by MacRae et al. (2010) and Khoo et al. (2014).

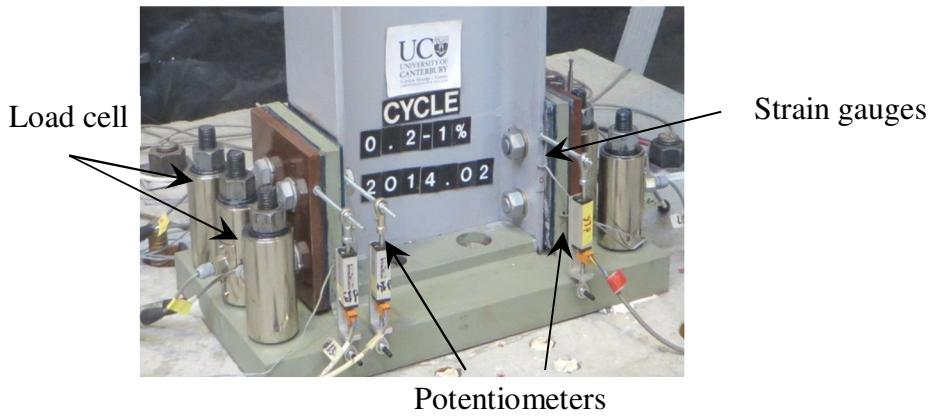

Figure 6-4: Instrumentation of the WAFC base connection

6.2.3. Analytical Predictions of Behaviour

In each test, the lateral force versus top displacement of the column was captured. The base moment and rotation were predicted using:

$$M_{Base} = V \times H_{Col} \tag{6-4}$$

$$\theta_{Base} = (\Delta_{top} - \frac{V \times {H_{Col}}^3}{3 \times E_{Col} \times I_{Col}}) \times \frac{1}{H_{Col}} \tag{6-5}$$

Where M_{Base} is base moment, V is lateral force applied, H_{Col} is the column height from the top of the plate to the point of lateral force application, θ_{Base} is the base rotation, and Δ_{Top} is the column top displacement. The shear deformation was ignored as it is small in long I-shaped members.

The sliding, prying and axial force are three mechanisms that provide moment resistance in this base connection, as shown in Figure 6-5. The nominal sliding force for each AFC bolt was calculated by (MacRae et al., 2010):

$$F_S = \mu \times \eta \times N_{tf} = 0.21 \times 2 \times 145 = 60.9\ kN \tag{6-6}$$

Where F_s is the sliding force of each bolt, μ is the friction coefficient, η is the number of shear planes, and N_{tf} is the proof load per bolt. The friction coefficient of steel on Bisalloy 500 is equal to 0.21 according to Chanchí et al. (2012b).

The maximum base moment from lateral loading causing strong axis bending, M_{Tot}, is defined:

$$M_{Tot} = M_{Slide} + M_{Prying} + M_{Axial}$$
$$= (n_{Bolt} \times F_S \times d) + \left(\frac{\theta_{Base} \times 3EI_{fp}}{H_{fp}}\right) + (P \times D_{Axial}) \quad (6\text{-}7)$$

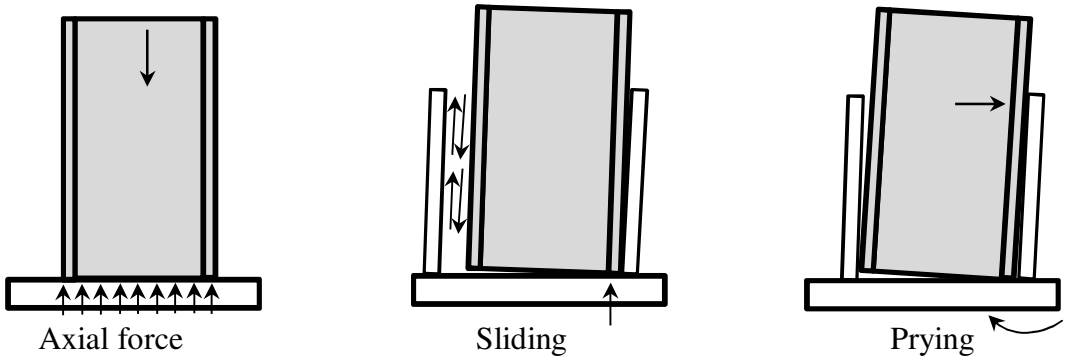

Figure 6-5: Mechanisms of load transfer at the base connection that are axial force, sliding, and prying from left to right, respectively.

Where M_{Slide} is the moment resulting from sliding friction, M_{Prying} is the elastic prying moment mainly from flange plate bending on the compression side of the column, and M_{Axial} is the moment from axial force. In Equation 6-7, n_{Bolt} is the number of the bolts in each AFC, F_s is the sliding force for each bolt as defined in Equation 6-6, θ_{Base} is the base rotation from Equation 6-5, H_{fp} is the distance from the top of the flange plate to the base plate, I_{fp} is the second moment of area about the weak axis of the flange plate, d is distance from the sliding bolts to the neutral axis, and D_{Axial} is perpendicular distance from the centre of axial force to the neutral axis.

For a member subject to a bidirectional displacement with loading components in the x and y directions, Δ_x, Δ_y and axial force N, it is often desired to obtain the moments M_x and M_y. This calculation is done by first taking the orientation of the neutral axis Θ perpendicular to bidirectional displacement, as shown in Figure 6-6. When moment is applied about the X

axis, Θ is equal to zero, and it is 90 degrees for moment about the Y direction. Iteration is conducted on the neutral axis depth, *c*, until the area of the compression side of the section, all at the yield stress as is commonly assumed in plastic design, resists the axial force, *N*. Such an assumption is appropriate when the friction forces on either side of the neutral axis have similar magnitude but opposite directions.

For weak axis bending, since only the AFCs in tension side slide, their sliding force should be added to the axial force for calculation of the neutral axis. Moments can then be obtained by summing forces multiplied by the distance about the neutral axis. Overstrength stress can also be used to compute overstrength actions.

The column base uplift displacement, Δ_{Uplift}, is thus given by:

$$\Delta_{Uplift} = \theta_{Base} c_{Tens} \tag{6-8}$$

Where c_{Tens} is the distance perpendicular to the neutral axis to the extreme fibre of the section on the gapping side, as shown in Figure 6-6.

Column base rotation may also be measured directly from the potentiometer readings at the base according to:

$$\theta_{Base} = \frac{\Delta_{Up} - \Delta_{Down}}{x_{UD}} \tag{6-9}$$

$$c = \Delta_{Down}/\theta_{Base} - x_{cp} \tag{6-10}$$

Where x_{cp} is the distance between the extreme fibre of the section and the position of the potentiometer measuring compression perpendicular to the neutral axis, Δ_{Down}. The uplift

displacement at the extreme tension side of the specimen, Δ_{Uplift}, is again given by Equation 6-8 using the experimental definition of the neutral axis.

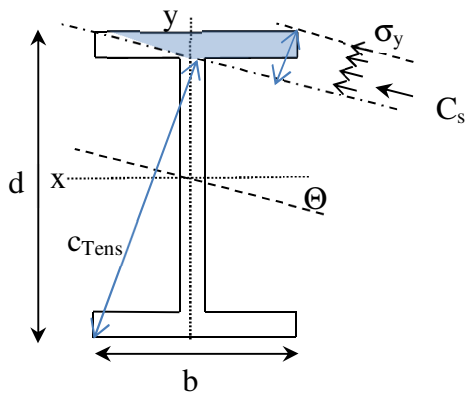

Figure 6-6: Section analysis of the column under bi-axial bending

When the column bends about the weak axis, prying effects, M_{prying}, do not contribute to the lateral resistance. Thus, the maximum base moment, when the column bends about its weak axis, M_{tot}, is the sum of the sliding moment, M_{slide}, and the moment from axial force, M_{axial}, defined in Equation 6-7. These equations are thus generated to both directions of loading.

For each test, a base moment-rotation curve is plotted. On this plot a bilinear curve is shown using the predicted values calculated using Equation 6-7. The base connection is assumed to be rigid with infinite stiffness before column sliding occurs, and the second line connects the first point to the maximum moment at 4% drift.

Predicted and experimental base moment, M_{Base}, column uplift, Δ_{uplift}, and neutral axis position, c, at 4% drift are also compared. For the bi-directional tests, a solid line gives the section capacity assuming it yields in axial tension and compression according to the alternative method in NZS3404 (2007). It can be regarded as an upper bound on the sliding/rocking capacity.

The proposed backbone curve is a simple estimation of the base friction performance with two lines. Some simplifying assumptions were made to present this method. The main objective is to develop a model for simple analyse and design of the base with AFCs. It is assumed the base acts rigidly up to the sliding in one side of AFC and the sliding on both sides of AFC occurred at the third point of backbone curve with the ultimate base rotation. Also, the resisting moment from axial force, sliding, and prying were considered in the simple backbone curve. Alternatively, the complex backbone curve will be presented for more precise design and modelling of friction base connections in Chapter 8. The stiffness from the flange plate on the tension side and bolt deformation in addition to the prying, axial force and friction sliding are considered to develop the full macro model. Furthermore, the performance of the base in the complex model are defined over four stages that are (i) before sliding (ii) initial sliding (iii) bearing-sliding (iv) cap plate sliding.

6.3. Results and Discussion

6.3.1. Test Summary

Table 6-2 summarizes the experimental test actions compared to the predicted values for recorded moments, M_{base}, about the X , and Y directions, position of the neutral axis, c, and column uplift, Δ_{uplift} for 4% drift. For bi-directional bending, Test No. 6, these values are presented for 4% drift in the X direction and 2.5% in the Y direction. These results are discussed in the following sections for the individual tests.

Table 6-2: Predicted and recorded actions for Tests No. 1 to 7

No	Bending Axis	Axial Force	No. AFC bolts	$M_{X,base}$, kN.m		$M_{Y,base}$, kN.m		c, mm		Δ_{uplift}, mm	
				Pred*	Expt*	Pred	Expt	Pred	Expt	Pred	Expt
1	Strong	Zero	Zero	11	11	0	0	0	0	12	12
2	Strong	Zero	Four	89	80	0	0	0	0	11.7	11
3	Weak	Zero	Four	0	0	40	31.64	0	0	4.2	4.8
4	Strong	320kN	Four	140.5	135	0	0	6	12.46	10.8	10.11
5	Weak	320kN	Four	0	0	35.5	39	74	67	3.2	2.75
6	Bi-directional	320kN	Four	145	127	35	26	29.5	19.7	11.52	10.5
7	Strong	320kN	Zero	62.6	68	0	0	6	19	11.53	10.56

* Pred: predicted value, Expt: recorded value from the experimental test

6.3.2. Test No. 1 - Strong Axis Bending without Axial Force and AFC bolts

At small levels of drift there is no initial resistance from bolts or axial force on the column to restrict the possibility of the column rocking over. Once rocking starts, resistance is provided by prying with the top of the flange plate on the compression side of the column and the bottom of the flange plate on the tension side. From the column base moment-rotation curve in Figure 6-7 it may be seen that some energy is dissipated, and that reloading occurs on the same loading curve as previously in the small magnitude cycles. This response indicates that no permanent damage or yield occurs. Instead, this energy is likely to be related to friction at the compressive interfaces between the column and flange plate where horizontal prying forces are developed due to vertical sliding at these locations.

During the larger magnitude cycles, some yielding occurs resulting in gapping near the zero displacement position. This yielding was also seen from the tests where the tops of the flange

plates moved apart by 2.5mm. The neutral axis depth is zero as there are no vertical forces on the column. The base rotation is almost equal to the applied column drift of 4% since there was little moment resistance at the base so the column moved over like a rigid body.

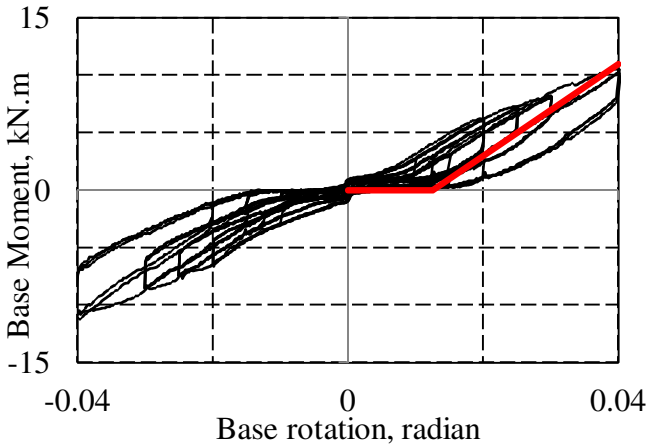

Figure 6-7: Moment-Rotation diagram of the base bending about the strong axis without AFC bolts and a red line showing the predicted performance from the described method in Section 6.2.3

The solid line in Figure 6-7 is obtained differently from the other tests because there is no initial moment resistance for that part. The prying rotational stiffness, M_{Prying}/θ_{base} calculated form Equation 6-7, and is drawn through the point of peak response to the zero moment line. The flat part of the curve between the rotations obtained of about 1.25% is an indication of the range of rotation where there is no rotational stiffness after prying yielding of the flange plates. The predicted quantified values in Table 6-2 generally match the experimental ones.

6.3.3. Test No. 2 - Bending without Axial Force (4 bolts in each AFC)

Figure 6-8 indicates the recorded base moment at 4% drift of 80 kN.m. This base moment is more than 7 times stronger than that of the previous specimen that resisted by prying alone. It was also 34% of the column gross section moment capacity assuming yielding in tension and

compression, which is 233 kN.m. Cap plate sliding initiated at 2% drift. No paint flaking was observed in the column and boundary plates and strains were less than the yield strain indicating likely elastic behaviour.

As larger drift cycles were applied, the base moment resistance at zero displacement increased compared to previous cycles to the same level of displacement. The reason for this is unclear. After testing, when the nuts were re-tightened with the torque wrench, the nut rotation was less than 0.1 rad, indicating no significant loss in post-tensioning, which was less than 15% of the bolt proof load. The predicted and recorded neutral axis depth, *c*, was again zero in this test because the tension and compression in the friction connections on the different sides of the specimen had approximately the same magnitude. The difference between predicted base moment and that from the experimental test at 4% drift is 10% and the predicted matched the recorded uplift within 6%, as recorded in Table 6-2. Possible reasons for 10% difference of base moment could be the bolts were tightened lower than the proof load level.

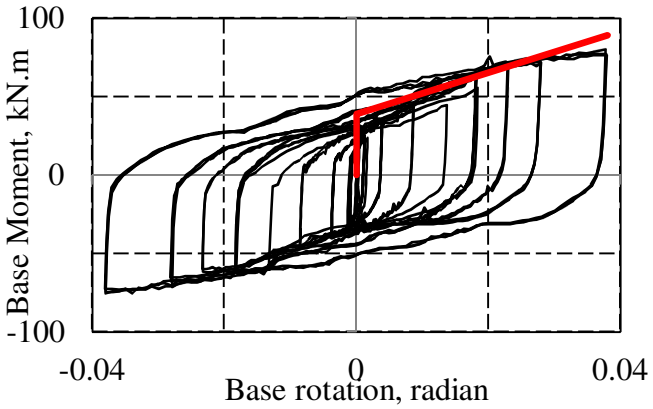

Figure 6-8: Moment-Rotation diagram of the base bending about the strong axis, where the red line is the predicted performance from the described method in Section 6.2.3

6.3.4. Test No. 3 - Weak Axis Bending without Axial Force (4 bolts in each AFC)

The maximum base moment due to weak axis bending was 31.6 kN.m, as shown in Figure 6-9. This is 40% less than the nominal moment capacity of the column section, which is 52 kN.m, and 39% of the strong axis strength. No paint flaking was observed on the column surface. When the bolts were retightened, no nut rotation was observed under applied torque. Since only bolts on the tension side slid, as shown in Figure 6-5, the centroid of the sliding force on the tension side occurs at the centre of the tension flange plate. This tension force is balanced by additional compression on the compression side of the column, as shown in Figure 6-5. However, since no axial force was applied to the column, a gap between the base plate and the column occurred by increasing the level of drift, and the neutral axis length was zero.

In the strength prediction it was assumed that sliding on two friction surfaces may occur. However, the cap plate did not slide during the test indicating that the full sliding strength on the second surface was not reached. This behaviour may be the reason for the 20% difference between the strengths as shown in Figure 6-9 and Table 6-2.

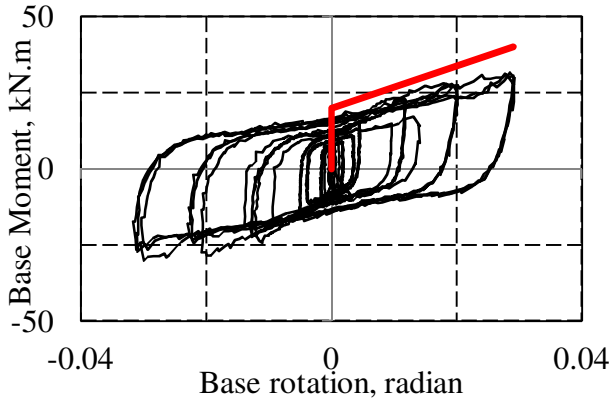

Figure 6-9: Moment-Rotation diagram of the base bending about the weak axis and a red line showing the predicted performance from the described method in Section 6.2.3

6.3.5. Test No. 4 - Strong Axis Bending with Axial Force (4 bolts in each AFC)

The maximum moment of 135kNm in Figure 6-10 is 70% of the nominal section moment capacity considering axial force, which is 192 kN.m, according to NZS3404 (2007) with the column section carrying tensile and compressive stresses. It is also 69% greater than that of the member without the 20% axial force ratio. The calculated self-centring base moment from both axial force and the prying effect, 61.5 kN.m, is smaller than the sliding moment, 76.5 kN.m, in Equation 6-7. This result indicates that the applied axial force is not sufficient for self-centring and it is consistent with the unloading from the negative displacement direction, where there is rotation at zero moment.

The cap plates slid at 2.25% drift. No yielding was indicated by the gauges and no paint flaking was observed in the column or any connection elements. No rotation occurred under the design torque when retightening the bolts at the end of the test. The flange plates also stayed vertical and did not move apart indicating that there was no permanent deformation.

Base moment and uplift at 4% drift were predicted to an accuracy of 4% and 6%. However, the neutral axis depth, c, was twice that predicted indicating that at this stage the force in the tension side friction connection was greater than in the compression side. The discrepancy in c does not have a significant effect on the uplift or strength.

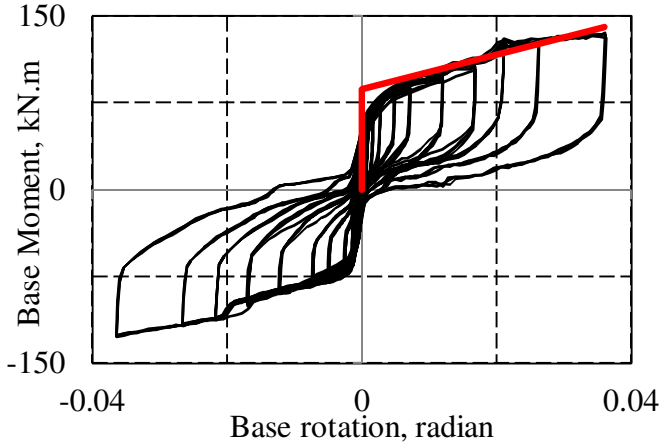

Figure 6-10: Moment-Rotation diagram of the base bending about the strong axis under axial force where the red line is the predicted performance from the described method in Section 6.2.3

6.3.6. Test No. 5 - Weak Axis Bending with Axial Force and 4 bolts in each AFC

The peak moment capacity of 39kNm, shown in Figure 6-11, was increased 23% by the presence of the 20% axial force ratio making it 90% of the nominal plastic section tension compression capacity considering axial force. For this axially loaded column bending about the weak axis, when the lateral force was reduced from the peak displacement, the rotation at the column base increased, as shown in Figure 6-11. This behaviour occurred even though the displacement at the loading point reduced. The reason is that during this unloading the elastic displacement of the column alone started to decrease making the column become straighter.

The effect of straightening, causing the base rotation to increase, was more significant than the effect of the decrease in displacement at the loading point that causes the column base rotation to decrease. The sliding force in the tension side was added to the axial force for calculation of the neutral axis as described before. The paint flaking was observed from 3%

drift that shows column flanges started yielding, but no other yielding was observed in the base connection or bolts. The base moment is under-predicted by 10% at 4% drift, and the difference between the positions of neutral axis, and the uplift is less than 10% in Table 6-2.

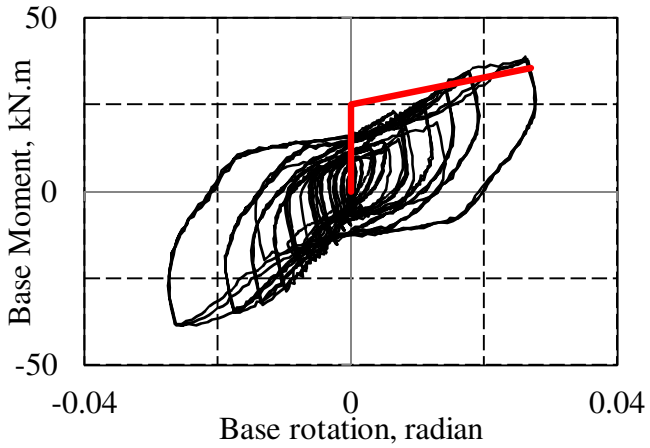

Figure 6-11: Moment-Rotation diagram of the base bending about the weak axis under axial force and a red line showing the predicted performance from the described method in Section 6.2.3

6.3.7. Test No. 6 - Bi-directional Bending with Axial Force and 4 bolts in each AFC

Figure 6-12 shows the predicted, capacity and experimental results of x-moment / y-moment interaction diagram considering the applied axial force. The moment is always less than that flexural capacity of the section assuming the gross section carries force in tension and compression the NZS3404 (2007) alternative method. The moment interaction curve is not symmetric as a result of load path dependency effects. For example, when $\Delta_x < 0$ the graph is not a smooth curve because the displacement was first increased in the Y direction and then in the X direction. In contrast, for $\Delta_x > 0$, displacement was first increased in the X direction and then in the Y direction resulting in a smoother curve. The calculated strength was obtained using Equation 6-7 considering interaction between the axial force and moments in

the 2 directions, but without considering load-path effects. The experimental moment at 4% drift in the *X* direction and 2.5% in the *Y* direction were 12% and 25% less than the predicted moments respectively possibly due to load path effects. The uplift was 8% less than predicted, and the neutral axis depth about 30% less than predicted.

During lateral loading it is possible that the centre of horizontal shear resistance at the base of the column may be on one corner, and may not line up with the centre of horizontal force at the top of the column. This non-alignment means that the column wants to twist. In the experiment, this twist is restrained by the two actuators in the column weak axis direction. The difference between the actuator loads at 4% drift in the *X* direction and 2.5% in the *Y* direction was 3.53 kN. This causes a 2.1kN.m twisting moment, over the column, which in addition to the load-path effects, causes the experimental moments to be less than that predicted. By assuming the shear resistance at the corner of the column and the applied force at the column section the twisting moment is equal to 2.92 kN.m. The twisting moment at the top of many similarly deforming columns in a building causes an additional building torsion. This building torsion related to the member deformation is in addition to that commonly considered a result of plan irregularity and ground motion.

The column base sustained up to 4% bi-directional drift under axial load without any damage to interrupt performance. The cap plate started to slide at 2% drift and the column flanges yielded at 2.5% drift as paint flaking was observed. However, no web or flange buckling was observed, and all of the flanges plates that are welded to the base plate showed no sign of yielding by observing no paint flaking.

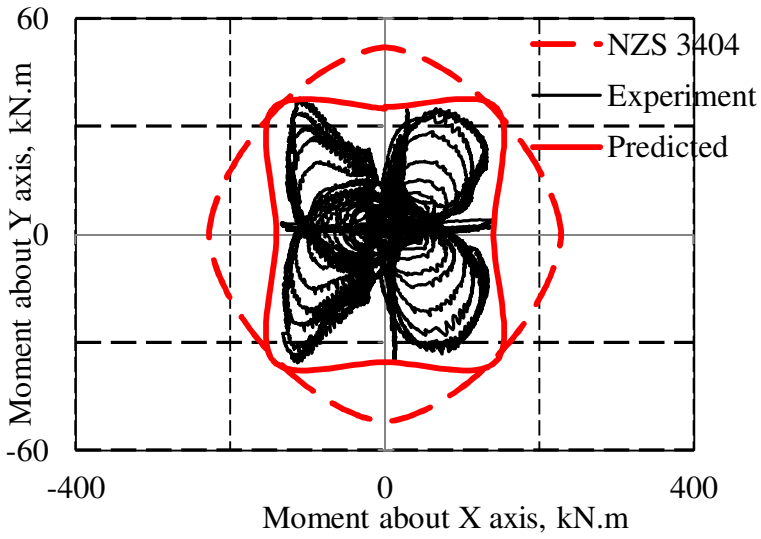

Figure 6-12: Moment-Rotation diagram of the base bending bi-directionally under axial force where a red line showing the predicted performance from the described method in Section 6.2.3 and the dashed red line is the flexural capacity of the section

A tear occurred at the connection of the web to the flange at 3% drift of bi-directional loading, as shown in Figure 6-13. The flange and web either side of the fracture were pushing on the shear key causing large tension strains at that location. It should be noted that there was no obvious change in global behaviour as a result of this tear. The shear that is provided by the flange plate and the friction of the column and the base plate can provide enough shear resistance against the lateral loading. Therefore, the shear keys can be removed.

Figure 6-13 shows the corner plastic compressive deformation of about 2mm at the flange tips after 4% clover leaf loading. The maximum flange tip deformation occurred in these cycles because all of the axial force needed to be resisted by the flange tip in some of the loading directions. Thus, the column and the base plate mainly contact at web-flange intersection, and the new position of contact caused changing of the neutral axis position from the predicted position.

a. Tear in the section

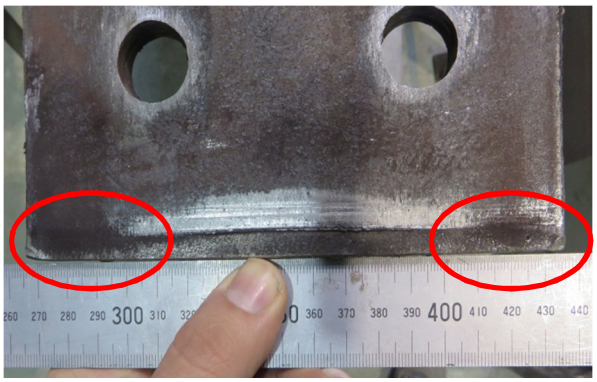

b. Localized compressive plastic deformation at the flange corners

Figure 6-13: Column section after bi-directional test. The left picture shows the tear in the column section, and the right picture shows the localized compressive plastic deformation at the flange corners

The bolts were retightened after the test to 480 N.m applied torque, and a nut rotation of 0.17 rad was recorded. This rotation indicates a loss equivalent to 25% of the proof load during testing. Although it was expected that some degradation occurred due to this nut rotation, there was no apparent strength loss shown in the hysteresis loop of Figure 6-12.

Shims and bolts after bi-directional loading cycles are shown in Figure 6-14. The level of degradation was small and the shims felt smooth with no gouging. In addition, there was no obvious deformation in the proof-loaded bolts.

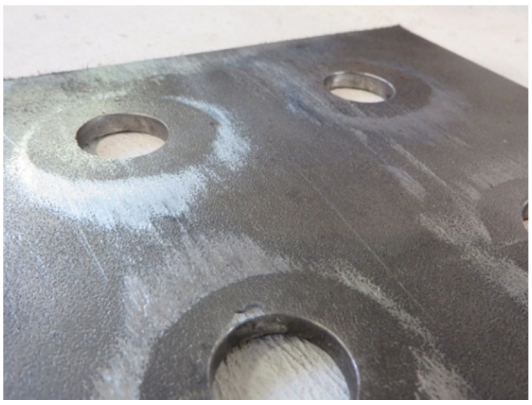

a. Tested shim

b. Tested bolt

Figure 6-14: Degraded shim is on left and the right picture shows the proof-loaded bolts after test

6.3.8. Test No. 7 - Strong Axis Bending with Axial Force and without AFC Bolts

In this final test, there were no bolts to provide additional strength and energy dissipation so non-linear elastic response was expected with a high initial stiffness before uplift, as described by the bilinear curve in Figure 6-15. However, the experimental results indicated that there was a low initial stiffness. The main reason is that the test was conducted after the bi-directional test where significant yielding of the flange tips had occurred. As a result the main contact points between the column and base-plate are at the points of web-flange intersection. Thus, the neutral axis is significantly further from the calculated location for a pristine specimen.

The experimental strength is 8% greater than predicted. This occurs possibly as a result of prying friction that was not considered in the calculations. In addition, the uplift prediction was reasonable. After the test, no paint flaking on the column was observed, which shows the column remained elastic.

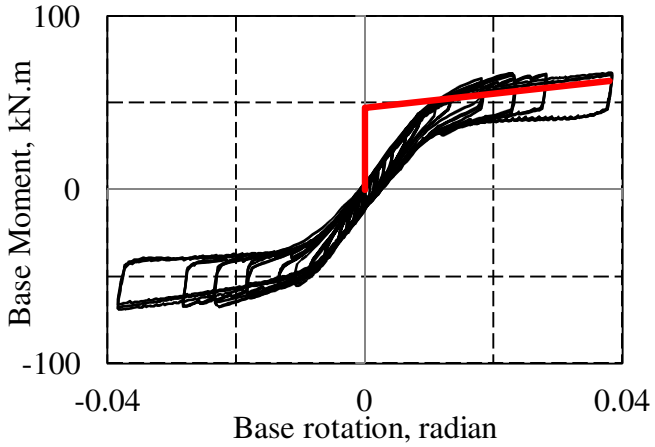

Figure 6-15: Moment-Rotation diagram of the base bending about the strong axis without bolts and a red line showing the predicted performance from the described method in Section 6.2.3

6.4. Summary

This chapter describes the design and experimental testing of column base strong axis aligned asymmetric friction connections (SAFC) bending about their strong and/or weak axis and subject to an axial force ratio of zero or $0.20Af_y$. It was shown that:

- Several cycles to a drift of 4% in strong and weak axis directions were obtained without significant damage. Cycles with axial force in a clover leaf pattern resulted in deformation of the flange tips that reduced the initial stiffness. In addition, a fracture occurred at the web-flange intersection during the bidirectional loading but this did not affect global behaviour. It is anticipated that the column would have been able to undergo significantly more cycles of displacement reaching the same loads without requiring replacement.

- A simple procedure to estimate the strength of this base connection was developed and verified experimentally. The predicted moment resistance varies from the experimental tests by an average of approximately 10%. This approach is thus simple and suitable for design.

- A new torsional demand on a column is described. It occurs because during bidirectional displacements, the centre of column base horizontal shear resistance may not be aligned with the applied shear force. The eccentricity of these forces causes a twisting moment on the column as was observed from the experiments. If many seismic columns deform similarly in a structure, this will cause a tendency for the

floor to twist. Therefore, in addition to torsion introduced by plan irregularity, and ground motions with a torsional component, there is also a torsion that can be caused by the characteristics of the members.

In the next chapter, the experimental testing of the column base weak axis aligned asymmetric friction connections (WAFC) subject to strong axis, weak axis and clover-leaf cyclic loading with and without axial force is described.

Chapter 7: Experimental Studies on Cyclic Performance of Column Base Weak Axis Aligned Asymmetric Friction Connection

7.1. Introduction

The other alternative to Chapter 6 for placement of the AFCs is the weak-axis-aligned asymmetric friction connection (WAFC) base. In this case, when the column bends about the weak axis, prying of the boundary plates provides moment resistance in addition to the moments from axial force and sliding. In contrast, this prying effect does not affect the base moment resistance when the column bends about the strong axis for the WAFC. Therefore, there is also a need to determine how this WAFC connection behaves in a low damage base configurations. This chapter describes experimental tests of column base weak axis aligned asymmetric friction connections (WAFC) to:

(i) Evaluate whether or not WAFC base connections can be considered low-damage considering the modes of deformation involved under in-plane loading, out-of-plane loading, and other 2-D deformation,

(ii) Determine if a simple model can be developed to represent WAFC mechanical behaviour,

(iii) Learn new lessons about the behaviour of WAFC column bases in the building.

7.2. Methodology

7.2.1. Design and Detailing of WAFC

The WAFC configuration is detailed in Figure 7-1 where the column and base plate are connected together by four AFCs. In each AFC, one plate is welded to the column, denoted the *column plate*, and a steel plate with oversized rounded holes welded to the base plate, denoted the *flange plate*. The round holes in the flange plate are sized to allow rotation of the column base relative to the base plate during strong axis bending, as well as for the deformations during weak axis bending.

Bisalloy500 shims, with high Brinell Hardness of 500, good abrasion resistance, and tensile strength of 1400 MPa are placed on all sliding surfaces to ensure stable hysteretic behaviour. According to Chanchí et al. (2012b) the static friction coefficient of Bisalloy500 on mild steel is 0.39, and the dynamic friction coefficient is 0.21. Khoo et al. (2014) defined the effective coefficient of friction for AFC. This definition seems more reasonable as no drop of sliding force occurred after the onset of sliding of in the AFC in past cyclic tests. This phenomenon indicates that the changing of states before and after sliding is not accompanied by changing of the friction coefficient as the sliding force was constant after the initial sliding.

Finally, a floating cap plate is placed on the inside of the flange plate and is connected to the rest of the joint with bolts. All plates are connected with Grade 8.8 high strength bolts.

The flange plate, shims and cap plate are placed a distance "*Cl A*" from the column face, as

shown in Figure 7-1. This distance is sufficient to prevent contact between the flange plate and column under large biaxial rotations. Clearance "*Cl B*" is provided to prevent contact between the column plate, shims, and cap plate with the base plate during expected weak axis rotations.

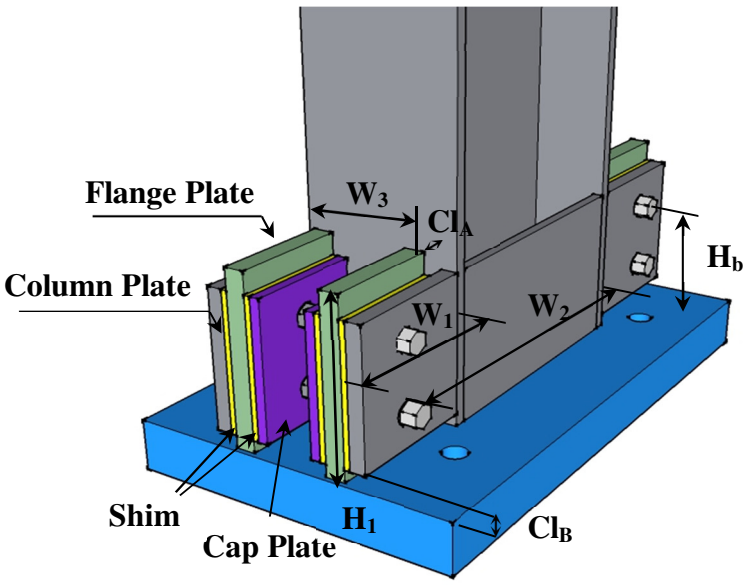

Figure 7-1: WAFC base showing boundary plates (shims, flange plates, column plates), column, base plate and clearances

The applied demands for design of the base plate and the anchor rods are shown in Figure 7-2. The over strength of 1.4 should be applied to the sliding force according to section 6.2.1 for design of the base plate and anchor rods.

The base connection sliding mechanism under column strong axis bending is shown in Figure 7-3. The column starts from its at-rest condition. When the base moment becomes equal to the frictional resisting moment on one shear plane, the column plates start sliding relative to the flange plate, as shown in Figure 7-3. At this stage, the cap plate does not slide. As top displacement of the column is increased, the AFC bolts become inclined, rather than

straight, providing a shear force on the cap plate-flange plate interface, pulling the cap plate and allowing it to slide. The shear force is twice the required shear for sliding on only one shear plane. When all column and cap plates start sliding, the rotational tangent stiffness at the base is 0. When the load is reversed, slip initially occurs on the shear plane between the flange plate and the column plate. For larger reverse deformation, sliding occurs in both sides of the flange plate and the tangent rotational stiffness is again equal to 0.

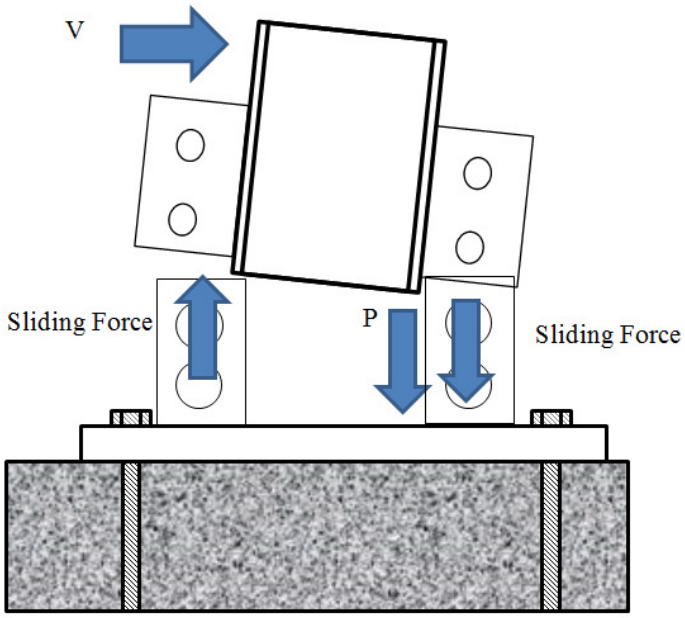

Figure 7-2: Applied demands for design of base plate and anchor rods of WAFC base

The base moment resistance can be increased by changing the size and number of bolts. To prevent column yielding, the sliding strength should be less than the column strength. Thus, the bolt size and number are influential design parameters.

Under column weak axis bending, the main difference compared to strong axis bending of WAFC is the additional prying effect of the flange plates as the column rotates about a point near the flange tips, as shown in Figure 7-4. This prying effect causes an additional elastic

stiffness in the moment-rotation behaviour that can be seen as the post-elastic stiffness after full sliding initiates. Otherwise, the onset of sliding at the different interfaces is similar, between strong and weak axes of WAFC.

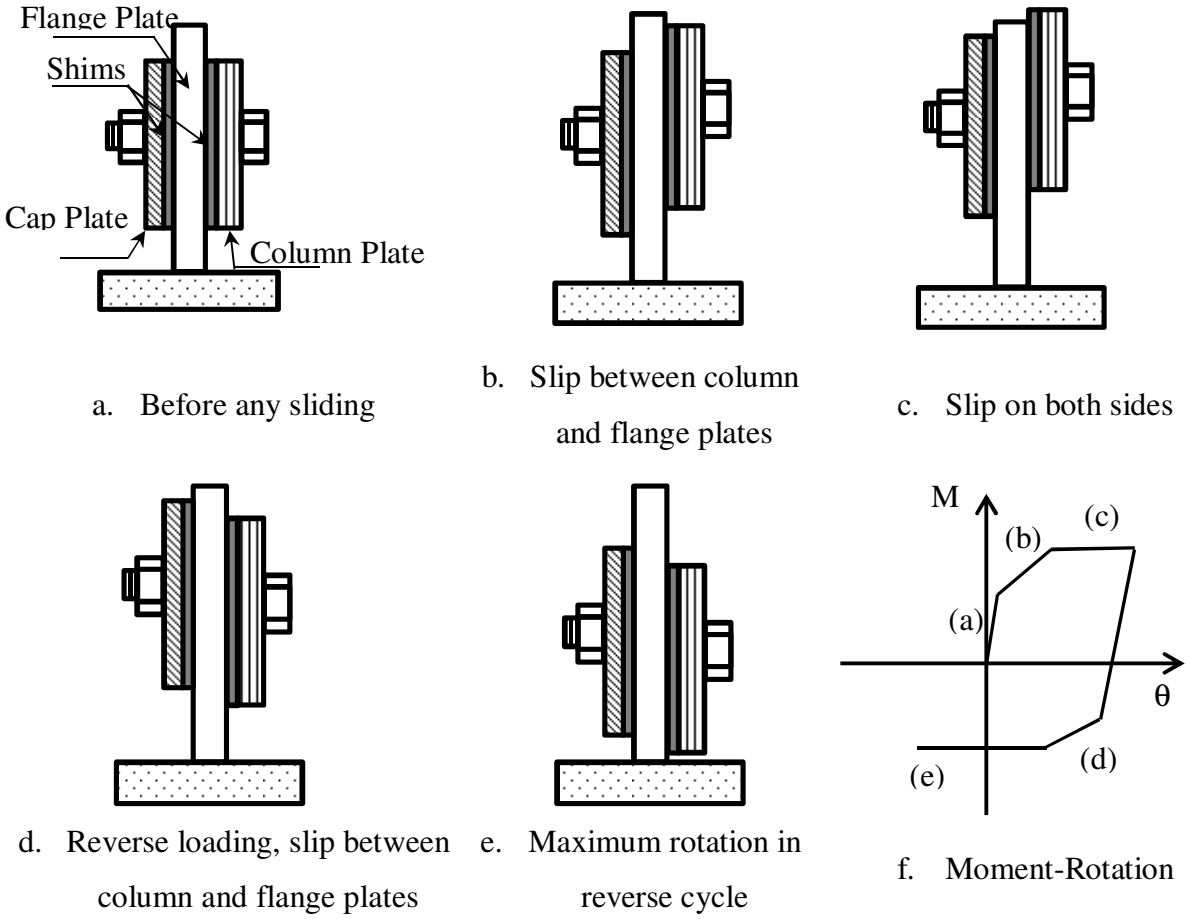

a. Before any sliding

b. Slip between column and flange plates

c. Slip on both sides

d. Reverse loading, slip between column and flange plates

e. Maximum rotation in reverse cycle

f. Moment-Rotation

Figure 7-3: WAFC column base behaviour due to bending about column strong axis

For design, the base rotation, $\theta_{rock,}$ under the applied lateral force is defined:

$$\theta_{rock} = \frac{\Delta_{total} - \Delta_{FB}}{H} \quad (7\text{-}1)$$

Where Δ_{total} is maximum design displacement, Δ_{FB} is the elastic column displacement alone under the same lateral force, and H is the distance from the base plate to the point of contraflexure in a strong-axis, x, or weak axis, y, loading direction. These rotations are

designated as θ_{rockx} and θ_{rocky}, respectively.

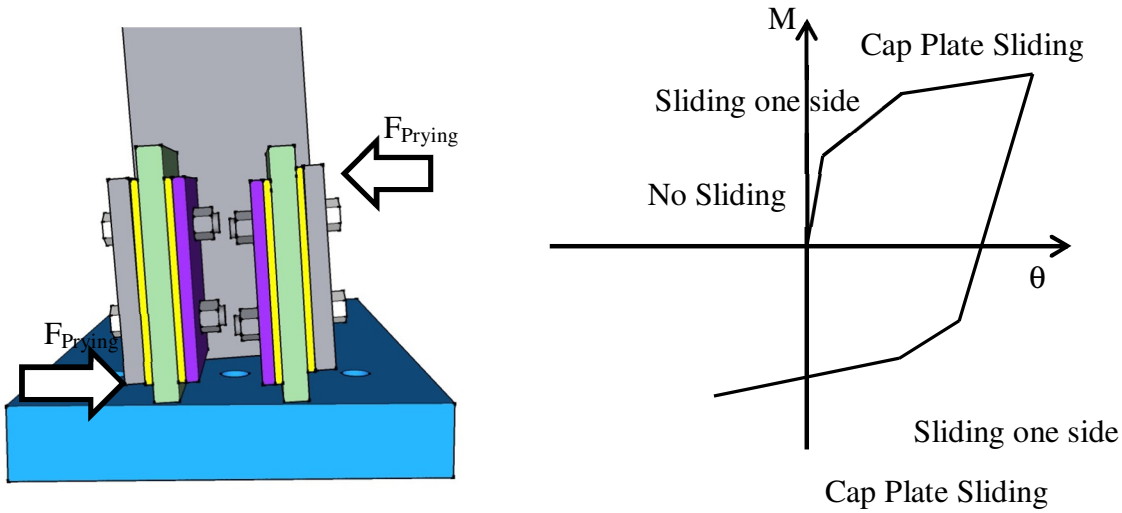

(a) Deformation (b) Hysteretic behaviour

Figure 7-4: WAFC Column base behaviour due to bending about column weak axis. Left is deformation of the column and the base connections and hysteretic behaviour of this connections is shown on right

The minimum clearances, Cl_A and Cl_B, and the diameter of the round hole in the flange plate, D, for strong axis bending may be estimated using:

$$Cl_{Ax} = \theta_{rockx} \times H_1 \quad (7\text{-}2)$$

$$Cl_{Bx} = \theta_{rockx} \times W_1 \quad (7\text{-}3)$$

$$D_x = 2(\theta_{rockx} \times \sqrt{W_2^2 + H_b^2} + d_{Sh} + 2\text{mm}) \quad (7\text{-}4)$$

Where Cl_A and Cl_B are clearances defined in Figure 7-1, H_1 is the height of the flange plate, W_1 is the width of the column's plate, W_2, and W_3 are the distance from the neutral axis up to the centre of the hole in the flange plate along length and width of the column section respectively, d_{sh} is the diameter of the bolt shank, and 2mm is the standard clearance. For weak axis bending, the values of Cl_{By} and D_y are defined:

$$Cl_{By} = \theta_{rocky} \times W_3 \quad (7\text{-}5)$$

$$D_y = 2(\theta_{rocky} \times \sqrt{b_f^2 + H_b^2}) + d_{Sh} + 2\text{mm} \quad (7\text{-}6)$$

When the column bends in two directions, the required Cl_B and D values may be obtained by vector superposition of the components in each direction.

7.2.2. Experimental Program

- **Detailing of the Base Connection and Tests Runs**

A 310UB46.2 test section was used for the column. The universal beam (UB) section, rather than a universal column (UC) section, was used as it is commonly used in the design of drift governed moment frames. The Grade 300 member had an actual tensile yield strength of 320 MPa. The distance from the top of the base plate to the column point of contraflexure was 1980 mm. All of the drift values are based on this height.

No shear key was placed between the column and the base plate and it was assumed that the shear resistance from the friction, bolts and the flange plate provide enough shear resistance. The calibrated torque control method was used for tightening bolts over the sliding surfaces of the AFCs to the proof load. The bolt calibration was conducted with five plate subassemblies with total thickness of 60mm. This thickness is equal to the total thickness of the sliding plates in the friction connection, which comprise the column plate, shims, cap plate, flange plate.

The grip length is 62 mm (thickness of the plates plus washers), and M16 bolts were cut at

length of 80 mm.

These elements are fastened with M16 Grade 8.8 bolts tightened by applying torques from 40 N.m up to 550 N.m. In each step, the specified torque was first applied and the bolt elongation and turn-of-nut were recorded. Bolt deformation corresponding to the proof load was calculated (Chanchí et al., 2012b) and the corresponding torque was applied to the bolt heads. The applied torque at the proof load was equal to 300 N.m for the M16 Grade 8.8 bolts tested according to the above procedure.

The column plates and flange plates were welded to the column and the base plate by full penetration respectively. This type of welding can provide a higher level of resistance against tensile and bending demands compare to the fillet welding. Moreover, fillet welding can prevent sliding of shims and cap plates for higher levels of rotation.

After testing the column bases, the bolt heads were retightened to the target torque and the corresponding nut rotation was recorded. A nut rotation of 0.1 rad caused 0.03mm elongation of the bolt that approximately corresponds to 15% of the proof load for these bolts with 2mm thread pitch. Hence, the loss of proof load due to the bolt elongation is measured after each test.

The base plate was placed on a 5mm layer of dental plaster to provide full contact. It was attached to the concrete by 6 M24 Grade 10.9 bolts anchored at the bottom of the concrete foundation block, as illustrated in Figure 7-5 and Figure 7-6. The anchor rods were post-tensioned until the axial force measured by the load cells beneath the nuts was 85% of the bolt minimum proof load, while twisting of the load cells was prevented. The value of 85%

was calculated to prevent any uplift of the base plate. In these tests, a 50mm thick base plate and post-tensioned anchor bolts were used to reduce the base flexibility.

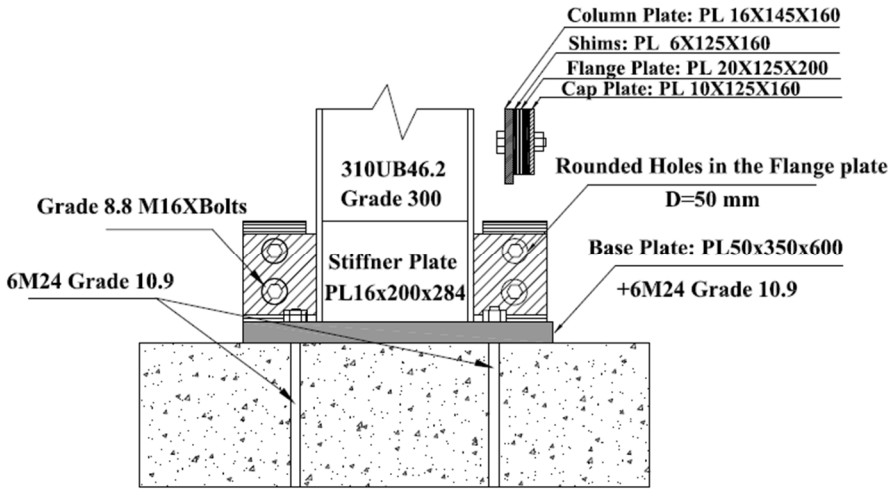

Figure 7-5: Detail of base connection

The five cyclic tests outlined in Table 7-1 were conducted in the order shown. Bolts and shims were replaced after each test but the same column was used. These tests mirror those used in Chapter 6 to allow direct comparison of SAFC and WAFC results.

Table 7-1: Tests conducted

No	Axis of Bending	Axial force
1	Strong	Zero
2	Weak	Zero
3	Strong	320kN (0.20Ns)
4	Weak	320kN (0.20Ns)
5	Bi-directional	320kN (0.20Ns)

- **Test Setup and Loading Regime**

The loading regime and test setup are as described in Chapter 2.

- **Test Instrumentation**

Four linear potentiometers with 25 mm stroke were attached between the column plates and the base plate to monitor the column base vertical sliding. Three potentiometers attached between the cap plate and the base plate monitored cap plate vertical sliding. Three other potentiometers, placed between the column stiffener and the base plate, recorded column uplift in different positions, and seven potentiometers on top of the base plate captured base plate uplift and deformation. Some of these sensors are shown in Figure 7-6. Strain gauges, with 6mm gauge length, were also placed on the column flange, column plate and the flange plates to measure localised st

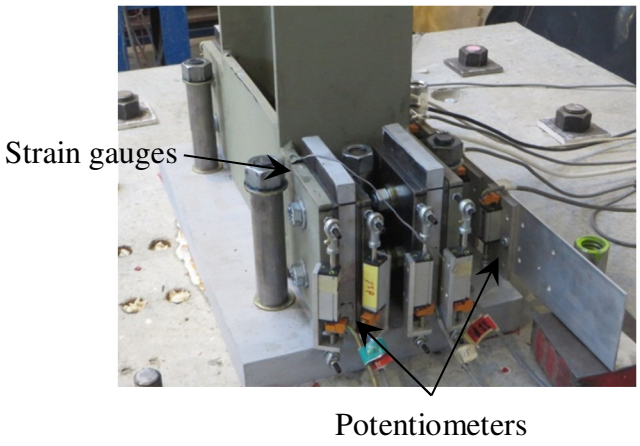

Figure 7-6: Instrumentation of the WAFC base connection

7.2.3. Analytical Prediction of Performance

In each test, the column base moment, M_{Base}, and column base rotation, θ_{Base}, were computed from the lateral force and column lateral displacement according to:

$$M_{Base} = V \times H_{col} \tag{7-7}$$

$$\theta_{Base} = (\Delta_{top} - \frac{V \times {H_{col}}^3}{3 \times E_{col} \times I_{col}}) \times \frac{1}{H_{col}} \quad (7\text{-}8)$$

Where V is the lateral force at column top, H_{col} is height of the column from the base plate to the point of contraflexure, Δ_{top} is top displacement of the column, E_{col} is the elastic modulus of the column, I_{col} is the second moment inertia of the column in the direction of testing. The shear deformation was ignored, as it is relatively small in long I-shaped members.

The nominal sliding force for each AFC bolt is defined (MacRae et al., 2010):

$$F_S = \mu \times \eta \times N_{tf} = 0.21 \times 2 \times 95 = 40\ kN \quad (7\text{-}9)$$

Where, F_s is sliding force of each bolt, μ is the friction coefficient, η is the number of shear planes, and N_{tf} is the proof load per bolt. The friction coefficient of steel on Bisalloy 500 was taken as 0.21 (Chanchí et al., 2012b).

The maximum base moment from lateral loading causing strong axis bending, M_{Xbaseu}, is the sum of the sliding moment, M_{Slide}, and the moment from axial force, M_{Axial}, as given:

$$M_{Xbaseu} = M_{Slide} + M_{Axial} = (n_{Bolt} \times F_S \times d) + (P \times D_{Axial}) \quad (7\text{-}10)$$

Where n_{Bolt} is number of the bolts in the AFCs on one side of the base connection, F_s, is the sliding force in each bolt as defined in Equation 7-9, d is the horizontal distance of sliding bolts up to the neutral axis, and D_{Axial} is the perpendicular distance from the centre of axial force, P, to the neutral axis. For calculation of the neutral axis, it is assumed that the area on the compression side of the section, is all at the yield stress of the material and resists the applied axial force, N, as is commonly assumed in plastic design.

When the column bends about its weak axis, a prying moment, M_{Prying}, occurs in addition to the moment resistance from the frictional sliding and axial force components, M_{Slide} and M_{Axial}. M_{Prying} mainly comes from bending of the column flange plates that is defined:

$$M_{Prying} = min\begin{cases} 2 \times \dfrac{\theta_{Base} \times 3EI_{fp}}{{L_1}^2} \times L_2 \\ 2 \times \dfrac{\sigma_y \times b_{fp} \times t_{fp}^2}{4} \end{cases} \quad (7\text{-}11)$$

Where L_1 is the distance from top of the column plate to the base plate; I_{fp} is the second moment of inertia about the weak axis of the flange plate; and L_2 is length of the column plate. This moment cannot be greater than the flange plate plastic flexural strength, $M_{P\text{-}fp}$, given by the second term in Equation 7-11. Where b_{fp} is the width of the flange plate, t_{fp} is the flange plate thickness, and σ_y is the flange plate yield stress.

For a member subject to a bidirectional displacement with components in the x and y directions, Δ_x, Δ_y and axial force N, the column base moments M_x and M_y are found by first taking the orientation of the neutral axis Θ perpendicular to bidirectional displacement, as shown in Figure 7-7. When moment is applied about the x axis, Θ is equal to zero, and it is 90 degrees for moment about the y axis direction. Iteration is conducted on the neutral axis depth, c, until the area on the compression side of the section is all at the yield stress, as is commonly assumed in plastic design, and resists the axial force, N. Moments can then be obtained by summing forces multiplied by distance about the neutral axis.

The column base uplift displacement, Δ_{Uplift}, is then found from:

$$\Delta_{Uplift} = \theta_{Base} c_{Tens} \quad (7\text{-}12)$$

Where c_{Tens} is the distance perpendicular to the neutral axis to the extreme fibre of the section on the gapping side, as shown in Figure 7-7. This section is almost a rectangular box with a central web as a result of the column stiffeners.

Column base rotation, θ_{Base}, may also be obtained from the potentiometer readings at the base:

$$\theta_{Base} = \frac{\Delta_{Up} - \Delta_{Down}}{x_{UD}} \quad (7\text{-}13)$$

where x_{UD} is the distance between potentiometers measuring tension and compression, Δ_{Up} and Δ_{Down}, respectively, perpendicular to the neutral axis.

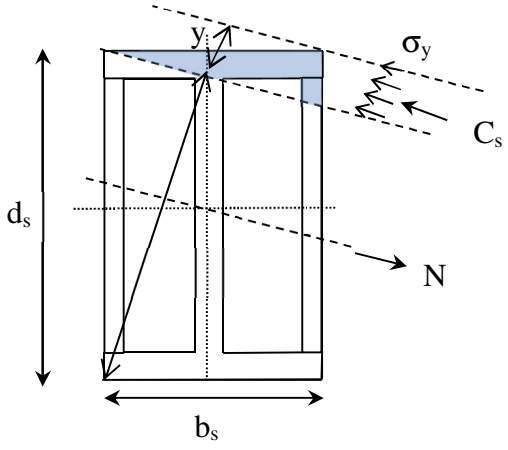

Figure 7-7: Column section under bi-axial bending

The neutral axis depth from the experimental test, *c*, is evaluated as:

$$c = \Delta_{Down}/\theta_{Base} - x_{cp} \quad (7\text{-}14)$$

Where x_{cp} is the distance between the extreme fibre of the section and the position of the potentiometer measuring compression perpendicular to the neutral axis, Δ_{Down}. The uplift displacement at the extreme tension side of the specimen, Δ_{Uplift}, is again given by Equation 7-12 using the experimental definition of the neutral axis.

For each test, the experimental moment-base rotation curve is plotted. The solid bilinear curve shows the predicted performance. The base connection is assumed rigid before sliding occurs at a base moment associated with sliding on the first surface using M_{Xbase} from Equation 7-10 with $\eta = 1$ in Equation 7-9. It is assumed that the strength is increased to that associated with cap plate sliding at 4%, drift again using Equation 7-10 with $\eta = 2$ in Equation 7-9. This bi-linear model provides a simple means for estimation and design of WAFC connection. For a more complex analytical study, a macro model of WAFC considering the interactions of different mechanisms should be used.

7.3. Results and Discussion

7.3.1. Test Summary

Experimental test parameters are compared with the predicted values of base moment in the *X* and *Y* directions, M_{base}, the position of the neutral axis, *c*, and column uplift, Δ_{uplift} for 4% drift. These results are summarized in Table 7-2. For the bi-directional bending test, Test No.5, these values are presented for 4% drift in the *X* direction and 2.5% in the *Y* direction. These results are discussed in detail in the following sections for the individual tests.

Table 7-2: Predicted and experimental actions for Tests No. 1 to 5

No	Bending Axis	Axial Force	No. AFC bolts	$M_{X,base}$, (kN.m)		$M_{Y,base}$, (kN.m)		c (mm)		Δ_{uplift} (mm)	
				Pred[1]	Expt[1]	Pred	Expt	Pred	Expt	Pred	Expt
1	Strong	Zero	Four	75	80.5	0	0	0	0	11.6	12.05
2	Weak	Zero	Four	0	0	36	32.7	$\frac{21^2}{1.6^3}$	12	4.9	4.3
3	Strong	320kN	Four	122	123.7	0	0	6	14	11	10.1
4	Weak	320kN	Four	0	0	52	47.4	$\frac{42^2}{3.2^3}$	36	3.4	2.28
5	Both	320kN	Four	118	131	28	26.5	20	13	12.3	12.6

[1] Pred: predicted value, Expt: value obtained from experimental test
[2] Neutral axis of the column above stiffener plates
[3] Neutral axis of the column with stiffener plates

7.3.2. Test No. 1- Strong Axis Bending without Axial Force

Figure 7-8 shows that the WAFC column base maximum strong axis moment reaches 80.5kN. This moment is 34% of the column plastic moment capacity of 233 kN.m assuming tension and compression yielding. No paint flaking was observed in the column or boundary plates, indicating that they remained elastic. In addition, when the nuts were re-tightened with the torque wrench after testing, the nut rotation was less than 0.1 rad, indicating less than 15% loss in post-tensioning. This loss is similar to the level of degradation seen in the cycles to a base rotation of 1.8%.

Table 7-2 shows that the uplift displacement and peak base moment were larger than that predicted. As larger drift cycles were applied, the level of base moment resisting was increased at zero rotation compared to the previous cycles for the same level of displacement. This performance is because the increase in strength after first sliding takes place occurs at a

similar rate irrespective of when the initial first sliding starts, as shown by the similar post-elastic slopes for small and large cycles before the plateau is reached. The depth of neutral axis, c, is 0 because the friction devices on the different sides of the column have similar forces in compression and tension and there is no axial force on the specimen. Hence, only friction sliding should be considered for calculation of the moment resistance.

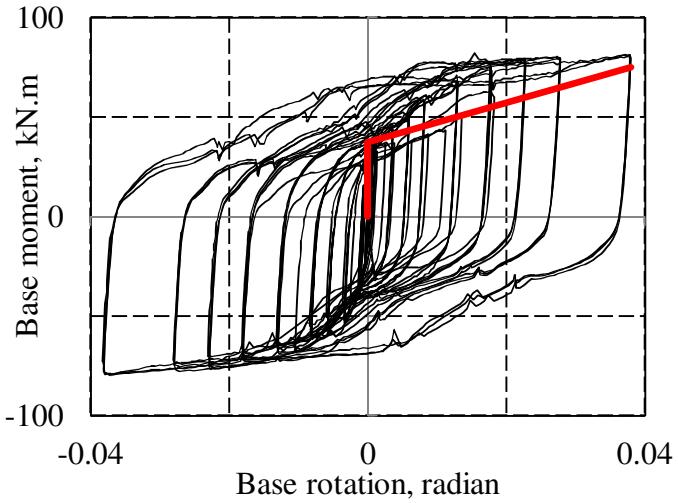

Figure 7-8: Strong axis bending tests response without axial force and a red line showing the predicted performance from the described method in Section 7.2.3

7.3.3. Test No. 2 - Weak Axis Bending without Axial Force

Figure 7-9 shows maximum base moment reaches 32.7 kN.m, which is 10% less than the column section nominal moment capacity of 35 kN.m for weak axis bending. Only the column plates slid and no cap plate sliding was recorded. In addition, no paint flaking was observed at the column and the boundary plates.

Nut rotation during bolt retightening was zero showing no significant AFC degradation. The computed M_{Base} at both initial sliding, and at larger drifts considering sliding on both surfaces

plus prying was reasonable. Column uplift, Δ_{Uplift} depth predictions were also accurate in Table 7-2 to better than 12% for this weak axis bending test.

The sliding force in the tension side is considered for calculation of the neutral axis. Since the stiffeners did not extend in the whole height of the column, two values for the neutral axis depth, *c*, are obtained. When stiffener plates are considered, *c* is 1.6 mm, and without stiffener plates *c* is 21 mm. The actual position of the neutral axis is between these two values.

After a few cycles a gap was also observed between the base plate and the column base over the whole depth of the column when the column was at zero lateral displacement. This gap opening indicates that the column moved up, and it could occur because no axial load was applied to the column and it could move up a little in each cycle. Some plastic deformation at the column corners happened as the strain recorded from deformation of the potentiometers connected to the column plates (4750×10^{-6}) was higher than the yielding strain of 1600×10^{-6}.

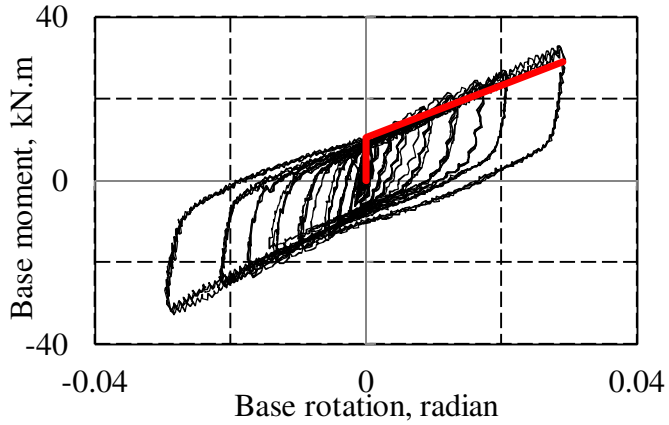

Figure 7-9: Weak axis bending for all cycles tested without axial force and a red line showing the predicted performance from the described method in Section 7.2.3

7.3.4. Test No. 3-Strong Axis Bending with Axial Force

Maximum moment resistance reached 123.7 kN.m, or 64% of the nominal section flexural strength considering the axial force according to NZS3404 (2007), as shown in Figure 7-10. In addition, first sliding occurred at about 80 kN.m. The self-centring base moment from the axial force, M_{Axial}, of 47 kN.m was smaller than the sliding moment on both sides using $\eta = 2$ in Equation 7-9, for the AFC yielded 75 kN.m, as predicted in Test No. 1, but greater that that associated with the initial sliding resistance on one side of the AFC, $\eta = 1$ in Equation 7-9, of 37.5 kN.m.

The overall results show that the applied axial force can provide self-centring for levels of peak moment less than the M_{Axial}, 47 kN.m obtained up to drifts of 0.75%. For greater levels of moment demand, the applied axial force could not provide static recentering. However, dynamic recentering after earthquake shaking is likely in these conditions (MacRae, 1994).

No yielding was observed in the column or any connection elements. In addition, no nut rotation was required to reach the torque associated with proof load after the tests that indicates very little AFC degradation.

Figure 7-10 shows that the peak moment, M_{Base} for strong axis bending with axial loading was predicted with 1% accuracy. Column uplift Δ_{Uplift} was 9% less than predicted. However, the recorded position of the neutral axis in the first cycle to 4% drift was less than one half the predicted value. This difference may occur because some limited column flange tip yielding occurred in Test No. 2 reducing the amount of section in direct contact with the

plate. Therefore, the position of the neutral axis is much closer to the centre of the column section, the initial stiffness was reduced, and base uplift occurred at a lower base moment than predicted.

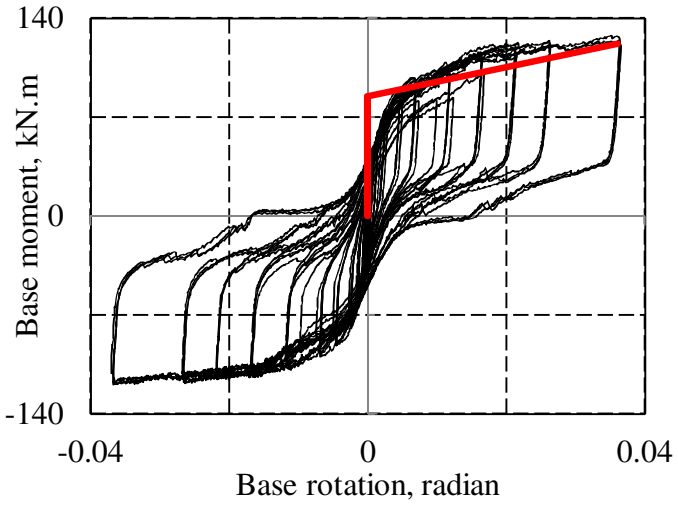

Figure 7-10: Strong axis bending cycles with axial force, where the red line is the predicted performance from the described method in Section 7.2.3

7.3.5. Test No. 4-Weak Axis Bending with Axial Force

Column base uplift occurred at about 10 kN.m, which is about one-third of that predicted in Table 7-2 and at about one-half of that estimated for uplift considering the axial force of 21 kN.m. This difference is due to previous yielding at the column base reducing the area in contact with the base. The position of neutral axis in Tests No. 2 and 3 indicates that plastic deformation mainly occurred at the flange tips. Therefore, at small base rotations the column flange tips did not contact the plate.

The predicted moment is 57 kN.m, which is higher than the column flexural capacity of 52 kN.m at 4% drift. Therefore, this value was considered as the predicted value in Table 7-2. The restoring moment from axial force and prying of 36.7kN.m was greater than the sliding

resisting moment of 20.7 kN.m indicating a tendency for self-centring based on the response at peak displacement. At zero displacement, the prying effect is zero, but static self-centering is still expected, as the restoring moment due to axial force of 25 kN.m was greater than the sliding resisting moment of 20.7 kN.m. However, there was no static self-centering because the experimental strength at low displacements was significantly less than the prediction due to the column base initial deformations.

Column flange yielding was observed from 3% drift based on paint flaking. For this axially loaded column bending about the weak axis, when the lateral force was reduced from the peak displacement, the rotation at the column base increased, as shown in Figure 7-11. This behaviour occurred because even though the displacement at the loading point reduced during unloading, the elastic displacement of the column alone started to decrease, making the column becomes straighter. The effect of this straightening, causing the base rotation to increase, was more significant than the effect of the decrease in displacement at the loading point that causes the column base rotation to decrease.

The uplift was about 53% of that for the column without axial force due to the column flexural/shear deformation being greater than that in Test No. 1. This result is due to the greater lateral force, and the greater amount of compressive yielding at the base of the column. If the column base had no stiffeners, the predicted neutral axis depth is 42mm. However, considering the effect of the column stiffeners the predicted neutral axis depth is 3.2mm that is within the 16mm stiffener plate depth. Since the stiffener plate does not extend over the full height of the column the neutral axis depth of a pristine column would be expected to lie between these two values. In this particular test, the experimental neutral axis depth of 36mm was close to the value assuming no stiffeners.

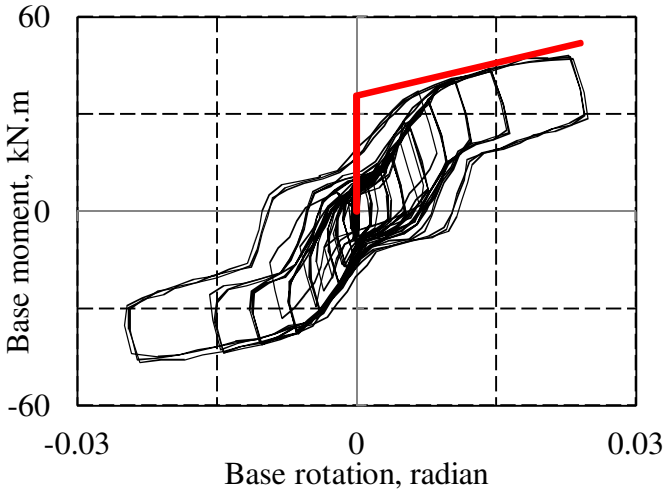

Figure 7-11: Weak axis bending test for all cycles with axial force, where the line is the predicted performance from the described method in Section 7.2.3

7.3.6. Test No. 5- Bi-directional Bending with Axial Force

Figure 7-12 shows the predicted x-moment / y-moment interaction diagram considering the applied axial force. This curve is within the interaction curve for NZS3404 (2007), where axial tension is also considered. The prediction provides a reasonable estimate of the actual strength. Since the column flange corners were yielded in Test No. 4, the neutral axis was shifted closer to the column centre mainly along Y axis direction. Therefore, the predicted value for points of loading with higher drift in Y direction and lower drift in X direction is different from the experimental results.

Table 7-2 showing the recorded and calculated values of moment, uplift, and neutral axis for 4% drift in the *X* direction and 2.5% in the *Y* direction. These results indicate that the prediction method evaluated base moments during bi-directional loading with accuracy of 10% for M_x and 5% for M_y. These errors provide good model prediction accuracy in design

for this case.

The centre of the shear resistance between the column and the base plate was at one corner during bi-directional loading. However, the resultant force of the column is applied to its centre causing the column tended to twist. During the experimental test, this twisting was restrained by the two parallel actuators that cause weak axis bending. The twisting moment, M_{tw}, from the experimental test was calculated as the force difference of the parallel actuators multiplied by the distance between actuators. M_{tw} can also be predicted by multiplying the resistance force calculated by Equation 7-10 in each direction by the perpendicular distances to the flange tip. Experimental and predicted M_{tw} were consistent, both being 5 kN.m at an applied drift of 4% in the X direction and 2.5% in the Y direction.

Such a torsional moment at the top of a column needs to be resisted by the building. Therefore, in addition to building torsion resulting from plan irregularity and torsional ground motions, buildings with a number of columns with WAFC bases or similar must account for the fact that the columns may together provide a twisting moment causing another component of building torsion. This additional torsional demand may lead to greater damage than intended in design.

The column base sustained up to 4% bi-directional drift under axial load without any strength degradation. Column paint flaking was observed at X=2% and Y=2.5% drift that described the yielding of the column. However, no web or flange buckling was observed up to the end of the test and there was no paint flaking observed in the column and flange plates.

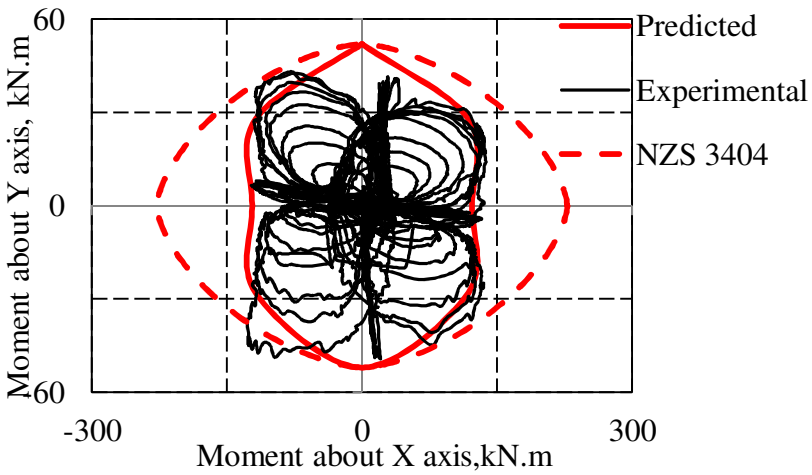

Figure 7-12: Bi-directional bending with axial force and a red line showing the flexural capacity of the section

The bolts were retightened, and the corresponding nut rotation was between 0.3-0.4 radians, which that corresponds to 45%-60% of the bolt proof loading, but no reduction of the resisting moment was recorded as the bi-directional drift was increased as the predicted and recorded value for X=4% drift had less than 3% difference. The shims and bolts after the bidirectional cyclic loading are shown in Figure 7-13. No bending was observed in the bolt and the shims were smooth indicating little degradation of the sliding surface. In addition, no low cycle fatigue of the bolts was observed under 43 cycles of displacement on the same set of bolts. However, it is recommended that after significant shaking bolts should be replaced to avoid potential issues.

No lateral sliding of the column towards the base plate was observed during cyclic loading. This phenomenon shows that provided shear resistance by AFC and friction between the column and the base plate can provide enough resistance to prevent sliding of the column. Therefore, no shear keys are required in the base with friction connection.

a. Tested shim

b. Tested bolt

Figure 7-13: Degraded shim on left and the pre-tensioned bolts after testing on right

7.4. Summary

This chapter describes experimental testing of the column base weak axis aligned asymmetric friction connections (WAFC) subject to strong axis, weak axis and clover-leaf cyclic loading with and without axial force. It was found that:

- The base connections did not have significant strength degradation even after cycles to a drift 4%. However stiffness degradation was observed, particularly after the cycles of the axially loaded specimen in the weak axis direction. Stiffener plates between the column flange tips did not stop column base yielding from occurring. In addition, the level of shim and steel plate degradation is minor and these can be reused after a strong earthquake. Axial load provided a degree of self-centring. No major damage occurred that interrupt the performance of the column and the base connection, and it can be categorized as a low-damage connection. Repair, if needed, may be undertaken by retightening, or replacing, bolts and possibly shims.

While full stiffness reinstatement is difficult, allowing grout to flow under sections of the column section where there is a gap, may increase the stiffness.

- A simple analytical method was developed to estimate the column base uplift moment resistance and the moment resistance at 4% drift. The method developed considers frictional resistance, axial force effects and prying effects. It provided a reasonable estimate of experimental strength. The stiffness was estimated well in initially untested specimens. However, during testing some yielding occurred at the column bases and this reduced the stiffness from the predicted level during subsequent tests.

- Columns, such as these, where the centre of applied lateral force at the top of the column is at a different vertical location to the resistance at the base of the column, can impose a torsional moment on the building they are supporting. This may affect the building response.

In the next chapter, the development and verification of a macro-model to represent the hysteretic moment-rotation backbone curve of the SAFC and WAFC under strong and weak axis displacements is described.

Chapter 8: Macro Modelling of Strong and Weak Axis Aligned Asymmetric Friction Connection Column Bases

8.1. Introduction

The observed performance of weak axis aligned asymmetric friction connections (WAFC) column bases, and strong axis aligned asymmetric friction connections (SAFC) showed no major strength degradation occurred that adversely affected performance of the column or the base connection. In addition, for low load levels, there is no stiffness degradation. Hence, these base connections can be categorized as low damage connections, as defined in Chapters 6 and 7.

To enable adoption, the design of these connections for specific applications must be as accessible and straight forward as possible. To this end, generalizable macro models provide a framework for design and inclusion into larger structure analyses. However, to date, no such models exist for these connections, which thus become the goal of this chapter.

An overview of the experiments used in the validation is given in Table 8-1. They are listed in the order conducted. One specimen, which consists of base connection and column, was used for each base type. The tests were selected to cover a range of variables, such as loading direction, number of AFC bolts, column axial force, and base connection type. For each test, the moment, M_{test}, was obtained at 4% drift and the secant base rotational stiffness, $K_{\theta,test}$, was calculated from the origin to the point on the column base moment-rotation curve when the

cap plate starts sliding. For the cases without sliding of the cap plate, the secant stiffness was calculated at the point of 4% drift on the column base moment rotation. The first yielding point that corresponds to the first rocking point is also important for design issues. For WAFC, and SAFC that bends about the strong axis without axial force the base moment at the first rocking point are 14.5 kN.m, 11.5 kN.m. Virgin specimens were used only for these two tests and they were re-used for Tests No. 2, 3, 4, 5, 7, 8, 9.

Table 8-1: Experimental Parameters

Test No	Base type	Direction[a]	n_{bolt} [b]	P_u [c], kN	M_{test}, kN.m	$K_{\theta,test}$ kN.m/rad
1	WAFC	X	4	0	80.5	5753
2	WAFC	Y	4	0	32.7	1150
3	WAFC	X	4	320	123.7	8994
4	WAFC	Y	4	320	51.4	2056
5	SAFC	X	0	0	11	399
6	SAFC	X	4	0	80	3295
7	SAFC	Y	4	0	31.64	1100
8	SAFC	X	4	320	135	5440
9	SAFC	Y	4	320	39	1493

[a] Direction of bending about the X, which is strong axis, or Y, which is a weak axis
[b] Number of the sliding bolts in one side of column
[c] Applied axial force

The data from these experiments provides an opportunity to validate analytical models characterizing the performance of these asymmetric friction column base connections that will be useful for their design. To make the most of this data, this chapter addresses the following questions:

a. Can a macro-model for WAFC and SAFC be developed?
b. How well does the developed macro-model work compared to extensive experimental data?

The main objective of this chapter is to develop the model for monotonic behavior as it can be used for simple hand calculation design and also to model these friction base connections as a link element in finite elements software products such as SAP2000, ETABS or as a zero length element in OpenSees.

8.2. Method and Model Design

For the design of friction connections, the base connection demands should be calculated at the first stage. The author recommends designing the base connection without any sliding up to the ultimate wind loading and serviceability earthquake. Size of the holes and clearances should be determined based on nonlinear analysis for ULS or MCE earthquake. The overstrength of 1.4 should be considered for design of friction connection as described in section 6.2.1. Therefore, maximum demand (axial force, and moment) on the column should be limited to 0.7 of the column capacity.

The main stiffness sources for columns with SAFC and WAFC base connections are the column, the base connection including friction, bending of the bolts, prying, and bending of the flange plate on the tension side, and the base plate. These elements are illustrated in Figure 8-1. These stiffnesses act in series, resulting in overall stiffness that is less than that of the most flexible component.

The performance of the SAFC and WAFC can be defined over four stages beginning with: (i) *Before sliding*, where column flexure dominates the response before there is sliding in the AFC; and (ii) *Initial sliding*, where column sliding occurs without bolts bearing on the hole edges. In addition, *prying-sliding* can occur for prying cases in stage (iii) *Bearing-sliding*,

where column sliding occurs with the AFC bolts bearing on the column flange in the SAFC, or on the column plate in the WAFC before sliding of the cap plate. Finally, stage (iv) *Cap-plate sliding* occurs after the onset of cap plate sliding. These four stages are all illustrated in Figure 8-2 for both the SAFC and WAFC and both bending directions.

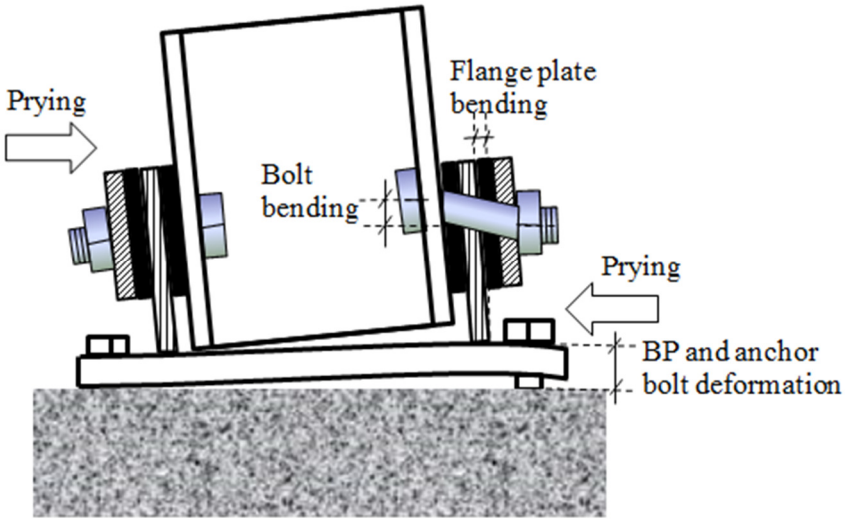

Figure 8-1: Sources of base stiffness

Figure 8-3 illustrates analytical models of the SAFC and WAFC connections for bending about the strong and weak axes for all four stages. The elements of Figure 8-3 are a direct match to those of Figure 8-2. These two figures thus connect the mechanism to the model elements. Importantly, prying occurs when the SAFC bends about the strong axis, or the WAFC bends about the weak axis, and the rotational stiffness is increased as column slides. Prying does not occur when the SAFC bends about the weak axis, or the WAFC bends about the strong axis as the AFCs are aligned in these cases. Thus, only bending of the bolts provides stiffness for the non-prying cases up to the level of cap plate sliding. Equally, in the non-prying cases, the AFCs do not provide any base rotational stiffness after the cap plate slides until it reaches the end of the bolt hole.

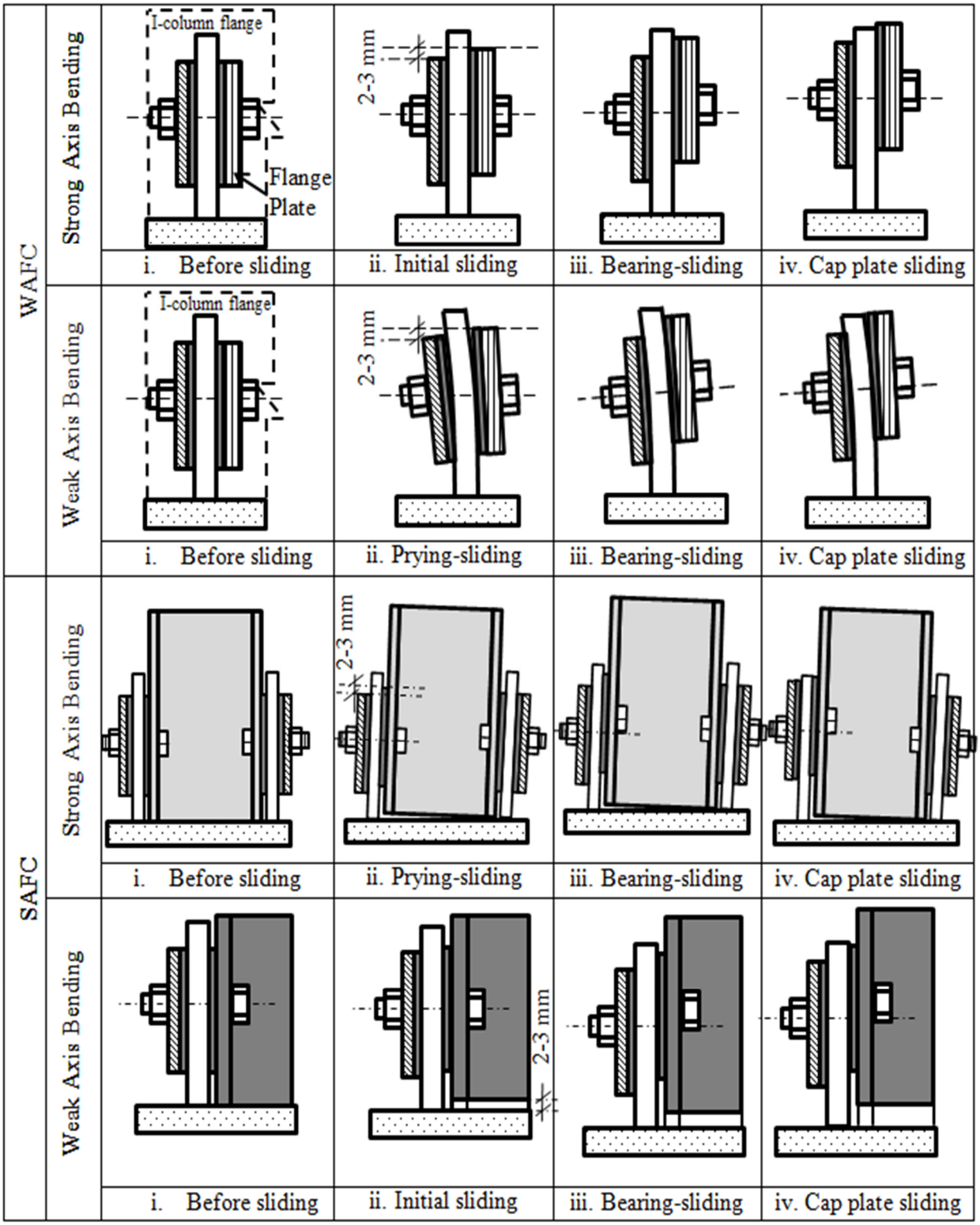

Figure 8-2: SAFC and WAFC under strong and weak axis bending deformation stages that are stage 1. Before sliding, stage 2. Initial sliding or prying sliding, stage 3. Bearing sliding, stage 4. Cap plate sliding

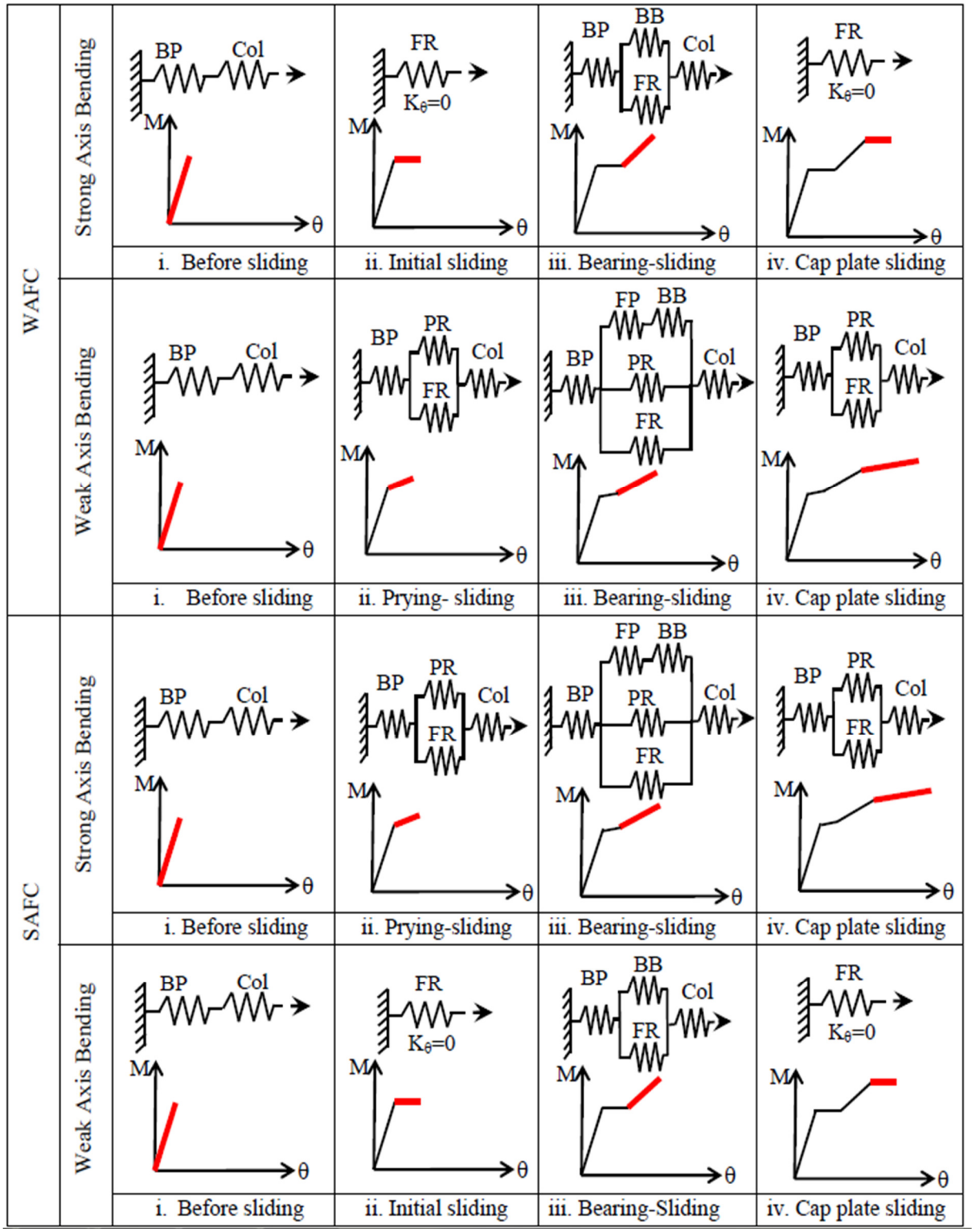

[**] ***BP***: Base plate, ***BB***: AFC Bolt Bearing, ***PR***: Prying, ***Col***: Column, ***FP***: Flange plate bending, ***FR***: Friction with zero stiffness

Figure 8-3: SAFC and WAFC deformation components for loading steps assuming FP and BB modes act in series that are stage 1. Before sliding, stage 2. Initial sliding or prying sliding, stage 3. Bearing sliding, stage 4. Cap plate sliding

8.2.1. Stage I: Before Sliding

When lateral force is first applied, there is no column base uplift or AFC sliding, as the column base acts like a rigid rotational spring. The column and base plates are in series, as shown in Figure 8-3 for stage (i). The AFC remains rigid until uplift initiates and sliding occurs in one of the AFCs on the tension side of the column. If the axial force is high enough to prevent column uplift, then only stage (i) happens. The base moment associated with this initial sliding, M_{Sl_col}, is defined:

$$M_{Sl_{col}} = M_{axial} + 0.5 \times M_{Sliding} \tag{8-1}$$

$$M_{axial} = P \times D_{axial} \tag{8-2}$$

$$M_{Sliding} = \sum_{i=1}^{n_{bolt}} (F_S \times d_i) \tag{8-3}$$

$$F_S = \mu \times \eta \times N_{tf} \tag{8-4}$$

Where, $M_{Sliding}$ is the moment where the *AFC* cap plates in Figure 8-2 for this stage start sliding without any axial force on the column. Since sliding needs to occur on both sides of the flange plate to obtain cap plate sliding, this moment is twice that required for sliding on one side of the flange plate that is associated with column uplift with no axial force, P. M_{axial} is the base uplift moment when the column is subject to P, and n_{bolt} is the number of AFC bolts that slide. For large deformations, if a bolt is on the tension side of the neutral axis it will slide in tension, and conversely in compression. Next, d_i is the horizontal distance from the centroid of the sliding surfaces of each bolt to the neutral axis; D_{axial} is horizontal distance from the centre of action of P, to the neutral axis; F_s is the sliding force for each bolt,

as defined in Equation 8-4 (MacRae et al., 2010); μ is the effective friction coefficient between steel and shims that is taken as 0.21 for Bisalloy 500 shims (Chanchí et al., 2012b); η is the number of shear planes that is always 2 for AFC; and N_{tf} is the proof load per bolt. If M_{Sl_col} goes higher than flexural capacity of the column section, the column yields before any column uplift.

Computationally, iteration must be conducted on the neutral axis location, *c*, until the area of the compression side of the section at the yield stress resists the applied axial force, *P,* as is commonly assumed in plastic design. Such an approach is appropriate when the friction forces on either side of the neutral axis have similar magnitude, but opposite directions. For cases with sliding in only the tension side, the sliding force from these bolts was added to the axial force, *P*, for calculation of the neutral axis location. This approach assumes that the entire axial load is carried by the column. In addition, the demands that are applied to the AFC connection in the compression side are sliding force and bending of the plates.

The base moment that AFC starts to slide is increased as the level of axial load is increased according to Equation 8-1. It should be noted that if the applied moment to the base connection is higher than M_{Sl_col} then no-sliding occurs and the base acts as a conventional base connection.

8.2.2. Stage II: Initial Sliding and Prying-Sliding

When uplift occurs, sliding takes place between the column flange and the flange plate for the SAFC, and between the column plate and flange plate for the WAFC. This sliding is assumed

to occur without force increase until the bolts reach the edge of the holes in the column flange or column flange plate. The sliding may be 1*mm* for a centrally located bolt in a hole with normal oversize, but could be different if the bolt is not centrally located. When the bolt shank makes contact with the edge of the hole in the column flange or column flange plate, the column base rotation, θ_{trans}, is given by:

$$\theta_{trans} = \frac{d_h - d_b}{2D} \tag{8-5}$$

Where d_h is hole diameter, d_b is bolt diameter, D is perpendicular distance from the hole to the neutral axis. For many normal holes $(d_h - d_b)/2 = 1mm$.

For the prying cases, weak axis bending for the WAFC and strong axis bending for the SAFC, as shown in Figure 8-2 and 8-3, the prying rotational stiffness, K_{θ_prying}, is assumed to be dominated by flange plate curvature deformation on the compression side. Based on this behaviour, it may be estimated:

$$K_{\theta\_prying} = \frac{{H_{fp}}^2}{\frac{{H_{fp}}^3}{12 \times E \times I_{fp}} + \frac{H_{fp}}{G \times A_{fp}}} \tag{8-6}$$

Where H_{fp} is the height to the top of the flange plate; I_{fp} is the flange plate second moment area about its weak axis; A_{fp} is the flange plate section area; and E and G are Young and shear modulus of steel, respectively. The effect of rounded holes of the flange plate, and composite action occurs here with the other boundary plates on changing of I_{fp} and A_{fp} were not considered. For non-prying cases, the stiffness in this state is 0. Therefore, the moment increment at this stage for non-prying cases is equal to zero and for prying cases, $\Delta M_{pryingSII}$, is defined as:

$$\Delta M_{Prying_{SII}} = K_{\theta\_prying} \times \theta_{trans} \quad (8\text{-}7)$$

Where K_{θ_prying} is the prying rotational stiffness, and θ_{trans} is the column base rotation at the second stage.

8.2.3. Stage III: Bearing-Sliding

After the bolts start bearing on the edge of the column flange or column flange plate hole, they start to pull on the cap-plate. However, the cap-plate is not moving. Thus, as rotation increases, bolt shear and bending forces increase in response to this load.

Interaction of flange plate bending on the tension side (FP), and the friction force between the cap-plate/shims and the flange plate when bolts are bearing and pulling on the cap plate (BB), depends on the bolt axial stiffness or clamping force. It is thus useful to consider the following points:

a) If the bolts have sufficient axial stiffness/clamping force such that the flange plates deform and move touching the face of the column, then the two mechanisms, BB and FP, act in parallel. In particular, if the stiffness of one of these mechanisms goes to 0, the other will resist force and motion. For example, if the flexural stiffness, *EI*, of the tension flange plate tends to 0, while the plate still has axial stiffness, EA ≠ 0, having similar behaviour to rope or cloth under tension, then there is still resistance on either side of the flange plate due to friction. Similarly, if the friction coefficient was 0, then there would be resistance due to bending of the tension flange plate.

   Thus, in Figure 8-3, the WAFC Weak-Axis (iii) and SAFC Strong-Axis (iii) cases would

show BB and FP in parallel, rather than in series. In addition, for the next stage of both these cases, shown as stage (iv), the FP will continue to act in parallel since BB=0 does not mean that the FP contribution to stiffness also disappears until yielding of the FP occurs. Similarly, when the bolts cause the flange plates to follow the column, no gap opening is expected between the flange plate and column during column testing. This performance was the case for all tests with bolts as usually observed.

b) If the bolts have low axial stiffness or clamping force to the column, such as in the case when no bolts are provided, then when uplift occurs at the column base, the tension side flange plate will not follow the deformation of the column. Instead, it will remain vertical. In this case, a gap opens between the column and flange plate and there is no frictional resistance at this interface. Bending at the base of the tension flange plate during column rotation will not contribute to the lateral force resistance at the top of the column. Even when there are bolts, and the tension flange plate is relatively stiff, the tension flange plate will not completely follow the column, as the stress on the column-tension flange plate interface will be reduced. However, the stress on the cap-plate column interface will still remain. Sliding resistance is reduced in this case, and the BB and FP mechanisms are assumed to act in series, as shown in Figure 8-3.

c) If bolts exist and have an intermediate bolt clamping force/axial stiffness, then the tension flange plate will be pulled over an intermediate amount. This case is intermediate the cases defined in (a) and (b).

Therefore, the tension flange plate flexural demand due to base rotation, θ, can be estimated by multiplying the rotation of the flange plate by the base rotational stiffness from deflection

of the tension flange plate, K_{θ_fp}, estimated using Equation 8-10. The modelling conducted thus utilizes the following assumptions:

a) **P**arallel BB and FP elements, the moment at the base of the compression and tension flange plate, M_{fp} was limited to the flange plate plastic flexural strength assuming a yield strength of 390 MPa for these experimental specimens without considering moment axial force interaction.

b) **S**eries BB and FP elements, the flange plates remained elastic. In this approach, due to a reduction of stress on the column-tension flange plate interface, η is effectively η<2 in Equation 8-4. Note that if the flange plate flexural yielding strength were explicitly considered, the lateral strength of the column drops from 47 *kN* to 30 *kN* ignoring the axial force in the plate.

Experimentally, for the SAFC bending about its strong axis with no axial load, the strength at peak displacement was 2 *kN* (i.e. 4%) less in the parallel model, with the yielding flange plate assumption, than in the series model, with the elastic flange plate assumption. However, the column top displacement at the initiation of first sliding of the cap plate was about 2 times greater for the parallel model than for the series model when it was assumed that the bolts remain at 90 degrees to the plates.

For the SAFC under strong axis bending without column axial force, the experimental secant rotational stiffness at cap-plate sliding was 3295 kN.m/rad. This stiffness was 7096 kN.m/rad in the parallel model and 3381 kN.m/rad in the series model. When column axial force was considered, the axial force secant stiffnesses were 5440 kN.m/rad, 10833 kN.m/rad and

5081 kN.m/rad for the experimental, parallel and series results, respectively.

It may be seen that these values were more consistent with the series assumption. An additional movement of 3.4*mm* in the holes for the parallel model for SAFC that bends about the strong axis without axial force is required if sliding is to occur at the same time as that in the experimental model. This behaviour is consistent with assuming that the bolts move on an angle before engaging the flange plates.

The AFC rotational stiffness ignoring prying, $K_{\theta\_AFC\_T}$, results from the stiffness due to: (i) bolt deformation, K_{θ_bolt}; and (ii) flange plate bending, K_{θ_fp}, in the tension side of the column based on series assumption. It is thus defined:

$$\frac{1}{K_{\theta\_AFC\_T}} = \frac{1}{K_{\theta\_bolt}} + \frac{1}{K_{\theta\_fp}} \tag{8-8}$$

$$K_{\theta\_bolt} = \sum_{i=1}^{n_{bolt}} \frac{{d_{1i}}^2}{\frac{{l_{bolt}}^3}{3 \times E \times I_{bolt}} + \frac{l_{bolt}}{G \times A_{bolt}}} \tag{8-9}$$

$$K_{\theta\_fp} = \frac{{H_m}^2}{\frac{{H_m}^3}{12 \times E \times I_{fp}} + \frac{H_m}{G \times A_{fp}}} \tag{8-10}$$

Where, n_{bolt} is the number of AFC bolts that slide, E and G are the Young and shear modulus of steel, respectively; L is the column height from the top of the plate to the point of lateral force application, A_{bolt} is the bolt cross sectional area, and I_{bolt} is the bolt section second moment of area, d_1 is distance between the point that the bolt force is applied to the column or column plate up to the neutral axis. For example, d_1 is assumed to the depth of the column section minus half of the thickness of the flange in the SAFC base that bends about the strong

axis. H_m is the average height of flange plate holes from top of the base plate; I_{fp} is the flange plate second moment area about the weak axis; A_{fp} is the section area of the flange plate; l_{bolt} is the lever arm of the bolt, l_{bolt} = *flange plate thickness* + 2×*shim thickness* + 0.2×*bolt diameter* according to Khoo et al. (2014). It is assumed that the bolts deform in single curvature, rather than double curvature as this performance fits better with the experimental results.

For non-prying cases, the prying stiffness and the flange plate bending on the tension side of the column do not participate in total base moment resistance and the column stiffness is only affected by the sliding spring, as shown in Figures 8-2 and 8-3. Hence, the column base flexural stiffness, K_{θ_bolt}, is as given by Equation 8-9.

For prying and non-prying cases, the increment of base moment, $\Delta M_{pryingSIII}$, $\Delta M_{Non\text{-}pryingSIII}$ and increment of base rotation, $\Delta\theta_{pryingSIII}$, $\Delta\theta_{Non\text{-}pryingSIII}$ are defined as below.

$$\Delta M_{Prying_{SIII}} = \frac{K_{\theta\_AFC\_T} + K_{\theta\_prying}}{K_{\theta\_AFC\_T}} \times \left(M_{axial} + M_{Sliding}\right) - \left(M_{Sl_{col}} + \Delta M_{Prying_{SII}}\right) \tag{8-11}$$

$$\Delta M_{Non-Prying_{SIII}} = 0.5 \times M_{Sliding} \tag{8-12}$$

$$\Delta\theta_{Prying_{SIII}} = \frac{\Delta M_{Prying_{SIII}}}{K_{\theta\_AFC\_T} + K_{\theta\_prying}} \tag{8-13}$$

$$\Delta\theta_{Non-Prying_{SIII}} = \frac{\Delta M_{Non-Prying_{SIII}}}{K_{\theta\_AFC\_T}} \tag{8-14}$$

Where K_{θ_prying} is the prying rotational stiffness, θ_{trans} is the column base rotation at stage II, $M_{Sliding}$ is the moment where the *AFC* cap plates start sliding without any axial force on the column, M_{axial} is the base uplift moment when the column is subject to *P,* M_{Sl_col} *is* the base

moment associated with this initial sliding, $\Delta M_{pryingSII}$ is the moment increment at the stage II for prying case, $K_{\theta\_AFC\_T}$ is the AFC rotational stiffness ignoring prying.

8.2.4. Stage IV: Cap plate sliding

When the shear force applied to the cap plate from the bolts is sufficient to initiate sliding, the bolts no longer provide stiffness as they have stopped deforming. Sliding occurs and the moment due to this sliding is $M_{sliding}$ from Equation 8-3. The secant stiffness is calculated when this moment is first reached. Any subsequent strength increase is due to prying in the prying cases according to Equation 8-6. For non-prying cases the rotational stiffness of the joint is 0, therefore the moment increment at this stage is 0. For prying cases, the increment of base rotation, $\Delta\theta_{SIV}$, and increment of base moment, $\Delta M_{pryingSIV}$, are defined:

$$\Delta\theta_{SIV} = \theta_{ULS} - \theta_{SIII} \tag{8-15}$$

$$\Delta M_{Prying_{SIV}} = K_{\theta\_prying} \times \Delta\theta_{Prying_{SIV}} \tag{8-16}$$

Where, θ_{ULS} is the ultimate base rotation from nonlinear analysis, θ_{SIII} is the total base rotation at the end of stage III, K_{θ_prying} is the prying rotational stiffness.

8.2.5. Model Summary

In summary, axial force, sliding, prying, bending of the flange plate in the tension side, and bolt bending are considered as mechanisms that affect the moment resistance and stiffness of

the sliding hinge joint connection as shown in Figure 8-4.

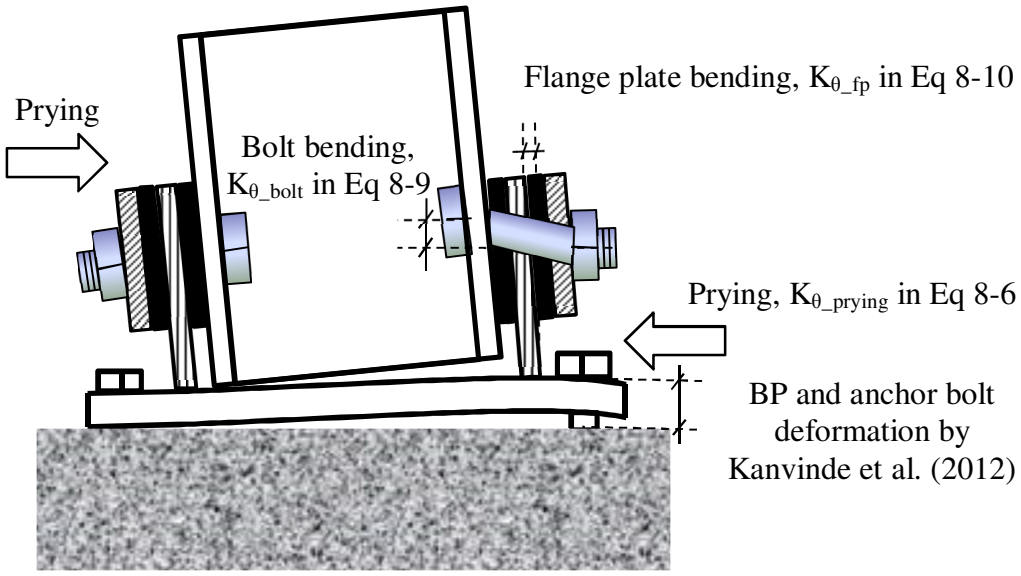

Figure 8-4: Summary of the macro model

Summary of the macro model including rotational stiffness, moment and rotation increment for each stage is described in Table 8-2.

Table 8-2: Summary of the macro model for each stage

Stage	Prying	Rotational Stiffness	Moment increment	Rotation Increment
I	Non-Prying	∞	Eq (8-1)	0
	Prying			
II	Non-Prying	0	0	Eq (8-5)
	Prying	Eq (8-6)	Eq (8-7)	Eq (8-5)
III	Non-Prying	Eq (8-8)	Eq (8-12)	Eq (8-14)
	Prying	Eq (8-8)+ Eq (8-6)	Eq (8-11)	Eq (8-13)
IV	Non-Prying	0	0	Eq (8-15)
	Prying	Eq (8-6)	Eq (8-16)	Eq (8-15)

8.3. Results and Discussion

8.3.1. General Interpretation

In this section, the experimental SAFC and WAFC behaviour is compared with the proposed analytical method. In the next step, the recorded moment from the experimental test at 4% drift, M_{test}, and the secant base rotational stiffness at the onset of cap-plate sliding, $K_{\theta,test}$ are compared with the calculated moment at 4% drift, M_{method}, and stiffness, K_{method}, from the mentioned method for all of the tests in a table. For cases where the cap plate did not slide, the rotational stiffness is presented for moment and rotation at 4% drift.

8.3.2. WAFC Base

Figure 8-5 shows the WAFC column experimental force-displacement response due to bending about the strong and weak axes, with and without applied axial force, compared to the proposed analytical model for the backbone curve shown by the solid red line. Figure 8-5 Tests No. 1 and No. 3 correspond to row 1 of Figures 8-2 and 8-3, where Figure 8-5 Tests No. 2 and No. 4 correspond to row 2 of Figures 8-2 and 8-3.

The backbone curve gives a good overall estimate of the response when there was no axial force applied. However, the overall shape is reasonable, but the model overestimates the moment for low levels of drift in Test No. 4, as illustrated in Figure 8-5. This over estimation is a result of column compressive section yielding, especially at the flange tips during

previous tests, as described in Chapters 6, and 7. This yielding reduces the area in contact with the base. Thus, at small base rotations, the column flange tips did not contact the plate resulting in the lower than predicted stiffness. This over estimation would not be expected in a virgin specimen.

Figures 8-4 Tests No. 1 and No. 3 illustrate that when the WAFC bends about the strong axis the four stage approximation seems reasonable up to 4% drift. In contrast, the cap plate did not slide before 4% drift for the weak axis bending of WAFC, as shown in Figures 8-4 Tests No. 2 and No. 4, and this performance was predicted according to the model. Overall, these figures validate the proposed method for WAFC for bending about the strong and weak axes, both with and without axial force.

According to Figure 8-5 Test No. 1, the base moment resistance at zero displacement increases at larger drift cycles compared to the previous cycles at the same level of displacement. The possible reason could be flange plates yielding that causes residual force at zero displacement. For this reason, the experimental force is larger than the predicted value at small displacement in the beginning of larger drift cycles.

At the end of each drift increment, a full cycle with half of the drift amplitude is also included to assess any degradation. This half cycle causes the level of strength in the last cycle of each level of drift is lower than initial or earlier cycles with the same drift. This outcome can be seen in Figures 8-4 for Tests No. 1 and No. 3.

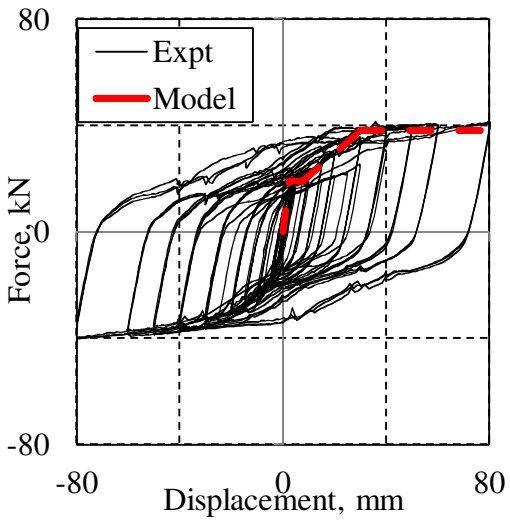

Test No. 1: Bends about the strong axis without axial force

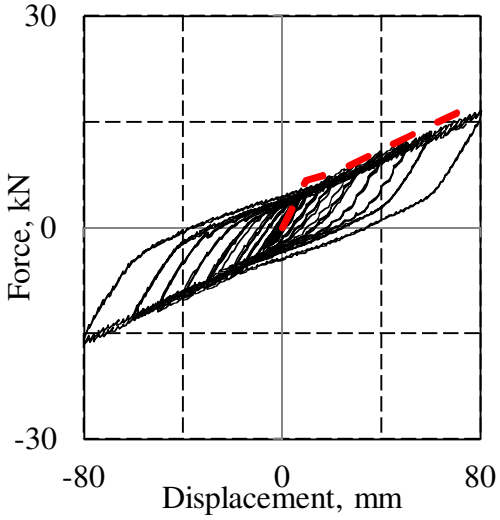

Test No. 2: Bends about the weak axis without axial force

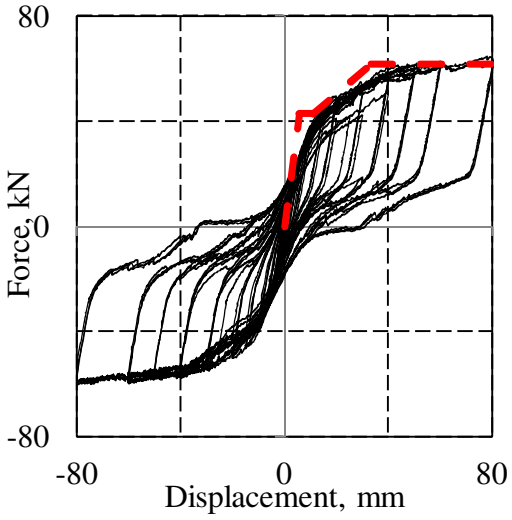

Test No. 3: Bends about the strong axis with axial force

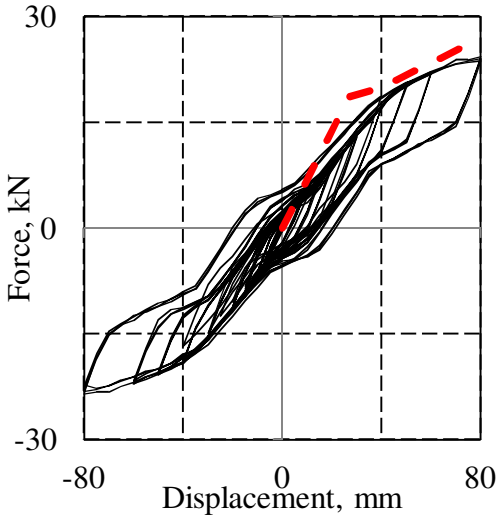

Test No. 4: Bends about the weak axis with axial force

Figure 8-5: Force-Displacement diagram of the WAFC bending about the strong and weak axis, with and without axial force, for Tests No. 1 to No. 4

8.3.3. SAFC Base

Figure 8-6 shows the strong axis bending force-displacement from the experimental test and the model for the SAFC without bolts in AFCs. The only effective element that provides

stiffness in the SAFC without bolts that bends about the strong axis is the prying actions on the compressive side. The plate on the tension side does not change the performance of the base connection, since no bolt is available to pull the plate over in this case.

From the column base moment-rotation curve in Figure 8-6 it may be seen that some energy is dissipated. This energy is likely to be related to friction at the compressive interfaces between the column and flange plate, where horizontal prying forces are developed due to vertical sliding at these locations. This test was conducted solely to verify the prying stiffness in the proposed method considering one plate and it seems to work well.

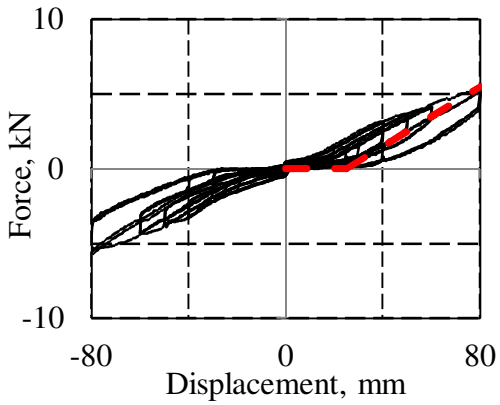

Figure 8-6: Force-Displacement diagram of the SAFC bending about the strong axis without AFC bolts

During the large magnitude cycles some yielding occurs on the flange plates, and gap opening occurs between the column flange and the flange plate. The effect of this yielding can be seen on the flat part of the curve between the drifts obtained of 25 *mm*. This flat part is an indication of the range of displacement where there is no rotational stiffness after prying yielding of the flange plates that was considered in the calculations. At larger drift cycles, this yielding causes the base moment resistance at zero displacement to increase compared to the previous cycles at the same level of displacement for prying cases, as shown in Figure 8-7

Test No. 6. This model does not consider yielding of flange plate explicitly.

Figure 8-7 shows experimental test and predicted model results for the SAFC with 4 bolts on each side of the column. Figure 8-7 Tests No. 6 and No. 8 correspond to row 3 of Figures 8-2 and 8-3, where Figure 8-7 Tests No. 7 and No. 9 correspond to row 4 of Figures 8-2 and 8-3.

The four stages listed previously represent the behaviour well for SAFC bending about the strong axis. In contrast, the cap plate did not slide up to 4% drift for the weak axis bending of the SAFC. Generally, this figure shows that the proposed mathematical model estimated the backbone of the SAFC for bending about X and Y axes except for:

i) In low magnitude cycles in Figure 8-7 Test No. 6, where sliding occurred at a lower force than predicted during the initial cycles. The reason for this behaviour is not known, but it is interesting to note that the predicted strength was reached in the larger cycles.

ii) In Figure 8-7 Test No. 9, where compressive yielding at the base of the column at the flange corners occurred in the previous tests. Therefore, the position of the neutral axis is closer to the middle of the section than predicted, which could be due to the previous yieldings at the flange corners.

Table 8-3 summarizes these results, along with the design critical predicted moment at 4% drift, M_{method}/M_{test}, and the secant base rotational stiffness at cap plate sliding. For the cases without cap plate sliding it was calculated at maximum drift, 4%, K_{method}/K_{test}. The following observations can be made from Table 8-3:

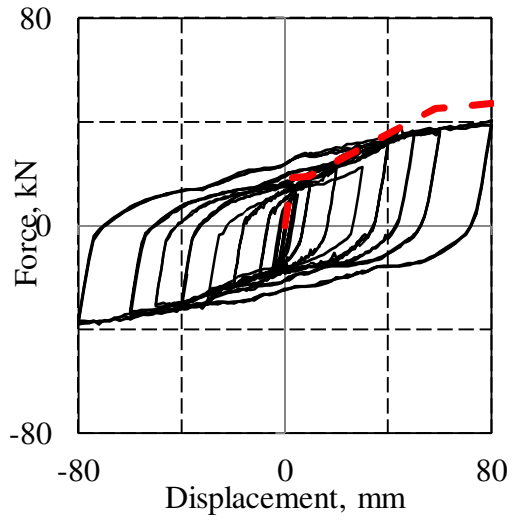

Test No. 6: Bends about the strong axis without axial force

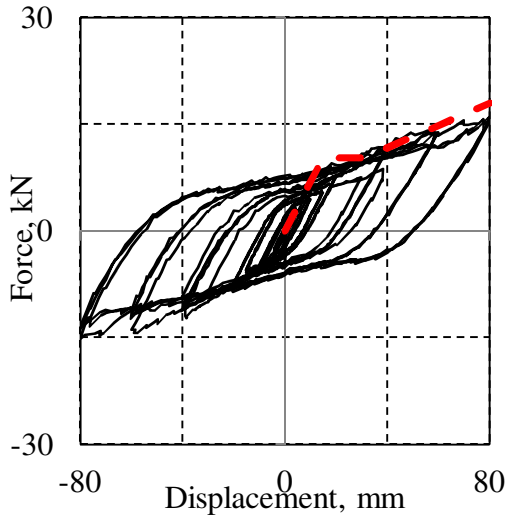

Test No. 7: Bends about the weak axis without axial force

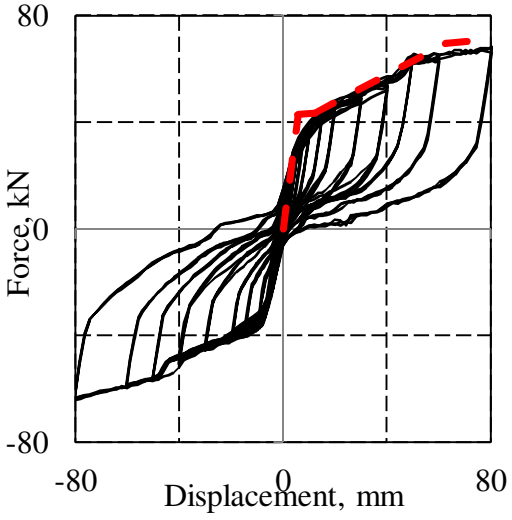

Test No. 8: Bends about the strong axis with axial force

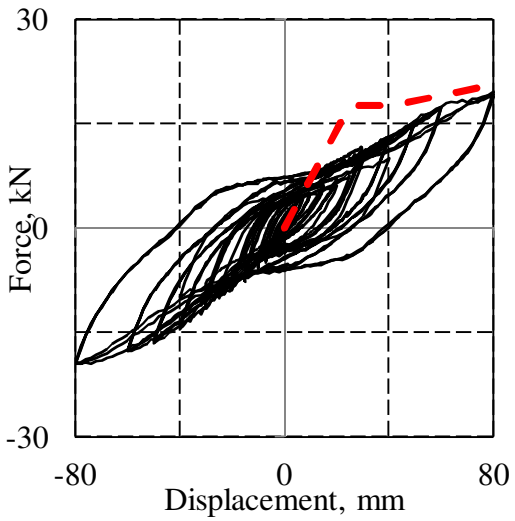

Test No. 9: Bends about the weak axis with axial force

Figure 8-7: Force displacement diagram of the SAFC bending about the strong axis, with and without axial force, for Tests No. 6 to 9

- Generally, the analytical method predicted the moment and stiffness with acceptable accuracy. On average, M_{method}/M_{test} at 4% drift was 1.025 with a coefficient of variation, COV, of 0.085, and K_{method}/K_{test} of 1.05 with a COV of 0.1. These results indicate the method can predict the overall performance of the SAFC and WAFC.

- When there was no prying the average M_{method}/M_{test} was 1.027 with a COV of 0.08, and K_{method}/K_{test} was 1.09 with a COV=0.06. For bending with prying the average of M_{method}/M_{test} was 1.07 with a COV=0.06, and K_{method}/K_{test} was 0.971 with a COV=0.07.

Table 8-3: Test data and comparison with analytical method

Test No	Type	Direction	Prying[a]	n_{bolt}[b]	P_u, kN	M_{method}/M_{test}	$K_{\theta method}/K_{\theta test}$
1	WAFC	Strong	No	Four	0	0.934	1.032
3	WAFC	Weak[d]	Yes	Four	0	1.107	0.867
2	WAFC	Strong	No	Four	320	0.997	1.072
4	WAFC	Weak[d]	Yes	Four	320	1.039	1.021
5	SAFC	Strong	Yes	0	0	1.000	1.005
6	SAFC	Strong	Yes	Four	0	1.163	1.026
8	SAFC	Weak[d]	No	Four	0	1.126	1.185
7	SAFC	Strong	Yes	Four	320	1.041	0.934
9	SAFC	Weak[d]	No	Four	320	1.051	1.082

[a] Does Prying affect the base performance?
[b] Number of the sliding bolts in one side of column
[c] Applied axial force
[d] Cap-plate sliding did not occur at 4% column drift.

8.4. Summary

This chapter develops a general macro model that describes the backbone curve of new low damage column base connections. The model is compared with the results of nine experimental tests. It was shown that:

i) The macromodel developed based on mechanics and a number of assumptions considering friction, bending of boundary plates, bolt bearing for loading in the two directions to represent the backbone response of the tests. The model is an advance on

similar models used for sliding hinge connections at the ends of beams in moment frames, not only because it is developed considering axial force, and bending about both axes, but also as it explicitly includes flange plate bending/prying and bolt hole oversize in the flexural stiffness/strength assessment. Prying was significant for strong-axis bending of the SAFC, and weak axis bending of the WAFC. The model considered 4 different stages of deformation.

ii) The macro model developed estimated the overall response of virgin specimens for testing in both directions including describing the appropriate modes of deformation. In addition, for columns that had been subject to some types of previous testing, the stiffness at low displacements was overestimated. Average peak strength and average secant stiffness to cap-plate sliding was predicted to an accuracy of better than 5%, and 2%, respectively.

In the next chapter, experimental testing of asymmetric friction connections (AFCs) using 2 M16 Grade 10.9 bolts with higher strength, but less ductility, compared to Grade 8.8 bolts is described to enable understanding of the effect of this change, and enable its inclusion into any modelling or design recommendations.

Chapter 9: Cyclic Performance of Asymmetric Friction Connections with Grade 10.9 Bolts

9.1. Introduction

One friction connection subject to significant research is the asymmetric friction connection (AFC) (Clifton, 2005; MacRae et al., 2010). As shown in Figure 9-1, this connection consists of 3 plates. The top structural steel plate, grey colour, is placed above a slotted structural steel plate that is, in turn, placed above a cap plate. Shims are placed between the top plate and the slotted plate and may also be placed between the slotted plate and the floating (or cap) plate. If a shim is not placed beside the cap plate, the cap plate itself may be made of shim material to obtain dependable sliding resistance. The floating plate, denoted the cap plate, is connected to the subassembly by means of the high strength bolts. Because sliding does not initiate at the same displacement on either side of the slotted plate, this connections is referred to as an *asymmetric friction connection* (AFC).

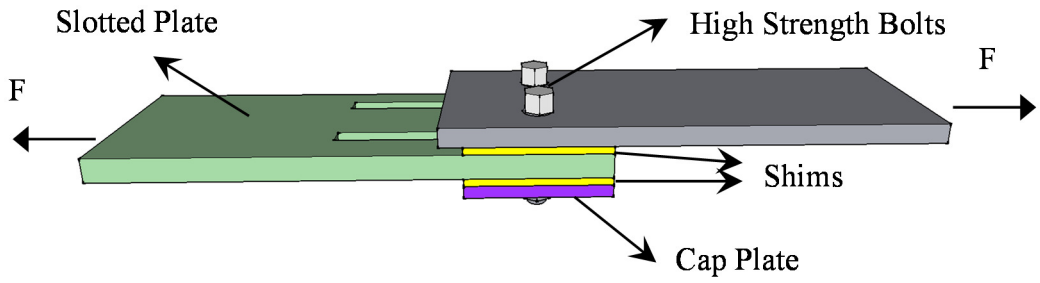

Figure 9-1: AFC configuration showing slotted plate, bolts, shims, and cap plate

The sliding force is dependent on both the shim-steel plate friction coefficient and the normal force on the surfaces. The normal forces are controlled by the bolt tension force. Bolt strength

and deformation capacity affect the ability of the bolt to provide reliable normal forces over large sliding displacements. Chanchí et al. (2012b) indicate that the most reliable friction sliding may be obtained if the hardness of the materials on either side of the sliding interface is very different. For this reason, high hardness shims are generally used.

Previous tests used Grade 8.8 bolts to provide interface clamping forces (Khoo et al., 2012b; Chanchí et al., 2012a). In the NZ steel standard, Clause 4.2.4.1.2c in NZS3404 (2007), the length of threaded bolt within the grip length is required to be at least 5 threads for a bolt length up to and including 4 times the bolt diameter. This constraint extends to 10 threads for a bolt length exceeding 8 times the bolt diameter, and 7 threads for intermediate bolt lengths. This requirement, which is not in many overseas codes, was developed based on bolt fractures during proof-loading on construction sites. They were not developed in consideration of any sliding friction issues.

It was considered that using higher strength bolts with greater clamping forces may be desirable because they result in more economical sliding connections. Such connections would require a lower number and/or size of bolts, which in turn would also reduce the length of the friction connection. However, there are concerns that the applied compressive force using lower numbers of bolts would not provide a uniform stress over the sliding surfaces, but could instead result in higher localized bearing stresses near the bolts, especially if the plate thicknesses are small. This stress may result in more degradation of the sliding surface, particularly near the bolt locations. In addition, there are concerns that the requirements of NZS3404 (2007) Clause 4.2.4.1.2c for the required number of threads in the grip length, may not be appropriate for higher strength, but less ductile, bolts.

Chanchí et al. (2014) conducted 2 cyclic tests using Grade 8.8 bolts with length of 120 mm and shank length of 80mm. The number of the threads within the grip length was 7. In addition, 21 cycles up to +/- 90 mm were applied and there was no bolt fracture and little connection strength degradation. The displacement regime for Test No. 1 was then re-applied after the connection had cooled several hours after Test No. 1 without retightening of the bolts and with the same plates as in Test No. 1. The shims, cap plate, and slotted plate were changed for Test No. 2. The second run (Test No. 2) was conducted without retightening of the bolts. The average of sliding force is 75 kN for both runs of Test No. 1, and 72.5 kN for Test No. 2, as shown in Figure 9-2.

From the standard nominal bolt properties in Table 9-1, it may be seen that the expected increase in initial sliding strength for Grade 10.9 bolts, compared to Grade 8.8 bolts, as estimated from the proof load ratio, is 830kN/600 kN = 1.38. In addition, the ultimate bolt elongation of Grade 10.9 bolts is 9%/12% = 0.75 times that of Grade 8.8 bolts, indicating that the stronger bolts are likely to fracture at a lower strain. Hence, there exists the normal trade-off between sliding force based on a bolt strength and reduced ductility.

Thus, there is a need to address concerns related to the use of higher strength bolts in sliding connections. In particular, answers are sought to the following questions:

1. How do AFC connections with Grade 10.9 bolts perform?
2. What minimum threaded length is appropriate to limit the possibility of Grade 10.9 bolt fracture to be similar to that for Grade 8.8 bolts?
3. Are special plate thickness requirements appropriate for Grade 10.9 bolts?

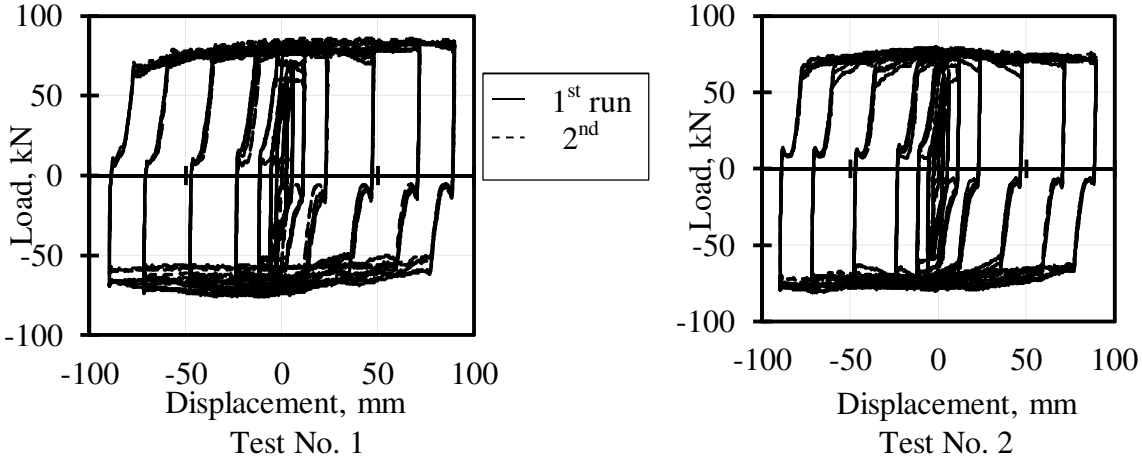

Figure 9-2: Force-displacement plot on AFC with grade 8.8 bolts (Chanchí et al., 2014). Left plot shows the force displacement for the 1st and 2nd runs of Test No.1. Right plot shows force-displacement of the new specimen in Test No. 2 with 1st and 2nd runs

Table 9-1: Standard Bolt Properties Grade 8.8 and 10.9 according to Bickford (1995)

Grade	Proof stress	Yield stress	Ultimate stress	Elongation
8.8	600	660	830	12%
10.9	830	940	1040	9%

9.2. Methodology

9.2.1. Details of AFC, Test setup, and Testing Plan

In the test configuration, a brace was placed horizontally, and the AFC was placed between the brace and a moving support, as illustrated in Figures 9-3 and 9-4 following Chanchí et al. (2014). The load cell and moving bracket were restricted against out-of-plane movement to prevent prying. The length of the 250 PFC Grade 300 brace was 2860 mm. A 16x200x300 bearing plate is welded to the inside of the PFC-section brace to increase brace buckling

resistance. The two 200 mm slotted holes were cut in the slotted plate attached to the moving bracket allowing 100 mm sliding in each direction. This sliding length is appropriate for a friction brace, rather than to a sliding hinge joint type connection (MacRae et al. 2010), where much smaller displacements are generally expected. The total thickness of the plates held together by the 2M16 120mm long Grade 10.9 bolts was 8mm + 2 x 6mm + 32mm + 16mm+ 16mm = 84 mm. The total grip, including washers, was 93 mm. The bolt shank length is 80 mm and the threaded length is 40 mm. The number of threads within the grip length was 7, which satisfied the NZ code requirement for a bolt length between 4 and 10 times the bolt diameter. All plates were Grade 300 steel. The 6mm shims were Bisalloy500 (2012) with a Rockwell hardness of 500, and the AFC bolts were Grade 10.9 bolts with actual ultimate and yielding stress of 1121 MPa, and 955 MPa, respectively.

Four linear potentiometers with 25mm stroke were attached between strong floor and the brace to monitor brace out-of-plane deformation, as shown in Figure 9-3. Horizontal movements of the brace and AFC were monitored by a rotary pot attached to the fixed bracket at the end of the brace. Horizontal force was monitored by the load cell attached to the actuator.

Five tests were conducted, as described in Table 9-2. In this table, a new number is used when the element is replaced. In the first test, slotted plate, shims, bearing plate, and bolts were new. However, for the remaining tests, Tests No. 2 to No. 5, the bearing plate was not changed, as it was welded to the brace. The slotted plate, shims and bolts were changed for Test No. 2. For Test No. 3 only the bolts were changed from Test No. 2. Test No. 4 was carried out without retightening of the bolt or changing of any plates to study AFC performance without retightening the Grade 10.9 bolts. In the last test, all bolts and shims

were replaced.

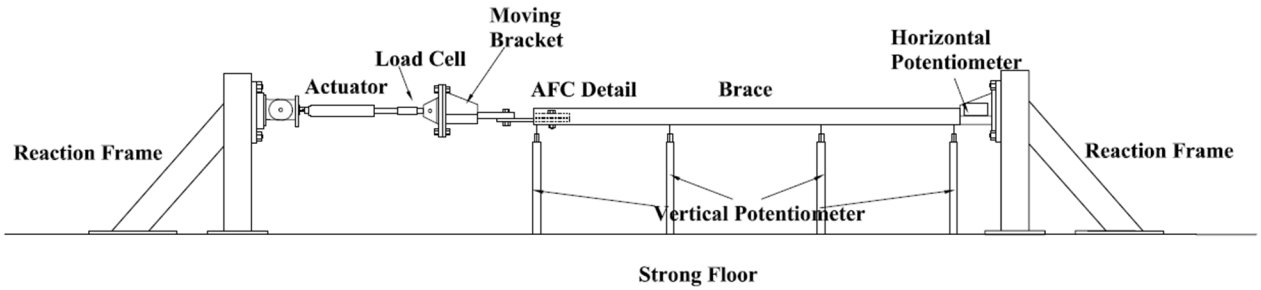

Figure 9-3: Test setup

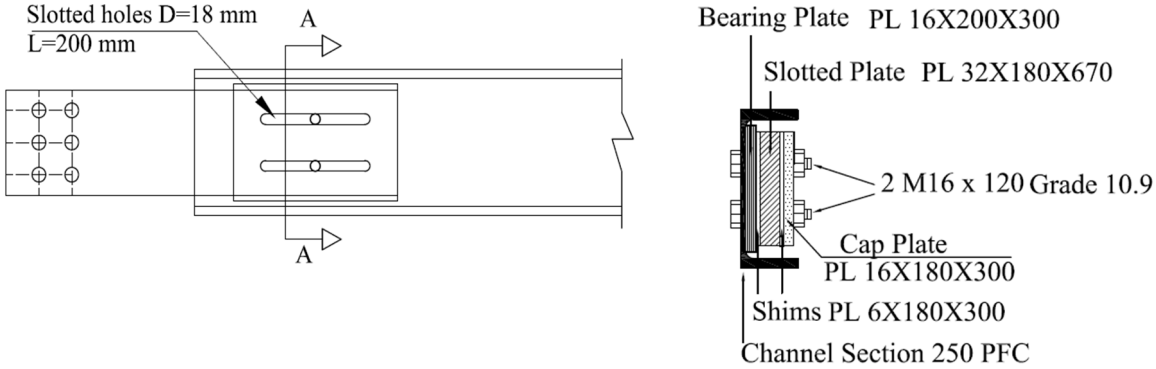

Figure 9-4: Tested AFC detail. Left is the longitudinal configuration of the specimen, and the section A-A is on right

Table 9-2: Tests Conducted

Test	Slotted Plate	Shims	Bolts	Bearing plate	Bolt retightened
1	1	1	1	1	Yes
2	2	2	2	1	Yes
3	2	2	3	1	Yes
4	2	2	3	1	No
5	2	3	4	1	Yes

9.2.2. Test Regime

The displacement regime was applied with a constant velocity of 3 mm/s. This loading regime consisted of 21 cycles with amplitudes between 3 mm and 90 mm. This value is 45%

of the slot length, as illustrated in Figure 9-5. Three cycles at each level of displacement were applied as shown.

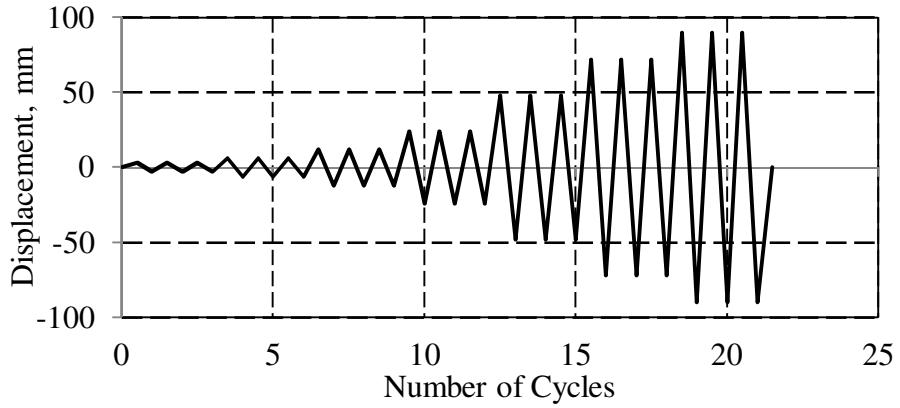

Figure 9-5: Test loading regime

9.2.3. AFC Bolt Tightening

According to New Zealand steel structures standard (NZS3404, 2007) all bolts in a friction connection must be tightened at least to the minimum bolt tension specified in the standard. This value is commonly referred to as the proof load. Five simple tests were conducted to obtain the torque and nut rotation for the bolt elongation corresponding to the proof load, Δ_{Bolt}, computed based on the bolt axial stiffness (Bickford, 1995) defined:

$$\Delta_{Bolt} = \frac{N_{tf}}{E}\left(\frac{L_{sh}}{A_{sh}} + \frac{L_{th}}{A_{th}}\right) = \frac{130 \times 10^3}{200 \times 10^3}\left(\frac{81}{201} + \frac{26.5}{157}\right) = 0.37\ mm \quad (9\text{-}1)$$

Where, N_{tf} is the proof load of the bolt, L_{sh} is the shank length plus half of the bolt head thickness, A_{sh} is the shank area, L_{th} is the threaded length of the bolt from the nut up to the shank plus half of the nut thickness, and A_{th} is the bolt tension area. For the total grip length of 91 mm, the M16 Grade 10.9 bolts were tightened by applying torques increasing from 40 N.m to 550 N.m. At each step, torque, bolt elongation and turn-of-nut were recorded and

the values at a bolt elongation of 0.37mm corresponded to the proof load, defined by Equation 9-1.

9.2.4. Analytical Predictions of Behaviour

The AFC connection initial nominal sliding force, F_s, was estimated using (MacRae et al., 2010):

$$F_S = n \times \mu \times \eta \times N_{tf} = 2 \times 0.21 \times 2 \times 130 = 109.2 \text{ kN} \quad (9\text{-}2)$$

Where, n is number of the bolts in the AFC, μ is the effective friction coefficient for the Bisalloy500-steel interface taken as 0.21 according to Chanchí et al. (2012b), η is the number of shear planes, and N_{tf} is the proof load per bolt. For design, a strength reduction factor, ϕ, of 0.70 is generally used acknowledging the uncertainty associated with friction connections. Based on recommendations used in construction (Leslie et al., 2013) an overstrength factor of 1.4 is reasonable. This factor is affected by factors including variability of bolt tightening, and different sliding surfaces.

9.3. Results

9.3.1. Torque, Nut Rotation, and Bolt Elongation

The median torque and nut rotation corresponding to the bolt proof load bolt elongation of 0.37mm are 370 N.m and 185 degrees, respectively, according to Figure 9-6. This result is similar to the NZS 3404 Clause 15.2.5.2 recommendation that the nut rotation from the snug

tight condition, for a bolt with the length of over 4 diameters, but not exceeding 8 diameters, is ½ turn. The equivalent torque and nut rotation for Grade 8.8 bolts tested the same way were 330 N.m and 550 degrees, respectively (Chanchí et al., 2012b). The bolts were cleaned by acetone before conducting the test to reduce the lubrication is much as possible.

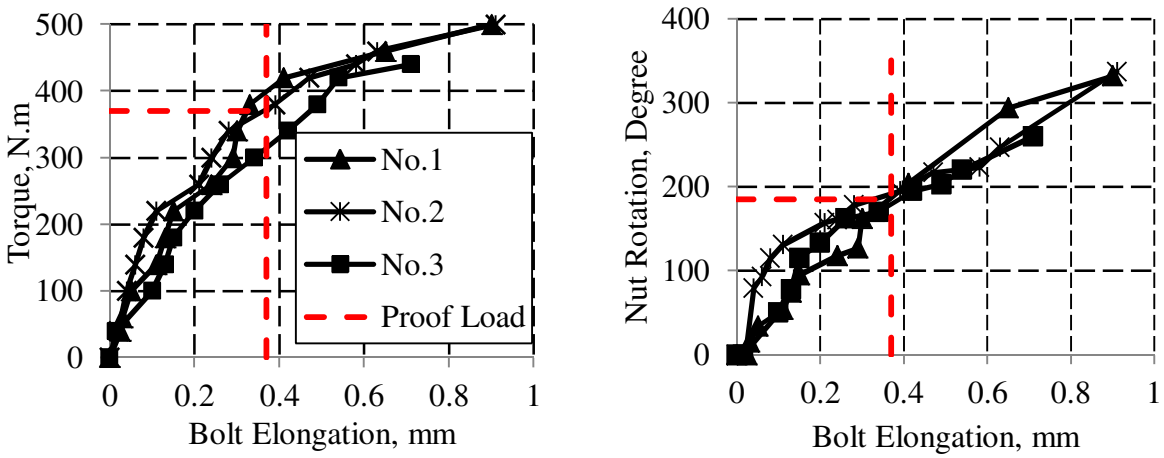

Figure 9-6: Nut rotation, torque, and bolt elongation relation. Left figure shows torque and the bolt elongation relation, and right is the nut rotation- bolt elongation relation

9.3.2. Sliding Tests

The hysteresis loop for Test No. 1 is shown in Figure 9-7, where positive force indicates compression. The hysteresis loops are not square because of the bolt-hole oversize. The bolts move on an angle, so there is approximately a 10mm slack displacement area before the bolt carries increased load. Initial tension and compression sliding forces were 123kN and 101kN, respectively giving an average initial sliding force of 112 kN. This value is close to the nominal value of 109kN computed in Equation 9-2 for Grade 10.9 bolts, shown as the solid line. In addition, the average sliding force of AFC with Grade 10.9 was 1.5 times that of the AFC with Grade 8.8 bolts. According to Chanchí et al. (2014), the tensile/compressive strength difference occurs due to bending in the non-clamped zone of the slotted plate, and this difference is caused by the AFC asymmetry.

In the third cycle to 48 mm displacement, the force increased to the maximum recorded value of 163 kN, as shown in Figure 9-7, and one of the bolts fractured. This force is 91% greater than the strength of 85 kN for the Grade 8.8 bolts reported by Chanchí et al. (2014). The increased sliding force is possibly due to larger particulates separating from the sliding surfaces due to the increased force. These particulates can be observed on the degraded slotted plate at the end of the test that is shown in Figure 9-8. No overlap of bearing area was observed in the slotted plate and the stress was distributed with 31 degrees angle according to the observed degradation on the plate.

As a result of the increased localised bearing stress causing material degradation, bolt elongation occurred, leading to causing higher sliding stresses until the bolt fractured. Bolt elongation occurs due to the separation of small steel particles during the material degradation as a result of the high localized stresses. At larger displacement levels, a greater number of small particles or bigger particles may separate.

The theoretical elongation of the Grade 10.9 bolts over the grip length at proof load was 0.37mm according to Equation 9-1. The strain at proof load over the threaded length, ε_{proof}, is 0.414%. The maximum bolt deformation before fracture, Δ_{ub}, may be estimated assuming all inelastic deformation occurs in threaded length of the bolt from the nut up to the shank plus half of the nut thickness, L_{th}, that is estimated from:

$$\Delta_{ub} = \left(\varepsilon_{ult} - \varepsilon_{proof}\right) \times L_{th} = (0.09 - 0.00414) \times 26.5 = 2.3\ mm \quad (9\text{-}3)$$

Where, ε_{ult} is the maximum bolt elongation in Table 9 1. For Grade 8.8 bolts, Δub = 3.1 mm. Bolts, slotted plate and shims were replaced after Test No. 2, and the average initial sliding force was 107 kN. The sliding force dropped to 70% of the initial sliding force at 24 mm

displacement, as shown in Figure 9-7, possibly as a result of permanent bolt elongation reducing the compressive test. No bolt fracture was observed at the end of this test.

In Test No. 3, only the bolts were replaced and they were tightened with a torque equal to 370 Nm to reach the proof load according to Figure 9-6. This test is similar to Test No. 2, with new bolts, except the shims were reused. Degradation of plates caused different levels of sliding force for the same level of drift, as illustrated in Figure 9-7. The minimum of the maximum sliding forces occurred in the last cycle and was 27% of the value measured in the first cycle. At 48mm displacement, the sliding force was 36% of that in the previous cycles, possibly due to bolt necking and nonlinear deformation. This behaviour was not observed for the AFC using Grade 8.8 bolts, except when the assembly materials were significantly worn causing instabilities in the behaviour of the AFC.

Test No. 4, evaluating the effect of previous cyclic loading on a joint, was conducted several hours after Test No. 3, so the joint had first cooled, and the test was run without retightening or replacing of plates and bolts. It may be seen from the force-displacement curve in Figure 9-7 that the sliding force was less than that of the previous tests, presumably as a result of bolt length elongation due to inelastic deformation. Such deformation reduces the interface force and thus the friction. During these additional cycles, one of the bolts fractured at 49 mm displacement. The sliding force of Test No. 4 is about 70% of Test No. 3 for displacements up to 48 mm. For Grade 8.8 bolts the sliding force of repeated tests was 90% of a test with new elements (Chanchí et al., 2014).

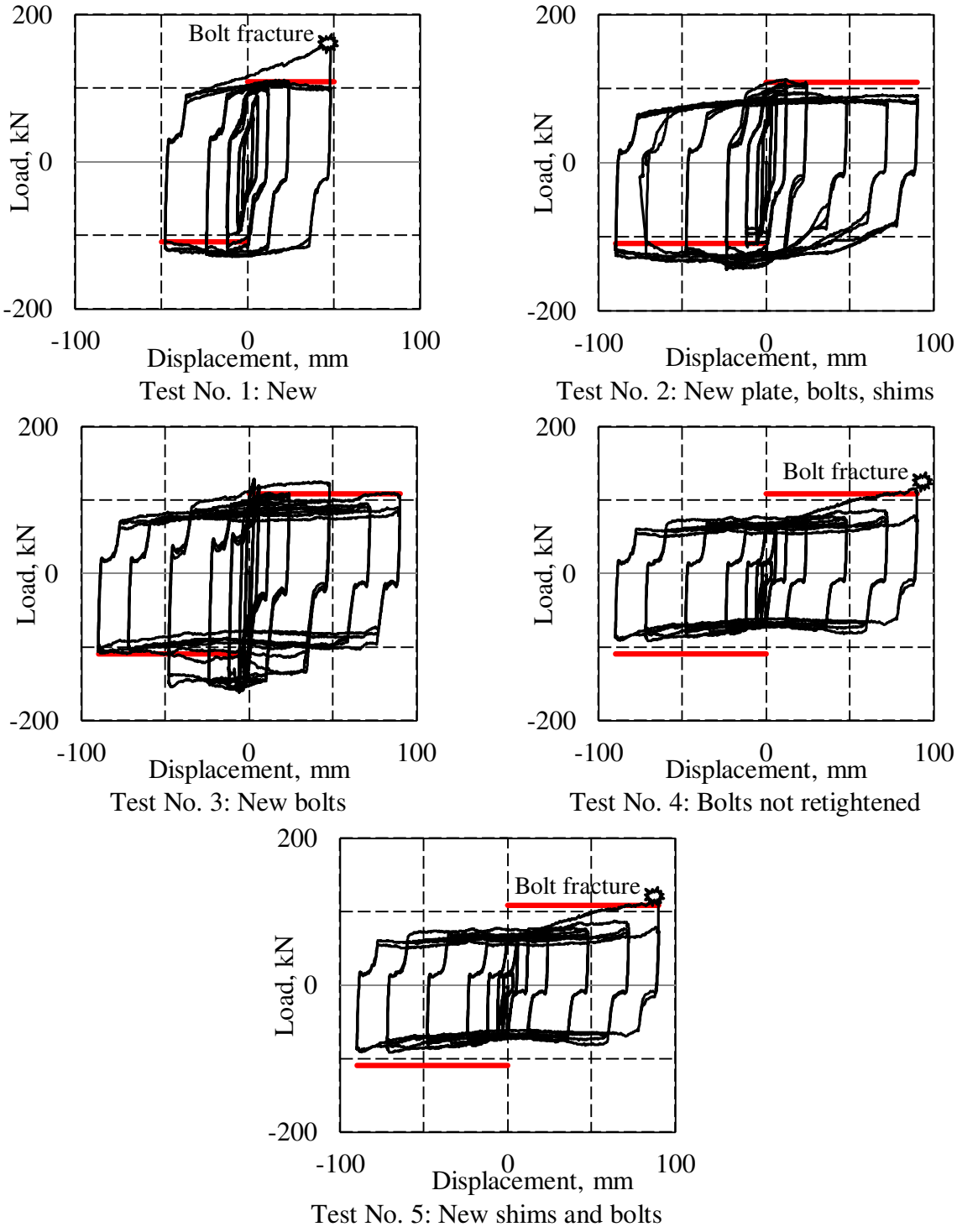

Figure 9-7: Force-Displacement Plot for AFC with Grade 10.9 bolts for Test No.1 to No. 5

In the final test, Test No. 5, both bolts and shims were replaced, but the same slotted plate was used. The average initial strength of 85kN was only 77% of the nominal value from

Equation 9-2 and from Test No. 1, as shown in Figure 9-7. This result occurred because 42 cycles were conducted on the slotted plate before this test. One of the bolts fractured in the second cycle to 90 mm displacement and the other bolt was highly deformed, as illustrated in Figure 9-9.

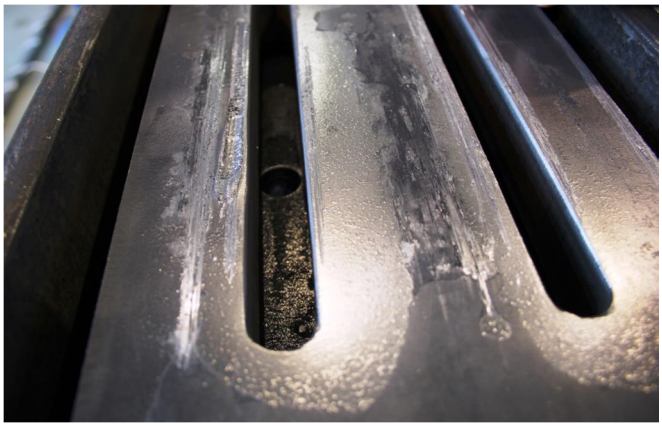

Figure 9-8: Degraded plate at the end of Test No. 1

Figure 9-9: Deformed and fractured bolts at the end of Test No. 5

The median sliding force for Tests No. 1 to No. 5 in the first cycle to different displacement levels is shown in Figure 9-10, and the dashed line shows the calculated nominal sliding force

from Equation 9-2. Generally, as sliding length increased, there is a reduction in the sliding force. This reduction is due to the bolt moving on an angle and greater MPV interaction that also can caused bolt nonlinearity.

The sliding force in each test, other than Test No. 4 where the bolts were not retightened, is also reduced due to reduction of the friction coefficient. This result occurs because the slotted plate was not changed from Tests No. 2 to No. 5. The maximum reduction of friction coefficient in Test No. 2 of the AFC with Grade 8.8 bolts was 0.9 of the friction coefficient in Test No. 1, as reported by Chanchí et al. (2014). The trend of Test No. 4 is slightly different to those of the other tests. After 48mm of displacement, the sliding force for Test No. 4 increases, whereas the sliding forces for other tests generally decrease with increasing displacement. This last behaviour could be caused by the debris being stuck between plates, causing extra force to be required to achieve sliding.

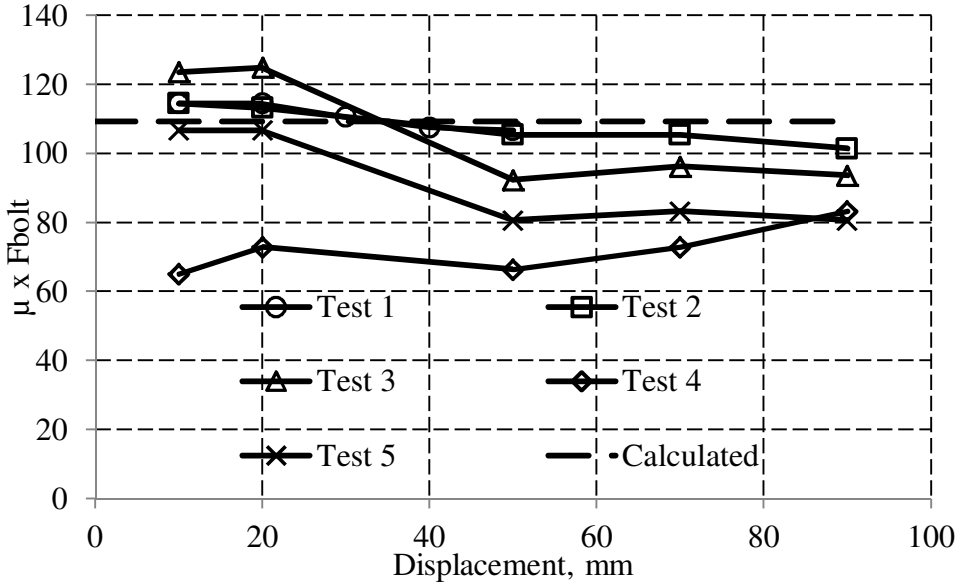

Figure 9-10: Tests No. 1 to No. 5 Sliding force at Different Displacements

9.4. Recommendations

I. A minimum thickness plate is required to prevent excessive localized bearing stress that can result in sliding surface deterioration. This thickness depends on the bolt strength and size of the bolt head. The bearing area, A_b, of the slotted plate from bolt tensile force is defined:

$$A_b = \frac{\pi \times (d_{eff}^2 - {d_h}^2)}{4} \tag{9-4}$$

Where, d_{eff} is effective diameter at the plate surface by assuming the stress is distributed with 30 degrees angle according to:

$$d_{eff} = d_{head} + 1.15 \times (t_{washer} + t_{shim} + t_{plate}) \tag{9-5}$$

d_h is hole size, d_{head} is diameter of bolt head that can be considered as the longest dimension, t_{washer}, and t_{shim} is thickness of the washer and shim, respectively, t_{plate} is thickness of the plates that are between the slotted plate and bolt, cap plate or bearing plate and brace web.

For more than one hole, the bearing area is as defined in Equation 9-4 minus the stress overlap area. From Figure 9-11, it appears that the greatest stress should be on the area between the slotted holes, as the stress areas overlap this area. For thicker plates, the average stress on the sliding interfaces from each bolt decreases due to the spread of stress with distance. Since the total compressive force is the same, the sliding compressive force is similar. However, thicker plates can also increase the likelihood of an area of stress overlap, where the average stress is *n* times that from one bolt, where *n* is the number of bolts

contributing to the stress there. It is recommended that the spacing of bolts be such that there is no stress overlap area. This point recommended that the peak stress, at the interface area, is the minimum plate thickness to prevent the overlap area since increasing thickness of the plates can prevent the overlap area from bolts.

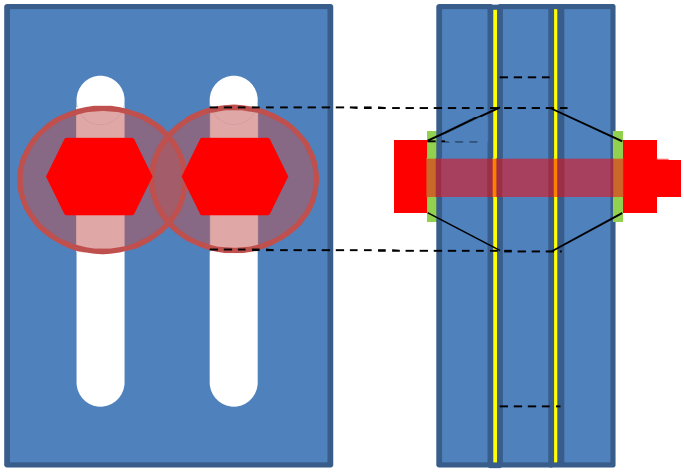

Figure 9-11: Localized bearing stress

II. Since the majority of inelastic deformation occurs in the threaded length of bolt in the grip length, the NZ standard should be modified for Grade 10.9 bolts considering that the ultimate elongation of Grade 10.9 bolts is 75% that of Grade 8.8 bolts (Bickford, 1995). Therefore, the length of threaded Grade 10.9 bolt within the grip length should be required to be 1/0.75 = 1.33 times that of the Grade 8.8 bolts. This length thus demands at least 7 threads for a bolt length up to and including 4 times the bolt diameter, 14 threads for a bolt length exceeding 8 times the bolt diameter, and 10 threads for intermediate bolt lengths.

III. The number of threads may need to be greater for shorter bolts since they have lower elastic deformations during the same bolt tightening than longer bolts.

IV. Retightened bolts should not be used since the level of sliding force is considerably reduced.

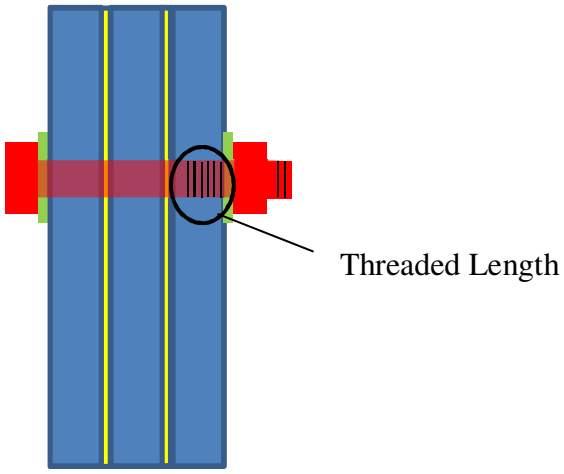

Figure 9-12: Threaded length within the grip length

9.5. Summary

This chapter describes the experimental testing of an asymmetric friction connection (AFC) with Grade 10.9 bolts under cyclic loading to displacements in one direction as large as 90mm. It was shown that:

- Some of the bolted connections with Grade 10.9 bolts suffered from fracture, and there was considerable wear on the sliding surfaces. Fracture did not occur to the same extent in similar tests using Grade 8.8 bolts.

- Since the nominal deformation capacity of Grade 10.9 bolts is 75% of that for Grade 8.8 bolts, the threaded length for these bolts should be at least 1/0.75 = 1.33 times that required for Grade 8.8 bolts.

- Since the nominal strength of Grade 10.9 bolts is approximately 38% greater than that of Grade 8.8 bolts, the thickness of plates required to limit localized bearing

stress and material scour during sliding should be increased. Calculation of bearing stress needs to consider the effect of the holes either side of the sliding interfaces. Dispersion angle of 31 degrees was obtained from the experiments.

In the next chapter, the cyclic performance of the base connection with yielding angles is described.

Chapter 10: The Base Connection with Yielding Angles

10.1. Introduction

One way to minimize damage at the base of columns in steel moment frames is to connect the column to the base plate by replaceable angles. The angles should be weaker than other components at the base of structure, so that the main inelastic actions occurred in the angles which can be replaced and after strong earthquake shaking. This type of connection is widely used for beam to column connections.

Many experimental studies have been performed on this connection (Rathbun, 1936; Maxwell et al., 1981; Stelmack et al., 1986; Roeder et al., 1996) to characterize its seismic performance. In addition macro models have been developed that were verified by experimental tests such as Frye and Morris (1975), Kishi and Chen (1990), and Pirmoz et al. (2009). The main differences between column base connections and beam to column joints is the existence of axial force and bidirectional loading in column base connections. Dundu (2012) conducted 16 monotonic tests on connections with angles and found satisfactory behaviour of this type of base connection.

From the above discussion, it can be seen that if low damage base connections with yielding angles are to be designed with confidence there is a need to develop models that allow their performance to be assessed considering axial load and bidirectional loading. This chapter seeks to address this need by seeking answers to the following questions:

i) Can a base connection with yielding angles be considered low damage if it is subject to axial force and bi-directional loading?

ii) Can simple models be developed to describe the performance of these connections?

iii) What lessons can be learnt about the behaviour of such connection?

Many analytical studies have been conducted to develop macro model for performance of beam to column joint with top and seat angles. In this chapter the models developed by Frye and Morris (1975), Kishi and Chen (1990), and Pirmoz et al. (2009) are used for test specimens. In particular, the Frye and Morris (1975) and Kishi and Chen (1990) studies were some of the pioneer models and highly referenced methods, and the method by Pirmoz et al. (2009) is one of the latest developed models in this area.

Frye and Morris (1975) developed the relation between moment, M, and rotation of the top and seat angle connection, θ_r, with the general format:

$$\theta_r = C_1(KM)^1 + C_2(KM)^3 + C_3(KM)^5 \quad (10\text{-}1)$$

Where the curve fitting constants C_1, C_2, and C_3 and the standardization constant, K, are summarized in Table 10-1, where l_a is length of the angles, d_b is diameter of the angle hole, d is depth of the beam, and t is the angle thickness.

Table 10-1: Curve fitting constants and standardizations constants for the Frye-Morris polynominal model

Curve fitting constants	$C_1 = 8.46\times10^{-4}$
	$C_2 = 1.01\times10^{-4}$
	$C_3 = 1.24\times10^{-8}$
Standardization constant	$K=d^{-1.5}\, t^{-0.5}\, l_a^{-0.7}\, d_b^{-1.5}$

Kishi and Chen (1990) proposed a macro modelling for estimation of the initial elastic stiffness, k_i, and ultimate moment capacity, M_u, of this type of connection by assuming:

$$k_i = \frac{3EI}{1 + (\frac{0.78t_t^2}{g_1^2})} \times (\frac{d_{1a}^2}{g_1^3}) \quad (10\text{-}2)$$

$$M_u = \frac{\sigma_y l_s t_s^2}{4} + \frac{V_p g_2}{2} + V_p(d + \frac{t_s}{2} + k) \quad (10\text{-}3)$$

Where: $(\frac{V_p}{V_0})^4 + \frac{g_2}{t_t}\left(\frac{V_p}{V_0}\right) - 1 = 0 \quad (10\text{-}4)$

Where EI is the bending stiffness of the angle's leg adjacent to the column face, $g_1=g_t-D/2-t_t/2$, D is the nut diameter, t_t is the thickness of the top angle, g_t is the gage distance from the top angle's heel to the centre of the fastener, d_{1a} is the distance between the centres of the legs of the top and bottom angles that is $=d+t_t/2+t_s/2$, t_t and t_s are the thickness of the top and bottom angles respectively, d is total depth of the beam section, σ_y is yielding stress of the angle, l_s is the width of the seat angle, t_s is the thickness of seat angle, g_2 is the distance between the plastic hinges as shown in Figure 10-1, k is the distance from the top angle's heel to the toe of the fillet as shown in Figure 10-1, V_p is ultimate force that causes formation of plastic hinges in the angle as given in Equation 10-4, and $V_0=\sigma_y l_l t_t/2$. In this model, two plastic hinges were assumed to occur in top angle at the ultimate condition as shown in Figure 10-1.

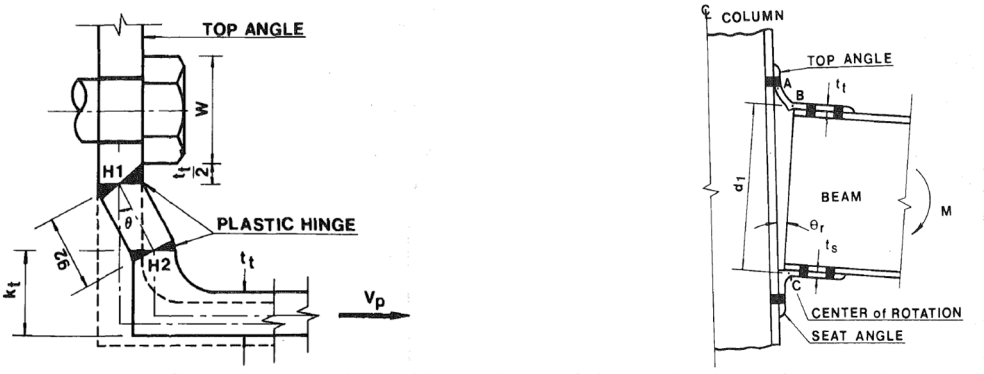

Figure 10-1: Deflected connection with angles. Left is mechanism of top angle at the ultimate condition, and right is deflected configuration at the elastic condition

Pirmoz et al. (2009) developed an analytical model for this connection by presenting equations for initial stiffness of the connection, K_i, connection plastic moment, M_p, yielding moment of the connection, M_y, defined as:

$$K_i = h_b^2 \times \frac{1}{\frac{(g-t)^3}{3\alpha E_a I_a} + \frac{l_b^3}{nE_b I_b}} \quad (10\text{-}5)$$

$$M_p = \frac{\beta \sigma_y b t^2}{4g} \times h_b \quad (10\text{-}6)$$

$$M_y = \frac{M_p}{1.5} \quad (10\text{-}7)$$

Where σ_y is yielding stress of the angle, l_b and n are the column top angle bolts' shank length and number of the bolts, respectively, E_a and I_a are the top angle cross section moment of inertia for vertical leg in bending and elastic modulus of angle material, E_b and I_b are the bolt cross section moment of inertia and elastic modulus of bolt material, t is the angle's thickness, g is the gage distance from the top angle's heel to the centre of the fastener, h_b is the beam depth, β is a representation of the formed mechanism and a method for its calculation was fully described by Pirmoz et al. (2009), b is length of the angle.

10.2. Methodology

10.2.1. Experimental Program

- **Detailing of the Base Connection with Angles**

The angles are bolted to the 310 UB 46.2 Grade 300 column section with 8M24 Grade 8.8 bolts that were snug tightened, as shown in Figure 10-2. In addition, they were connected to

the base plate and the foundation by 4M24 Grade 10.9 un-bonded anchor rods with effective length of 550 mm passed through steel tubes placed in the concrete foundation and were anchored at the bottom of the foundation, as shown in Figure 10-2.

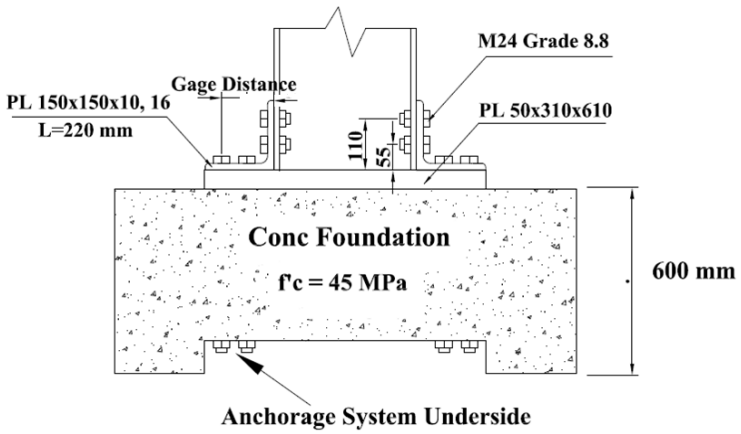

Figure 10-2: Base connection detail

The test column was universal beam (310 UB 46.2) since UB sections are more efficient and common in drift-governed ductile moment resisting frames than universal column (UC) and welded column (WC) sections. The distance from top of the base plate to the point of lateral force application was 1980 mm. All drift values are based on this height. The base plate was placed on top of a 5 mm layer of dental plaster to provide full contact. The anchor rods were post-tensioned until the axial force measured by the load cells beneath the nuts was 85% of the bolt minimum proof load, while twisting of the load cells was prevented. The value of 85% was calculated to prevent any uplift of the base plate. In these tests, a 50mm thick base plate and post-tensioned anchor bolts were used to reduce the base flexibility.

To have a comprehensive estimation of the performance of the base connection with yielding angles the five cyclic tests shown in Table 10-2 were conducted in the order shown. The main

objective in Tests No. 1 and 2 is to find the effect of the gage distance on performance of this type of base connection. The effect of angle thickness on base performance can be studied by comparing Tests No. 1 and 3. To find the effect of axial load on performance of base connection Test No. 4 was carried out. Finally, Test No. 5 was conducted to study the performance of this type of base connection under actual circumstances, which are generally bi- directional loading under axial load.

Table 10-2: Tests Conducted

No	Axis of Bending	Axial force	Angle	Gage distance, mm
1	Strong	Zero	150X150X10	110
2	Strong	Zero	150X150X10	55
3	Strong	Zero	150X150X16	110
4	Strong	320kN ($0.20N_s$)	150X150X10	110
5	Bi-directional	320kN ($0.20N_s$)	150X150X10	110

- **Test Setup and Loading Regime**

The loading regime and test setup are as described in Chapter 2.

- **Test Instrumentation**

Foundation rods passing through 125mm long 30mm diameter 600kN load cells recorded anchor rod tension, while holding down the baseplate, as shown in Figure 10-3. Four linear potentiometers with 25 mm stroke were attached between the column flange and the base plate to monitor the column base vertical sliding. One manual potentiometers on top of the base plate capture base plate uplift and deformation. Some of these sensors are shown in Figure 10-3. Strain gauges, with 6mm gauge length, were placed on the column flange and the angles to measure localised strains.

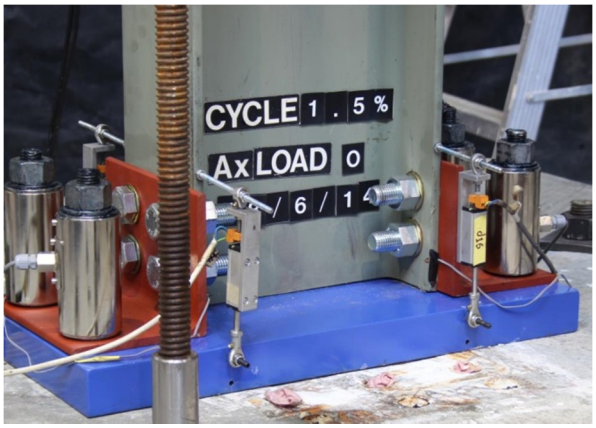

Figure 10-3: Instrumentation of the base connection

10.2.2. Analytical Prediction of Performance

In each test, column base moment, M_{Base}, and column base rotation, θ_{Base}, were computed from the lateral force and column lateral displacement according to:

$$M_{Base} = V \times H_{col} \tag{10-8}$$

$$\theta_{Base} = (\Delta_{top} - \frac{V \times {H_{col}}^3}{3 \times E_{col} \times I_{col}}) \times \frac{1}{H_{col}} \tag{10-9}$$

Here V is the lateral force at column top, H_{col} is height of the column from the base plate to the point of contraflexure, Δ_{top} is top displacement of the column, E_{col} is the elastic modulus of the column, I_{col} is the second moment inertia of the column in the direction of testing. The shear deformation was ignored as it is small in long I-shaped member.

For Tests No. 1, 2, and 3 the analytical methods by Frye and Morris (1975), Kishi and Chen (1990), and Pirmoz et al. (2009) are used for estimation of yielding and ultimate moments, moment at 4% drift and initial stiffness. These methods were presented for semi rigid beam to column connections with angles. Hence, they can be used for the column without axial force

that bends about the strong axis.

A method with more accurate prediction of demands will be modified for estimation of moment resistance and rotational stiffness of specimen in Test No. 4 that conducted under axial force. The moment resistance, M_{base}, is increased by axial force that is calculated:

$$M_{base} = M_{angle} + M_{axial} \tag{10-10}$$

$$M_{Axial} = P \times D_{axial} \tag{10-11}$$

Here, M_{axial} is the base moment from the axial force that is given in Equation 10-11, M_{angle} is the base moment from angles, D_{axial} is the neutral axis depth from the experimental test. For calculation of the neutral axis, it is assumed that the area on the compression side of the section is all at the yield stress of the material and resists the applied axial force, P, as is commonly assumed in plastic design. In addition, the base rotational stiffness at the first yielding point, K_{base}, is increased by applying axial force:

$$K_{base} = \frac{M_{y\_angle} + M_{axial}}{\theta_{y\_angle}} \tag{10-12}$$

Where, M_{y_angle} is the base moment that angles yield, M_{axial} is the base moment from the axial force as given in Equation 10-11, θ_{y_angle} is rotation of the base connection when the angles yield that can be calculated by methods of Kishi and Chen (1990), and Pirmoz et al. (2009).

10.3. Results and Discussion

10.3.1. Tests No. 1, 2, 3- Strong Axis Bending without Axial Force

In Test No. 1, the maximum strong axis moment at 4% drift reaches 10% of the column plastic moment capacity of 233 kN.m assuming tension and compression yielding, as shown in Figure 10-4. The first line of paint flaking that shows angle yielding occurred at 1% drift in the leg adjacent to the base plate as shown in Figure 10-5. Then, the second line was observed on the leg adjacent to the column face at 1.5% drift. Another yield line also formed under the angle adjacent to the base plate that cannot be observed during loading due to its position. No paint flaking was observed in the column indicating that the column remained elastic during cyclic loading. The residual force at zero displacement and displacement at zero force on top of the column was 0.44, and 0.62 of the force and displacement at 4% drift, as described in Table 10-3. Since no column yielding occurred at the end of the test, these residual actions can be removed by replacing the angles.

The measurements in Table 10-3 are moment at the first angle yielding, My, ultimate moment at the level of second yielding in angles, M_u, moment of the base connection at 4% drift, $M_{4\%}$, rotational stiffness of the base connection in the first yielding point, K_θ, residual force at top of the column at zero displacement, $P_{\Delta=0}$, residual displacement at top of the column at zero force, $\Delta_{P=0}$.

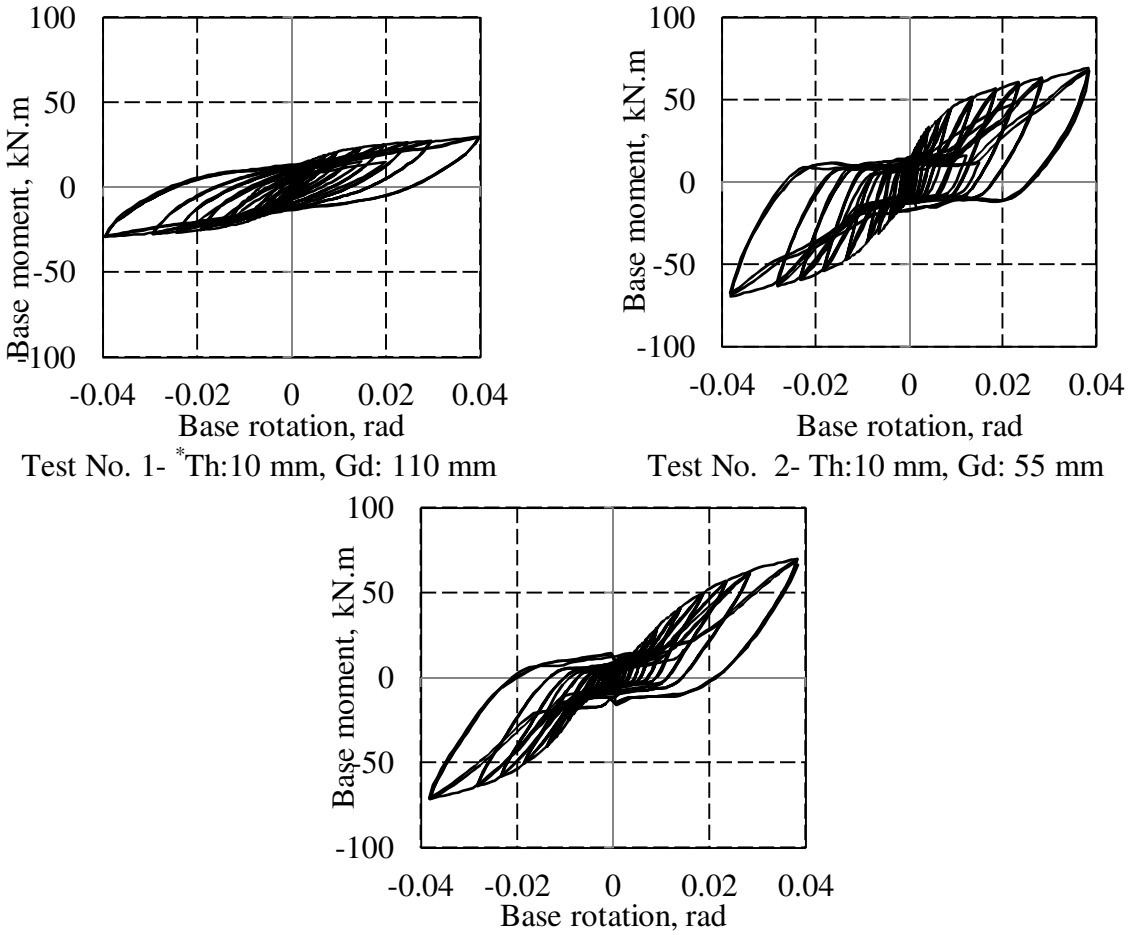

* Th: angle thickness, Gd: the gage distance from the column face to centre of the fastener holes in the leg adjacent to the base plate.

Figure 10-4: Moment-Rotation for specimens without axial force (Tests No. 1, 2, 3)

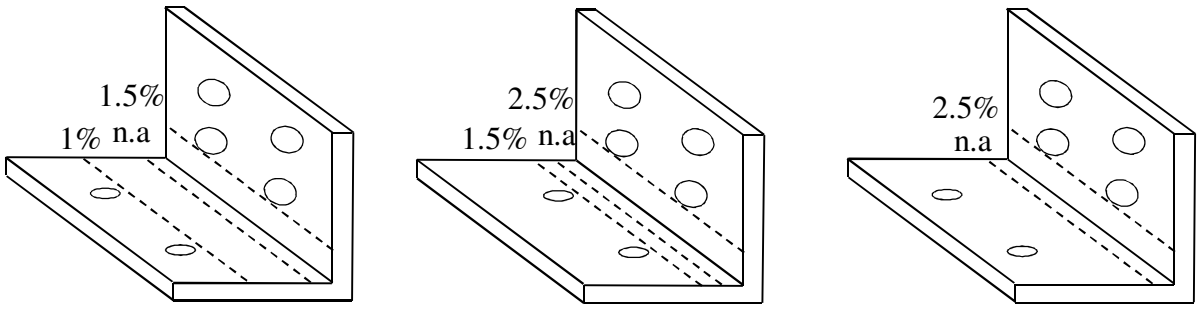

Figure 10-5: Angles yield lines for Tests 1-5

Table 10-3: Experimental recorded demands for Test 1-5

Test No		M_y kN.m	M_u kN.m	$M_{4\%}$ kN.m	K_θ		$P_{\Delta=0}$ kN	$\Delta_{P=0}$ mm
					kN.m/rad	EI/H		
1		19.8	23.2	29	2039	0.2	6.5	50
2		49.5	59.4	70	2931	0.29	8	52
3		49	57.5	71.5	2665	0.26	7	40
4		74	77	80	4182	0.41	5	5
5	X	65.5	75.4	82.5	12148	1.2	7.5	10
	Y	9.5	22.8	29.8	2653	2.9	3.7	5

In Test No. 2, the anchor rods were placed closer to the column face, with the gage distance of 55 mm. This distance is half of the specimen in Test No.1. Shifting of anchor rods from 110 mm of the column face in Test No. 1 to 55 mm in Test No. 2 caused the yielding, and ultimate moments increased up to 2.5 times of Test No. 1 according to Table 10-3, and Figure 10-4. In addition, the base rotational stiffness in Test No. 2 was 1.45 of Test No. 2. It shows that placing of the anchor rods closer to the column face increased strength and stiffness of the connection. The first yielding line was observed in the leg adjacent to the base plate at 1.5% drift, and the second line formed at 2.5% drift in the leg adjacent to the column face, as shown in Figure 10-5. Another yield line was formed under the leg adjacent to the base plate that cannot be observed until taking off the angles. Although, the residual force at zero displacement (8 kN) at the end of cyclic load is near to Test No. 1 (6.5 kN) as shown in Table 10-3, the ratio of residual base moment over maximum resisting moment for Test No. 2 is half of this ratio for Test No. 1.

The angles were replaced with same leg size (150 mm) but higher thickness angles (16 mm) in Test No. 3. In addition, the anchor rods were placed at distance of 110 mm from the column face. The M_y, M_u, and $M_{4\%}$ for Test No. 3 are close to recorded values in Test No. 2

with less than 4% difference according to Table 10-3, and Figure 10-4. Further, the rotational stiffness of base in Test No. 3 is 0.9 of Test No. 2. This result describes the economic way to increase performance (moment resistance and stiffness) of this base connection is placing the anchor rods closer to the column face rather than using angles with larger dimensions. The first paint flaking line was observed at 2.5% drift in the leg adjacent to the column as shown in Figure 10-5. Although some local paint flaking was observed around holes in the other leg, no obvious yield line was formed on top of the holes in the leg adjacent to the base plate. The third yield line was formed underneath the angle, and the level of drift is unknown, as it could not be observed.

The mathematical model by Pirmoz et al. (2009) presents a more accurate estimation of yielding, ultimate moment and initial stiffness compared to methods by Kishi and Chen (1990), and Frye and Morris (1975), as shown in The prying of the bolts was not significant as the thickness of the angle is low, meaning that the flexural stiffness of the angle is much lower than the axial stiffness of the bolts. The effect of bolt prying could be significant for the case with thicker angle and smaller bolt size

Table 10-4. In this table, the measurements are yielding base moment from the analytical model over the experimental yielding base moment, M_y/M_{y_exp}, ultimate base moment from analytical model over the experimental ultimate base moment, M_u/M_{u_exp}, base moment from analytical model at 4% drift over the experimental base moment at 4% drift, $M_{4\%}/M_{4\%\_exp}$, initial stiffness from analytical method over experimental initial stiffness, K_i/K_{i_exp}. Therefore, the Pirmoz et al. (2009) method is used for estimation the base performance under axial loading.

The prying of the bolts was not significant as the thickness of the angle is low, meaning that the flexural stiffness of the angle is much lower than the axial stiffness of the bolts. The effect of bolt prying could be significant for the case with thicker angle and smaller bolt size

Table 10-4: Comparing experimental yielding moment, ultimate moment, and initial stiffness with valus from analytical methods suggested by Pirmoz et al. (2009), Frye and Morris (1975), Kishi and Chen (1990) for Tests No. 1-3

Test No	Pirmoz et al. (2009			Frye and Morris (1975		Kishi and Chen (1990	
	M_y/M_{y_exp}	M_u/M_{u_exp}	K_i/K_{i_exp}	M_u/M_{uexp}	$M_{4\%}/M_{4\%\_exp}$	M_u/M_{uexp}	K_i/K_{i_exp}
1	0.78	0.99	0.68	0.49	0.64	0.49	0.75
2	0.57	0.72	0.84	0.19	0.26	0.19	11.34
3	0.67	0.87	0.82	0.56	0.54	0.56	3.02
Median	0.67	0.87	0.82	0.49	0.54	0.49	3.02

10.3.2. Test No. 4- Strong Axis Bending with Axial Force

The maximum strong axis moment for this column base with 320 kN axial force reached 80 kN.m, which is 41% of the nominal section moment capacity considering axial force (192 kN.m), as shown in Figure 10-6. The solid line shows the bilinear performance of this base connection according to the method by Pirmoz et al. (2009) that was modified to consider the axial load effect. Yielding moment, ultimate moment, and rotational stiffness from this method is 0.85, 0.91, and 1.34 of the experimental values, respectively. The first line of angle paint flaking was observed on the leg adjacent to the column at the first cycle of 2% drift and the second line appeared in the leg adjacent to the base plate in 2.5% drift. The third yield line formed under the angle in the leg adjacent to the base plate. This yield line could not be observed until the angles were taken off, as shown in Figure 10-6. Some local yielding in the column around holes could be observed at 4% cycles. The residual force at

zero displacement and residual displacement at zero force at the end of the test were 5 kN, and 5 mm, respectively, according to Table 10-3. The main portion of this residual displacement could be removed by replacing the angles since they were the main sacrificial element.

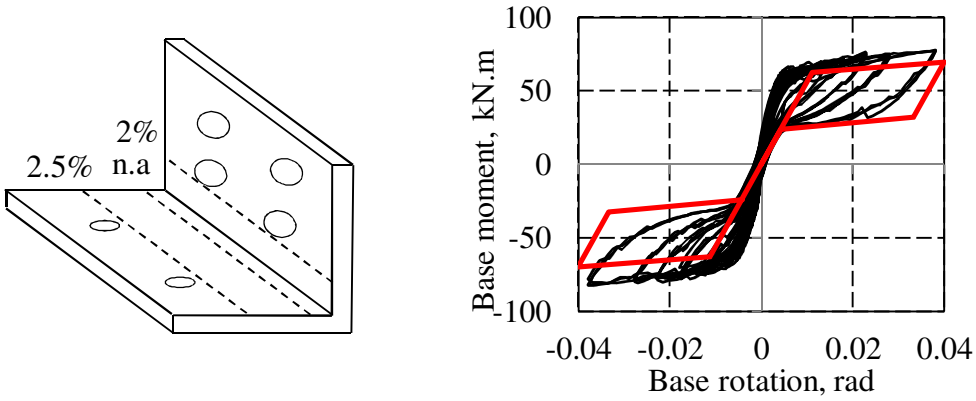

a. Yield Line b. Moment-Rotation

Figure 10-6: Yield lines on angles, and moment-rotation for Test No. 4. Left is the yielding lines on angles and the moment-rotation hysteretic curve is shown on right.

10.3.3. Test No. 5- Bi-directional Bending with Axial Force

The moment capacity in Test No. 5 is always less than the flexural capacity of the section, assuming the gross section carries force in tension and compression from the NZS 3404 (2007) alternative method, as shown in Figure 10-7. The moment interaction curve is not symmetric as a result of load path dependency effects. For example, when $\Delta_x < 0$, the graph is not a smooth curve because the displacement was first increased in the Y direction and then in the X direction. In contrast, for $\Delta_x > 0$, displacement was first increased in the X direction and then in the Y direction resulting in a smoother curve. The first yielding line was observed at 0.75% drift in the leg adjacent to the base plate. The other leg yielded at 2.5% drift and at the same level, column paint flaking was observed on the compression side that contacted to the base plate. Finally, at 4% drift the other line of paint flaking was observed on the leg adjacent to the base plate as shown in Figure 10-7.

During bi-directional loading the centre of the shear resistance at the column base can be placed on one corner, and may not align with centre of the horizontal force at the top of the column. It causes twisting of the column. In these experimental tests, two actuators were restrained the column along weak axis to restrain column twisting. The difference between actuator loads at 4% drift in *X* direction and 2.5% in the *Y* direction was 7.4 kN. This causes a 4.4 kN.m twisting moment over the column. By assuming the shear resistant at the corner of the column and the applied force at the column section the twisting moment is calculated equals to 5 kN.m. The twisting moment at the top of many similarly deforming columns in a building causes an addition building torsion. This building torsion is related to the member deformation, is in additional to that commonly considered as a result of plan irregularity and ground motions.

The corner plastic compressive deformation occurred (about 1.5 mm) at the flange tips after 4% clover leaf loading. The maximum flange tip deformation occurred in these cycles because all of the axial force was resisted by the flange tip in some of the loading directions.

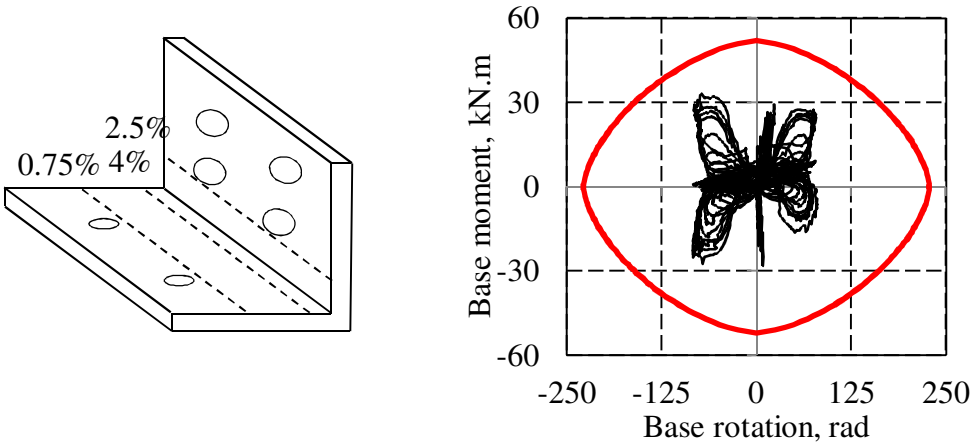

a. Yield Line b. Moment-Rotation

Figure 10-7: Yield lines on angles, and moment-rotation for Test No. 5

10.4. Summary

This chapter describes the design and experimental testing of column base with replaceable angles bending about their strong and weak axis and subject to an axial force ratio of zero or $0.20Af_y$. It was shown that:

- Several cycles to a drift of 4% in strong and bi-directions with and without axial force were obtained without significant damage. Although some yielding lines were observed in angles, and the corner plastic compressive deformation at the flange tips after bi-directional loading that reduced the initial stiffness, it is anticipated that the column base would have been able to undergo significantly more cycles of displacement reaching the same loads, before requiring replacement.

- The mathematical model by Pirmoz et al. (2009) presents more accurate method for estimation of yield and ultimate moment resistance, and initial stiffness. This method was modified to consider the effect of axial force. This enables yielding moment, ultimate moment, and rotational stiffness to be estimated with 0.85, 0.91, and 1.34 of the experimental values, respectively.

- Columns, such as these, where the centre of applied lateral force at the top of the column is at a different vertical location to the resistance at the base of the column, can impose a torsional moment on the building they are supporting. This outcome may affect the building response.

In the next chapters the performance of proposed low damage base connections are compared with the performance of the exposed base plate connections that were described in Chapter 3.

Chapter 11: Comparison of Tested Base Connections

11.1. Introduction

The cyclic performance of the exposed base plate connections, column base strong axis aligned asymmetric friction connections (SAFC), column base weak axis aligned asymmetric friction connections (WAFC), and base connections with yielding angles were each experimentally characterised and quantified in Chapters 3, 4, 6, 7 and 10, respectively. To enable selection of base connections in structural design, this chapter presents a summary comparison of their construction, stiffness and damage performance. Three criteria are considered for comparing of these bases, construction, stiffness and damageability.

11.2. Importance of Assessed Criteria

Construction time, cost and complexity are increased by adding more drilling holes and welding to the base connection. Comparing the number of base connections, which corresponds to the number of the columns, to other structural elements, such as beam to column connections, shows that the required time and cost for a base connection is a small portion of total construction time and cost. Therefore, the main construction parameter considered in this chapter is complexity of the base connection based on the detailing.

Stiffness of the base connection is related to the drift and structural performance as described in Chapter 5. Drift is generally reduced by increased rotational stiffness at the base. In

addition, it should also be noted that higher storey drift causes more damage to the building and non-structural elements. Therefore, using the base connection with high rotational stiffness can lead to less damage in the building.

Damage at the base of a structure can cause high residual deformation. In addition, replacing the damaged base plate and column may be difficult since these elements are under high axial force and integral to structural stability. Therefore, a base connection where damage occurs in only replaceable elements can be more easily repaired after an earthquake, and it is possible that residual deformation may also be ameliorated replacing these elements.

11.3. Rating of Tested Connections

11.3.1. Construction Comparison

Table 11-1 describes the special construction considerations for each tested base connection. According to Table 11-1, the base connection with yielding angles is the easiest base to be constructed, since no welding is required. Therefore, it is given the lowest and best ranking of 1 in Table 11-1. Positions of the holes and the plates that are welded to the column and the base plate in SAFC and WAFC are the main complexity considerations in the detailing and construction of these bases. Therefore, the SAFC and WAFC are given the lowest ranking of 3 and 4, respectively. Finally, special welding inspection is required for the exposed base plate connection, since its performance is highly dependent on the welding details between the column and the base plate.

Table 11-1: Special construction considerations of tested bases

Base Connection	Special considerations	Ranking
Exposed base plate connection	Special detailing is required for column to the base plate welding	2
SAFC	Position of the flange plate on the base plate	3
	Position of the holes in the column and the flange plate	
WAFC	Position of the flange plate on the base plate	4
	Position of the column plate on the column	
	Position of the holes in the column plate and the flange plate	
	Size of the base plate is larger than SAFC	
Base with yielding angles	Position of the holes in the column and angles	1

11.3.2. Stiffness Comparison

The rotational stiffness of exposed base plate, SAFC and WAFC connections, and bases with yielding angles are presented in Table 11-2. The secant rotational stiffness of the base connection, K_θ, was calculated from the origin to the point on the column base moment-rotation curve when the cap plate starts sliding for the SAFC and WAFC connections, to the point that the column yields for the exposed base plate connection, and to the point that angles yield for the base connection with yielding angles. The comparison shows that the WAFC connection can provide higher stiffness in both bending directions due to the longer lever arm of the bolts when the column bends about the strong axis, and also incorporation of flange plate prying for bending about the weak axis. However, by increasing number and size of the bolts in the SAFC connection, the same level of stiffness can be obtained. For this reason the WAFC is given a better ranking of 2 than the SAFC ranking of 3.

Table 11-2: Experimental recorded stiffness for exposed base plate, SAFC, WAFC, and yielding angles

Base		Axis of Bending		Axial force kN	K_θ kN.m/rad	Ranking
Exposed Base Plate 4M24 Grade 8.8		Strong		0	14700	1
Exposed Base Plate 4M24 Grade 10.9		Strong		0	14700	
Exposed Base Plate 4M24 Grade 10.9		Strong		320	23200	
Exposed Base Plate 4M24 Grade 10.9		Bi-directional	Strong axis	320	38200	
			Weak axis	320	14600	
SAFC		Strong		0	3295	3
		Weak		0	1100	
		Strong		320	5440	
		Weak		320	1490	
		Bi-directional	Strong axis	320	12100	
			Weak axis	320	3700	
WAFC		Strong		0	5750	2
		Weak		0	1150	
		Strong		320	8990	
		Weak		320	2060	
		Bi-directional	Strong axis	320	13650	
			Weak axis	320	7600	
Yielding Angles	150X150X10 GD*: 110 mm	Strong		0	2040	4
	150X150X10 GD: 55 mm	Strong		0	2930	
	150X150X16 GD: 110 mm	Strong		0	2670	
	150X150X10 GD: 110 mm	Strong		320	4180	
	150X150X10 GD: 110 mm	Bi-directional	Strong axis	320	12150	
			Weak axis	320	2650	

* GD is the gage distance

The rotational stiffness of base connections with yielding angles is 0.5 and 0.8 of the rotational stiffness of the WAFC and SAFC connections, on average. Therefore, the SAFC and WAFC provide more rigidity at the base compared to bases with yielding angles. Moreover, the rotational stiffness of SAFC and WAFC bases and base with yielding angles

are 0.25, 0.4 and 0.2 of the exposed base plate connections, respectively. Therefore, exposed base plate connections provide more rotational stiffness compared to the proposed low damage bases and are given a ranking of 1. The base with flexible yielding angles is ranked with a 4.

11.3.3. Damage Comparison

The summary of the damage observed during experimental tests is presented in Table 11-3.

Exposed Base Plate Connections: During cyclic loading some failures, such as weld fracture, anchor rod yielding, column and base plate, and buckling of the column flange and web were observed. These failures cause permanent deformation at the top of the column and also in the base connection, and the column may thus need to be replaced. This connection is ranked at number 4 from a low damage aspect.

SAFC and WAFC: No major damage occurred to interrupt the performance of the column and the base connection. Repair, if needed, may be undertaken by retightening, or replacing, bolts and possibly shims. While full stiffness reinstatement is difficult, allowing grout to flow under sections of the column section where there is a gap, due to corner plastic compressive deformation at the flange tips, may increase the stiffness. The column can be re-straightened after the earthquake by loosening and retightening of the bolts. The axial force provides sufficient moment for reinstatement. These bases are ranked number 1 due to their low damage performance.

Table 11-3: Damage of the exposed base plate, SAFC, WAFC, and base with yielding angles

Base		Axis of Bending	Axial Force	Damage	Drift, %	Damage	Drift %	Damage	Drift %	Ranking
Exposed Base Plate 4M24 Grade 8.8		Strong	0	BP yielding	0.85	Column and Anchor rod yielding	2.5	Anchor rod fracture	4	4
Exposed Base Plate 4M24 Grade 10.9		Strong	0	BP yielding	0.85	Column and Anchor rod yielding	2.5	Welding fracture	4	
Exposed Base Plate 4M24 Grade 10.9		Strong	320 kN	Column yielding	1	BP yielding	1.25	Flange buckling	3.5	
Exposed Base Plate 4M24 Grade 10.9		Bi-directional	320 kN	BP and Col yielding	0.5	Flange buckling	2.5			
SAFC		Strong, Weak, Bi-directional	0, 320 kN	No major damage, some corner plastic compressive deformation at the flange tips after weak axis bending and bi-directional loading						1
WAFC		Strong, Weak, Bi-directional	0, 320 kN	No major damage, some corner plastic compressive deformation at the flange tips after weak axis bending and bi-directional loading						1
Yielding Angles	150X150X10 GD[1]: 110 mm	Strong	0	1st YL[2] angles	1	2nd YL angles	1.5			3
	150X150X10 GD: 55 mm	Strong	0	1st YL angles	1.5	2nd YL angles	2.5			
	150X150X16 GD: 110 mm	Strong	0	1st YL angles	2.5					
	150X150X10 GD: 110 mm	Strong	320	1st YL angles	2	2nd YL angles	2.5			
	150X150X10 GD: 110 mm	Bi-directional	320	1st YL angles	0.75	2nd YL angles	2.5	3rd YL angles	4	

[1]GD is the gage distance

[2] yield line

Base with Yielding Angles: Although some yielding lines were observed in angles and there was corner plastic compressive deformation at the flange tips after bi-directional loading that reduced the initial stiffness, the performance of the base connections was not reduced by yielding and more cycles could still be applied. After an earthquake, the angles may require

replacement. This base connection is thus ranked at number 3.

11.4. Effect of Changing Base Connection Properties

Changing the number and size of the bolts in SAFC and WAFC connections, the thickness of the base plate, the position of the anchor rod and anchor rod diameter in the exposed base plate connections, or the thickness of the angle and position of the anchor rod in the base with yielding angles, can change the stiffness of these bases. Therefore, the order of these base connections, according to base rotational stiffness, can be changed according to the base connection properties. Hence, the stiffness is customizable to the specific application within a given base connection approach.

11.5. Comparison

Table 11-4 summarizes the order of the base connection according to the three metrics that are low damage performance, stiffness, and simple construction. The values in Table 11-4 can be summed to provide an overall view. However, the final result is dependent on the weighting of the different criteria, but assigning weighting factor to these three criteria was not considered here.

The SAFC and WAFC bases are good candidates for structures where low damage performance is a top priority, but the stiffness is reduced possibly due to corner plastic deformation of the column section affecting response in future events. In contrast, when

simple construction detailing is required, then a base with yielding angles is an appropriate choice. Finally, based on the tested specimens the exposed base plate connections provided more rotational stiffness compared to other specimens. However, the stiffness of SAFC, WAFC, and yielding angle bases can be increased by design, mitigating this advantage. Hence, the order of stiffness in Table 11-4 can change for different properties of base connections, changing the overall summary as a result.

Table 11-4: Order of bases according to the experimental performance

Base Connection	Ease of Construction	Stiffness	Low Damage
Exposed base plate	2	1	4
SAFC	3	3	1
WAFC	4	2	1
Base with yielding angle	1	4	3

11.6. Summary

This chapter presents a summary comparison of exposed base plate connection, SAFC, WAFC, and yielding angle base connections in terms of damageability, stiffness and construction. It was shown that:

- Selection of the base connection for a structure depends on importance of construction or performance factors. If low damage performance is important, then SAFC and WAFC connections are good selections. If simple detailing and construction is a top priority, then bases with yielding angles are a reasonable choice, while the exposed base plate connection can provide more stiffness and less rotation at the base.

- Although the rotational stiffness of the tested exposed base plate connection was

higher than other specimens, the stiffness of the SAFC, WAFC and yielding angles connections can be increased by changing the design parameters, and this advantage can be mitigated.

- Moment resistance and stiffness of the WAFC about both the strong and weak axis are higher than the SAFC with the same number and size of the bolts. However, the same level of moment resistance and rotational stiffness can be reached by using higher numbers and sizes of bolts in the SAFC. Thus, each of these connections should be considered on its own merits.

Chapter 12: Conclusion

This thesis explores the experimental and analytical studies on performance of steel column base connections under likely seismic demands. Base connections are critical elements of low damage structures. Failure to create low damage base connections would reduce the potential of low damage designs.

A subjective quantitative assessment (SQA) rubric showed that the base connections with yielding angles and AFC have higher likelihood to act as a low damage connections compared to bases with yielding base plate, post tensioned rods, yielding anchor rods and exposed base plate connections. These systems were all compared in terms of damageability, cost and construction difficulty. A final choice will depend on the potential target building value and ease of access for repair.

Experimental tests on exposed base plate connections with and without preloading anchor rods showed that these base connections remained elastic at low levels of drift. They can be categorized as "low damage", but only at low levels of drift. Beyond this point, plastic base rotation occurred, leading to brittle fracture or residual column deformation, and thus significant damage for even moderate drift demands.

Nonlinear time history analysis of a single storey structure illustrated that nonlinear base rotation, which has a direct relation to the base connection damage, is not generally reduced by the base flexibility. Therefore, base flexibility effects may not always reduce damage, as is often assumed and implied in design codes. In addition, neglecting the base flexibility effects arising from soil, foundation and base connection flexibility, can lead to non-conservative

structural demand estimation. Hence, there is a need to update design codes and methods based on these results.

From cyclic testing of the base connections with yielding angles it was found that this base endured several cycles under bi-directional bending without significant damage although some yielding lines were observed in angles.

Experimental testing of SAFC and WAFC connections showed that these connections did not have significant strength degradation even after cycles to a drift 4%. However stiffness degradation was observed, particularly after the cycles of the axially loaded specimen in the weak axis direction. The level of shim and steel plate degradation was minor. Importantly, axial load provided a degree of self-centring not available in other connector designs. From a strength point of view, since no degradation occurred, these connections can be categorized as low-damage connections. Repair, if needed, may be undertaken by retightening, or replacing, bolts and possibly shims. If low damage performance is defined predominantly in terms of base stiffness, rather than strength, then it is possible to also reinstate some or all of the lost stiffness after a major event.

Although no bolt fracture was observed during cyclic loading of Grade 8.8 bolts in AFCs that were placed in the brace, some Grade 10.9 bolts suffered from fracture in AFC. This type of fracture may be solved by considering longer threaded length for Grade 10.9 bolts. Hence, there are results to update design codes for AFCs in general and for base connections with AFCs in particulars.

Overall, selection of an appropriate base connection depends on a number of factors. If low

strength loss is important, then SAFC and WAFC connections are good selections. If simple detailing and construction is a top priority, then bases with yielding angles are a reasonable choice, while exposed base plate connections provide more stiffness and less rotation at the base for connections expected to have lower demands. The stiffness of the SAFC, WAFC and yielding angles connections may be increased by changing the design parameters, and so any disadvantage associated with initial stiffness may be mitigated.

Macro models of these base connections were developed or modified to enable design of these base connections by practitioners. This step includes developing simple and complex macro models for SAFC, WAFC, base with yielding angles, and modifying the available methods for estimation of the base plate connection performance to consider anchor rod preloading. These results enable translation of this research into direct practice to specify any type of AFC or other base connection.

In summary, the unique contributions this research and thesis make to the field of steel structure include:

- Developing two novel friction base connections that can be categorized as low damage connections in terms of their strength. They may also be repaired, if needed, in a short time and with low cost.
- Illustrating the new torsional demand on these columns during bi-directional loading. In addition to torsion introduced by plan irregularity, and ground motions that induce a torsional component, there is also torsion that can be caused by the characteristics of the members. This research ensures performance in the presence of torsion.

- Developing macro models for performance of SAFC, WAFC, base with yielding angles and the exposed base plate connections with pre-loaded anchor rods. These models can be used for practitioners to create specific designs to desired capacity and behaviour.
- Assessing the effect of anchor rod preloading on the cyclic performance of the exposed base plate connection and developing a model that can be used in design.
- Evaluating the effect of column base rotational stiffness on the seismic demands of single storey frames with a range of periods. This evaluation gives practitioners a better understanding of the demands at the base of structures due to the base flexibility, and thus enables easy initial design specification of base connections.
- Describing the cyclic performance of AFC connections with Grade 10.9 bolts. Previous testing has used lower grade bolts, and assumed similar behaviour from higher strength elements. These results lead to better understanding of AFC performance and design.

Chapter 13: Future Work

The research within this thesis provided significant insight into the development of low damage base connections. Several areas that have potential for further studies have been identified as a result of this work, and these are detailed within this chapter.

13.1. Friction Base Connections

The presented experimental tests in this thesis showed that SAFC and WAFC are promising connections. However, there is the possibility of different column sections.

13.1.1. Columns with Square Hollow Sections

Square hollow sections, SHS, are widely used as column sections. Friction base connections for such columns required special detailing to perform well. Some sections of this column are shown in Figure 13-1. The one on the left has been used by Aurecon in the Terrace project in 2014. Here, vertical plates were placed to allow the axial force to be resisted by a shear key beneath the base. Varieties on this connection could be to allow the column to rock about a corner or edge thereby eliminating the need for the shear key internal cross plates. The RCTF WAFC on the right may also need cross plates to stop the slide of the tube pulling away from the concrete.

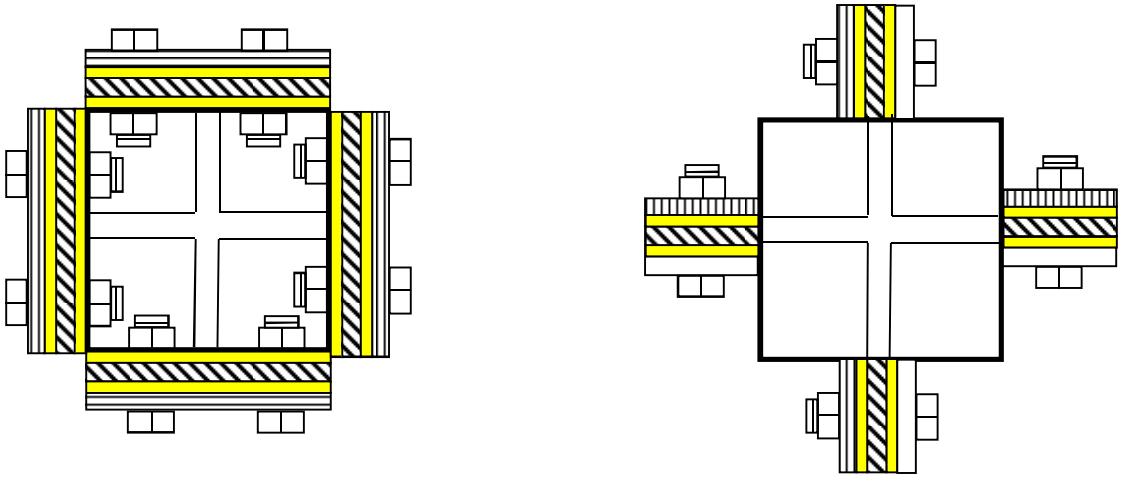

Figure 13-1: Detail of friction base connection in the column with SHS. Left is the base with SAFC and the base with WAFC is shown on right

13.1.2. Merging of SAFC and Yielding Angles

The main advantage of the SAFC base is its low damage performance. Angles provide easy construction. These base connection types can be merged to use these advantages as shown in Figure 13-2. The column is connected to the base plate by yielding angles while the angles connected to the column by AFCs. The slotted holes are required to be considered in the angle leg connected to the base plate to be tightened to the anchor rods. These slotted holes provide enough space for easy installation of angles. The thickness of the angles should be enough to prevent any yielding in the column and to ensure initial stiffness provided. The rotational stiffness of this base connection can be increased by increasing the angle thickness or placing anchor rods closer to the column flange as describe in Chapter 10. This study provides another innovative base connection types that uses advantages of bases with angles and friction connections.

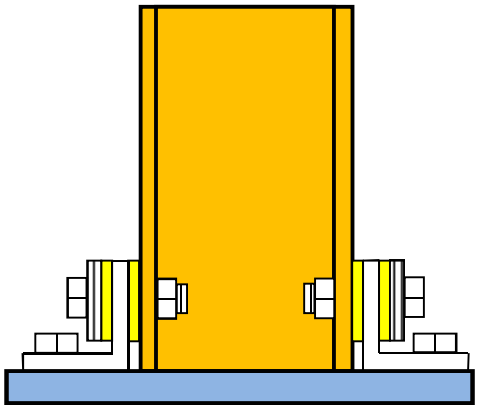

Figure 13-2: Detail of SAFC merged with angle at the base connection

13.1.3. Low Damage Bases for Composite Columns

Columns may be required to carry high axial force. High axial force can considerably move the neutral axis of a column making the strains in the columns due to axial force and flexure predominantly compressive as shown in Figure 13-3. As a result, low damage column base connections which rely on uplift are ineffective and column yielding becomes the main mode of energy dissipation under high axial force.

The idea proposed is to use composite columns in the base level of structures in order to develop low damage bases under high axial force (MacRae and Borzouie, 2013). Composite columns may be concrete-filled tubular columns, steel reinforced concrete columns (SRC), or columns with concrete infill between then flanges. The concrete provided will also have the advantages that it will limit buckling of the steel, add fire resistance, and reduce the possibility of damage due to impact or collision.

This system is desirable because the concrete carries the compression, so the neutral axis of the section is toward the compression side of the section. This means that there will be uplift

on the tension side of the section thereby activating energy dissipating mechanisms. The capacity of the column is also increased by this way. The difference in strain is illustrated in Figure 13-3. The experimental testing on the bare steel columns with SAFC or WAFC bases and the steel column filled with concrete can evaluate the effectiveness of this idea.

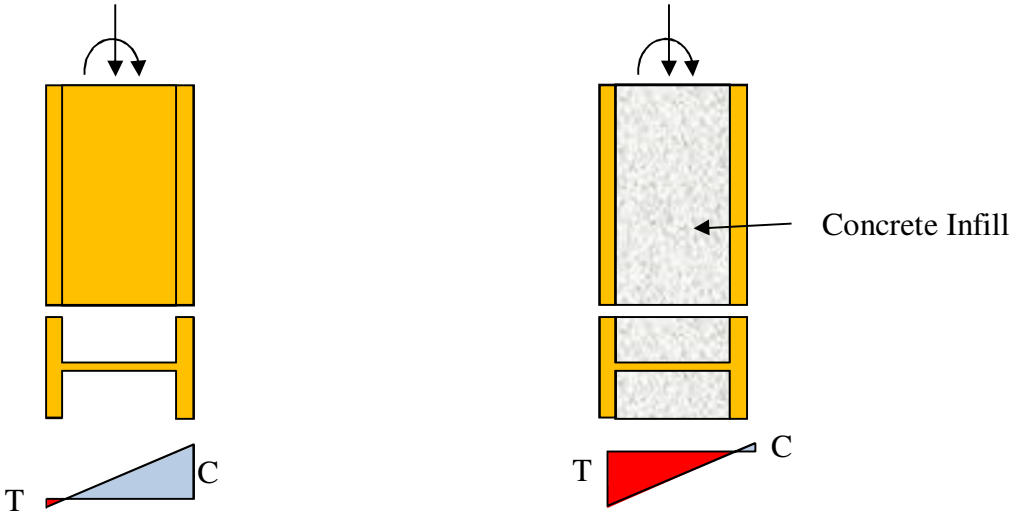

Figure 13-3: Column and approximate position of neutral axis under high axial force. Left is for the bare steel column and right is the steel column section filled with concrete

13.1.4. Developing Methods for Repairing of SAFC and WAFC

As it was observed during experimental testing of SAFC and WAFC, the stiffness of the column base was reduced by plastic deformation of the column flange during bi-directional loading. This plastic deformation was recorded under severe bi-directional loading (4% drift). Therefore, this effect could be lower for lower level of drifts. Also, this plastic deformation does not change the sliding force of the bolts. There are some possible ways to solve this issue after high bi-directional loading such as grout injection to fill gaps resulting from the yielding, between the column flange tips and the base plate, welding steel plates at the flange

tips after loading. Studying the effectiveness of these methods in future studies would be useful.

13.1.5. Effect of Heat on Performance of Friction Connection

A few studies were conducted with high speed Past studies by

According to a few studies that have been conducted to observe performance of AFC under high speed loading (Chanchí et al., 2012a, and the new study that is undertaken at the University of Auckland) no welding of sliding connections due to high temperature was observed. The following reasons can reduce the adverse effects of heat in this type of connection:

i. All of the elements of AFC are from steel with the same expansion coefficient

ii. Thermal conductivity of steel is high.

iii. This connection is open to air from all sides that can help to reduce temperature of steel in a short time

Still more experimental tests are required to fully study the effect of heating effects on the performance of AFCs.

13.1.6. Finite Element Modelling of SAFC and WAFC

Finite element modelling of friction base connections is useful to quantify the plastic deformation of column flange tips under different levels of axial force and bi-directional loading. From these analyses, the column stiffness can also be obtained and compared after different displacement histories. Comparison may also be made with these experimental studies. Any stiffness reduction can therefore be obtained for:

iv. Development of a simple method for stiffness reduction estimation

v. Further analyses to understand stiffness reduction effects

vi. Support decisions based on an acceptable base connection stiffness.

13.1.7. SAFC and WAFC Under Tensile Force

The cases without axial force and with compressive force were considered in these experimental tests. For the case with the net tensile force, the following solutions are required further studies:

i. Maximum uplift is determined by nonlinear analysis and the hole size is adjusted according to the uplift demand.

ii. Special detailing can be suggested such as placing a tie between column and the base plate to limit the uplift

13.2. Overall System Modelling

The provided macro model of the sliding hinge joint in Chapter 8 is a key next step in the analysis. Modelling of the SAFC and WAFC macro model directly in response history analysis would provide a better indication of the behaviour. The effect of changing base friction connection characteristics would be studied using this approach.

In addition, although nonlinear analysis of structures with these friction connections provides more realistic understanding of low damage structures, most of practitioners are not familiar with nonlinear analysis and make usage of these systems hard to be applied in construction. Therefore, analytical study is required to develop a simple methodology for linear analysis of these structures that corresponds to the nonlinear performance. This study will result in low damage technology being more used by practitioners.

13.3. Base Flexibility Effects on Multi Storey Structures

This research provides the effect of base flexibility on single-storey structures for wide range of structural periods. Understanding of this effect on multi-storey structures leads to more accurate estimation of building demands due to the base flexibility. The next step in this field can consider the effect of base flexibility on multi-storey structures in addition to developing simple analytical equations to estimate changing of the structural demands due to the base flexibility.

13.4. Implementation in the Field

The final step for any useful research is implementing by practitioners. A few consultant engineers have used low damage steel structures in their projects, and their interest has been expressed in different stages of this research. The presented research in this thesis, in addition to the published papers from this study, provided all the basic tools needed for these devices to be implemented into a design. Future research topics may result from discussing with practitioners, fabricators and contractors. Ongoing work will hopefully result in widespread implementation of the low damage technology in both new building designs and retrofit applications.

References

ASCE 1997, "Anchor Bolt Design for Petrochemical Facilities." Task Committee on Wind Induced Forces and Task Committee on Anchor Bolt Design, American Society of Civil Engineers.

AISC 2005, "Seismic provisions for structural steel buildings", American Institute of Steel Construction, Inc, Chicago, IL.

ACI Innovation task group 1. 2001." Acceptance criteria for moment frames based on structural testing and commentary (T1.1R-01)", American Concrete Institute, Farmington Hills, Mich.

Adany, S., Calado, L.,Dunai, L. 2000, "Experimental studies on cyclic behavior modes of base-plate connections." Third International Conference on the Behavior of Steel Structures in Seismic Areas (STESSA), 21-24 August. Montreal, Canada. 8 Pages.

Akiyama, H. 1984. "Strength and deformation of exposed type of steel column bases." Transactions of the Architectural Institute of Japan, Vol (342)**,** pp**.** 46-54.

Akiyama, H., Yamada, S., Takahashi, M., Katsura, D., Kumura, K.,Yahata, S. 1998. "Full scale shaking test of the exposed-type column bases." Journal of Structural and Construction Engineering, Vol 514 pp**.** 185-192.

Astaneh, A., Bergsma, G.,H., S. J. 1992, "Behavior and design of base plates for gravity, wind and seismic loads." National Steel Construction Conference, 3-5 June Las Vegas Hilton. 10 Pages.

Aviram, A., Stojadinovic, B.,Der Kiureghian, A. 2010. "Performance and reliability of exposed column base plate connections for steel moment-resisting frames." Report No. 2010/107, Report submitted to the Pacific Earthquake Engineering Research Center, August, 2010.

Bickford, J. 1995. "An introduction to the design and behavior of bolted joints, fourth edition." CRC Press, ISBN: 978-0-8493-8176-8.

Bisalloy. 2012, "Bisplate technical guide." Bisalloy Steels Pty Ltd, 2012. Unanderra, Australia.

Borzouie , J., MacRae, G. A., Chase, G. J., Rodgers, G. W.,Clifton, C. G. 2013, "The effect of base flexibility on demands of the structure." New Zealand Society of Earthquake Engineering Annual Conference, 26-28 April. Wellington, New Zealand. 8 Pages.

Burda, J. J.,Itani, A. M., (1999). "Studies of seismic behavior of steel base plates ." Rep. No. CCEER 99-7, Center for Civil Engineering Earthquake Research, Dept. of Civil Engineering, Univ. of Nevada, Reno, NV.

Cannon, R. W. 1992. "Flexible baseplates: Effect of plate flexibility and preload on anchor loading and capacity." ACI Structural Journal, Vol 89 (3), pp. 315-324.

Chanchí, J. C., MacRae, G. A., Chase, J. G., Rodgers, G. W.,Clifton, C. G. 2012a, "Clamping force effects on the behaviour of asymmetrical friction connections." 15WCEE, 24-28 September. Lisbon. 8 Pages.

Chanchí, J. C., MacRae, G. A., Chase, J. G., Rodgers, G. W.,Clifton, C. G. 2012b, "Behaviour of asymmetrical friction connections using different shim materials." New Zealand Society of Earthquake Engineering Annual Conference, 13-15 April. Christchurch, New Zealand. 7 Pages.

Chanchí, J. C., MacRae, G. A., Chase, G. J., Rodgers, G. W.,Clifton, C. G. 2013, "Hysteretic behavior of symmetrical friction connections (sfc) using different steel grade shims." The Pacific Structural Steel Conference, 8-11 October. Singapore. 6 Pages.

Chanchí , J. C., Xie, R., MacRae, G., Chase, G., Rodgers, G.,Clifton, C. 2014, "Low-damage braces using asymmetrical friction connections (afc)." New Zealand Society of Earthquake Engineering Annual Conference, 21-23 March. Auckland, New Zealand. 9 Pages.

Chaudhari, T., MacRae, G., Bull, D., Chase, G., Hobbs, M., Clifton, C.,Hicks, S. 2014, "Composite slab effects on beam-column subassemblies: Further development." NZSEE, 21 – 23 March,. Auckland, New Zealand. 9 Pages.

Chi, H.,Liu, J. 2012. "Seismic behavior of post-tensioned column base for steel self-centering moment resisting frame." Journal of Constructional Steel Research, Vol 78 pp. 117-130.

Christopoulos, C., Filiatrault, A., Uang, C.,Folz, B. 2002. "Posttensioned energy dissipating connections for moment-resisting steel frames." Journal of Structural Engineering, Vol 128 (9), pp. 1111-1120.

Clifton, C. G. 2000. "Design concepts for moment resisting column base plate connection in a seismic resisting system." HERA steel design & constrcution Bulltin, Vol 56 pp. 11-29.

Clifton, C. G. 2005. "Semi-rigid joints for moment resisting steel framed seismic resisting systems ". PhD, Department of Civil and Environmental Engineering, University of Auckland.

Cui, Y., Nagae, T.,Nakashima, M. 2009. "Hysteretic behavior and strength capacity of shallowly embedded steel column bases." Journal of Structural Engineering, Vol 135 (10), pp. 1231-1238.

Dewolf, J. T. 1978. "Axially loaded column base plates." Journal of the Structural Division, Vol 104 (5), pp. 781-794.

Dewolf, J. T.,Sarisley, E. F. 1980. "Column base plates with axial loads and moments." Journal of the Structural Division, Vol 106 (11), pp. 2167-2184.

Dieter, G.,Schmidt, L. 2012. "Engineering design." McGraw-Hill Higher Education ISBN: 978-0073398143.

Dundu, M. 2012. "Base connections of single cold-formed steel portal frames." Journal of Constructional Steel Research, Vol 78 pp. 38-44.

European Committee for Standardisation 2005. "En 1993-1-8:2005 eurocode 3: Design of steel structures- part 1-8: Design of joints." Brussels, Belgium: European Committee for Standardization

Fahmy, M., Stojadinovic, B.,Goel, S. C. 1999, "Analytical and experimental studies on the seismic response of steel column bases." Proceeding of the 8th Canadian Conference of Earthquake Engineering, Vancouver, 13-16 June. British Columbia, Canada. 6 Pages.

Fisher, J. M.,Kloiber, L. A. 2006. "Design guide 1:Base plate and anchor rod design,2nd ed." American Institute of Steel Construction, Chicago

Fitzgerald, T. F., Anagnos, T., Goodson, M.,Zsutty, T. 1989. "Slotted bolted connections in aseismic design for concentrically braced connections." Earthquake Spectra, Vol 5 (2), pp. 383-391.

Frye, M. J.,Morris, G. A. 1975. "Analysis of flexibly connected steel frames." Canadian Journal of Civil Engineering, Vol 2 (3), pp. 280-291.

Garlich, S.,Thorkildsen, E. T. 2005. "Guidelines for the installation, inspection, maintenance and repair of structural supports for highway signs, luminaires, and traffic signals." No. FHWA NHI 05-036. 2005, Report submitted to the The Federal Highway Administration (FHWA)

Gledhill, S., Sidwell, G.,Bell, D. K. 2008, "The damage avoidance design of tall steel frame buildings - fairlie terrace student accommodation project, victoria university of wellington." New Zealand Society of Earthquake Engineering Annual Conference, 11-13 April. Wairakei, New Zealand. 19 Pages.

Gomez, I. R. 2010. "Behavior and design of column base connections". PhD, Civil and Environmental Engineering, University of California Davis.

Gomez, I. R., Kanvinde, A.,Deierlein, G. G. 2010. "Exposed column base connections subjected to axial compression and flexure." Report submitted to the American Institute of Steel Construction, 29 August, 2010.

Grauvilardell, J. E., Lee, D.,Hajjar, J. F. 2005. "Synthesis of design, testing and analysis research on steel column base plate connections in high-seismic zones." Structural Engineering Report. No. ST-04-02, Report submitted to the University of Minnesota,

Hobbs, M., MacRae, G. A., Bull, D., Gunasekaran, U., Leon, R.,Clifton, C. G. 2013, "Slab column interaction - significant or not?" SCNZ Steel Innovations Conference, 21-22 February. Christchurch, New Zealand. 11 Pages.

Hon, K. K.,Melchers, R. E. 1988. "Experimental behaviour of steel column bases." Journal of Constructional Steel Research, Vol 9 (1), pp. 35-50.

Inoue, K., Suita, K., Takeuchi, I., Chusilp, P., Nakashima, M.,Zhou, F. 2006. "Seismic-resistant weld-free steel frame buildings with mechanical joints and hysteretic dampers." Journal of Structural Engineering, Vol 132 (6), pp. 864-872.

Jaspart, J.-P., Wald, F., Weynand, K.,Gresnigt, A. 2008. "Steel column base classification." Heron Journal, Vol 53 (1/2), pp. 69-86.

Jaspart, J. P.,Vandegans, D. 1998. "Application of the component method to column bases." Journal of Constructional Steel Research, Vol 48 (2), pp. 89-106.

Kanvinde, A., Grilli, D.,Zareian, F. 2012. "Rotational stiffness of exposed column base connections: Experiments and analytical models." Journal of Structural Engineering, Vol 138 (5), pp. 549-560.

Khoo, H.-H., Clifton, C., Butterworth, J., MacRae, G.,Ferguson, G. 2012a. "Influence of steel shim hardness on the sliding hinge joint performance." Journal of Constructional Steel Research, Vol 72 pp. 119-129.

Khoo, H.-H., Clifton, C., Butterworth, J., MacRae, G.,Ferguson, G. 2012b. "Influence of steel shim hardness on the sliding hinge joint performance." Journal of Constructional Steel Research, Vol 72 (0), pp. 119-129.

Khoo, H.-H., Clifton, C., MacRae, G., Zhou, H.,Ramhormozian, S. 2014. "Proposed design models for the asymmetric friction connection." Earthquake Engineering & Structural Dynamics, Vol 44 (8), pp. 1309-1324.

Kishi, N.,Chen, W. 1990. "Moment-rotation relations of semirigid connections with angles." Journal of Structural Engineering, Vol 116 (7), pp. 1813-1834.

Koetaka, Y., Chusilp, P., Zhang, Z., Ando, M., Suita, K., Inoue, K.,Uno, N. 2005. "Mechanical property of beam-to-column moment connection with hysteretic dampers for column weak axis." Engineering structures, Vol 27 (1), pp. 109-117.

Latham, D., Reay, A.,Pampanin, S. 2013, "Kilmore street medical centre: Application of a post-tensioned steel rocking system." SCNZ Steel Innovations Conference, 21-22 February. Christchurch, Nw Zealand. 13 Pages.

Latour, M., Piluso, V.,Rizzano, G. 2011. "Experimental analysis of innovative dissipative bolted double split tee beam-to-column connections." Steel Construction, Vol 4 (2), pp. 53-64.

Latour, M.,Rizzano, G. 2011. "Experimental behavior and mechanical modeling of dissipative t-stub connections." Journal of Structural Engineering, Vol 138 (2), pp. 170-182.

Latour, M., Piluso, V.,Rizzano, G. 2013. "Experimental behaviour of friction t-stub beam-to-column joints under cyclic loads." Steel Construction, Vol 6 (1), pp. 11-18.

Latour, M., Piluso, V.,Rizzano, G. 2014. "Experimental analysis on friction materials for supplemental damping devices." Construction and Building Materials, Vol 65 pp. 159-176.

Latour, M., Piluso, V.,Rizzano, G. 2015. "Free from damage beam-to-column joints: Testing and design of dst connections with friction pads." Engineering Structures, Vol 85 pp. 219-233.

Leslie, B., Gledhill, S.,Moghaddassi, M. 2013, "Concentric braced frames with afc connections–a designers view." SCNZ Steel Innovations Conference, 21-22 February. Christchurch, New Zealand. 13 Pages.

Loo, W. Y., Quenneville, P.,Chouw, N. 2014. "A new type of symmetric slip-friction connector." Journal of Constructional Steel Research, Vol 94 pp. 11-22.

Maan, O.,Osman, A. 2002, "Influence of column bases flexibility on the seismic response of steel framed structures." 4th Structural Specialty Conference of the Canadian Society for Civil Engineering, 2002. Montréal, Québec, Canada. 10 Pages.

MacRae, G. A.,Borzouie , J., 2013;"Composite Columns for Low Damage Bases", HERA Idea Registration, No: IR GAM, Date: 23 May 2013.

MacRae, G. A. 1994. "P-δ effects on single-degree-of-freedom structures in earthquakes." Earthquake Spectra, Vol 10 (3), pp. 539-568.

MacRae, G. A., Urmson, C. R., Walpole, W. R., Moss, P., Hyde, K.,Clifton, C. 2009. "Axial shortening of steel columns in buildings subjected to earthquakes." Bulletin of the New Zealand Society for Earthquake Engineering, Vol 42 (4), pp. 275-287.

MacRae, G. A., Clifton, G. C., Mackinven, H., Mago, N., Butterworth, J.,Pampanin, S. 2010. "The sliding hinge joint moment connection." Bulletin of the New Zealand Society for Earthquake Engineering, Vol 43 (3), pp. 202-212.

MacRae, G. A. 2013, "Low damage construction–some systems issues." 10th International Conference on Urban Earthquake Engineering (10CUEE), 1-2 March Tokyo Institute of Technology, Tokyo, Japan. 4 Pages.

Mashal, M. 2015. "Post-tensioned earthquake damage resistant technologies for accelerated bridge construction". PhD, Civil Engineering, Univer sity of Canterbury.

Maxwell, S. M., Howlett, J. H., Jenkins, W. M.,Bose, B. 'A realistic approach to the performance and application of semi-rigid joints in steel structures', Joints in Structural Steelwork (Ed. J. H. Howlett, et aL) Pentech Press, 1981, 2.71-2.98

Melchers, R. E. 1992. "Rotational stiffness of shallow footings." Journal of Computers and Geotechnics, Vol 13 (1), pp. 21-35.

Menegotto, M.,Pinto, P. E. 1973, "Method of analysis for cyclically loaded reinforced concrete plane frames including changes in geometry and non-elastic behaviour of elements under combined normal force and bending." IASBE Proceedings, 1973. Lisbon, Portugal.

Midorikawa, M., Hori, H., Ishihara, T., Azuhata, T., Kusakari, T.,Asari, T. 2010. "Three-dimensional shaking table tests on seismic response of reduced-scale steel frames with yielding base plates allowed to uplift." Journal of Structural and Construction Engineering, Vol 75 (647), pp. 213-221.

Midorikawa, M., Nishiyama, I., Tada, M.,Terada, T. 2012, "Earthquake and tsunami damage on steel buildings caused by the 2011 tohoku japan earthquake." International Symposium on Engineering Lessons Learned from the 2011 Great East Japan Earthquake, March. Tokyo, Japan. 16 Pages.

Miyasaka, H., Arai, S., Uchiyama, M., Yamada, T.,Hashimoto, A. 2001. "Elasto-plastic behavior of structural elements consist in exposure fixed-type steel column base. Part i – behavior to bending moment." Journal of Structural and Construction Engineering, Vol 550 pp. 167-174.

Morino, S., Kawaguchi, J., Tsuji, A.,Kadoya, H. 2003, "Strength and stiffness of cft semi-embedded type column base." Proceedings of the International Conference on Advances in Structure, 22-25 June. Sydney, Australia. 12 Pages.

Muir, C. 2014. "Seismic performance of the slotted beam detail in reinforced concrete moment resisting frames". PhD, Department of Civili Engineering University of Canterbury.

Murray, T. M. 1983. "Design of lightly loaded steel column base plates." Engineering Journal, Vol 20 (4), pp. 143-152.

Myers, A. T., Kanvinde, A. M., Deierlein, G. G.,Fell, B. V. 2009. "Effect of weld details on the ductility of steel column baseplate connections." Journal of Constructional Steel Research, Vol 65 (6), pp. 1366-1373.

Nakashima, S.,Igarashi, S. 1986. "Behavior of steel square tubular column bases embedded in concrete footings under bending moment and shearing force: Part 1 – test program and load-displacement relations." Journal of Structural and Construction Engineering

Journal, Vol 366 pp. 106-118.

Oh, S.-H., Kim, Y.-J.,Ryu, H.-S. 2009. "Seismic performance of steel structures with slit dampers." Engineering structures, Vol 31 (9), pp. 1997-2008.

Pall, S.,Marsh, C. 1982. "Response of friction damped braced frames." Journal of structural engineering, Vol 108 (6), pp. 1313-1323.

Picard, A.,Beaulieu, D. 1985. "Behaviour of a simple column base connection." Canadian Journal of Civil Engineering, Vol 12 (1), pp. 126-136.

Piluso, V., Montuori, R.,Troisi, M. 2014. "Innovative structural details in mr-frames for free from damage structures." Mechanics Research Communications, Vol 58 pp. 146-156.

Pirmoz, A., Khoei, A. S., Mohammadrezapour, E.,Daryan, A. S. 2009. "Moment–rotation behavior of bolted top–seat angle connections." Journal of Constructional Steel Research, Vol 65 (4), pp. 973-984.

Process Industry Practices Structural, 2006 “Anchor Bolt Design Guide”, PIP STE05121.

Rathbun, J. C. 1936. "Elastic properties of riveted connections." American Society of Civil Engineers Transactions, Vol 101 pp. 524-563.

Ratner, S. B.,Sokol'skaya, V. D. 1956. "The influence of the hardness of rubber on its coefficient of static friction without lubrication." Rubber Chemistry and Technology, Vol 29 (3), pp. 829-833.

Robertson, A. P. 1991. "A study of base fixity effects on portal frame behaviour." The Structural Engineer, Vol 69 (2), pp. 17-24.

Rodgers, G., Solberg, K., Mander, J., Chase, J., Bradley, B.,Dhakal, R. 2012. "High-force-to-volume seismic dissipators embedded in a jointed precast concrete frame." Journal of Structural Engineering, Vol 138 (3), pp. 375-386.

Rodgers, G. W., Chase, J. G., Mander, J. B., Leach, N. C.,Denmead, C. S. 2007. "Experimental development, tradeoff analysis and design implementation of high force-to-volume damping technology." NZSEE Bulletin, Vol 40 (2), pp. 35-48.

Roeder, C. W., Knechtel, B., Thomas, E., Vaneaton, A., Leon, R. T.,Preece, F. R. 1996.

"Seismic behavior of older steel structures." Journal of Structural Engineering, Vol 122 (4), pp. 365-373.

Ruiz-Garcia, J.,Kanvinde, A. 2013, "Effect of column base flexibility on residual drift demands of low-rise steel moment-resisting frames " Advances in Structural Engineering and Mechanics (ASEM13), 8-12 September. Jeju, Korea. 13 Pages.

Salmon, C. G., Schenker, L.,Johnston, B. G. 1957. "Moment-rotation characteretics of column anchorage." ASCE, Vol 122 (1), pp. 132-154.

Solberg, K., Mashiko, N., Mander, J. B.,Dhakal, R. P. 2009. "Performance of a damage-protected highway bridge pier subjected to bidirectional earthquake attack." Journal of Structural Engineering, Vol 135 (5), pp. 469-478.

Somerville, P., Smith, N., Punyamurthula, S.,Sun, J. 1997. ""“Development of ground motion time histories for phase ii of the fema/sac steel project,” sac background document." Report submitted to the Report SAC/DB-97/04, USA,

Somiya, Y., Fukuchi, Y.,Chin, B. 2002. "Experimental study on elasto-plastic behavior and strength estimation of exposed-type column base with variable axial force." Journal of Structural and Construction Engineering, Vol 562 pp. 137-143.

Steel Structures Standard (Incorporating Amendments 1 and 2), NZS 3404:1997, Standards New Zealand, Wellington, 2007.

Stelmack, T. W., Marley, M. J.,Gerstle, K. H. 1986. "Analysis and tests of flexibly connected steel frames." Journal of Structural Engineering, Vol 112 (7), pp. 1573-1588.

Tamai, H., Miura, K., Kitagawa, Y.,Fukuta, T. 2003, "Application of sma rod to exposed-type column base in smart structural system." Smart Structures and Materials Conference. Shih-Chi Liu. International Society for Optics and Photonics, 8 Pages.

Tamai, H., Kitagawa, Y.,Fukuta, T. 2004, "Application of sma rods to exposed-type column bases in smart structural systems." 13th World Conference on Earthquake Engineering, 1-6 August. Vancouver, B.C., Canada. 15 Pages.

Thambiratnam, D.,Paramasivam, P. 1986. "Base plates under axial loads and moments." Journal of Structural Engineering, Vol 112 (5), pp. 1166-1181.

Till, R. D.,Lefke, N. A. 1994. "The relationship between torque, tension, and nut rotation of

large diameter anchor bolts." No. R-1330, Report submitted to the Michigan Department of Transportation, USA,

Tremblay, R. 1995. "Performance of steel structures during the 1994 northridge earthquake." Canadian Journal of Civil Engineering, Vol 22 (2), pp. 338-360.

Voce, G. J. 1958. "Restraint at stanchion bases." The Structural Engineer, Vol 36 (4), pp. 136-137.

Website. of California State University Northridge. Available: http://library.csun.edu/About/Quake/Gallery.

Winterkorn, H. F.,Fang, H.-Y. 1975. "Foundation engineering handbook." London, Van Nostrand Reinhold ISBN: 10: 0442295642.

Zareian, F.,Kanvinde, A. 2013. "Effect of column base flexibility on the seismic response and safety of steel moment resisting frames." Earthquake Spectra, Vol 29 (4), pp. 1537-1559.

Appendix A: MATLAB Code for Base Flexibility

```
function Time_history_analysis_nonlinear_Second_Stiffness

clear
clc
E= 2.1e10;    % Kg/m2
H= 3.5;       % Height of structure (m)
zi1 = 0.05;   % damping of structure (define the fraction of critical damping)
zi2 = 0.05;    % damping of base (define the fraction of critical damping)
zi3= 0.05;
%zi3 = 0.05;    % damping of top (define the fraction of critical damping)
I= 3.526e-4;  % Moment of inertia for column 2IPE300
kfb= 12*E*I/(H^3); % stiffness of fixed base structure
%ev= [1;0;0]; % Influence vector
ev= [1;0;0]; % Influence vector
Beta= 10;
ktt=2000*E*I/H;

l=1;
for My = 10e5%[1e5 5e5 8e5]
    My2=1.1*My;
   j=2; %j>1 linear, j<1 nonlinear
for ktb =2000*E*I/H%[5*E*I/H,2000*E*I/H, 5*E*I/H]
   k2= 0.1*ktb;

   i=1;
   for period =0.1:0.1:5.0
      m= (period^2)*kfb/(4*pi^2);   % mass of the frame (Kg)
      M= [ m,0,0;0,0.001*m,0; 0,0,0.001*m];
      K=          [12*E*I/(H^3),          -6*E*I/(H^2),          -6*E*I/(H^2);          -6*E*I/(H^2),
(4*E*I/H)+ktt,2*E*I/H;-6*E*I/(H^2),2*E*I/H,(4*E*I/H)+ktb];  % Kg/m    % Calculating
stiffness matrix

      [V,U]= eig (K,M);  % V= eigen vectors, U= diagonal eigen values% calculating
eigenvalues
      Cstar= [2*zi1,0,0;0,2*zi2,0;0,0,2*zi3] *sqrt(U); % Calculating Damping matrix
     % Cstar= [2*zi1,0;0,2*zi2] *sqrt(U);  % Calculating Damping matrix
      C= M*V*Cstar*V'*M;
        if j>1
          %K= [12*E*I/(H^3), -6*E*I/(H^2); -6*E*I/(H^2), (4*E*I/H)+ktb];
          K=          [12*E*I/(H^3),          -6*E*I/(H^2),          -6*E*I/(H^2);          -6*E*I/(H^2),
(4*E*I/H)+ktt,2*E*I/H;-6*E*I/(H^2),2*E*I/H,(4*E*I/H)+ktb];  % Kg/m    % Calculating
stiffness matrix
      else
```

```
        % K= [12*E*I/(H^3), -6*E*I/(H^2); -6*E*I/(H^2), (4*E*I/H)];
        K= [12*E*I/(H^3), -6*E*I/(H^2), -6*E*I/(H^2); -6*E*I/(H^2), (4*E*I/H)+ktt,2*E*I/H;-6*E*I/(H^2),2*E*I/H,4*E*I/H]; % Kg/m  % Calculating stiffness matrix

      end
    if period < 0.5
       load kobe_1e-3
    elseif period < 1
       load kobe_2e-3
    else
       load kobe_4e-3
    end

    % Set-up initial conditions (usually zero)
    x0 = 0;     % x0 = x_zero = initial displacement
    xd0 = 0;    % xd0 = x_dot_zero = initial velocity
    xdd0 = 0;   % xdd0 = x_dot_dot_zero = initial acceleration

    if j>1;
       F = -M*ev*f;% Use the ground acceleration to determine the input inertia force
       [x xd xdd] = NBmdof(M, C, K, F, dt, x0, xd0, xdd0);
    else
       [x xd xdd teta M_MP] = NBmdofNL(M, C, K, ev, f, dt, x0, xd0, xdd0,My,ktb,Beta,k2,My2);
    end
    periodector = period;
    spectral_disp1(i,j,l)     = max(abs(x(1,:))')
    spectral_top_mom(i,j,l)   = ktt*max(abs(x(2,:))')
    spectral_bot_rot(i,j,l)   = max(abs(x(3,:))')

    %spectral_top_moment(i,j,l)   = 9.806*(1/1000)*ktt*max(abs(x(2,:)));
    % spectral_veloc(i,:) = max(abs(xd)');
    %  spectral_accel(i,:) = max(abs(xdd)');
    i = i + 1
  end
  j=j+1
end
l=l+1
end
for l=1:3
  for i=1:48
    RFSDNL(i,l)= spectral_disp1(i,1,l)/spectral_disp1(i,2,l);
    RFSDL(i,l)= spectral_disp1(i,1,l)/spectral_disp1(i,3,l);
    rot(i,l)= spectral_rot(i,1,l)/spectral_rot(i,3,l);
end
end
% figure(1)
```

```
%  plot(teta,M_MP),grid on
 %plot the spectra against period
set(0,'DefaultAxesFontSize',14)
figure(1)
title('Reduction factor of SD (NL to fixed linear) against Structural Period for Ktbot=5EI/H')
subplot(1,1,1),grid on,hold on
plot(0.3:0.1:5,RFSDNL(:,1),'blue--','linewidth',3)
plot(0.3:0.1:5,RFSDNL(:,2),'red','linewidth',3)
plot(0.3:0.1:5,RFSDNL(:,3),'green','linewidth',3)
legend('My=1e+5','My=5e+5','My=8e+5')
xlabel('Period of fixed base (s)'),ylabel('Reduction factor for SD')

figure(2)
title('Reduction factor of SD (NL to linear) against Structural Period for Ktbot=5EI/H')
subplot(1,1,1),grid on,hold on
plot(0.3:0.1:5,RFSDL(:,1),'blue--','linewidth',3)
plot(0.3:0.1:5,RFSDL(:,2),'red','linewidth',3)
plot(0.3:0.1:5,RFSDL(:,3),'green','linewidth',3)
legend('My=1e+5','My=5e+5','My=8e+5')
xlabel('Period of fixed base (s)'),ylabel('Reduction factor for SD')

figure(3)
title('base rotation against Structural Period for Ktbot=5EI/H')
subplot(1,1,1),grid on,hold on
plot(0.3:0.1:5,spectral_rot(:,1,1),'blue--','linewidth',3)
plot(0.3:0.1:5,spectral_rot (:,1,2),'red','linewidth',3)
plot(0.3:0.1:5,spectral_rot (:,1,3),'green','linewidth',3)
legend('My=1e+5','My=5e+5','My=8e+5')
xlabel('Period of fixed base (s)'),ylabel('base rotation')

figure(4)
title('Reduction factor of rotation (NL to linear) against Structural Period for Ktbot=5EI/H')
subplot(1,1,1),grid on,hold on
plot(0.3:0.1:5,rot(:,1),'blue--','linewidth',3)
plot(0.3:0.1:5,rot (:,2),'red','linewidth',3)
plot(0.3:0.1:5,rot (:,3),'green','linewidth',3)
legend('My=1e+5','My=5e+5','My=8e+5')
xlabel('Period of fixed base (s)'),ylabel('Reduction factor for base rotation')

function [x xd xdd teta M_MP] = NBmdofNL(M, C, K, ev, fp, dt, x0, xd0,
xdd0,My,ktb,Beta,k2,My2)

% Constant average acceleration Newmark-Beta
% MDOF case
[mmm,iii]=min(abs(fp')) ;
N = iii(1,1);
for j=1:N
   f(1,j)= fp(1,j);
```

```
end
ndof = length(diag(M));
x = zeros(ndof,N); x(:,1) = x0;
xd = zeros(ndof,N); xd(:,1) = xd0;
xdd = zeros(ndof,N); xdd(:,1) = xdd0;
M_MP = zeros(1,N);
zero= zeros (1,N);
M_reset = 0;
teta_reset = 0;

for i = 2:N
   xerr= 100;
   A1 = (4*M/dt/dt + 2*C/dt +K);
   A2 = M*((4/dt/dt)*x(:,i-1) + (4/dt)*xd(:,i-1) + xdd(:,i-1));
   A3 = C*((2/dt)*x(:,i-1) + xd(:,i-1));
  M_MP (1,i)=  M_MP (1,i-1);
  F = (-M*ev*f)-[zero;zero;M_MP];

   x(:,i) = inv(A1)*(F(:,i) + A2 + A3);
   xd(:,i) = -xd(:,i-1) + (2/dt)*(x(:,i) - x(:,i-1));
   xdd(:,i) = (4/dt/dt)*(x(:,i) - x(:,i-1) - xd(:,i-1)*dt) - xdd(:,i-1);
   teta= x(3,:);
   [M_MP,M_reset,teta_reset,My]                                                    =
Menegotto_Pinto_Model_Second_Stiffness(teta,i,M_MP,My,ktb,Beta,M_reset,teta_reset,k2,
My2);

   while abs(xerr) > 1e-5
     xold=x(3,i);
%       F = (-M*ev*f)-[zero;zero; M_MP];
      F = (-M*ev*f)-[zero;zero; M_MP];
      A1 = (4*M/dt/dt + 2*C/dt +K);
      A2 = M*((4/dt/dt)*x(:,i-1) + (4/dt)*xd(:,i-1) + xdd(:,i-1));
      A3 = C*((2/dt)*x(:,i-1) + xd(:,i-1));
      x(:,i) = inv(A1)*(F(:,i) + A2 + A3);
      xd(:,i) = -xd(:,i-1) + (2/dt)*(x(:,i) - x(:,i-1));
      xdd(:,i) = (4/dt/dt)*(x(:,i) - x(:,i-1) - xd(:,i-1)*dt) - xdd(:,i-1);
      xerr= x(3,i)-xold;
  end


end
function                                [M_MP,M_reset,teta_reset,My]                    =
Menegotto_Pinto_Model_Second_Stiffness(teta,i,M_MP,My,K,beta,M_reset,teta_reset,k2,M
y2)

M_MP= M_MP';
dteta = diff(teta);
```

```
if i < 3

   M_MP(i,1) = K*teta(i);
else
   M_MP1(i,1)                =                (K*(teta(i)-teta_reset)+M_reset)/((1+((abs((K*(teta(i)-
teta_reset)+M_reset)/(My*sign(teta(i)-teta(i-1)))))^beta))^(1/beta));

   if (dteta(i-1)*dteta(i-2)) < 0

      M_reset = M_MP1(i);
      teta_reset = teta(i);
   end

   teta_y= teta_reset-((M_reset- My*sign(teta(i)-teta(i-1)))/K);

   if k2*(teta(i)-teta_y)*sign(teta(i)-teta(i-1))<0

      M_MP2(i,1)= 0;
   else
      M_MP2(i,1)= k2*(teta(i)-teta_y);
   end
   M_MP(i,1)= M_MP1(i,1)+ M_MP2(i,1);

   if abs(M_MP (i,1))> My2;
      M_MP (i,1)= My2*sign(teta(i-1)-teta(i-2));
   end
   if (dteta(i-1)*dteta(i-2)) < 0

      My=max (My,(M_MP(i-1,1)*sign(teta(i-1)-teta(i-2))));

   end
end
M_MP= M_MP';
```

Appendix B: Details of Tested Base Connections

B.1. Concrete Foundation

The foundation was designed based on ACI 318-05 and the details are shown in Figure B-1.

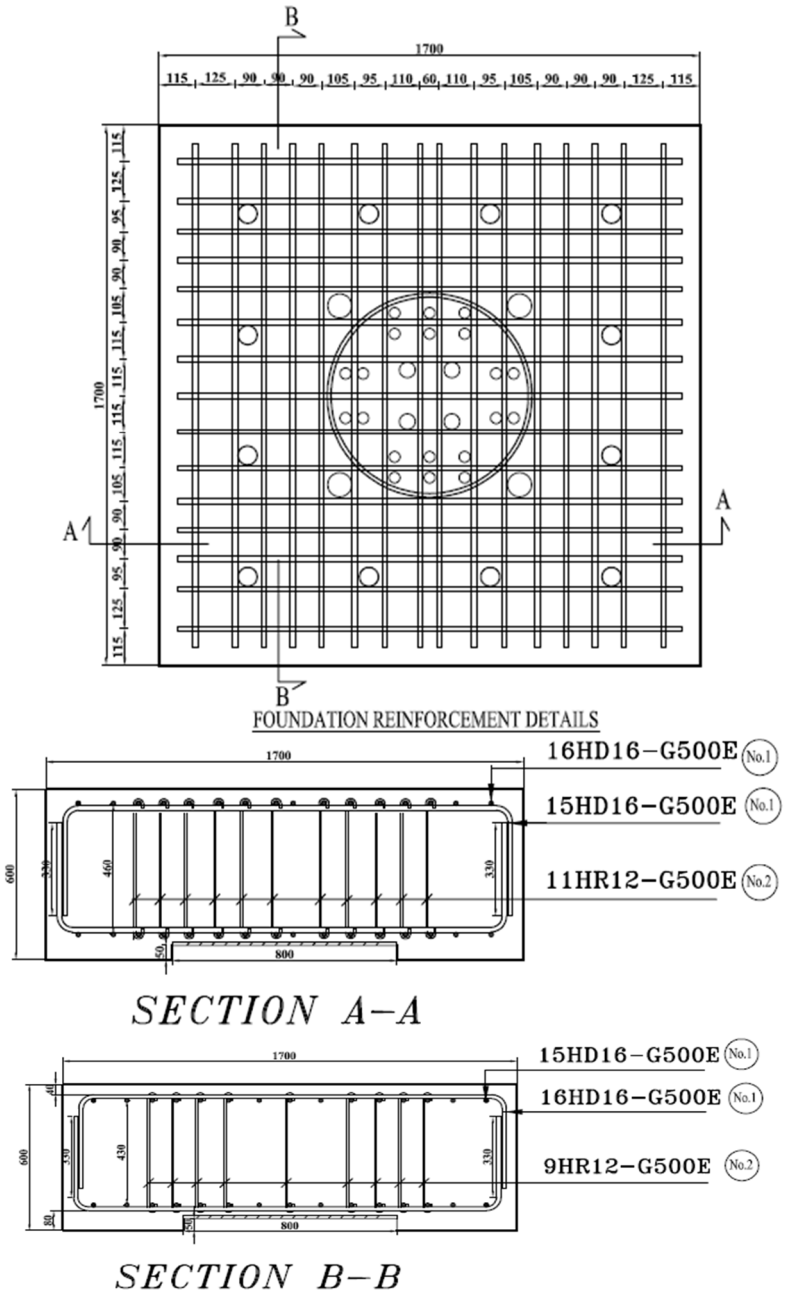

Figure B-1: Detail of tested concrete foundation

Steel tubes were placed in the concrete to provide a pathway for rods. These holes are shown in Figure B-2. Rods in holes A connected the concrete foundation to the strong floor, rods in holes B connected the column to the foundation for applying axial force, rods in holes C connected base connections with yielding angles to the foundation, rods in holes D connected exposed base plate and WAFC to the foundation, rods in holes E connected SAFC to the foundation.

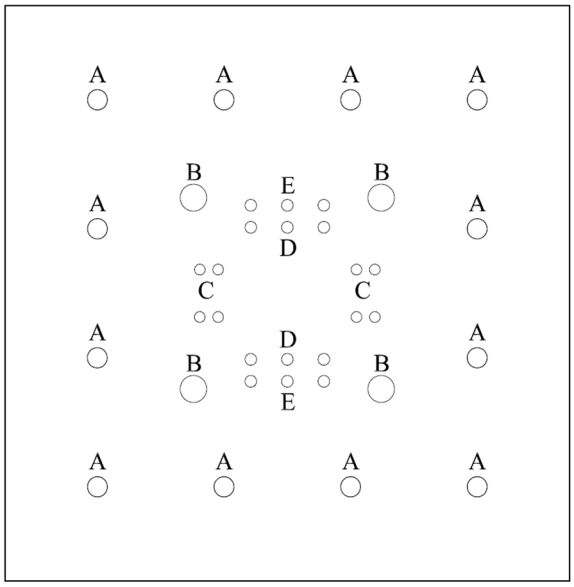

Figure B-2: Position of the holes and tubes in the concrete foundation

The concrete foundation was connected to the strong floor by 12 M36 Grade 8.8 threaded rods as shown in Figure B-3. These rods prevented the concrete foundation from uplift and sliding during lateral loading.

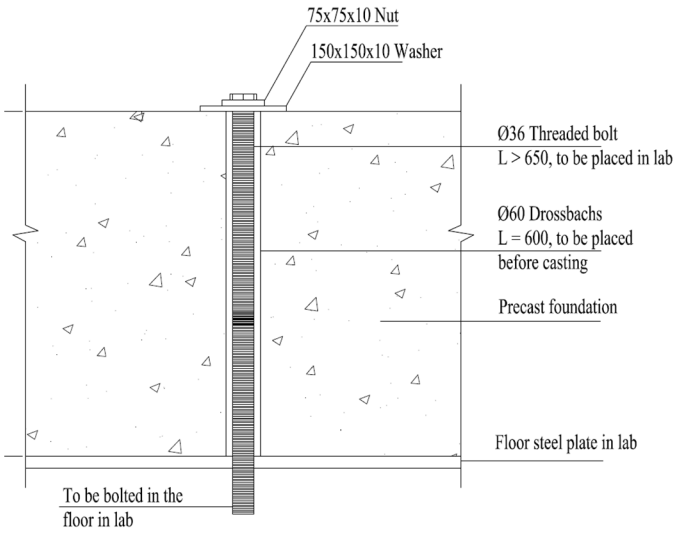

Figure B-3: Connection between the concrete foundation and the strong floor

The anchor rods passed through the steel tubes of concrete (holes C, D and E in Figure B-2) and anchored at the bottom of the concrete foundation as shown in Figure B-4. A void was considered at the bottom of the concrete foundation to provide enough space for nuts as shown in Figure B-1.

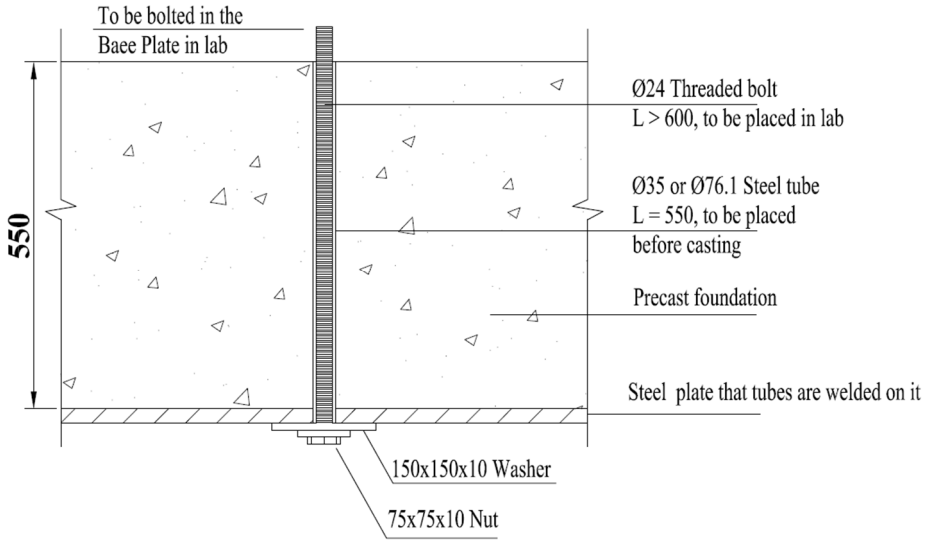

Figure B-4: Connection between the anchor rod and bottom of the concrete foundation

B.2. Base Connections

The following Figures show base connection details that were tested, and the results are presented in Chapters 3, 4, 6, 7, 9 and 10.

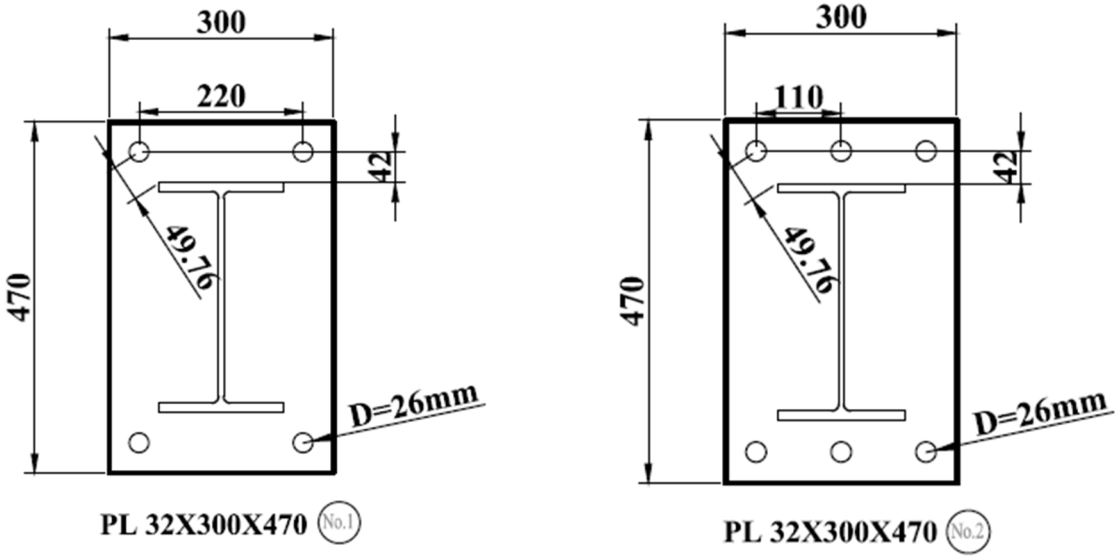

PL 32x300x470- Grade 300 PL 32x300x470- Grade 300

Figure B-5: Details of the exposed base plate for specimens of Chapter 3 and Chapter 4

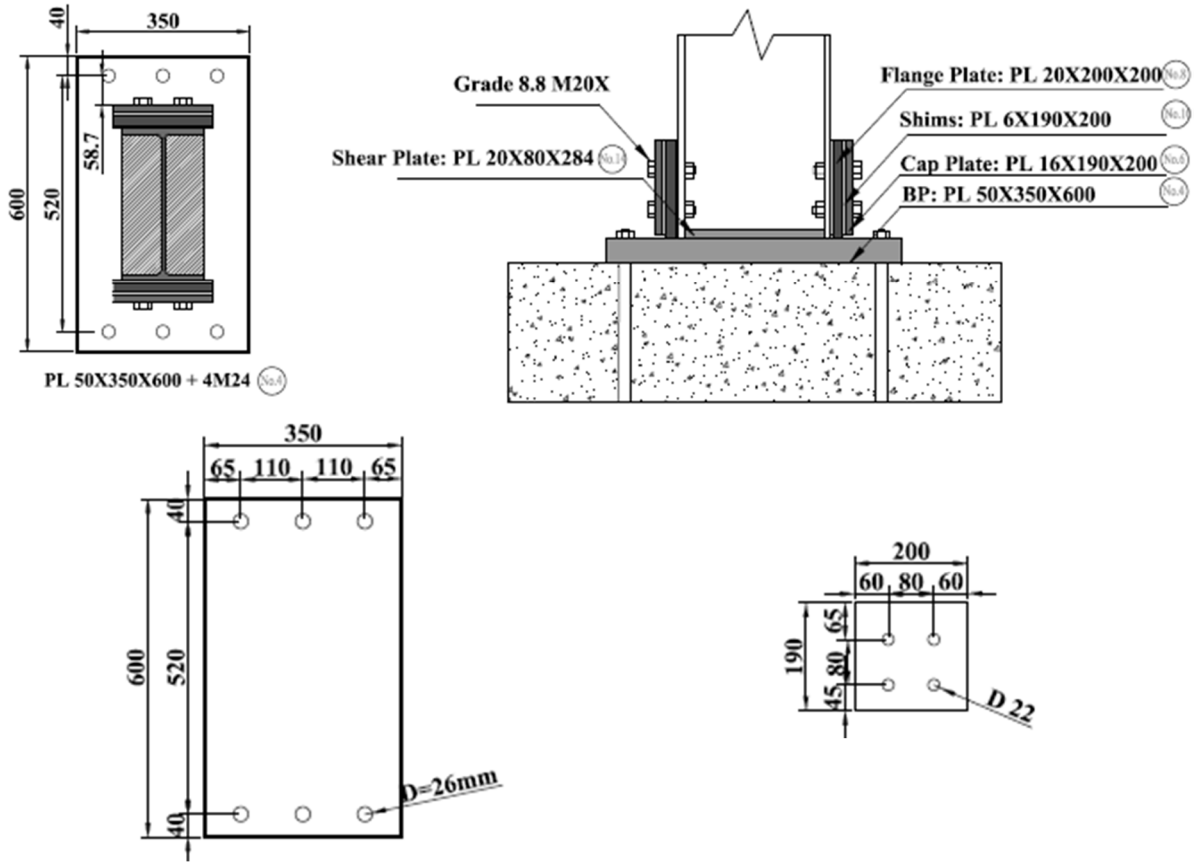

PL 50x350x600-- Grade 300
Base Plate

PL 160x190x200- Grade 300
Cap Plate

PL 20x200x200- Grade 350
Flange Plate

PL 160x190x200- Bisalloy 500
Shim

Figure B-6: Details of the SAFC

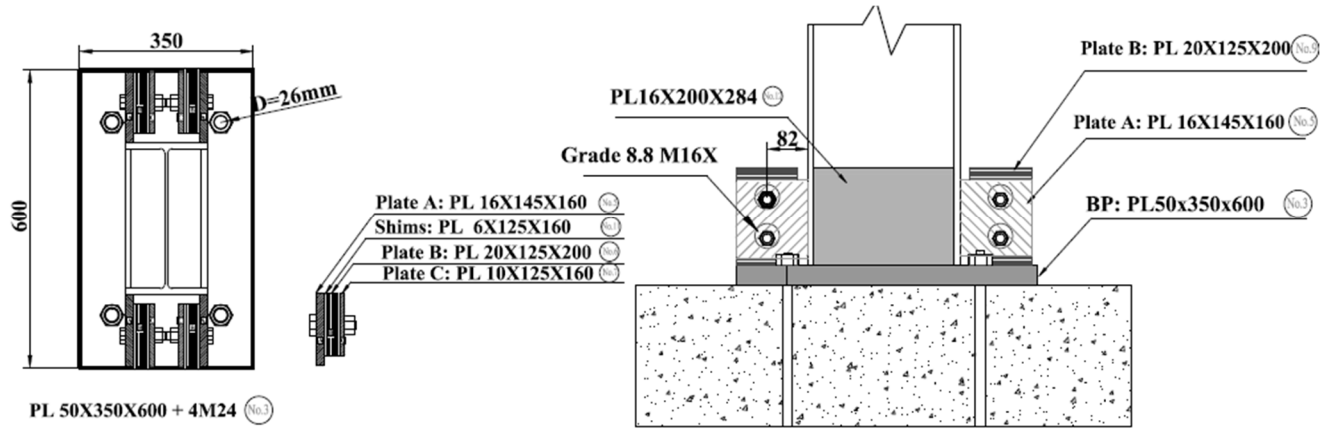

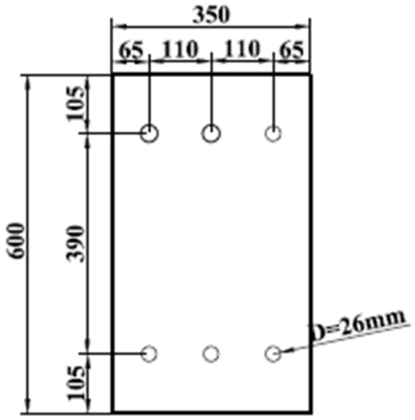

PL 50x350x600- Grade 300
Base Plate

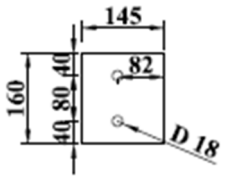

PL 16x145x160- Grade 350
Column Plate

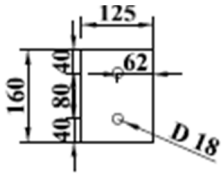

PL 10x125x160- Grade 300
Cap Plate

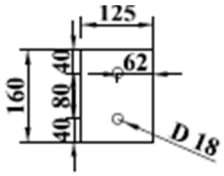

PL 6x125x160- Bisalloy 500
Shim

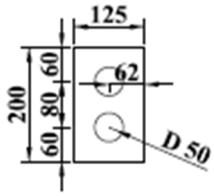

PL 20x125x200- Grade 350

Figure B-7: Details of the WAFC

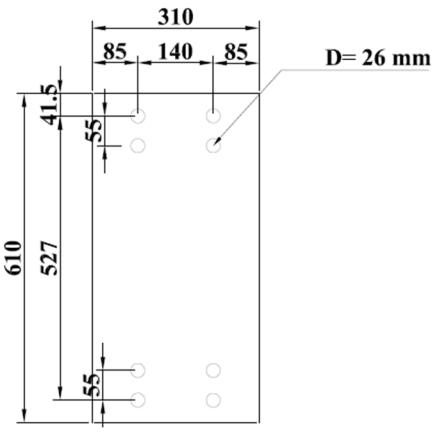

PL 50x310x610- Grade 300
Figure B-8: Details of the base with yielding angle

B.3. Asymmetric Friction Connection

The following details were used for asymmetric friction connection that is used in Chapter 9.

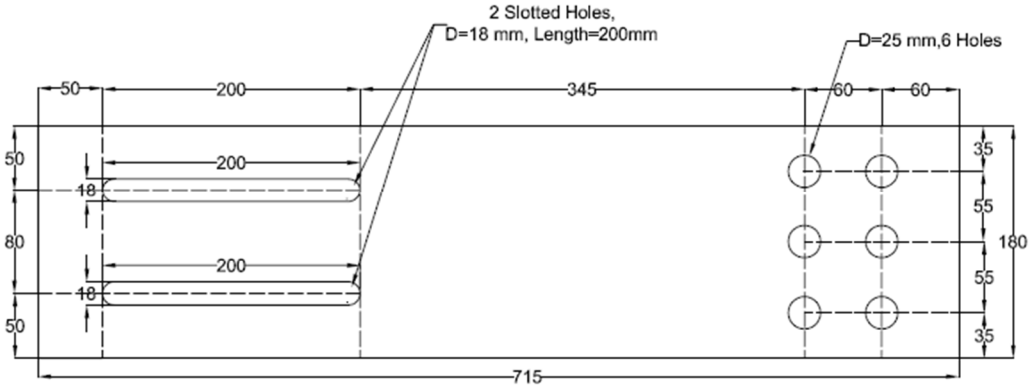

Slotted Plate: PL 32x180x670- Grade 300

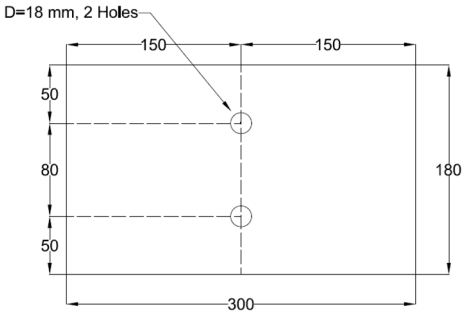

Bearing Plate and Cap Plate: PL 16x180x300- Grade 300
Shim: PL 6x180x300- Bisalloy 500

Figure B-9: Details of AFC for related tests in Chapter 9

Appendix C: SAFC and WAFC Design Examples

For design of these base connections the following steps are required:

- Determining maximum demands based on the interaction of axial force and the column bending moment

- Calculating the number of bolts in the AFC connection to satisfy the required sliding moment of the base connection.

- Designing and detailing of the boundary plates (shims, flange, column and cap plates), the base plate and anchor rods.

- Develop the macro model for the SAFC and WAFC.

In the following examples, the design and detailing of SAFC and WAFC for the column section of 460UB82 with an effective length of 3.0m under 300 kN axial compression force are described. It is assumed maximum rotation at ULS is 0.04 radian.

This example considers bi-directional loading. Loading is different in different directions should also be considered.

In the first step, the design bending moments about the principle axes are calculated as given by Equations (C-1) and (C-2). Assigning M^*_x and M^*_y equal to 140 kN.m and 58 kN.m can satisfy these equations (NZS 3404, 1997)

Section capacity (clause 8.3.4.2):

$$\left(\frac{M_x^*}{\emptyset M_{rx}}\right)^{\gamma} + \left(\frac{M_y^*}{\emptyset M_{ry}}\right)^{\gamma} \leq 1 \text{ where } \gamma = 1.4 + \left(\frac{N^*}{\emptyset N_s}\right) = 0.77 \leq 1 \quad \text{(C-1)}$$

Biaxial bending capacity (clause 8.4.5.1):

$$\left(\frac{M_x^*}{\emptyset M_{cx}}\right)^{1.4} + \left(\frac{M_y^*}{\emptyset M_{iy}}\right)^{1.4} \leq 1 \quad \text{(C-2)}$$
$$1.01 \approx 1$$

Where M_r is the nominal section moment capacity reduced by axial force that is 491 kN.m for M_{rx} and 87.6 kN.m for M_{ry}, M^* is the design bending moment, M_i is the nominal in-plane member moment capacity of the column section that is equal to 74.3 kN.m for M_{iy}, M_c is lesser of M_i and nominal out of plane member capacity about major principal x-axis that is 336 kN.m for $M_{cx.}$

C.1. Design of WAFC

The neutral axis (NA) depth, *c*, is calculated as:

$$c_x = \frac{P}{W \times \sigma_y} = \frac{300 \times 10^3}{191 \times 300} = 5\ mm$$
$$c_y = \frac{P}{2 \times t_f \times \sigma_y} = \frac{300 \times 10^3}{2 \times 16 \times 300} = 31\ mm \quad \text{(C-3)}$$

Where P is the axial force, W is the width of the section, t_f is the flange thickness, σ_y is the yielding stress of the column. It is assumed that bolt friction force on either sides of connection are equal and opposite and therefore do not contribute to computation of *c*.

The base uplift moment when the column is subject to axial compression force, M_{Axial}, is estimated from:

$$M_{Axial-X} = P \times D_{axial} = 300 \times \left(\frac{460}{2} - \frac{5}{2}\right) = 68\ kN.m$$
$$M_{Axial-y} = P \times D_{axial} = 300 \times \left(\frac{191}{2} - \frac{31}{2}\right) = 24\ kN.m \quad \text{(C-4)}$$

Where, P is the column axial force, and D_{axial} is perpendicular distance from the centre of axial force to the neutral axis. The remaining maximum moment before overstrength is considered, that will prevent column flexural yielding in X direction, $M_{slide\text{-}X}$, is equal to:

$$M_{Slide-X} = \frac{M^*_x - M_{Axial-X}}{\emptyset_{\text{OS-Sliding}}} = \frac{140 - 68}{1.4} = 52kN.m \quad \text{(C-5)}$$

Where M^*_x is the maximum moment that is applied to the column obtained by their bi-directional loading case as shown in Equation (C-2), M_{Axial} is the moment from axial force, and $\phi_{OS\text{-}Sliding}$ is over strength of sliding that is 1.4. M_{slide} is the ideal resistance we wish the bolts to provide with friction in the direction considered.

For calculation of the prying moment due to Y-axis bending of the WAFC initial estimation of flange plate size is required. Size of the flange plate and column plate are assumed 25x125x200 mm, and 16x150x160 mm. The prying moment about y direction is given below from Equation (7-11) of Chapter 7.

$$M_{Prying} = min\begin{cases} 2 \times \dfrac{\theta_{Base} \times 3EI_{fp}}{{L_1}^2} \times L_2 = 2 \times \dfrac{0.04 \times 3 \times 200 \times 162 \times 10^6}{170^2} \times 200 \\ 2 \times \dfrac{\sigma_y \times b_{fp} \times t_{fp}^2}{4} = 2 \times \dfrac{300 \times 125 \times 25^2}{4} \end{cases} = 11\ kN \quad \text{(C-6)}$$

Where L_1 is the distance from top of the column plate to the base plate; I_{fp} is the second moment of inertia about the weak axis of the flange plate; and L_2 is length of the column plate. This moment cannot be greater than the flange plate plastic flexural strength, $M_{P\text{-}fp}$, given by the second term in Equation 7-11. Where b_{fp} is the width of the flange plate, t_{fp} is the flange plate thickness, and σ_y is the flange plate yield stress. Therefore, the sliding moment about Y direction, $M_{slide\text{-}Y}$, is defined as:

$$M_{Slide-Y} = \frac{M_Y - M_{Prying-Y} - M_{Axial-Y}}{\emptyset_{\text{OS-Sliding}}} = \frac{58 - 11 - 24}{1.4} = 17\ kN.m \qquad \text{(C-7)}$$

Where, M is the column base moment, M_{Prying} is the column base prying moment, M_{Axial} is the moment from the axial force, and $\phi_{OS\text{-}Sliding}$ is the sliding over strength factor.

The required sliding force based on the sliding in X direction, F_s as shown in Figure C-10, is 52 kN.m/ 600mm= 87 kN that corresponds to 2M16 on each side of the base connection. 2M16 can provide 80 kN in AFC sliding that is less than 87 kN. This configuration can provide the following moment resulting from sliding friction that is close to the required moment in Equations (C-5) and (C-7). In addition, no column yielding is expected for this bi-axial yielding.

$$M_{Slide-x} = \text{n} \times F_{s-M16} \times d = 2 \times 40 \times 0.6 = 48\ kN.m$$
$$M_{Slide-y} = \text{n} \times F_{s-M16} \times (\frac{W}{2} - \frac{c}{2}) = 4 \times 40 \times (\frac{0.191}{2} - \frac{0.031}{2}) = 13\ kN.m \qquad \text{(C-8)}$$

Where, n is the number of the bolts in AFC, F_s is the nominal sliding force for each AFC bolt, d_i is horizontal distance from the centroid of the sliding surfaces of each bolt to the neutral axis, W is the width of the section, c is the neutral axis distance from the edge.

The sliding force causes moment and shear in the column plate and tension and compression force in the flange plate as shown in Figure C-10. Demands and capacities for these plates are compared as follows:

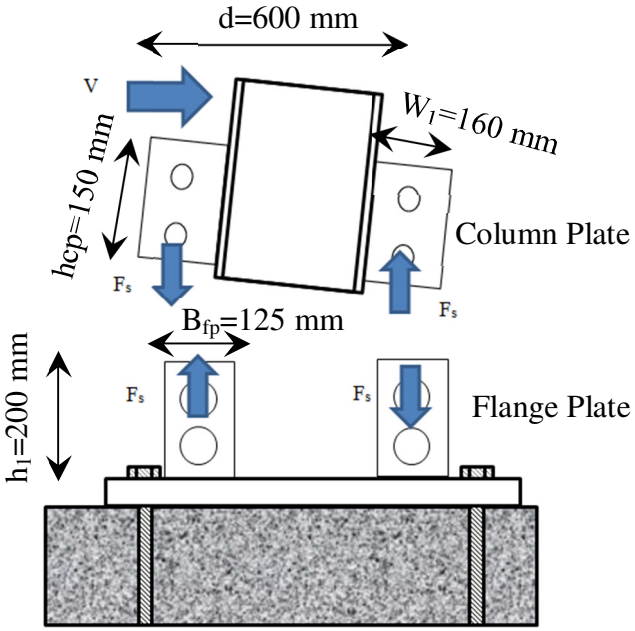

Figure C-10: Applied demands on the column plates and flange plates of WAFC

For flange plate in tension: (Clause 7.1 NZS 3404,1997)

$$N_t^* \leq \emptyset N_t = \emptyset \min\left(A_g f_y, 0.85 k_{te} A_n f_u\right)$$

$$80 \text{ kN} \leq \emptyset N_t = 0.9 \times \min(875\ kN, 685\ kN) = 616\ kN \quad OK \tag{C-9}$$

In compression: (Clause 6.1 NZS 3404,1997)

$$N_c^* \leq \emptyset \min(N_s, N_C) = \emptyset k_f A_n f_y \rightarrow 80 \text{ kN} \leq 472\ kN \quad OK \tag{C-10}$$

Where N^* is the applied tension force to the plate that is the same N^*_t, N^*_c, F_s, A_g is the gross area of the plate cross section, A_n is the net area of the plate cross section, N_t is the nominal section capacity of the plate in tension, k_{te} is the correction factor for distribution of forces in

a tension member, k_f is the form factor for members subject to compression, N_c is the nominal member capacity and N_s is the nominal section capacity.

For Column Plate:

$$\begin{aligned} \mathrm{M}_S^* \le \emptyset M_s \rightarrow (\mathrm{F}_S \times \frac{W_1}{2} = 80 \times \frac{0.16}{2} = 6.4\ kN.m) \le (\phi \times \mathrm{Ze} \times \mathrm{fy} \\ = 0.9 \times 9000 \times 300 \times \frac{1}{10^6} = 24.3\ kN.m) \quad OK \\ V^* \le \emptyset V_V \rightarrow (\mathrm{F}_S = 80\ kN) \le 0.9 \times 0.6\mathrm{fy} \times A_w = 414\ kN \quad \mathrm{OK} \end{aligned} \tag{C-11}$$

Where M^* and V^* are applied demand and M_s (f_y Z_e=300MPa × 21 mm^3), and V_v are flexural and shear resistance of the column plate. Clearances and size of the hole can be calculated by the method in Section 7.2.1. These are defined as:

$$Cl_A = \theta_{rock} \times H_1 = 0.04 \times 200 = 8\ mm \rightarrow (oversize\ hole\ 2mm) 10\ mm \tag{C-12}$$

$$Cl_B = \theta_{rock} \times W_1 = 0.04 \times 150 = 6\ mm \rightarrow 10\ mm \tag{C-13}$$

$$\mathrm{D} = 2(\theta_{rock} \times \sqrt{W_2^2 + H_b^2} + d_{Sh} + 2\mathrm{mm}) = 2\left(0.04 \times \sqrt{535^2 + 130^2} + 18 + 2\mathrm{mm}\right) = 85\mathrm{mm} \tag{C-14}$$

Where Cl_A and Cl_B are clearances defined in Figure 7-1, H_1 is the height of the flange plate, W_1 is the width of the column's plate, W_2, and W_3 are the distance from the neutral axis up to the centre of the hole in the flange plate along length and width of the column section respectively, d_{sh} is the diameter of the bolt shank, and 2mm is the standard clearance.

The applied demands to the base plate and anchor rods are shown in Figure 7-2. Based on these demands the minimum size of the base plate and anchor rods are: PL 32x760x350+4M24 Grade 8.8. The final details of the WAFC connection are as follows:

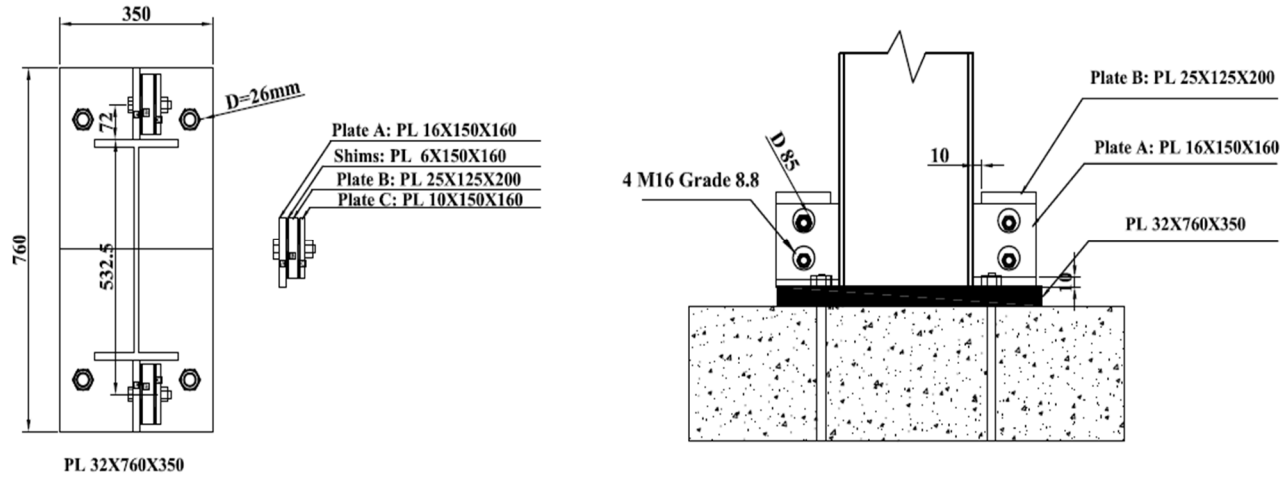

Figure C-11: Details of WAFC base

Table C-1 and Figure C-11 present the details of macro model based on Chapter 8.

Table C-1: Macro model output parameters- using nominal input values of the WAFC base

Stage	Direction	Rotational Stiffness, kN.m/rad	Moment increment, kN.m	Rotation Increment, mrad
I	X	∞	Eq (8-1)= 92.3	0
	Y	∞	Eq (8-1)= 30.4	0
II	X	0	0	Eq (8-5)=1.88
	Y	Eq (8-6)=533	Eq (8-7)=1.9	Eq (8-5)=9.15
III	X	Eq (8-8)=2739	Eq (8-12)=24.2	Eq (8-14)=8.8
	Y	Eq (8-8)+ Eq (8-6)=583	Eq (8-11)=11.5	Eq (8-13)=0.02
IV	X	0	0	Eq (8-15)=0.029
	Y	Eq (8-6)=533	Eq (8-16)=1.1	Eq (8-15)=0.011

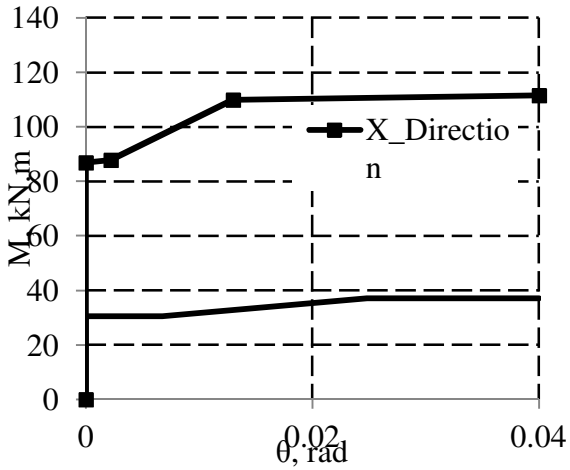

Figure C-12: Macro model of the WAFC

C.2. Design of SAFC

The neutral axis depth and the base uplift moment when the column is subjected to the axial compression force is similar to WAFC (c_x=5mm, c_y=31mm, M_{Axial}-x=68 kN.m, M_{Axial}-y=24 kN.m).

Initial estimation of the flange plate size is required for calculation of the prying moment. The size of the flange plate is assumed to be 20x200x200 mm. The prying moment about X direction is given below from Equation (8-6):

$$M_{Prying} = min\begin{cases} \dfrac{{H_{fp}}^2}{\dfrac{{H_{fp}}^3}{12 \times E \times I_{fp}} + \dfrac{H_{fp}}{G \times A_{fp}}} \times \theta = 16 \text{ kN.m} \\ \dfrac{\sigma_y \times b_{fp} \times t_{fp}^2}{4} = 6 \text{ kN.m} \end{cases} = 6\ kN.m \qquad \text{(C-15)}$$

Where H_{fp} is the height to the top of the flange plate, I_{fp} is the flange plate second moment area about its weak axis, A_{fp} is the flange plate section area, b_{fp} is the width of the flange plate, and E and G are Young and shear modulus of steel, respectively Therefore, the sliding moment about X direction is defined:

$$M_{Slide-x} = \frac{M_x - M_{Pryin-x} - M_{Axial-x}}{\emptyset_{\text{OS-Sliding}}} = \frac{140 - 6 - 68}{1.4} = 47\ kN.m \qquad \text{(C-16)}$$

The remaining moment that should be provided by sliding in Y direction is equal to:

$$M_{Slide-y} = \frac{M_y - M_{Axial-y}}{\emptyset_{\text{OS-Sliding}}} = \frac{58 - 24}{1.4} = 24\ kN.m \qquad \text{(C-17)}$$

Where M is the maximum moment that is applied to the column, M_{Axial} is the moment from axial force, and $\phi_{OS\text{-}Sliding}$ is the sliding over strength factor. The required sliding force based on the sliding in X direction, F_s as shown in Figure C-13, is 47 kN.m/ 480mm= 98 kN that is close to the provided shear from 2M16 (80 kN) on each side of base connection. This configuration can provide the following moment resulting from the sliding friction that is close to the required moment in Equations (C-16) and (C-17). In addition, no column yielding is expected for this bi-axial yielding.

$$M_{Slide-x} = \text{n} \times F_{s-M16} \times d = 2 \times 40 \times 0.48 = 38.5\ kN.m$$
$$M_{Slide-y} = \text{n} \times F_{s-M16} \times (w - c) = 2 \times 40 \times (0.191 - 0.031) = 13\ kN.m \quad \text{(C-18)}$$

Where, n is the number of the bolts in AFC, F_s is the nominal sliding force for each AFC bolt, d_i is horizontal distance from the centroid of the sliding surfaces of each bolt to the neutral axis, W is the width of the section, c is the neutral axis distance from the edge.

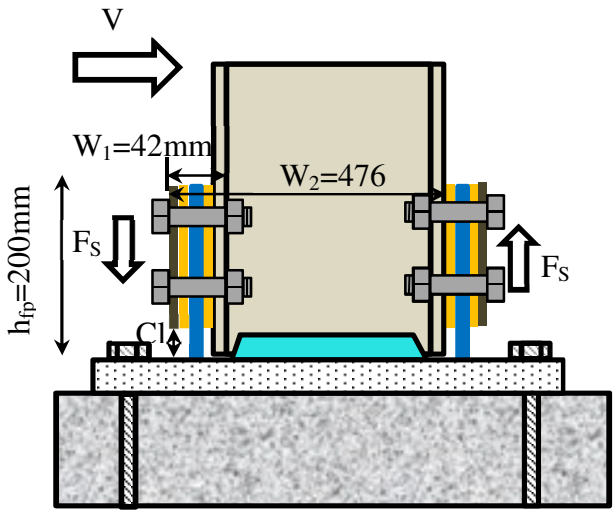

Figure C-13: Applied demands on the flange plate

The sliding force causes tension and compression of the flange plate. The demand and capacity for the flange plate are compared using:

For flange plate in tension: (Clause 7.1 NZS 3404,1997)

$$\text{N}^* \leq \emptyset N_t = \emptyset \min\left(A_g f_y, 0.85 k_{te} A_n f_u\right)$$
$$80 \text{ kN} \leq 756 \quad OK \tag{C-19}$$

In compression: (Clause 6.1 NZS 3404,1997)

$$\text{N}^* \leq \emptyset \min(N_s, N_C) = \emptyset k_f A_n f_y \rightarrow 80 \text{ kN} \leq 529\ kN \quad OK \tag{C-20}$$

Where N^* is the applied tension force to the plate, A_g is the gross area of the plate cross section, A_n is the net area of the plate cross section, N_t is the nominal section capacity of the plate in tension, k_{te} is the correction factor for distribution of forces in a tension member, k_f is the form factor for members subject to compression, N_c is the nominal member capacity and N_s is the nominal section capacity. Clearances and size of the hole can be calculated by the method in Section 6.2.1. These are defined as follows:

$$Cl = \theta_{rock} \times W_1 = 0.04 \times 42 = 2\ mm \tag{C-21}$$
$$D = 2(\theta_{rock} \times W_2) + d_{Sh} + 2mm = 2(0.04 \times 476) + 16 + 2 = 56\ mm \tag{C-22}$$

Where W_1 is total thickness of the shims as shown in Figure C-13, column flange, flange plate, and cap plate on one side of the column as shown in Figure 6-1. Where d_{sh} is the bolt shank diameter and W_2 is the minimum of: (i) the depth of the column plus W_1 for strong axis bending; and (ii) the distance from the flange tip to the furthest bolt for weak axis bending. The base plate and anchor rods are designed similar to the conventional base plate and anchor rods. The only modification is the position of the tensile force is shifted from the tensile column flange to the flange plate in the tension side as described in Section 6.2.1. The final

details of the SAFC connection are shown in Figure C-14. Table C-2 and Figure C-14 describe the details of macro model of the SAFC based on Chapter 8.

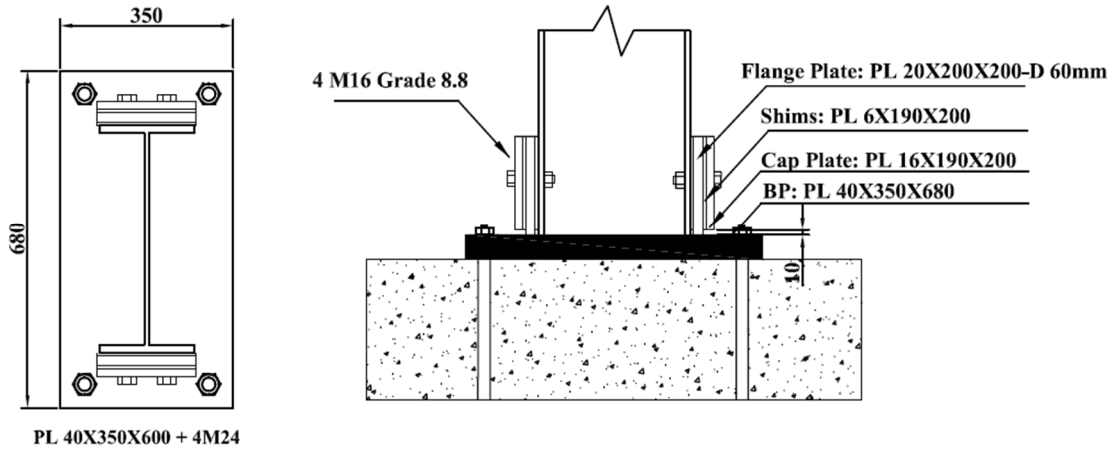

Figure C-14: Details of SAFC base

Table C-2: Macro model output parameters- using nominal input values of the SAFC base

Stage	Direction	Rotational Stiffness, kN.m/rad	Moment increment, kN.m	Rotation Increment, mrad
I	Y	∞	Eq (8-1)=30.5	0
	X	∞	Eq (8-1)=87	0
II	Y	0	0	Eq (8-5)=6.8
	X	Eq (8-6)=397	Eq (8-7)=0.8	Eq (8-5)=2.21
III	Y	Eq (8-8)=700	Eq (8-12)=6.4	Eq (8-14)=18
	X	Eq (8-8)+ Eq (8-6)=2268	Eq (8-11)=22.7	Eq (8-13)=11
IV	Y	0	0	Eq (8-15)=15
	X	Eq (8-6)=397	Eq (8-16)=0.5	Eq (8-15)=26

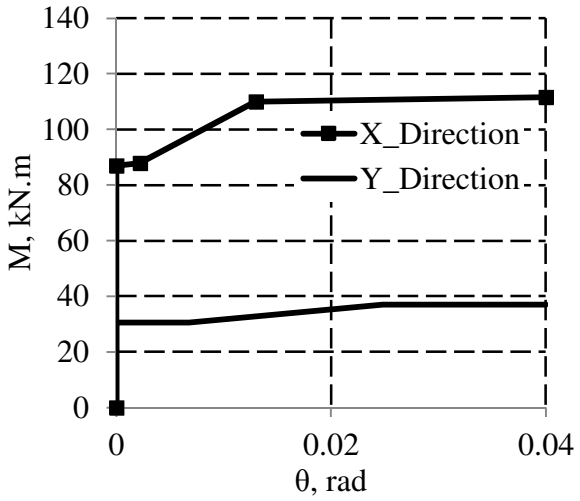

Figure C-15: Macro model of the SAFC

Appendix D: Notation

A_b: bearing area on the plate, mm^2

$A_{foundation}$: foundation area, mm2

A_{fp}: flange plate section area, mm^2

A_g: gross area of the plate cross section, mm^2

A_n: net area of the plate cross section, mm^2

A_{rod}: area of the anchor rod, mm^2

A_{sh}: shank area, mm^2

A_{th}: bolt tension area, mm^2

*B:*base plate width, mm

b: length of the angle, mm

b_{fp}: width of the flange plate, mm

Cl: distance/clearance from the cap plate and shims to the base plate, mm

c: neutral axis depth, mm

c_{Tens}: distance perpendicular to the neutral axis to the extreme fibre of the section on the gapping side, mm

D: diameter of the flange plate holes, *mm*

D_{Axial}: perpendicular distance from the centre of axial force to the neutral axis, mm

D_{rod}: Rod diameter, mm

d: distance from the sliding bolts to the neutral axis, mm

d_1: depth of the column section minus half of the thickness of the flange, mm

d_{1a}: distance between the centres of the legs of the top and bottom angles, mm

d_b: bolt diameter, mm

d_c: depth of the column section, mm

d_{eff}: effective diameter at the plate surface, mm

$d_{footing}$: footing height, mm

d_h: hole diameter, mm

d_{head}: diameter of bolt head, mm

d_i: horizontal distance from the centroid of the sliding surfaces of each bolt to the neutral axis

d_{sh}: bolt shank diameter, mm

E: elastic modulus of material, MPa

e: axial load eccentricity, mm

F_s: The nominal sliding force for each AFC bolt, kN

f_p: bearing stress between the baseplate and concrete, MPa

f_c': specific compressive strength of concrete, MPa

G: shear modulus of material, MPa

g: gage distance from the top angle's heel to the centre of the fastener, mm

g_2: distance between the plastic hinges of angle, mm

g_t: gage distance from the top angle's heel to the centre of the fastener, mm

H_1: height of the flange plate, mm

H_{col}: height of the column, m

H_{fp}: distance from the top of the flange plate to the base plate, mm

H_m: average height of flange plate holes from top of the base plate, mm

H_{st}: Column height to the point of contraflexure from the base, m

h_b: beam depth, mm

I: second moment inertia, mm^4

I_a: top angle cross section moment of inertia for vertical leg in bending, mm^4

I_{BP}: base plate moment of inertia, mm^4

I_{fp}: second moment of area about the weak axis of the flange plate, mm^4

$K_{bot.}$ base rotational stiffness of the column, kN.m

k_f: form factor for members subject to compression

K_{i_exp}: experimental initial stiffness, kN.m/rad

K_{method}: base rotational stiffness predicted from the analytical method, kN.m

K_{top}: top rotational stiffness of the column, kN.m

k_{te}: correction factor for distribution of forces in a tension member

$K_{\theta\_AFC\_T}$: AFC rotational stiffness ignoring prying, kN.m/rad

K_{θ_bolt}: base rotational stiffness due to bolt deformation, kN.m/rad

K_{θ_fp}: base rotational stiffness due to flange plate bending in the tension side of the column, kN.m/rad

K_{θ_prying}: prying rotational stiffness, kN.m/rad

$K_{\theta,test}$: secant base rotational stiffness, kN.m/rad

$k_{i:}$ initial elastic stiffness, kN.m/rad

$k_{\theta:}$ base rotational stiffness, kN.m/rad

L_1: distance from top of the column plate to the base plate, mm

L_2: length of the column plate, mm

L_{rod}: length of the anchor rod, mm

L_{sh}: shank length plus half of the bolt head thickness, mm

L_{th}: threaded length of the bolt from the nut up to the shank plus half of the nut thickness, mm

l_a: length of the angles, mm

l_{bolt}: lever arm of the bolt, mm

l_s: width of the seat angle, mm

$M_{4\%\_exp:}$ experimental base moment at 4% drift, kN.m

M^*: design bending moment, kN.m

M_{Axial}: the moment from axial force, kN.m

M_{angle}: base moment from angles, kN.m

M_{base}: column base moment, kN.m

M_c: lesser of M_i and nominal out of plane member capacity, kN.m

$M_{Elastic,FB}$: maximum elastic moment of the fixed top and base column, kN.m

M_i: nominal in-plane member moment capacity of the column section, kN.m

M_{method}: base moment predicted from the analytical method, kN.m

M_p: column plastic capacity, kN.m

$M_{P\text{-}fp}$: flange plate plastic flexural strength, kN.m

M_{Prying}: elastic prying moment mainly from flange plate bending on the compression side of the column, kN.m

M_r: nominal section moment capacity reduced by axial force, kN.m

M_{Slide}: moment resulting from sliding friction, kN.m

M_{test}: moment from experimental test that was obtained at 4% drift, kN.m

M_{Tot}: maximum base moment from lateral loading causing strong axis bending, kN.m

M_u: ultimate moment capacity, kN.m

M_y: base yielding moment, kN.m

M_{y_angle}: base moment that angles yield, kN.m

$M_{y\_exp:}$ experimental ultimate base moment, kN.m

m: distance from edge of the base plate up to edge of the column flange, mm

N: length of the base plate, mm

N_c: the nominal member capacity, kN

N_t: nominal section capacity of the plate in tension, kN

N_{tf}: the proof load per bolt, kN

n_{AB}: number of anchor rods in the tension side

n_{bolt}: number of AFC bolts that slide

P: Axial load, kN

P_r: applied axial force, kN

q_{max}: uniform bearing stress per width, MPa/mm

T_{apply}: applied torque for tightening the rods, kN.m

T_{BP}: tension force on the tension side of the base plate, kN

T_{dc}: double curvature period

T_{rod}: final tensile force of the rods, kN

T_{PT}: anchor rod tension force, kN

t_{fp}: flange plate thickness, mm

t_{plate}: thickness of the plates that are between the slotted plate and bolt, cap plate or bearing plate and brace web

t_s: thickness of the top and bottom angles, mm

t_{shim}: thickness of the shim, mm

t_t: thickness of the top angle, mm

t_{washer}: thickness of the washer, mm

V: column lateral force, kN

V_p: ultimate force that causes formation of plastic hinges in the angle, kN

W: width of the section, mm

W_1: total thickness of the shims, column flange, flange plate, and cap plate on one side of the column, mm

W_2: distance from the neutral axis up to the centre of the hole in the flange plate along length the column section, mm

W_3: distance from the neutral axis up to the centre of the hole in the flange plate along width the column section, mm

x: length of the base plate from the rods up to the column flange, mm

x_{cp}: distance between the extreme fibre of the section and the position of the potentiometer measuring compression perpendicular to the neutral axis, mm

x_e: distance between the edge of the column flange up to the centre of the anchor rod in the tensions side, mm

x_{UD}: distance between potentiometers measuring tension and compression, mm

Y: bearing length, mm

Y_2: bearing length on the tension side of the base plate, mm

η: number of shear planes

$\Delta_{plate}^{compression}$: flexural deformation of the base plate on the compression side, mm

$\Delta_{concrete}$: compressive deformation under the toe of the base plate, mm

Δ_{FB}: elastic displacement of the column alone under the lateral force, mm

$\Delta_{Kbot=\alpha EI/H}^{Ktop=\beta EI/H}$: Column median lateral displacement with a top flexibility of $\beta EI/H$ and the base flexibility of $\alpha EI/H$, *mm*

$\Delta M_{non\text{-}pryingSIII}$: the moment increment at stage III for non-prying cases, kN.m

$\Delta M_{pryingSII}$: the moment increment at stage II for prying cases, kN.m

$\Delta M_{pryingSIII}$: the moment increment at stage III for prying cases, kN.m

$\Delta M_{pryingSIV}$: the moment increment at stage IV for prying cases, kN.m

Δ_{top}: lateral displacement of the column, m

$\Delta_{plate}^{tension}$: flexural deformation of the base plate on the tension side, mm

Δ_{Uplift}: uplift displacement at the extreme tension side of the specimen, mm

Δ_{ub}: maximum bolt deformation before fracture, mm

$\Delta\theta_{non\text{-}pryingSIII}$: the base rotation increment at stage III for non-prying cases, kN.m

$\Delta\theta_{pryingSIII}$: the base rotation increment at stage III for prying cases, kN.m

$\Delta\theta_{pryingSIV}$: the base rotation increment at stage IV for prying cases, kN.m

$\Delta\theta_{SVI}$: the base rotation increment at stage IV, kN.m

ε_{proof}: bolt elongation due to the proof load

ε_{ult}: maximum bolt elongation

Θ: orientation of the neutral axis

θ_{base}: base rotation, rad

θ_{beam}: beam rotation, rad

θ_{column}: the rotation of the column, rad

$\theta_{footing}$: footing rotation, rad

$\theta_{NL,Fixed}$: nonlinear base rotation of the fixed top and base frame, rad

$\theta_{NL,Kbot}$: nonlinear base rotation for a frame that is fixed at the top with base rotational stiffness, rad

θ_{plate}: baseplate rotation, rad

θ_{rock}: column design base rotation, rad

θ_{trans}: base rotation at the transitional stage, rad

θ_{y_angle}: rotation of the base connection when the angles yield, rad

μ: friction coefficient

σ_y: yield stress of material, Mpa

ϕ: strength reduction factor

$\phi_{OS\text{-}Sliding}$: Over strength of sliding